CHARACTERIZATION AND COMPENSATION OF THE ELECTROMECHANICAL DELAY DURING FES-CYCLING

By

BRENDON CONNOR ALLEN

A DISSERTATION PRESENTED TO THE GRADUATE SCHOOL
OF THE UNIVERSITY OF FLORIDA IN PARTIAL FULFILLMENT
OF THE REQUIREMENTS FOR THE DEGREE OF
DOCTOR OF PHILOSOPHY

UNIVERSITY OF FLORIDA

2021

To my wife, *Breanna*, to my parents, *Craig* and *Kimberly*, and to my siblings, *Cory*, *Kyli*, *Morgan*, and *Mackenzie*, who have provided invaluable support and encouragement throughout my life, and to God for his inspiration and blessings.

ACKNOWLEDGMENTS

I would like to acknowledge Dr. Warren Dixon, for his support, guidance, mentorship, and encouragement throughout my graduate studies at the University of Florida. He has helped me to grow both intellectually and as an individual. I would also like to thank Dr. Steven Charles for helping me as I began my graduate studies at Brigham Young University and for his constant support and guidance. I would like to thank Drs. Scott Banks, Emily Fox, and Amor Menezes, for their recommendations and oversight throughout the completion of this dissertation. I am thankful for the current and past members of the Nonlinear Controls and Robotics Laboratory for their time, support, and dedication. I would like to thank the National Defense Science and Engineering Graduate Fellowship Program for their generous financial support. Further, I would like to thank my family and friends, for their support and role in making me who I am.

TABLE OF CONTENTS

LIST OF TABLES

LIST OF FIGURES

LIST OF ABBREVIATIONS

CD	Contraction Delay
CP	Cerebral Palsy
EMD	Electromechanical Delay
FES	Functional Electrical Stimulation
LG	Left Gluteal
LH	Left Hamstring
LK	Lyapunov-Krasovskii
LQ	Left Quadriceps
LQLG	Left Quadriceps and Left Gluteal
MVT	Mean Value Theorem
MS	Multiple Sclerosis
NCs	Neurological Conditions
PD	Parkinson's Disease
RD	Residual Delay
RG	Right Gluteal
RH	Right Hamstring
RPM	Revolutions Per Minute
RQ	Right Quadriceps
RQRG	Right Quadriceps and Right Gluteal
SCI	Spinal Cord Injury
W	Watts

$\equiv$	indentically equal
$\approx$	approximately equal
$\neq$	not equal
$\triangleq$	defined as
$<\ (>)$	less (greater) than
$\leq\ (\geq)$	less (greater) than or equal to
$\times$	cross product
$\forall$	for all
∞	infinity
$\in$	belongs to
$\subset\ (\subseteq)$	subset (strict) of
$\cup$	union
$\cap$	intersection
$\rightarrow$	tends to
$\Longleftrightarrow$	equivalent to, if and only if
$\sum$	summation
$\lvert\cdot\rvert$	absolute value
$\lVert\cdot\rVert$	the norm of a vector
$\max$	maximum
$\min$	minimum
$\sup$	supremum, the least upper bound
$\inf$	infimum, the greatest lower bound

$\mathbb{N}$	the set of natural numbers
$\mathbb{R}^n$	the n-dimensional Euclidean space
$f : S_1 \to S_2$	a function f mapping a set S_1 into a set S_2
∇f	the gradient vector
∂f	the Clarke generalized gradient
$\dot{y}$	the first derivative of y with respect to time
$\ddot{y}$	the second derivative of y with respect to time
$[a_1, ..., a_n]$	a diagonal matrix with diagonal elements a_1 to a_n
A^T $\left(x^T\right)$	the transpose of matrix A (of a vector x)
$\mathcal{L}_\infty$	the space of all essentially bounded functions
sgn $(\cdot)$	the signum function
$\ln(\cdot)$	the natural logarithm
a.e.	almost everywhere
$\mathcal{O}^2$	higher order terms of a Talyor series expansion
$\square$	designation of end of proofs

Abstract of Dissertation Presented to the Graduate School
of the University of Florida in Partial Fulfillment of the
Requirements for the Degree of Doctor of Philosophy

CHARACTERIZATION AND COMPENSATION OF THE ELECTROMECHANICAL DELAY DURING FES-CYCLING

By

Brendon Connor Allen

August 2021

Chair: Warren E. Dixon
Major: Mechanical Engineering

Within the United States alone there are tens of millions of individuals who suffer from neurological conditions (NCs), such as stroke, Parkinson's disease (PD), multiple sclerosis (MS), cerebral palsy (CP), spinal cord injury (SCI), among others. The average age of the global population is increasing, which is resulting in an increased number of people with NCs each year. In fact, annually there are millions of new cases of NCs throughout the world. A consequence of NCs is that people may experience muscle weakness, paralysis, partial/total loss of coordinated limb control, and secondary effects such as obesity, diabetes, and cardiovascular disease resulting from sedentary lifestyles. Consequently, performance of activities of daily living is significantly impaired and culminates in annual health care costs of upwards of 150 billion dollars. In an effort to combat the severity of disability, limit the complications, and reduce the cost of treatment of NCs, clinicians and researchers have turned to technological solutions such as functional electrical stimulation (FES) and motor assistive devices (e.g., rehabilitation robotics, motorized stationary cycles) to facilitate rehabilitative therapies, both of which are the focus of this dissertation.

FES uses electrical stimulation to evoke muscle contractions, despite a damaged nervous system, to perform a functional task. Evoking muscle contractions has numerous health benefits such as improved muscular strength, motor control, and cardiovascular parameters. Additional benefits include increased bone mineral density,

lean muscle mass, sensory ability, and range of motion. A common application of FES is FES cycling, since it is an active therapy that is both low-impact and low-risk. However, closed-loop FES control has numerous challenges including uncertain nonlinear dynamics, unmodeled disturbances, fatigue, and that the muscle characteristics are unknown and vary with time. Furthermore, the complex electro-physiological mechanism involved in FES induced force production results in an electromechanical delay (EMD) between the instant stimulation is applied and the onset of muscle force, which may result in instability of the control system. Practically, fatigue is a challenge because it limits the duration of an exercise, which has been shown to lower the rehabilitative effectiveness of the exercise. To help reduce fatigue, motorized FES-cycling is often implemented, which intermittently provides motor inputs to assist the rider as required. However, coordinating control between the motor and FES, particularly when FES is used on multiple muscles, requires a switched system stability analysis to be performed to guarantee stability of the system.

In Chapter 1, an overview and motivation of the dissertation is provided, including a review of relevant literature. Chapter 2 includes a dynamic model for the delayed combined-cycle rider system, where the EMD is modeled as an input delay. In Chapter 3, the effect of cycling time (i.e., fatigue) and lower limb position (i.e., crank angle) on the EMD are characterized to develop models of the EMD as a function of cycling time and as a function of crank angle. Chapters 4 and 5, develop EMD-compensating cadence tracking motor and FES controllers for the FES-cycle system in Chapter 2. Chapter 4 implements a constant estimate of the EMD, whereas Chapter 5 implements a time-varying estimate of the EMD using the results in Chapter 3. In Chapters 6 and 7, cadence tracking controllers are again developed for the combined cycle-rider system that is modeled in Chapter 2; however, now the FES and motor controllers are designed to be saturated to compensate for the fact that the controllers are functions of the system's states, which without saturation could result in high FES inputs that cause

discomfort/pain or motor inputs that exceed motor capabilities. Relative to Chapter 6, Chapter 7 modifies the control development and stability analysis to ensure both position and cadence tracking. In Chapter 8, unlike in the prior chapters, a dual objective control structure for simultaneous position/cadence and power tracking is developed for the FES cycle-rider system modeled in Chapter 2. The FES and motor controllers are designed to track a desired power and cadence, respectively, which results in uncontrolled periods for the power tracking objective due to intermittent FES application. Chapters 4-8 provide Lyapunov-like analyses to ensure the designed controllers achieve their tracking objective and Chapter 8 includes a dwell-time analysis. Furthermore, experiments on both able-bodied participants and participants with NCs are included in Chapters 4-8 to validate the developed control systems. In Chapter 9, the dissertation is concluded by summarizing the contributions and future efforts are discussed.

CHAPTER 1
INTRODUCTION

1.1 Background

Neurological conditions (NCs) such as traumatic brain injury (TBI), stroke, spinal cord injury (SCI), and Parkinson's Disease (PD), multiple sclerosis (MS), cerebral palsy (CP), among others, often result in a deterioration of quality of life for affected individuals [1]. Individuals suffering from NCs may experience paralysis, muscle weakness, partial or total loss of coordinated limb control, reduced endurance or strength, in addition to secondary health effects such as diabetes, obesity, muscle atrophy, reduced cardiovascular fitness, osteoporosis, cardiovascular diseases, etc. that result from a sedentary lifestyle, and a predisposition to depression [2–6]. Within the United States alone there are over 900,000 new cases of NCs annually, which culminates in annual health care costs of upwards of 150 billion dollars [2]. In an effort to combat the severity of disability, reduce the cost of treatment of NCs, and limit the complications, researchers and clinicians have turned to technological solutions such as hybrid exoskeletons, which combine rehabilitation robots (e.g., exoskeletons, motorized stationary cycles) with functional electrical stimulation (FES) to facilitate rehabilitative therapies [7].

FES involves the application of an electric field to induce muscle contractions yielding functional tasks (e.g., walking [8, 9], cycling [3, 10–17], or arm curls [18, 19]). Evoking muscle contractions has been shown to have numerous health benefits such as improved muscular strength, motor control, and cardiovascular parameters, and increased bone mineral density, lean muscle mass, sensory ability, and range of motion [20–23]. FES-cycling is a common rehabilitative exercise for those with a variety of NCs such as stroke, PD, CP, MS, etc. [1, 3, 10–15], because FES-cycling is a low-impact and low-risk (e.g., minimal risk of a fall) intensive and repetitive exercise and has been

shown to have numerous health benefits, such as improved cardiovascular parameters and musculoskeletal fitness, increased bone mineral density and muscle mass, nervous system reorganization, among other benefits [20–27]. Those with NCs often lack the strength, limb control, or endurance to voluntarily maintain cycling intensities needed to achieve desired training effects. As a result, FES of the lower body muscles is used to facilitate cycling tasks, yielding improvements in neurological, physiological, and psychological measures, as well as in musculoskeletal and cardiorespiratory fitness [28].

A critical factor for facilitating nervous system reorganization and potentially beneficial change in the neuromuscular system is sufficient intensity and repetitive practice of coordinated limb movements. Therefore, coordinated motion of multiple muscle groups and limbs over long durations is motivated to yield rehabilitative outcomes; yet, the potential effectiveness of current FES methods is limited by the onset of muscle fatigue which impedes the user's ability to intensely and repeatedly practice the activity. Further, evidence indicates that to derive neural adaptation and plasticity, a person must be actively participating in functional activities [29]. Moreover, as discussed in [30] an assistive device, that allows the rider to passively participate, could even potentially decrease recovery if it encourages a decrease in motor output, effort, energy consumption, and/or attention during training. Additionally, each individual has different injuries, medical conditions, abilities, and initial conditions. However, despite the vast differences between people, a one-size-fits-all approach is used in current commercially available FES-cycles. Specifically, a motor is typically always on to maintain a desired cadence (independent of the person's capabilities or activity) while providing FES intensities based on iterative open-loop designs. However, this approach encourages passive riding instead of active engagement and the FES intensities are typically insufficient to allow a person to pedal without the motor.

Dynamic or adaptive FES therapy (i.e., closed-loop FES control) is more effective than such traditional passive rehabilitation approaches in the promotion of muscle strength and neurological recovery [31, 32]. However, implementing closed-loop control of a FES-cycle has numerous challenges [1, 3, 11–13, 33]. For example, from a control systems perspective, FES-cycling is a prime example of a switched system because there are continuous physical dynamics of the limbs and the cycle, yet there are discrete logical jumps that are required to engage different muscle groups, to potentially engage a motor for assistance/resistance, or to discretely turn on/off the motor control (motivated by the desire to allow the rider to contribute all the torque or by different stimulation schemes) [3]. Additional challenges are nonlinearity and uncertainty of the muscle activation dynamics [34], unmodeled disturbances [35], uncertain parameters in the nonlinear dynamic model [35], and fatigue. Fatigue reduces the FES-induced muscle force under a fixed stimulation intensity [36] and decreases the duration an exercise can be performed (e.g., the number of repetitions), which may lower rehabilitative effectiveness. Additionally, a challenge of FES control is that participants may be sensitive to the stimulation, requiring limits to be placed on the FES controller for a participant's comfort and safety [1]. Furthermore, FES cycling typically has a lower metabolic efficiency than cycling volitionally due to several factors, including fatigue, poor control of each muscle group, or less than optimal stimulation parameters [37–41]. Metabolic efficiency during FES cycling can be improved by increasing the power output (PO), such as by implementing a power tracking controller, which cultivates fatigue resistant muscle fibers and reverses muscle atrophy, among other benefits [38, 41].

Another challenge of closed-loop FES control is that there exists a complex electro-physiological mechanism involved in force production in response to electrical stimulation. A result of this complex energy conversion process is that there exists an input delay between the application of an electric field and the onset of force production, (i.e.,

an electromechanical delay (EMD)) [33, 42, 43]. Often in literature the EMD corresponds to the time latency between the onset of EMG activity and muscle force [44], however, in this dissertation we refer to the EMD in a broader sense as the time latency between the application of stimulation and the corresponding torque, such as the EMD is defined in [11–13, 33, 45–48]. EMD can potentially destabilize a control system such as FES-cycling (e.g., the cadence tracking error is not contained in a bounded set). To prevent delay-induced instability, EMD needs to be included in the dynamic model that is used in the stability analysis of the closed-loop system. Practically, the EMD can be modeled as an input delay.

Few studies have developed FES controllers to compensate for an FES-induced input delay, and these studies have focused on continuous exercises (e.g., leg extensions) with FES of a single muscle group [45, 46, 48, 49]. For example, results such as [45, 46, 48, 49] all consider a continuous leg extension exercise with FES of the quadriceps femoris muscle group. In [48], uncertain dynamics with a known delay were assumed to yield a uniformly ultimately bounded result. A global asymptotic tracking controller was developed in [49]; however, a constant but unknown delay and exact model knowledge of the lower limb dynamics was assumed. An unknown, time-varying input delay is examined in [45] and [46]; however, the delay is estimated by a constant. A constant estimate is not ideal because EMD has been shown to change due to FES-induced fatigue and a more accurate estimate will improve performance [33]. Prior studies on continuous exercises only considered the contraction delay (CD), where the CD is the time latency between the start of stimulation and the onset of torque. Recently, closed-loop FES controllers have been developed to compensate for FES-induced input delays for FES-cycling as will be detailed in this dissertation [11–15]. When a coordinated exercise is performed, such as cycling, switching is required between multiple muscle groups and the residual delay (RD) must also be considered, where the RD is the time latency between the end of stimulation and the cessation of

torque. If the RD is unaccounted for it could result in residual forces being produced by antagonistic muscles, which oppose the desired motion and may increase the rate of fatigue, and hence, may effect the rehabilitative effectiveness.

Each of the prior results to compensate for the EMD require for certain aspects of the EMD to be known. For example, often the EMD is assumed to be bounded by a known lower and upper bound. However, all previous studies to understand the time-varying effects of FES-induced fatigue on torque production and EMD have focused on simple single joint (e.g., knee extension [33, 48, 50, 51]) tasks, and the effects of FES-induced fatigue during more complex tasks that involve multiple muscle groups (e.g., cycling) remains unclear. In fact, it is unclear if closed-loop control during motorized FES-cycling produces enough fatigue to cause the EMD to vary and bounds on the EMD are unknown. As previously stated, the CD and RD must be considered (and hence known) for the more complex interaction and timing of multiple muscle groups involved in FES-cycling. An increased understanding of the CD and RD will allow closed-loop controllers to determine when to apply/cease stimulation to reduce muscle contractions in antagonistic muscles [11–13].

Although results that compensate for FES-induced input delays are sparse, input delayed systems have been extensively studied for general systems [52–74]. Often results either assume exact model knowledge (cf. [58–60]) or that the input delay is known (cf. [60–62]). However, there are uncertainties in many practical engineering systems and the input delay may be unknown and potentially time-varying (e.g., an FES-induced input delay is time-varying and difficult to measure outside of isometric conditions [75]). Therefore, results such as [63–68] have analyzed systems with an unknown input delay. In recent years, some results have begun to examine input delay compensation for switched systems [11–15, 56, 69–74]. A linear system with a constant input delay is considered in [69], while stability is achieved for a class of nonlinear systems with time-varying delays in [70] and [71]. However, the aforementioned results

do not compensate for FES-specific factors such as the development of a complex state-dependent switching signal to produce effective agonist muscle contractions despite the contraction delay, while simultaneously preventing or minimizing residual antagonistic forces that remain after the stimulation has ceased.

Non-FES related systems with input delays have been studied extensively; however, few studies have implemented saturated control [76–82]. Most saturated controllers for input delayed systems have been for linear systems [76–78], with a few exceptions that include nonlinear systems [79–82]. Strict-feedforward nonlinear systems are considered with no disturbances in [79] and with no uncertainties in [80]. A class of uncertain nonlinear systems are considered in [81] with known and constant input delays and in [82] with unknown delays. However, the aforementioned results either are not for switched systems or do not implement a saturated controller. Additionally, non-FES related systems do not compensate for FES specific factors, such as the need to properly time stimulation to yield effective agonist muscle contractions and to remove/limit residual antagonistic forces.

As has been previously stated, it is desired to increase the PO to increase the metabolic efficiency during FES cycling. Multiple strategies have been employed to increase the PO of FES cycling such as cadence strategies [39, 83], releasing the ankle joint [84], creating the optimal pedal path [85], using higher stimulation currents [38], using a fixed gear cycle [86], and modifying the stimulation frequency and pattern [40]. In recent decades, closed-loop controllers have been developed to ensure torque/power tracking[1] during FES cycling to increase the PO. For example, in [87] torque tracking is performed when it is kinematically efficient, in [88, 89] discretized power tracking is achieved, and in [14, 41, 90–92] there is instantaneous power tracking. However, of the

[1] Power and torque tracking are synonymous within the scope of this dissertation.

prior torque tracking results, only the author's prior work in [14] provided compensation for the EMD.

1.2 Outline of the Dissertation

In Chapter 2, a nonlinear switched dynamic model is presented for a combined cycle-rider system. The model consists of a modified motorized recumbent tricycle. The participant is seated on the cycle and then coupled to the cycle using orthotic boots. The cycle is then actuated by using either the motor or FES. The FES is applied across the participant's quadriceps femoris, hamstrings, and gluteal muscle groups to elicit muscle contractions to yield pedaling of the cycle. Switching signals are introduced to determine when to activate each actuator (e.g., the muscles and motor) to pedal the cycle.

In Chapter 3, two protocols were performed to better understand the EMD. The objective of the first protocol, called the cycling protocol, is to test the hypothesis that FES-induced cycling will induce sufficient fatigue such that the EMD and torque about the cycle crank axis will vary with cycling time and to then establish bounds on the torque and EMD and on the rate of change of the torque and EMD. The objective of the second protocol, called the angle protocol, is to determine if the crank angle has an effect on the EMD. A focus of prior works has been to examine the underlying physiological factors for the latency between electrical input and force output [93–95], but in this chapter the EMD is considered at the macro level, motivated by the desire to compensate for the phenomenological effects within a closed-loop control structure, and the underlying physiological factors are beyond the scope. To provide additional information for the control designer, two types of EMD were considered, the CD and RD, and both the CD and RD were measured in three different ways for the cycling protocol and two different ways for the angle protocol. To test both protocols, experiments were performed on five able-bodied individuals and five individuals with NCs. The cycling protocol consisted of 10 minutes of FES-cycling. Both protocols consisted of using the

motor to fix the crank at preset angles to create isometric conditions. Transcutaneous electrical stimulation was delivered to a combination of the quadriceps femoris and gluteal muscle groups in these isometric conditions. The resultant torque data was then examined to determine information about the torque and EMD. Multiple linear regressions were performed on the data and the results provide evidence that FES-cycling does result in fatigue, that the EMD is time-varying, and that the EMD is angle dependent. Figures were constructed to show how the torque and EMD vary with cycling time and with the crank angle. The results in this chapter can be used to improve the future development of closed-loop controllers for FES-cycling that are robust to time-varying input delays.

In Chapter 4, closed-loop FES and motor cadence-tracking controllers were developed for the FES-cycle modeled in Chapter 2 that compensates for the unknown and time-varying EMD. Further, an extension is provided with a modified control objective in the sense that motorized assistance is continuously provided to further align with current clinical practice in rehabilitation cycles. A delay-free FES control input is injected into the dynamics via an auxiliary tracking error signal. Trigger conditions are developed to appropriately schedule the activation and deactivation of stimulation for each muscle group and the motor such that the muscle forces occur in desired locations and the residual muscle forces are less likely to come from antagonist muscles, which would impede cycling and increase fatigue. These trigger conditions are significant because cycling requires complex state-dependent switching conditions, which are further complicated by the input delay, to ensure muscle contractions occur in more efficient regions of the crank. A Lyapunov-like switched systems stability analysis is performed to prove a cadence tracking error with semi-global exponential convergence to a uniform ultimate bound. To demonstrate the performance of the developed controller, in-depth experiments were performed on six able-bodied participants and four participants with different NCs (spina bifida, quadriplegia, MS, and CP). The experiments compare the developed

controller, the extended controller, and for comparison, a controller that was developed assuming the system has no input delay. The developed controller achieved an average cadence error of 0.01 $\pm$ 2.00 revolutions per minute (RPM) for the able-bodied participants and 0.01 $\pm$ 2.72 RPM for the participants with NCs. The experimental results validate the controller and indicate that delay compensation can result in an improved FES-cycling experience when compared to a controller of the same form, but without delay compensation.

Chapter 5, building upon our work in Chapter 4, implements a time-varying estimate of the EMD, includes volitional effort from the participant in the dynamic model, includes comparative experiments on nine participants (including four with NCs), and modifies/improves the error system, switching signals, and Lyapunov-based stability analysis to yield improved FES/motor controllers, improved gain conditions, and exponential position/cadence tracking for the delayed, switched, uncertain, and nonlinear FES-cycling system. Furthermore, FES and motor switching signals are designed to maintain control authority, to ensure efficient muscle contractions, and to mitigate contractions in antagonistic muscles. Passive therapy (i.e., no volitional contributions) experiments were conducted on able-bodied participants to compare the developed FES/motor controllers to an alternate control method, of similar form, that was developed by assuming the EMD was negligible. Likewise, active therapy (i.e., with volitional contributions) experiments were conducted on participants with varied NCs. Experimental results show that compensating for the EMD significantly improves the cadence tracking performance, and the developed control system can safely and effectively yield cadence tracking for individuals with varied capabilities during both active and passive therapy exercises.

In Chapter 6, a cadence tracking control system is developed for the switched FES-cycle modeled in Chapter 2 that is robust to uncertainties in the system, unknown disturbances, and a time-varying input delay. Similar to Chapters 4 and 5, a delay-dependent trigger condition is developed to schedule the activation/deactivation of FES

to yield effective muscle contractions. However, in Chapters 4 and 5, the controllers are functions of the system's states and unmodeled disturbances or large initial conditions may result in large FES or motor inputs, and although the controllers are proven to be bounded, the bounds are unknown, which could result in high FES inputs that cause discomfort/pain or motor inputs that exceed motor capabilities. The focus of this chapter is to guarantee safety and comfort by developing saturated FES and motor controllers where the control bounds are known and can be adjusted a priori. Further, a Lyapunov-like stability analysis is performed to guarantee uniformly ultimately bounded cadence tracking errors despite using saturated controllers. To validate the control system a preliminary experiment was performed on a single able-bodied participant and demonstrated a cadence of 48.24 $\pm$ 2.09 RPM for a desired cadence of 50 RPM. Chapter 7 is motivated to reduce the offset in the cadence tracking error.

Chapter 7, building on our precursory result in Chapter 6, modifies the control development and Lyapunov-based stability analysis to compensate for the EMD and to ensure both exponential position and cadence tracking of a switched FES-cycle system using saturated FES control. Furthermore, compared to Chapter 6, Chapter 7 improves the gain conditions and provides comparative experiments on four and five participants with and without NCs, respectively. The controllers developed in this chapter are robust to unknown disturbances, uncertainties in the dynamics, and the unknown time-varying EMD. To properly schedule the application of the FES, switching signals and trigger conditions were developed that are state and delay dependent, which ensure muscle contractions occur in efficient regions of the crank cycle. An important feature of the bound on the developed saturated FES controller is that, similar to Chapter 6, it is known a priori and can be adjusted by tuning the control gains to limit the stimulation levels, providing a more comfortable experience for the participant. Comparative passive therapy experiments were performed on five able-bodied participants using the controllers developed in Chapters 6 and 7 to compare the performance of each

method. The results indicate that the controllers developed in Chapter 7 significantly improved the cadence tracking while simultaneously reducing the required control effort, relative to the controllers developed in Chapter 6. Furthermore, active therapy (i.e., the participant provided volitional effort) experiments were performed on four participants with NCs (e.g., CP, spina bifida, and MS), which further validated the performance of the developed control system.

In Chapter 8, unlike in the prior chapters, a dual objective control structure for simultaneous position/cadence and power tracking is developed for an uncertain, nonlinear, switched FES cycle-rider system with an unknown and time-varying EMD. Furthermore, switching conditions are designed to properly schedule the application/deactivation of FES to efficiently contribute to forward pedaling, and rider asymmetries are accounted for by implementing instantaneous power tracking via a running integral [14, 41]. This chapter includes an in-depth description and presentation of the developed methods, the complete stability analysis, volitional effort from the participant in the dynamic model, and a series of comparative experiments with a statistical analysis and discussion for nine participants, including four with NCs. The position/cadence objective is regulated by the motor, similar to clinical practice, and the power objective is regulated using FES to increase the PO and ensure participant contribution. However, due to intermittent FES application there exists uncontrolled periods for the power tracking objective, which requires a dwell-time analysis, which was further complicated by the existence of the EMD. For example, the EMD required the development of an auxiliary signal to inject a delay free FES input into the closed-loop error system and Lyapunov-Krasovskii (LK) functionals to aid the stability analysis. Although the auxiliary signal provides a delay free FES input, the cost is additional delayed FES input terms. Thus, each term included in the FES controller requires special consideration. The torque error system was specially designed such that the FES controller does not need to consider the motor input,

to reduce the complexity of the FES control design. Uncertainty in the EMD further complicates the mathematical development (FES input terms are delayed by the actual EMD and an estimate of the EMD) and resulted in more complex and conservative gain and dwell-time conditions. Overall, a switched systems Lyapunov-like analysis is provided to develop dwell-time conditions and to ensure uniformly ultimately bounded torque/power tracking and global exponential position/cadence tracking of a delayed and switched FES cycle system. A series of experiments were conducted on four participants with NCs and five able-bodied participants. Experiments on the able-bodied participants compared the control system developed in this chapter to the control system developed in [41], which did not consider the EMD. It was concluded from the experimental results that the presented control system improved the power tracking performance while reducing the control inputs. Furthermore, the experiments on the participants with NCs included volitional effort and further demonstrated the validity of the developed control system.

Chapter 9 concludes the dissertation by providing a summary of each chapter, the contributions, and potential future research direction.

CHAPTER 2
DYNAMIC MODEL

In this chapter, the dynamic model for the combined cycle-rider system is developed. The dynamic model is an extension of the model from [3, 30] with the main difference being that the EMD is included in the model. The rider is seated in the modified recumbent tricycle and then coupled to the cycle using orthotic boots. Electrodes are then placed on the quadriceps femoris, hamstring, and gluteal muscle groups to allow for the application of FES. The application of FES must be coordinated appropriately to produce effective muscle contractions that yield efficient forward pedaling of the cycle crank. In [34], it was observed that based on the position of the cycle (e.g., the crank angle), it is more kinematically efficient to use certain muscles rather than others [34]. Therefore, each muscle has a set of crank angles over which its contractions are more efficient. However, there also exists some crank angles over which muscle contractions of each muscle group are not kinematically efficient to contribute torque to pedal the cycle (e.g., kinematic deadzones). Therefore, it is desired for the developed controllers to switch control between multiple inputs (i.e., six muscle groups and a motor) in such a manner that a muscle produces contractions when it is kinematically efficient and that the motor is activated as required to yield continuous pedaling of the cycle. Thus, although the state dynamics are continuous (i.e., position, cadence, etc.) the inputs into the system are discontinuous, which results in the development of a switched system. Further, the existence of the EMD requires the development of state and delay dependent switching conditions such that muscle contractions occur when it is kinematically efficient. The dynamic model developed in this chapter is used in Chapters 4-8 to facilitate the control development.

2.1 Experimental Testbed: FES Cycle

The experimental testbed for Chapters 3-8 was created by modifying an existing recumbent tricycle (TerraTrike Rover) to include actuators and sensors as described

in other papers and dissertations [3, 88, 96–98]. The dynamic model of the combined cycle-rider system is developed in [3, 88, 96–98]; however, in these prior works the EMD was assumed to be non-existent and was not included in the dynamic model. In this dissertation, the model is modified to include the EMD, which is modeled as an input delay on the FES controller. Orthotic boots (Össur Rebound Air Tall) were used to couple the rider to the cycle, to securely constrain the ankles, and to maintain sagittal alignment of the legs. A Kinetic Bike Trainer and rider rings were used to offset the cycle from the ground. The original bike crank was replaced with a SRM Science Road Wireless Powermeter crankset to measure the torque. A US Digital H1 encoder was mounted to the cycle and attached to the crank via spur gears to measure the position and cadence. A 250 W, 24 V DC brushed motor (Unite Motor Co. Ltd. MY1016Z2) was coupled to the drive train and actuated using a current-controlled Advanced Motion Controls[1] (AMC) AB25A100 motor driver and an AMC PS300W24 power supply, and an AMC FC15030 filter card was added in-line with the motor. A current-controlled, 8-channel HASOMED RehaStim 1 stimulator (operating in science mode) was used to deliver symmetric, biphasic, and rectangular pulses via self-adhesive electrodes (Axelgaard ValuTrode CF7515).[2] For all experiments, the stimulation is applied at 60 Hz and amplitudes are fixed at 90, 80, and 70 mA for the quadriceps, hamstrings, and gluteals, respectively. The stimulation pulse width for each muscle group is determined by the subsequently designed controllers and commanded to the stimulator by the control software. For safety, an emergency stop switch was mounted to the cycle's handle to allow the rider to halt the experiment if required. The power

[1] ADVANCED Motion Controls supported the development of this testbed by providing discounts on their branded items.

[2] Surface electrodes for this study were provided compliments of Axelgaard Manufacturing Co., Ltd.

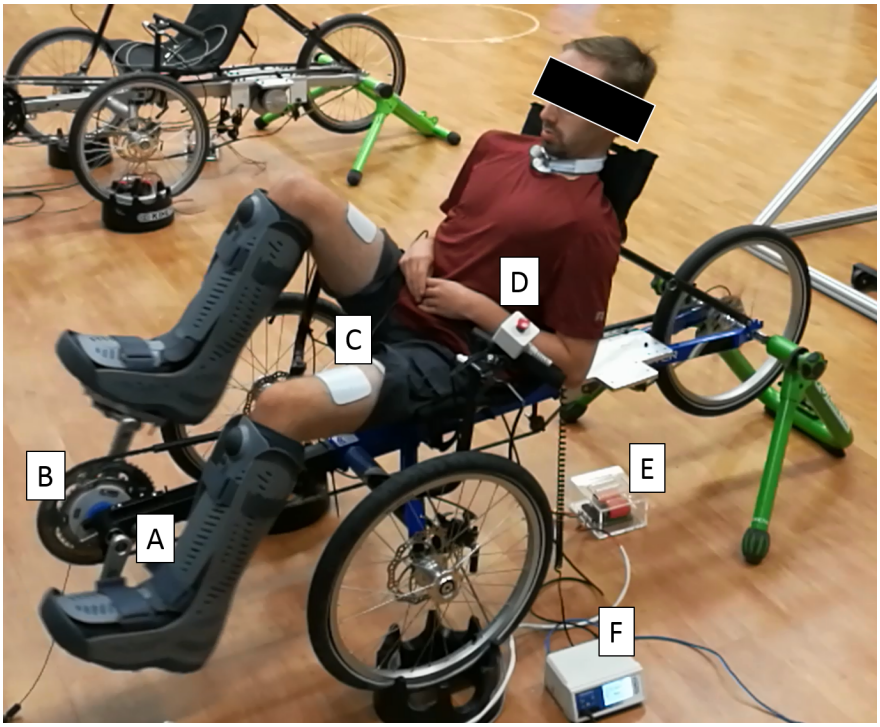

Figure 2-1. Motorized FES cycle: (A) Encoder (B) Power Meter (C) Electrodes (D) E-Stop (E) Filter Card (F) Stimulator. Photo courtesy of Christian Cousin [1].

meter, encoder, motor, and stimulator were interfaced with a desktop computer running MATLAB/Simulink/Quarc through a Quanser Q-PIDe data acquisition board at 500 Hz. The motorized FES cycle with a rider is depicted in Fig. 2-1.

2.2 Cycle-Rider Dynamic Model

Throughout the dissertation, delayed functions are defined as

$$h_\tau \triangleq \begin{cases} h\left(t-\tau\left(t\right)\right) & t-\tau\left(t\right) \geq t_0 \\ 0 & t-\tau\left(t\right) < t_0 \end{cases}, \tag{2–1}$$

where $t, t_0 \in \mathbb{R}_{\geq 0}$ denote the time and initial time, respectively. The time-varying EMD, i.e., the delay between the application/removal of the current and the onset/elimination of muscle force production is denoted by $\tau : \mathbb{R}_{\geq 0} \to \mathbb{S}$, where $\mathbb{S} \subset \mathbb{R}$ represents a set of all possible delay values [75, 99, 100]. The combined cycle-rider dynamics, are

considered as[3] [3]

$$\tau_e(t) = \tau_c(\dot{q}, \ddot{q}, t) + \tau_r(q, \dot{q}, \ddot{q}, t), \tag{2–2}$$

where $q : \mathbb{R}_{\geq 0} \to \mathcal{Q}$, $\dot{q} : \mathbb{R}_{\geq 0} \to \mathbb{R}$, and $\ddot{q} : \mathbb{R}_{\geq 0} \to \mathbb{R}$ denote the measurable crank angle, measurable angular velocity (cadence), and unmeasured acceleration, respectively. The set of $\mathcal{Q} \subseteq \mathbb{R}$ denotes the possible angles of the crank. The torque from the motor applied about the crank axis is denoted by $\tau_e : \mathbb{R}_{\geq 0} \to \mathbb{R}$ and is defined as

$$\tau_e(t) \triangleq B_e u_E(t), \tag{2–3}$$

where the unknown motor control effectiveness is denoted by $B_e \in \mathbb{R}_{>0}$ (In Chapter 8 B_e is assumed to be known) and the designed motor control input (i.e., current) is denoted by $u_E : \mathbb{R}_{\geq 0} \to \mathbb{R}$. The torques applied about the crank axis by the cycle and the rider are denoted by $\tau_c : \mathcal{Q} \times \mathbb{R}^2 \times \mathbb{R}_{\geq 0} \to \mathbb{R}$ and $\tau_r : \mathcal{Q} \times \mathbb{R}^2 \times \mathbb{R}_{\geq 0} \to \mathbb{R}$, respectively, and are defined as

$$\tau_c(q, \dot{q}, \ddot{q}, t) \triangleq J_c(q)\ddot{q} + b_c\dot{q} + d_c(t), \tag{2–4}$$

and

$$\tau_r(q, \dot{q}, \ddot{q}, t) \triangleq \tau_p(q, \dot{q}, \ddot{q}) - \tau_M(q, \dot{q}, \tau, t) + d_r(t), \tag{2–5}$$

respectively. The cycle inertial effects, cycle viscous damping effects, and the cycle disturbances are denoted by $J_c \in \mathbb{R}_{>0}$, $b_c \in \mathbb{R}_{>0}$, and $d_c : \mathbb{R}_{\geq 0} \to \mathbb{R}$, respectively. The torque applied by the rider about the crank can be decomposed into the passive effects denoted by $\tau_p : \mathcal{Q} \times \mathbb{R}^2 \to \mathbb{R}$, the muscle contribution due to the FES-induced muscle contractions or volitional efforts from the participant are denoted by $\tau_M : \mathcal{Q} \times \mathbb{R} \times \mathbb{S} \times \mathbb{R}_{\geq 0} \to \mathbb{R}$, and the disturbances (e.g., spasticity or changes in load)

[3] For notational brevity, all explicit dependence on time, t, within the terms $q(t)$, $\dot{q}(t)$, $\ddot{q}(t)$, and $\tau(t)$ is suppressed.

denoted by $d_r : \mathbb{R}_{\geq 0} \to \mathbb{R}$. The passive torques applied by the rider are defined as

$$\tau_p(q, \dot{q}, \ddot{q}) \triangleq M_p(q)\ddot{q} + V(q, \dot{q})\dot{q} + G(q) + P(q, \dot{q}), \tag{2–6}$$

where the inertial effects, gravitational effects, centripetal-Coriolis effects, and passive viscoelastic tissue forces are denoted as $M : \mathcal{Q} \to \mathbb{R}_{>0}$, $G : \mathcal{Q} \to \mathbb{R}$, $V : \mathcal{Q} \times \mathbb{R} \to \mathbb{R}$, and $P : \mathcal{Q} \times \mathbb{R} \to \mathbb{R}$, respectively. The torque applied by the muscles due to the FES-induced muscle contractions can be expanded into the sum of their individual contributions and is defined as

$$\tau_M(q, \dot{q}, \tau, t) \triangleq \sum_{m \in \mathcal{M}} B_m(q, \dot{q}, t)\, u_m(t - \tau) + \tau_{vol}(t), \tag{2–7}$$

where the volitional torque contribution from the participant is denoted by $\tau_{vol} : \mathbb{R}_{\geq 0} \to \mathbb{R}$ and the unknown muscle control effectiveness is denoted by $B_m : \mathcal{Q} \times \mathbb{R} \times \mathbb{R}_{>0} \to \mathbb{R}_{>0}$, $\forall m \in \mathcal{M}$, where $m \in \mathcal{M} \triangleq \{RH, RQ, RG, LH, LQ, LG\}$ indicates the right (R) and left (L) hamstrings (H), quadriceps femoris (Q), and gluteal (G) muscle groups. The delayed FES input (i.e., pulse width) to the rider's muscles is denoted by $u_{m,\tau} : \mathbb{S} \times \mathbb{R}_{\geq 0} \to \mathbb{R}$, $\forall m \in \mathcal{M}$. Substituting (2–3)-(2–7) into (2–2) yields

$$\sum_{m \in \mathcal{M}} B_m(q, \dot{q}, t)\, u_{m,\tau} + \tau_{vol}(t) + B_e u_E(t) = M(q)\ddot{q} + V(q, \dot{q})\dot{q} + G(q) + P(q, \dot{q}) + b_c\dot{q} + d(t), \tag{2–8}$$

where $M : \mathcal{Q} \to \mathbb{R}$ is defined as $M(q) \triangleq J_c(q) + M_p(q)$, and $d : \mathbb{R}_{\geq 0} \to \mathbb{R}$ is defined as $d(t) \triangleq d_c(t) + d_r(t)$.

2.3 Switched System Dynamic Model

As in results such as [2, 3, 30, 88, 101], FES-cycling often stimulates the muscles in regions of the crank cycle where it is efficient. The crank angles where it is efficient to stimulate a given muscle can be determined a priori based on the kinematic effectiveness of the torque transferred to the crank axis from the muscle. Stimulation is not applied in the kinematic dead zones (KDZ) where it is not efficient for any of the muscle groups to significantly contribute to the forward motion of the crank. In the KDZ regions

the electric motor is used to provide the torque. For a given muscle, the efficient crank angles are denoted by $\mathcal{Q}_m \subset \mathcal{Q}$, $\forall m \in \mathcal{M}$, where $\mathcal{Q}_m$ is defined using the definition in [3] as

$$\mathcal{Q}_m \triangleq \{q \in \mathcal{Q} \mid T_m(q) > \varepsilon_m\}, \tag{2–9}$$

$\forall m \in \mathcal{M}$, where $\varepsilon_m \in (0, \max(T_m)]$ denotes a selectable lower threshold for each torque transfer ratio that is denoted by $T_m : \mathcal{Q} \to \mathbb{R}$. The region, $\mathcal{Q}_m$, is called the FES region for the muscle $m \in \mathcal{M}$. Thus, (2–9) limits the FES regions for each muscle group such that FES-induced muscle contractions efficiently contribute to forward pedaling (i.e., positive crank motion). The union of all muscle regions defined in (2–9) represents the FES region, denoted by $\mathcal{Q}_{FES}$, and defined as $\mathcal{Q}_{FES} \triangleq \bigcup_{m \in \mathcal{M}} \{\mathcal{Q}_m\}$. The kinematic dead zones are defined as $\mathcal{Q}_{KDZ} \triangleq \mathcal{Q} \setminus \mathcal{Q}_{FES}$. The FES and KDZ regions are depicted in Figure 2-2.

Now switching signals must be developed to determine when to activate the FES and the motor. For each muscle, a state and delay dependent FES switching signal, denoted by $\sigma_m : \mathcal{Q} \times \mathbb{R} \to \{0, 1\}$, is designed to compensate for the delay by activating/deactivating the muscle at the appropriate locations of the crank at time t such that contractions occur in the more efficient FES regions. For Chapters 4 and 8, the designed piecewise right-continuous switching signal for each muscle group is defined as

$$\sigma_m(q, \dot{q}) \triangleq \begin{cases} 1, & q_\alpha(q, \dot{q}) \in \mathcal{Q}_m \\ 1, & q_\beta(q, \dot{q}) \in \mathcal{Q}_m \\ 0, & \text{otherwise} \end{cases}, \forall m \in \mathcal{M}, \tag{2–10}$$

and for Chapters 5, 6, and 7, $\sigma_m(q, \dot{q})$ is defined as

$$\sigma_m(q, \dot{q}) \triangleq \begin{cases} 1, & q_\alpha(q, \dot{q}) \in \mathcal{Q}_m \\ 0, & \text{otherwise} \end{cases}, \forall m \in \mathcal{M}, \tag{2–11}$$

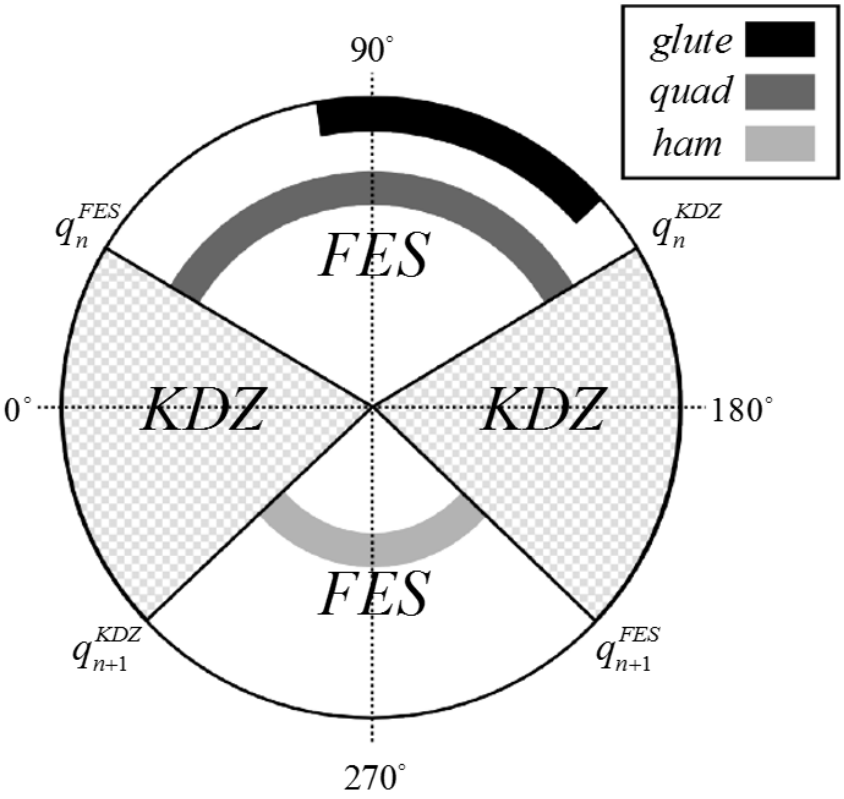

Figure 2-2. Sample crank cycle illustrating the FES and KDZ regions for a single leg. The crank positions q_n^{FES} and q_n^{KDZ} denote the points at which the crank enters the FES and KDZ regions of cycle n, respectively. Cycle n refers to the nth time the crank enters the FES/KDZ region [102].

where $q_\alpha, q_\beta : \mathcal{Q} \times \mathbb{R} \to \mathbb{R}$ denote trigger conditions. The functions q_α and q_β are designed to stimulate the rider's muscles sufficiently prior to the crank entering an FES region and for the stimulation to cease sufficiently prior to the crank leaving the FES region. The trigger conditions, q_β and q_α, use the fact the delay can be lower and upper bounded, respectively, (e.g., see the experimental results in [75, 99, 100]) and do not require explicit knowledge of the actual delay. The trigger conditions, q_α and q_β, are thus used to adjust the activation/deactivation of the FES input to ensure that the FES-induced muscle contractions occur in desired FES regions, denoted by $\mathcal{Q}_m \subset \mathcal{Q}, \forall m \in \mathcal{M}$, and to reduce/eliminate the residual torques in antagonistic muscles. The switching signal in (2–10) ensures the muscle contractions occur over the entire FES region, whereas (2–11) ensures a muscle contraction occurs before entering a FES region. To indicate when stimulation is applied, the following piecewise right-continuous switching signal, denoted by $\sigma_s : \mathbb{R}_{\geq 0} \to \{0, 1\}$, is defined

$$\sigma_s(t) \triangleq \begin{cases} 1, & \sum_{m \in \mathcal{M}} \sigma_m > 0 \\ 0, & \text{otherwise} \end{cases}. \tag{2–12}$$

For Chapters 4-7, the piecewise right-continuous switching signal for the activation/deactivation of the motor, denoted by $\sigma_e : \mathcal{Q} \times \mathbb{R} \to \{0, 1\}$, is defined as

$$\sigma_e(q, \sigma_s) \triangleq \begin{cases} 1, & q \in \mathcal{Q}_{KDZ} \\ 1, & q \in \mathcal{Q}_{FES}, \sigma_s = 0 \\ 0, & \text{otherwise}. \end{cases}. \tag{2–13}$$

In Chapter 8, the motor is active for all $t \geq t_0$ (i.e., the motor switching signal is defined as $\sigma_e \triangleq 1$).

Based on the aforementioned switching laws, the FES input to each muscle group that is implemented at time t is defined as

$$u_m \triangleq k_m \sigma_m(q, \dot{q})\, u(t), \forall m \in \mathcal{M}, \tag{2–14}$$

where $u : \mathbb{R}_{\geq 0} \to \mathbb{R}$ is a subsequently designed FES control input and $k_m \in \mathbb{R}_{>0}$, $\forall m \in \mathcal{M}$ are selectable constants, which allows for the FES input into each muscle group to be different for a given control input. However, as was previously stated, the EMD causes the implemented FES input to be delayed. The delayed FES input (i.e., pulse width) to the rider's muscles is defined as

$$u_{m,\tau} \triangleq k_m \sigma_{m,\tau} u_\tau, \forall m \in \mathcal{M}. \tag{2–15}$$

Notice that the delayed switching signals, $\sigma_{m,\tau}$, $\forall m \in \mathcal{M}$, indicate which muscle groups received the FES input u_τ at $t - \tau(t)$.

Based on the aforementioned switching laws, the current input to the motor windings is defined in Chapters 4 and 6 as

$$u_E \triangleq k_e \sigma_e(q, \sigma_s) u_e(t), \tag{2–16}$$

and in Chapters 5, 7, and 8 as

$$u_E \triangleq k_e u_e(t), \tag{2–17}$$

where $k_e \in \mathbb{R}_{>0}$ is a selectable constant and the subsequently designed motor input is denoted by $u_e : \mathbb{R}_{\geq 0} \to \mathbb{R}$. Substituting (2–15) and (2–16) (or (2–17)) into (2–8) yields[4]

$$\underbrace{B_M^\tau u_\tau + \tau_{vol}}_{\tau_M} + B_E u_e = M\ddot{q} + V\dot{q} + G + P + b_c\dot{q} + d, \tag{2–18}$$

where the lumped switched muscle control effectiveness, denoted by $B_M^\tau : \mathcal{Q} \times \mathbb{R} \times \mathbb{S} \times \mathbb{R}_{\geq 0} \to \mathbb{R}_{\geq 0}$, is defined as

$$B_M^\tau \triangleq \sum_{m \in \mathcal{M}} B_m k_m \sigma_{m,\tau}, \tag{2–19}$$

[4] For notational brevity, all functional dependencies are hereafter suppressed unless required for clarity of exposition.

and the motor control effectiveness, denoted by $B_E : \mathcal{Q} \times \mathbb{R} \to \mathbb{R}_{\geq 0}$, is defined in Chapters 4 and 6 as

$$B_E \triangleq B_e k_e \sigma_e, \tag{2–20}$$

and in Chapters 5, 7, and 8 as

$$B_E \triangleq B_e k_e. \tag{2–21}$$

The parameters in (2–18) capture the torques that affect the dynamics of the combined motorized cycle-rider system, however the exact values of these parameters are unknown. The subsequently designed FES and motor controllers only require known bounds on the aforementioned parameters. Specifically, the switched system in (2–18) has the following properties, which are used in Chapters 4 and 6 for the cycle-rider system [3, 75, 99, 100].

Property 2.1. $c_m \leq M(q) \leq c_M$, where $c_m,\ c_M \in \mathbb{R}_{>0}$ are known constants.

Property 2.2. $|V(q, \dot{q})| \leq c_V |\dot{q}|$, where $c_V \in \mathbb{R}_{>0}$ is a known constant and $|\cdot|$ denotes the absolute value.

Property 2.3. $|G(q)| \leq c_G$, where $c_G \in \mathbb{R}_{>0}$ is a known constant.

Property 2.4. $|P(q, \dot{q})| \leq c_{P1} + c_{P2} |\dot{q}|$, where $c_{P1},\ c_{P2} \in \mathbb{R}_{>0}$ are known constants [2].

Property 2.5. $|b_c| \leq c_c$, where $c_c \in \mathbb{R}_{>0}$ is a known constant [2].

Property 2.6. $|d| \leq c_d$, where $c_d \in \mathbb{R}_{>0}$ is a known constant.

Property 2.7. $||\tau_{vol}| \leq c_{vol}$, where $c_{vol} \in \mathbb{R}_{>0}$ is a known constant.

Property 2.8. The muscle control effectiveness B_m is lower and upper bounded $\forall m \in \mathcal{M}$; thus, $c_b \leq B_M^{\tau} \leq c_B$, whenever a muscle contraction is occurring (i.e., $\sigma_{s,\tau} = 1$), where $c_b, c_B \in \mathbb{R}_{>0}$ are known constants. Otherwise (i.e., $\sigma_{s,\tau} = 0$), $B_M^{\tau} = 0$.

Property 2.9. In Chapters 4 and 6, the motor control effectiveness is bounded such that whenever the motor is active (i.e., $\sigma_e = 1$), $c_e \leq B_E \leq c_E$, where $c_e,\ c_E \in \mathbb{R}_{>0}$ are known constants, and otherwise (i.e., $\sigma_e = 0$), $B_E = 0$. In Chapters 5 and 7, the motor control effectiveness is bounded such that $c_e \leq B_E \leq c_E$. Recall that B_E is assumed to be known in Chapter 8.

Property 2.10. $\dot{M}(q) - 2V(q, \dot{q}) = 0$, by skew-symmetry.

Property 2.11. The delay is upper and lower bounded such that $\underline{\tau} \leq \tau \leq \bar{\tau}$, where $\underline{\tau}, \bar{\tau} \in \mathbb{R}_{>0}$ are known constants. The EMD estimate error, defined as $\tilde{\tau} \triangleq \hat{\tau} - \tau$, is bounded such that $|\tilde{\tau}| \leq \overline{\tilde{\tau}}$, where $\overline{\tilde{\tau}}, \hat{\tau} \in \mathbb{R}_{>0}$ denotes a known constant estimate of the EMD, respectively. Note, the EMD estimate is time-varying in Chapter 5 and is constant in all other chapters.

To aid the control design and analysis in Chapter 6, the vector $\text{Tanh}(\cdot) \in \mathbb{R}^n$ is defined as follows

$$\text{Tanh}(\xi) \triangleq [\tanh(\xi_1), ..., \tanh(\xi_n)]^T, \tag{2–22}$$

where $\xi = [\xi_1, ..., \xi_n]^T \in \mathbb{R}^n$. Based on the definition in (2–22), the following inequalities hold $\forall \xi \in \mathbb{R}^n$ [103]:

$$\|\xi\|^2 \geq \sum_{i=1}^{n} \ln(\cosh(\xi_i)) \geq \ln(\text{cosh}(\|\xi\|)) \geq \frac{1}{2}\tanh^2(\|\xi\|), \tag{2–23}$$

$$\|\xi\| > \|\text{Tanh}(\xi)\|, \quad \|\text{Tanh}(\xi)\|^2 \geq \tanh^2(\|\xi\|), \tag{2–24}$$

$$\frac{\|\xi\|}{\tanh(\|\xi\|)} \leq \|\xi\| + 1. \tag{2–25}$$

CHAPTER 3
CHARACTERIZATION OF THE TIME-VARYING NATURE OF ELECTROMECHANICAL DELAY DURING FES-CYCLING

In this chapter, the FES-induced torque production and EMD are quantified on an FES-cycle for the quadriceps femoris and gluteal muscle groups. Two protocols were performed on five able-bodied individuals and five individuals with NCs. The EMD was examined by considering the CD and the RD, where the CD (RD) is the time latency between the start (end) of stimulation and the onset (cessation) of torque. For the first protocol, called the angle protocol, the motor fixed the crank arm in 10-degree increments and at each angle stimulation was applied in a random sequence to a combination of the quadriceps femoris and gluteal muscle groups to understand how the torque and EMD vary at different crank angles of an FES cycle system. The crank angle was determined to be statistically relevant for both the CD and RD. For the second protocol, called the cycling protocol, closed-loop FES-cycling was applied to induce fatigue and torque and EMD measurements were made during isometric conditions before and after each minute of cycling to quantify the effect of fatigue on EMD and torque production. A multiple linear regression and other descriptive statistics were performed to establish a range of expected EMD values and bounds on the rate of change of the EMD across a diverse population. Further, the EMD was found to increase slightly and the torque to decrease significantly during the cycling experiment. The results from these experiments can be used to assist in the development of closed-loop controllers for FES-cycling that are robust to time-varying EMD and changes in torque production. In fact, the results of this chapter are used to bound the EMD in Chapters 4-8 and to estimate the EMD in Chapter 5.

3.1 Methods

Transcutaneous electrical stimulation was applied to the quadriceps femoris and the gluteal muscle groups and the resulting crank arm torque was recorded during isometric conditions to examine the torque production and EMD. During dynamic conditions

the recorded torque measurements are a complex function of the leg and muscle dynamics, disturbances such as volitional movement, motor contribution, FES-induced muscle contribution, and the muscle effectiveness across various angles and velocities. Since the FES-induced muscle contribution cannot be extracted from dynamic torque measurements the EMD cannot be measured during dynamic conditions; thus, isometric conditions are utilized in this chapter. The current amplitude (90 mA for the quadriceps and 70 mA for the gluteals) and stimulation frequency (60 Hz) were fixed while the pulse width was used as the control input.[1] When recording the torque, each protocol used the motor to hold the crank at a pre-specified angle to create isometric conditions and then the pulse width was varied in an open-loop manner (i.e., the stimulation pattern was predetermined) to induce muscle contractions. The pulse width pattern was designed to enable repeated EMD and torque measurements throughout the experiment. To fatigue the muscle, FES-induced cycling was implemented in one-minute intervals between torque measurements for the cycling protocol.

3.1.1 Subjects

Five able-bodied individuals and five individuals with NCs, whose demographics are listed in Table 3-1, participated in the study. Since an objective of this study is to characterize and establish bounds on the EMD and the torque about the cycle crank axis to inform the development of closed-loop controllers, participants with and without NCs and with varied demographics were recruited. However, to investigate the EMD for specific NCs including differences in levels of severity, clinical trials would need to be pursued to yield a larger data set. Able-bodied participants are referred to by the letter "S" followed by their participant number, while participants with NCs are referred to by the letter "N" followed by their participant number. Prior to participation, written informed

[1] These current amplitudes and stimulation frequency were selected based on prior literature [3].

Table 3-1. Participant Demographics

Participant	Age	Sex	Condition	Time Since Diagnosis
S1	27	M	None	- -
S2	28	M	None	- -
S3	22	F	None	- -
S4	21	M	None	- -
S5	23	M	None	- -
N1	26	M	Spina Bifida (L5-S1)	26yr
N2	57	F	Multiple Sclerosis	10yr
N3	42	F	Cerebral Palsy	42yr
N4	34	F	Multiple Sclerosis	5yr
N5	64	F	Multiple Sclerosis	23yr

consent was obtained from each participant, as approved by the University of Florida Institutional Review Board (IRB201901676).

3.1.2 Apparatus

The experimental testbed used in this chapter is the FES cycle, introduced in Chapter 2.

3.1.3 Experimental Protocol

Two protocols were performed in this study, the Angle Protocol and the Cycling Protocol. Prior to either protocol, electrodes were placed medial-distal and lateral-proximal over the quadriceps femoris muscle and over the proximal and distal components of the gluteal muscle group in accordance with the Axelgaard electrode placement manual.[2] The participant was then seated in the recumbent tricycle with their legs constrained using orthotic boots. Next, a participant specific angle was determined for efficient stimulation of both their left (right) quadriceps and left (right) gluteal muscle groups called the left (right) angle, denoted by $q_L \in \mathbb{R}$ ($q_R \in \mathbb{R}$). To allow for a comparison between participants, q_L and q_R were selected using the torque transfer ratios from [3], denoted

[2] If desired, images of electrode placement can be found under Knee-Extension and Hip-Extension at https://www.axelgaard.com/Education.

by $T_m : \mathcal{Q} \to \mathbb{R}$, where $m \in \mathcal{M} \triangleq \{RQ,\, RG,\, LQ,\, LG\}$ indicates the right (R) and left (L) quadriceps femoris (Q) and gluteal (G) muscle groups and the set of all possible crank angles is denoted by $\mathcal{Q} \subseteq \mathbb{R}$. The left and right angle were selected as

$$q_* \triangleq \{q \in \mathcal{Q} \mid [T_* (q) = \max (T_*)] \,\&\, [T_{*Q} (q) \,, T_{*G} (q) > 0]\} \,,$$

where the * can be replaced by R or L to create distinct expressions, q denotes the crank angle, and where

$$T_* (q) \triangleq \sqrt{\left(\frac{T_{*Q}}{\max (T_{*Q})} \right)^2 + \left(\frac{T_{*G}}{\max (T_{*G})} \right)^2} .$$

Lastly, a proportional–integral–derivative (PID) controller was used to fix the crank at the left (right) angle to create isometric conditions and comfort limits on the pulse width, called the comfort threshold, were determined for the left (right) leg's muscle groups. During both protocols the participant was instructed to be a passive rider and to provide no volitional effort and no practice was allowed.

The purpose of this study is to understand the effect of fatigue and the crank angle on the EMD and torque production of two muscle groups in response to FES-induced cycling. In previous studies, the gluteal muscle group is often stimulated only when the quadriceps femoris group is also being stimulated [1, 3, 11, 12]. Therefore, in this study the EMD and torque production are examined for two muscle combinations: quadriceps only, and quadriceps and gluteal together.

3.1.3.1 Angle protocol

During the angle protocol, the motor fixed the crank arm in 10 degree increments (from 10 degrees to 350 degrees) while 0.25 s of stimulation, at each muscle's comfort threshold, was provided at each angle in a random sequence to the right quadriceps (RQ), left quadriceps (LQ), right quadriceps and gluteal (RQRG), and left quadriceps and gluteal (LQLG) muscle groups. The pulse width input and resulting output torque

were recorded with a 500 Hz sampling frequency. Rest periods of 2 s were provided between each application of 0.25 s of stimulation.

3.1.3.2 Cycling protocol

The cycling protocol has two components: the measurement sequence and the cycling sequence. For the measurement sequence, the motor randomly fixed the crank at the right or left angle, followed by fixing the crank at the other angle. When at the right (left) angle, 0.25 s of stimulation, at each muscle's comfort threshold, was applied in a random sequence to the RQ, RQRG (LQ, or LQLG) muscle groups with a 2 s rest period provided between each bout of stimulation. The cycling sequence was 80 s and the first 20 s consisted of the motor tracking a smooth cadence ramp from 0 to 50 RPM, at which point the closed-loop FES controller from [3] was implemented for a one minute duration of FES-cycling. For added comfort, the maximum allowed stimulation for each muscle, during the cycling sequence, was set between 80% to 90% of each muscle's comfort threshold based on user comfort. The cycling protocol consisted of an initial measurement sequence and thereafter a combination of a cycling sequence followed (after a brief cool down of 5 s) by a measurement sequence repeated ten times for a total of ten minutes of cycling.

3.1.4 Precautions

Since an aim of this chapter was to characterize the effect of fatigue on the EMD and torque production, the experiments were only performed if the participant reported that their muscles were adequately rested (i.e., no sore muscles from previous exercises or activities). Additionally, an aim was to understand the effect of fatigue in various muscle groups in both legs. However, only one leg and one muscle group combination can be tested at a time. Therefore, during the measurement sequence, the order in which the leg and muscle groups were stimulated was randomized. Randomization and consistent timing were each managed automatically through the feedback controller software.

Due to the non-selective nature of FES [104, 105], fatigue should be similar across intensity levels. Therefore, the comfort threshold for each muscle was used to set the pulse width for each participant. During the cycling portion, 80% to 90% of the comfort threshold was used as an upper limit of the stimulation input in each muscle. These thresholds ensure comfort for the participant while simultaneously producing strong contractions from each muscle group. To provide additional safety, an emergency stop button was provided to halt the experiment if required.

3.1.5 Measurements

FES inputs (pulse width) and the resulting torque output were recorded with a sampling frequency of 500 Hz. To reduce noise in the torque data, a 2nd order Butterworth IIR low-pass filter with a half power frequency of 8 Hz was implemented using the MATLAB functions designfilt and filtfilt to forward and reverse filter the torque data so that the filter would not introduce a delay.

The pulse width and torque data were segmented such that each segment contained 0.25 s of stimulation and its associated torque response. Each segment included 1 s of data from the moment the 0.25 s of stimulation began. The torque response in each segment contained 3 distinct regions: a pre-contraction region called the initial torque baseline, a region that represented the muscle contraction, and once the contraction ceased, a post-contraction region called the post torque baseline. The torque data of each segment was shifted so that the average torque of the initial torque baseline was 0 to remove the inertia effects of the leg pushing against the torque sensor. A plot of a single segment after being shifted is shown in Fig. 3-1.

During FES-cycling, generally stimulation is only applied when the resulting muscle contraction yields efficient forward pedaling of the cycle. For the cycling protocol, measurements only occurred at efficient angles. However, the angle protocol performed isometric experiments at both efficient and inefficient angles. Therefore, it was desired to only consider the data that resulted in efficient forward pedaling for the angle protocol,

which was accomplished by measuring the peak (T_{max}) and average (T_{avg}) torques as defined below. The torque measurements were converted into a percent, for a given participant and muscle combination, by dividing each T_{max} (T_{avg}) measurement by the maximum T_{max} measurement over the entire experiment and multiplying by 100. The percent torques were then plotted, and a subset of angles over which it is efficient (i.e., the median $T_{max} \geq 40\%$ for both muscle combinations) to stimulate the left and right muscle groups was determined, and the data associated with non-efficient stimulation was removed (e.g., all data associated with stimulation of a given muscle group at a non-efficient angle for that muscle group).

3.1.5.1 Torque

The peak and average torques were measured to determine the effect of fatigue and the effect of crank angle on the FES-induced torque. The peak torque (T_{max}) and the average torque (T_{avg}) are defined as the maximum and average value of the resultant torque after 0.25 s of stimulation, respectively.

3.1.5.2 Delay

CD was measured in three ways: the initial CD (CD0), the CD to reach 25% of the peak torque (CD25), and the CD to reach 75% of the peak torque (CD75). CD0 is the time difference between when the first electrical pulse was delivered to the muscle and the time the torque increased to 0.05 Nm above the initial torque baseline. CD25 (CD75) is the time difference between when the first electrical pulse was delivered to the muscle and the time the torque increased to 25% (75%) of the peak torque value. RD was measured in three ways: the initial residual delay (RD0), the RD to decay to 25% of the peak torque (RD25), and the RD to decay to 75% of the peak torque (RD75). RD0 is the time the difference in time between when the last electrical pulse was delivered to the muscle and the time that the torque fell to 0.05 Nm below the peak torque. RD25 (RD75) is the time difference between when the last electrical pulse was delivered to the muscle and the time that the torque fell to 25% (75%) of the difference between the

peak torque value and the average value of post torque baseline. For the angle protocol the measurements CD0 and RD0 were not considered. Fig. 3-1 illustrates the different delay measurements.

3.1.6 Statistical Analysis

3.1.6.1 Angle protocol

To characterize the effect of the crank angle on the EMD, a multiple linear regression was performed separately on the CD25, CD75, RD25, and RD75 measurements using the fitlm function in MATLAB and the data obtained from the angle protocol. However, since the left and right muscle groups are effective over different sets of angles (e.g., 50 to 160 degrees for the right muscle groups and 230 to 340 degrees for the left muscle groups), two regressions were performed for each measurement: one for the left muscle groups and another for the right. To allow for a comparison between the left and right muscle groups, the angle was shifted before performing a regression. For the right (left) angle data, the angle was subtracted by 50 (230). The regressions used the following predictors: crank angle (Angle; quantitative predictor ranging from 0 to 110 for both muscle groups due to shifting the data), the muscle combination (Side; RQ or RQRG for the right muscle groups and LQ or LQLG for the left muscle groups), the individual being tested (Subject; N1, . ., N5, S1, . ., S5), and the quadratic term Angle^2. The reference levels for the categorical predictors were selected as N1 for Subject and RQ (LQ) for the right (left) muscle groups. Thus, the subsequent regressions do not include a coefficient for N1, RQ, or LQ since their effects are included in the constant term of the regression table.

3.1.6.2 Interpretation for the angle protocol

To determine if the crank angle (and hence lower limb position) has a significant effect on the EMD the statistical significance of the Angle and Angle^2 predictor coefficients were used. The coefficients for categorical predictors represent vertical shifts, while the coefficients for quantitative predictors represent slopes. The regression over the right

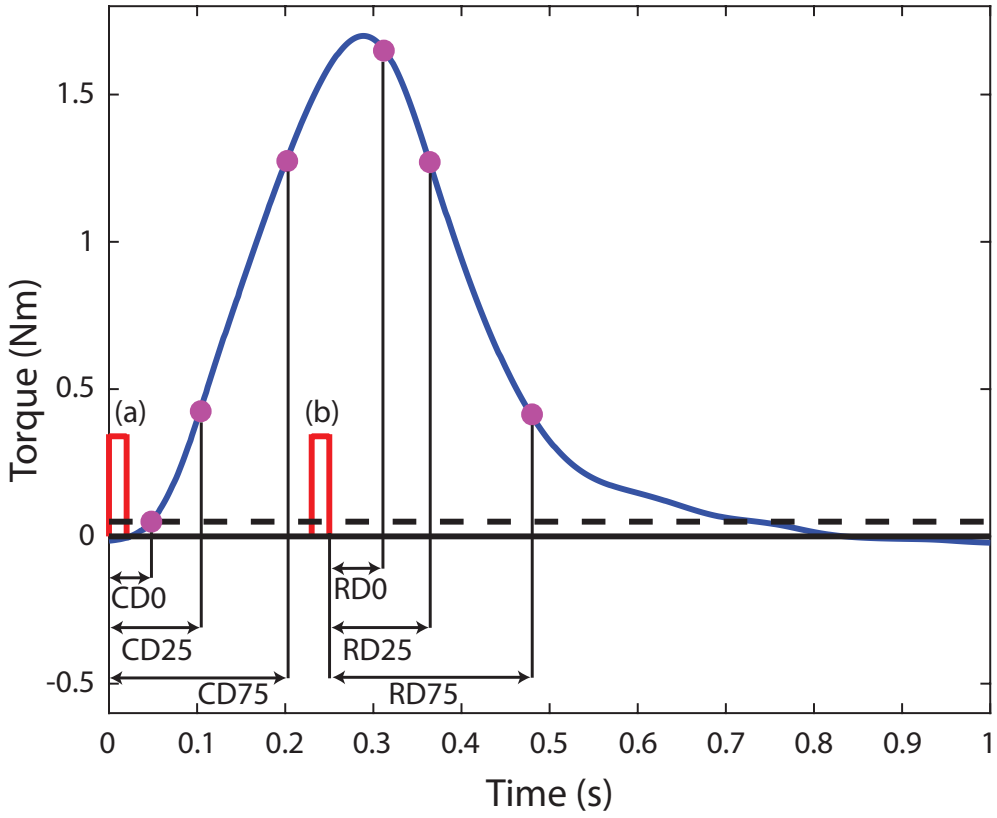

Figure 3-1. Schematic illustration to depict the six EMD measurements, where (a) represents the initial pulse of a pulse train and (b) denotes the final pulse. The first and last pulse of the pulse train are shown to represent timing information for 0.25 s of stimulation where the height and width is arbitrarily drawn. The EMD measurements are the initial contraction delay (CD0), the contraction delay to reach 25% of the peak torque (CD25), the contraction delay to reach 75% of the peak torque (CD75), the initial residual delay to decay to 0.05 Nm below the peak torque (RD0), the residual delay to decay to 25% of the peak torque (RD25), and the residual delay to decay to 75% of the peak torque (RD75). The dashed black line indicates a torque threshold of 0.05 Nm.

(left) muscle groups provides a result that is effective over the crank angles 50 to 160 (230 to 340) degrees. However, recall that the angles were shifted prior to performing the regressions. Therefore, as an example, the CD25 regression for the right muscle groups, for a given Subject and Side, would yield a model with the following form

$$CD25(q) = A + B(q-50) + C(q-50)^2, q \in [50, 160], \tag{3–1}$$

where the coefficients A, B, and C are scalars obtained from the CD25 regression table for the right muscle groups.

3.1.6.3 Cycling protocol

To quantify the effect of fatigue on FES-cycling, a series of multiple linear regressions were performed using the fitlm function in MATLAB and using the cycling protocol data. For each regression the dependent variable was selected as one of the measurements (T_{max}, T_{avg}, CD0, CD25, CD75, RD0, RD25, and RD75). Each of the regression analyses used the following predictors (independent variables): number of minutes spent cycling (CycleTime; quantitative predictor ranging from 0 to 10), leg dominance[3] (Side; Non-dominant or Dominant), if the gluteal muscle group was stimulated (Muscle; No Glute or Glute), and the individual being tested (Subject; S1, . . ., S5, N1, . ., N5). To improve the model, the following quadratic and interaction terms were included in all the regressions: CycleTime^2, Side$\times$Muscle, Side$\times$Subject, Muscle$\times$Subject, and CycleTime$\times$Subject. The interactions CycleTime$\times$Side and CycleTime$\times$Muscle were initially included, however they were subsequently removed because they did not have a significant effect (P-value > 0.05) for any of the regressions. The model for each regression included each independent variable, the quadratic term, and the aforementioned

[3] Each participant was asked to self-identify their dominant leg. If they were uncertain they were asked, “which leg would you use to kick a ball?” to identify their dominant leg [106].

interactions. To provide additional information about how the delay varies with time the quantitative predictors CD0, CD25, RD0, and RD75 were included in the regression on CD25, CD75, RD75, and RD25, respectively. To assess goodness of each model the adjusted R^2 was utilized.

3.1.6.4 Interpretation for the cycling protocol

The statistical significance of the CycleTime, CycleTime$\times$Subject, and CycleTime^2 predictor coefficients was used to infer the effect of FES-cycling induced fatigue on each measurement. The coefficients for quantitative predictors represent slopes. For example, the quantitative predictor, CycleTime, being a significant predictor of CD0, and CycleTime having a coefficient of 2, indicates that on average the CD0 increases by 2 ms per minute of cycling and the effect is significantly different from zero. Likewise, if the quadratic term, CycleTime^2, had a significant coefficient of 3 for the CD0, then on average the CD0 would increase by 3 ms per squared minute of cycling. A significant effect of the CycleTime$\times$Subject interaction indicates that the effect of CycleTime on the measured parameter depends on the subject. As an example, if CycleTime$\times$Subject has a significant S2 interaction coefficient of 5 for the CD0, then this indicates that the CD0 increased by 5 ms more per cycling minute for S2 than for S1. This means that the slope that CycleTime represents is steeper for S2 than for S1 (i.e., the delay increased faster for S2).

To interpret the additional quantitative predictors, consider the CD25 regression as an example. Including CD0 in the CD25 regression essentially segments the measurements. The CycleTime parameter from the CD25 regression indicates the rate CD25 is changing per minute of cycling relative to the CD0 measurement. For example, if CycleTime is 2 from the CD0 regression and CD0 and CycleTime from the CD25 regression are 1 and 3, respectively, then on average CD25 would increase by 3 ms per minute of cycling relative to CD0 and would increase by 5 ms per minute of cycling (3 + 2(1) = 5) relative to the instant the stimulation began.

Table 3-2. Angle Protocol: Regressions on CD measurements for the right muscle groups, where the angle coefficients are multiplied by $(q - 50) \in [0, 110]$, where q is the crank angle.

	CD25 (ms)				CD75 (ms)			
Term	Coef	SE	P-Value	Sig.	Coef	SE	P-Value	Sig.
Constant	85.06	2.69	0.000	***	164.34	6.73	0.000	***
Angle	-0.29	0.07	0.000	***	-0.12	0.18	0.507	ns
Angle^2	0.0054	0.0006	0.000	***	0.0073	0.0015	0.000	***
Side								
RQRG	0.76	1.20	0.528	ns	0.38	3.01	0.899	ns
Subject								
N2	-1.12	2.65	0.674	ns	-1.03	6.61	0.877	ns
N3	-13.58	4.31	0.002	**	-33.71	10.76	0.002	**
N4	-4.04	2.52	0.110	ns	-10.68	6.29	0.091	ns
N5	-7.57	3.03	0.013	*	-24.98	7.56	0.001	***
S1	-0.12	2.84	0.967	ns	-22.37	7.08	0.002	**
S2	5.42	2.49	0.031	*	-10.30	6.23	0.100	ns
S3	0.65	2.53	0.799	ns	-4.12	6.32	0.515	ns
S4	-12.24	2.51	0.000	***	-40.55	6.27	0.000	***
S5	-3.02	2.61	0.250	ns	-11.93	6.53	0.069	ns
R^2_{adj}	73.1%				67.5%			

3.2 Results

3.2.1 Angle Protocol

Plots of the percent torques are depicted in Figure 3-2 and plots of the EMD measurements are shown in Figures 3-3 and 3-4. Regressions were performed on each EMD measurement for both the left and right muscle groups using the data depicted in Figures 3-3 and 3-4, and the results are included in Tables 3-2 to 3-5. For visual clarity, non-significant (P-Values > 0.05) regression coefficients in each table are denoted by ns, and statistical significance is indicated by *, **, and *** for P-values less than or equal to 0.05, 0.01, and 0.001, respectively. Each regression model was validated by generating normal probability plots of the residual errors and visually confirming normality. Additionally, the adjusted R^2 was between 67% and 76% (45% and 68%) for each CD (RD) regression, indicating a good fit. Angle and/or Angle^2 were statistically significant predictors (P-value < 0.05) for each CD and RD regression, indicating the crank angle has a significant effect on both the CD and the RD, and hence the EMD.

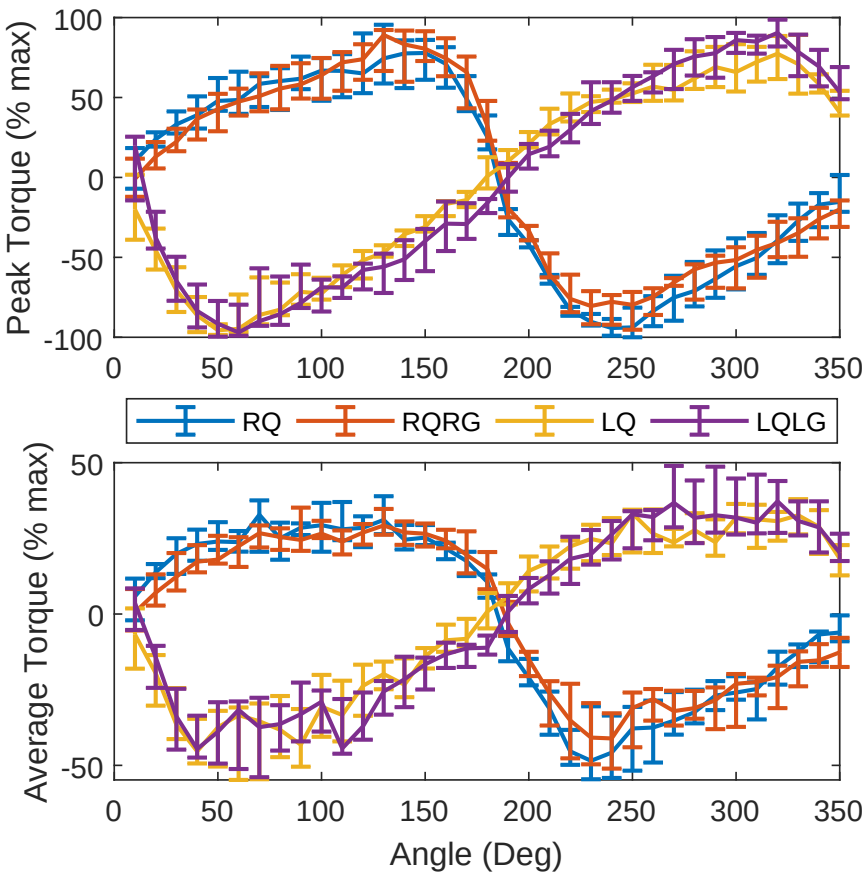

Figure 3-2. Angle Protocol: Torque measurements for each muscle combination (i.e., right quadriceps (RQ), left quadriceps (LQ), right quadriceps and gluteal (RQRG), and left quadriceps and gluteal (LQLG) muscle groups). The values show the median across all subjects and the lower and upper error bar denote the 25th (Q1) and 75th (Q3) percentiles, respectively. For a given muscle combination and participant, the peak (average) torque was converted into a percent by dividing each peak (average) torque measurement by the maximum peak torque measurement for the same participant and muscle combination over the entire experiment and multiplying by 100. The 0 degree crank angle corresponds to the crank being horizontal with the ground and the right leg extended. Consistent with the findings in Bellman *et al.* [3], the peak and average torques vary in a sinusoidal manner with the crank angle. The torque measurements show that at some angles there is negligible torque production, known as kinematic deadzones [1, 3, 107], and other angles are more efficient for positive torque production.

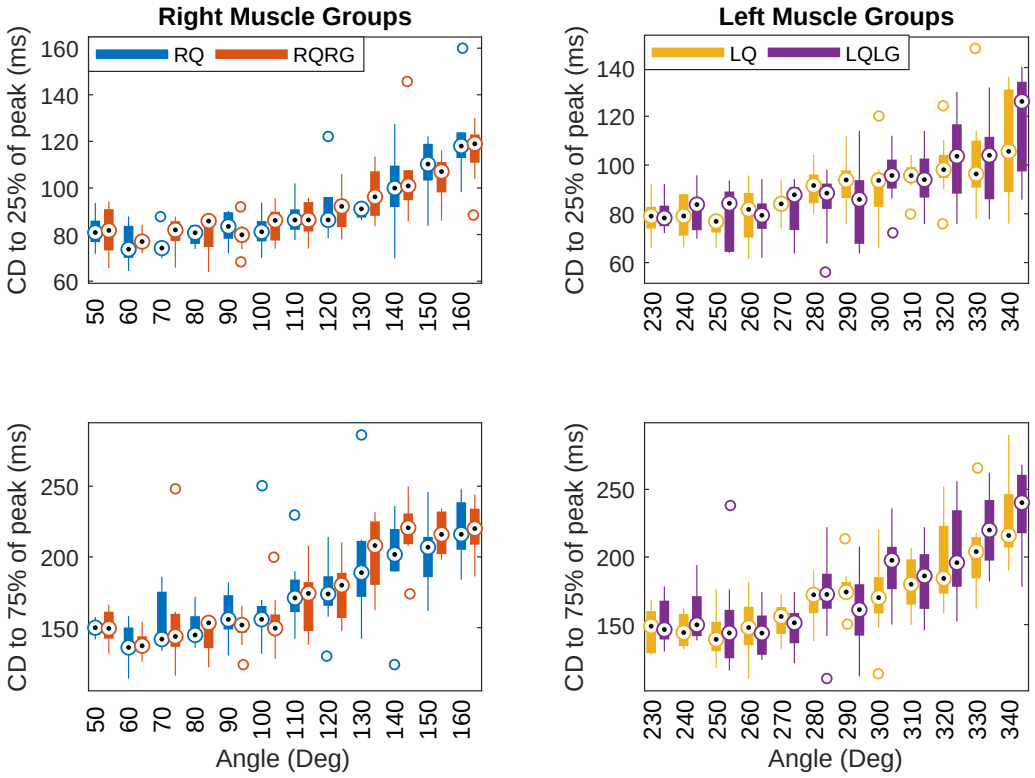

Figure 3-3. Angle Protocol: Box plots of the contraction delay (CD) measurements for each muscle combination (i.e., right quadriceps (RQ), left quadriceps (LQ), right quadriceps and gluteal (RQRG), and left quadriceps and gluteal (LQLG) muscle groups). The black dot within a white circle denotes the median, and the box edges denote the the 25th (Q1) and 75th (Q3) percentiles. The most extreme, non-outlier, data points are indicated by the whiskers and the outliers are indicated by circles. An outlier is a point above Q3+1.5(Q3-Q1) or below Q1-1.5(Q3-Q1). The 0 degree crank angle corresponds to the crank being horizontal with the ground and the right leg extended. In each subplot, the CD appears to initially be relatively flat and to then increase with the crank angle. In Muraoka *et al.*, the delay was measured at multiple joint angles and it was determined that the delay is dependent on the joint angle until the tendon slack is taken up, at which point the delay becomes constant for further joint angle changes [108]. Therefore, it is possible that the crank angles where the CD was relatively constant correspond to the crank angles where the tendon slack is taken up.

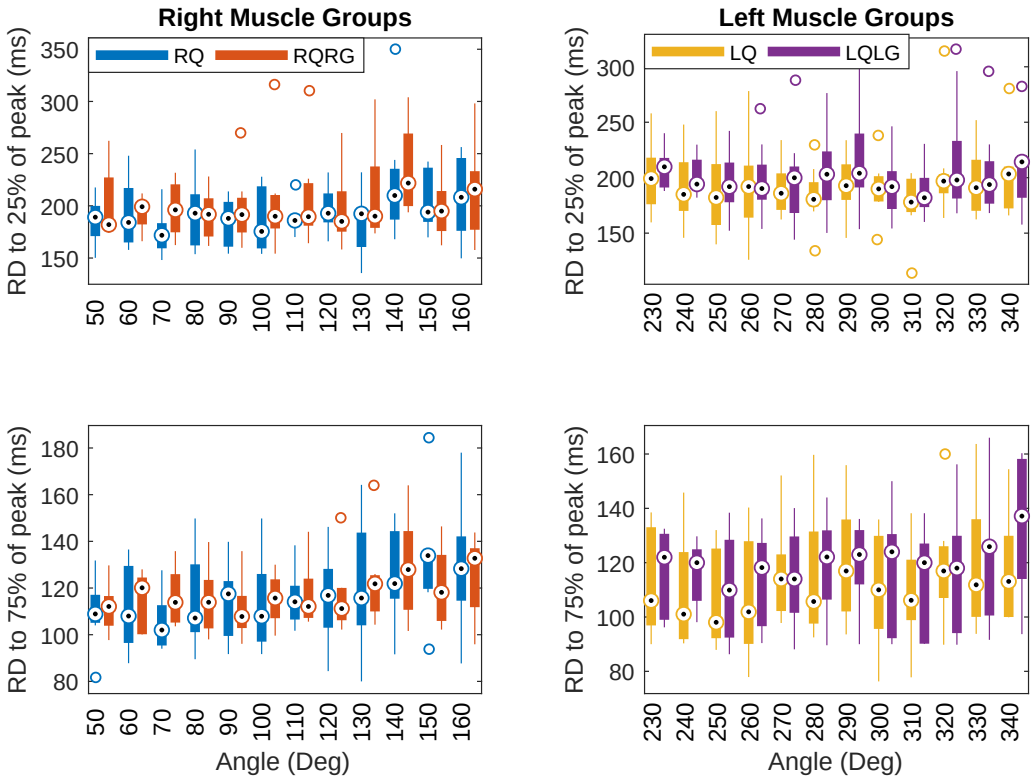

Figure 3-4. Angle Protocol: Box plots of the residual delay (RD) measurements for each muscle combination (i.e., right quadriceps (RQ), left quadriceps (LQ), right quadriceps and gluteal (RQRG), and left quadriceps and gluteal (LQLG) muscle groups). The black dot within a white circle denotes the median, and the box edges denote the the 25th (Q1) and 75th (Q3) percentiles. The most extreme, non-outlier, data points are indicated by the whiskers and the outliers are indicated by circles. An outlier is a point above Q3+1.5(Q3-Q1) or below Q1-1.5(Q3-Q1). The 0 degree crank angle corresponds to the crank being horizontal with the ground and the right leg extended. By visual inspection of the RD subplots the effect of the angle on the RD appears to be unclear.

Table 3-3. Angle Protocol: Regressions on RD measurements for the right muscle groups, where the angle coefficients are multiplied by $(q - 50) \in [0, 110]$, where q is the crank angle.

	RD25 (ms)				RD75 (ms)			
Term	Coef	SE	P-Value	Sig.	Coef	SE	P-Value	Sig.
Constant	171.02	6.83	0.000	***	102.40	4.39	0.000	***
Angle	-0.26	0.18	0.141	ns	-0.05	0.11	0.653	ns
Angle^2	0.0041	0.0015	0.008	**	0.0020	0.0010	0.043	*
Side								
RQRG	6.39	3.05	0.038	*	0.161	1.96	0.754	ns
Subject								
N2	28.42	6.72	0.000	***	18.50	4.32	0.000	***
N3	16.42	10.92	0.134	ns	6.83	7.02	0.332	ns
N4	47.27	6.38	0.000	***	33.60	4.11	0.000	***
N5	31.56	7.67	0.000	***	14.08	4.93	0.005	**
S1	-17.39	7.19	0.017	*	-7.95	4.62	0.087	ns
S2	12.31	6.32	0.053	ns	6.53	4.07	0.110	ns
S3	7.92	6.41	0.218	ns	1.75	4.13	0.673	ns
S4	6.27	6.36	0.325	ns	4.18	4.09	0.309	ns
S5	44.05	6.62	0.000	***	8.62	4.26	0.045	*
R^2_{adj}	49.9%				47.1%			

Table 3-4. Angle Protocol: Regressions on CD measurements for the left muscle groups, where the angle coefficients are multiplied by $(q - 230) \in [0, 110]$, where q is the crank angle.

	CD25 (ms)				CD75 (ms)			
Term	Coef	SE	P-Value	Sig.	Coef	SE	P-Value	Sig.
Constant	67.33	2.29	0.000	***	134.66	5.56	0.000	***
Angle	-0.12	0.07	0.092	ns	-0.29	0.165	0.083	ns
Angle^2	0.0033	0.0006	0.000	***	0.0084	0.0014	0.000	***
Side								
LQLG	0.56	1.18	0.643	ns	5.80	2.85	0.043	*
Subject								
N2	21.98	2.53	0.000	***	23.29	6.15	0.000	***
N3	-0.59	3.04	0.846	ns	-9.18	7.37	0.214	ns
N4	18.72	2.37	0.000	***	15.16	5.74	0.009	**
N5	20.61	2.45	0.000	***	26.25	5.95	0.000	***
S1	24.94	2.61	0.000	***	27.21	6.34	0.000	***
S2	12.51	2.48	0.000	***	25.67	6.02	0.000	***
S3	2.40	2.42	0.3237	ns	2.19	5.88	0.710	ns
S4	35.59	2.79	0.000	***	58.28	6.76	0.000	***
S5	15.05	2.39	0.000	***	7.05	5.81	0.227	ns
R^2_{adj}	75.3%				68.9%			

Table 3-5. Angle Protocol: Regressions on RD measurements for the left muscle groups, where the angle coefficients are multiplied by $(q - 230) \in [0, 110]$, where q is the crank angle.

	RD25 (ms)				RD75 (ms)			
Term	Coef	SE	P-Value	Sig.	Coef	SE	P-Value	Sig.
Constant	175.69	6.59	0.000	***	94.22	3.13	0.000	***
Angle	-0.39	0.196	0.048	*	-0.16	0.09	0.078	ns
Angle^2	0.0044	0.0017	0.009	**	0.0022	0.0008	0.007	**
Side								
LQLG	7.54	3.38	0.027	*	2.51	1.61	0.120	ns
Subject								
N2	49.10	7.29	0.000	***	42.17	3.47	0.000	***
N3	84.37	8.73	0.000	***	39.29	4.15	0.000	***
N4	28.70	6.81	0.000	***	31.75	3.24	0.000	***
N5	26.85	7.06	0.000	***	28.22	3.35	0.000	***
S1	12.66	7.52	0.094	ns	16.28	3.57	0.000	***
S2	10.46	7.14	0.145	ns	5.63	3.39	0.099	ns
S3	-16.34	6.97	0.020	*	-2.38	3.31	0.474	ns
S4	53.23	8.02	0.000	***	40.42	3.81	0.000	***
S5	8.23	6.89	0.234	ns	14.75	3.27	0.000	***
R^2_{adj}	54.3%				67.8%			

A couple of examples are presented to demonstrate the model provided by the regression tables. The form of the model for the CD25 regression for the right muscle groups is included in (3-1), where coefficient A is obtained by adding the Constant, Subject, and Side coefficients from the CD25 data in Table 3-2 as applicable. Note that the Subject and Side coefficients are associated with a specific participant or muscle combination and recall that Tables 3-2 to 3-5 do not include a coefficient for N1, RQ, or LQ since their effects are included in the constant terms of the regression tables. Furthermore, coefficients B and C are obtained from the Angle and Angle^2 coefficients from the CD25 data in Table 3-2, respectively. For example, the model of CD25 for participant S1 and the RQ muscle is $CD25(q) = 84.94 - 0.29(q - 50) + 0.0054(q - 50)^2, q \in [50, 160]$. Likewise, using the CD25 data in Table 3-4, the model of CD25 for participant S1 and the LQ muscle is $CD25(q) = 92.27 - 0.12(q - 230) + 0.0033(q - 230)^2, q \in [230, 340]$.

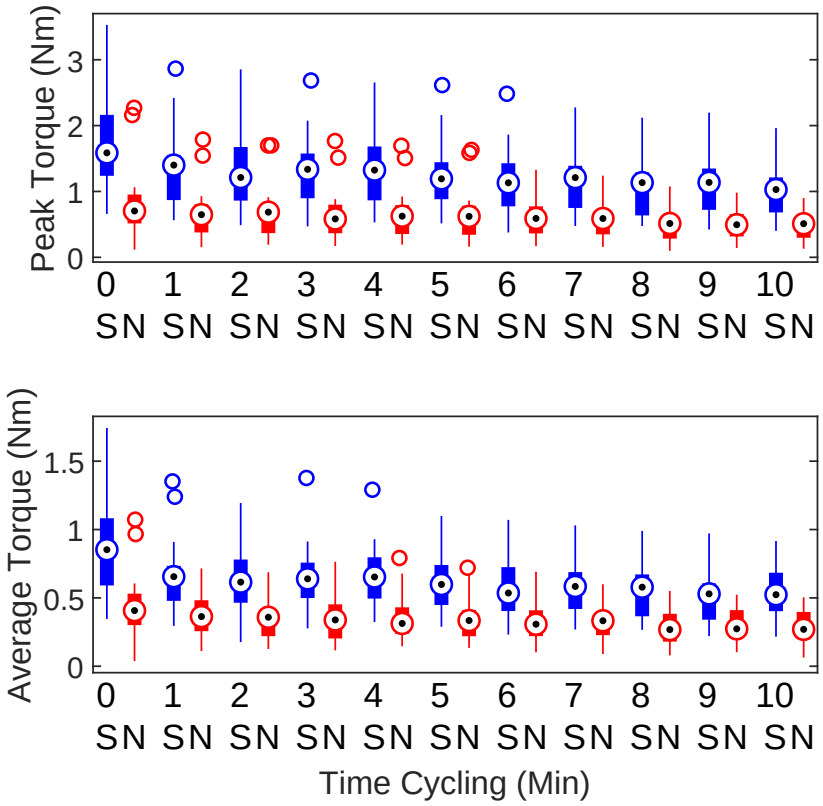

Figure 3-5. Cycling Protocol: Box plots of the torque measurements for participants with (N) and without (S) NCs. The median is depicted by a black dot within a white circle, the edges of the box denote the 25th (Q1) and 75th (Q3) percentiles, the whiskers denote the most extreme data points that are not considered to be outliers, and the outliers are indicated by circles. A data point is considered an outlier if it is below Q1-1.5(Q3-Q1) or above Q3+1.5(Q3-Q1). As the cycling time increased the peak and average torques tended to decrease, indicating that cycling resulted in fatigue.

3.2.2 Cycling Protocol

The effect of the number of minutes spent cycling on the T_{max} and T_{avg} is depicted in Fig. 3-5 and the effect of the number of minutes spent cycling on the six delay measurements is depicted in Fig. 3-6. To better understand the range of the two torque and six delay measurements over all the experiments, a table of descriptive statistics for each measurement is provided in Table 3-6. Measurements for 10 subjects in Table 3-6 resulted in N = 440 samples. Regressions were performed on T_{max}, T_{avg}, CD0, CD25, CD75, RD0, RD25, and RD75 and the results for CD0, CD25, and CD75

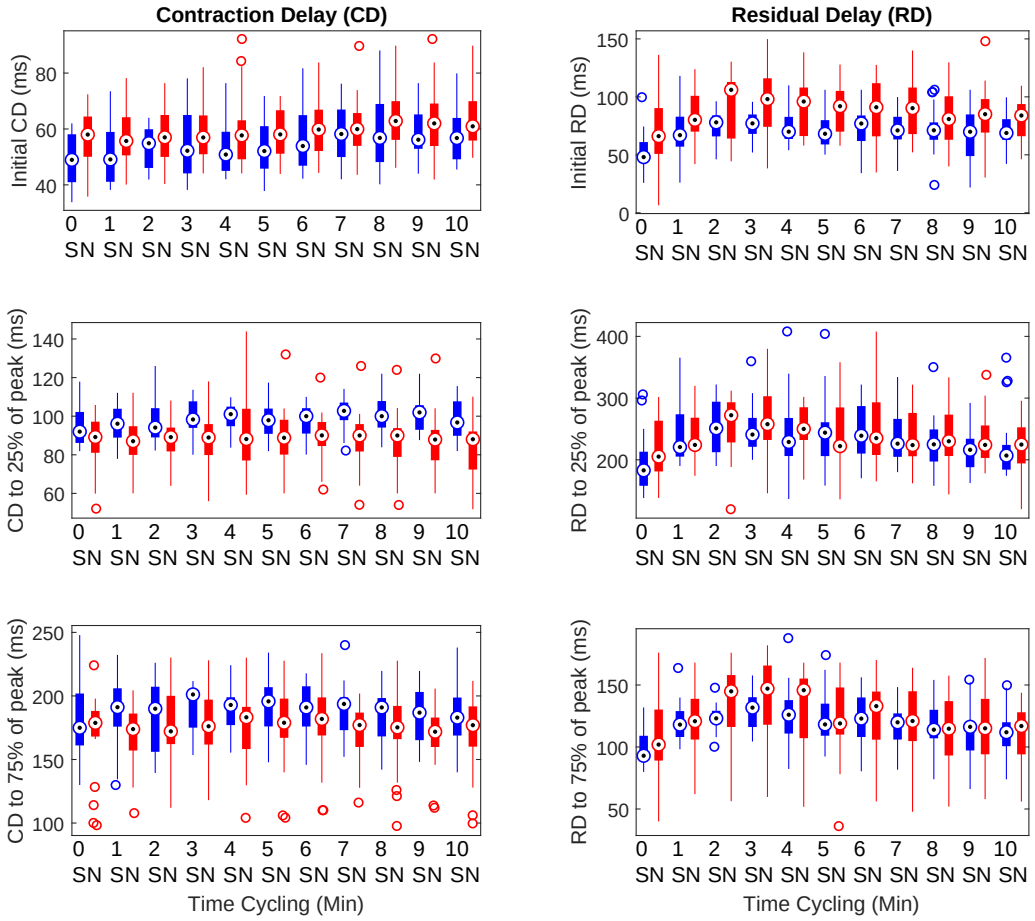

Figure 3-6. Cycling Protocol: Box plots of the delay measurements for participants with (N) and without (S) NCs. The median is depicted by a black dot within a white circle, the edges of the box denote the 25th (Q1) and 75th (Q3) percentiles, the whiskers denote the most extreme data points that are not considered to be outliers, and the outliers are indicated by circles. A data point is considered an outlier if it is below Q1-1.5(Q3-Q1) or above Q3+1.5(Q3-Q1). The CD subplots show a general increasing or flat trend. The RD subplots depict that the RD initially increased and later began to decrease.

Table 3-6. Cycling Protocol: Descriptive statistics

Variable	Units	Min	Q1	Median	Q3	Max
T_{max}	Nm	0.116	0.538	0.796	1.265	3.529
T_{avg}	Nm	0.038	0.296	0.427	0.632	1.742
CD0	ms	33.8	49.7	56.3	64.2	92.2
CD25	ms	51.8	85.8	93.9	102.1	143.9
CD75	ms	97.7	164.3	182.0	198.1	247.9
RD0	ms	6.5	62.1	75.8	94.2	149.8
RD25	ms	119.9	204.3	226.2	272.0	408.0
RD75	ms	36.2	104.1	119.8	138.2	187.8

are provided in Table 3-7 and the results for RD0, RD25, and RD75 are provided in Table 3-8. For visual clarity, statistical significance of the fitted coefficients is indicated in each table by *, **, and *** for P-Values less than or equal to 0.05, 0.01, and 0.001, respectively. Fitted coefficients that are not significant (P-Values > 0.05) are indicated by ns. For each regression the adjusted R^2 was between 66% and 95%, which indicates a good fit was achieved [33]. To validate each regression model, normal probability plots were created and normality of the residual errors was visually confirmed for each measurement. To quantify the rate at which the two torque and six delay measurements vary with cycling time (fatigue), a table of descriptive statistics for the rates of change of each variable is provided in Table 3-9.

3.2.2.1 Torque

CycleTime, CycleTime$\times$Subject, and CycleTime^2 were all statistically significant predictors (P-value < 0.05) of T_{max} and T_{avg}, indicating that fatigue (induced by cycling) occurs and has a significant effect on the FES-induced torque production confirming a hypothesis of this chapter. By using the coefficients from the regression analyses for CycleTime and CycleTime$\times$Subject, it was determined that both T_{max} and T_{avg} tended to decrease for each participant per cycling minute. Since CycleTime^2 had a positive coefficient for both T_{max} and T_{avg}, the rate at which T_{max} and T_{avg} decreases per cycling minute becomes less steep as the cycling time progresses.

Table 3-7. Cycling Protocol: Regressions on CD measurements (ms)

	CD0				CD25				CD75			
Term	Coef	SE	P-Value	Sig.	Coef	SE	P-Value	Sig.	Coef	SE	P-Value	Sig.
Constant	66.60	2.12	0.000	***	28.43	3.38	0.000	***	50.45	8.97	0.000	***
CycleTime	1.35	0.42	0.001	***	0.13	0.361	0.711	ns	2.04	0.898	0.024	*
CycleTime^2	-0.017	0.031	0.594	ns	-0.089	0.027	0.001	***	-0.169	0.067	0.012	*
CD0/CD25*					1.03	0.04	0.000	***	1.19	0.08	0.000	***
Side												
Dominant	-1.80	1.83	0.326	ns	0.60	1.57	0.704	ns	12.84	3.91	0.001	***
Muscle												
Glute	-13.40	1.83	0.000	***	21.68	1.67	0.000	***	10.81	3.96	0.007	**
Subject												
S2	-6.65	2.90	0.022	*	5.05	2.49	0.043	*	20.20	6.18	0.001	***
S3	-13.47	2.90	0.000	***	4.58	2.54	0.072	ns	6.35	6.22	0.308	ns
S4	-22.46	2.90	0.000	***	7.08	2.65	0.008	**	-6.57	6.31	0.298	ns
S5	-11.78	2.90	0.000	***	5.63	2.53	0.026	*	1.92	6.20	0.757	ns
N1	-17.24	2.90	0.000	***	3.71	2.58	0.151	ns	30.18	6.28	0.000	***
N2	2.34	2.90	0.420	ns	-4.69	2.48	0.059	ns	31.43	6.18	0.000	***
N3	-5.49	2.90	0.059	ns	-31.04	2.49	0.000	***	-13.40	6.84	0.051	ns
N4	-15.31	2.90	0.000	***	6.28	2.56	0.015	*	14.60	6.22	0.019	*
N5	3.95	2.90	0.174	ns	5.02	2.48	0.044	*	-3.88	6.22	0.533	ns
Side×Muscle												
Dominant×Glute	1.80	1.11	0.105	ns	-4.34	0.95	0.000	***	-5.69	2.36	0.016	*
CycleTime×Subject												
S2	-1.00	0.39	0.010	**	0.13	0.34	0.709	ns	-0.03	0.84	0.970	ns
S3	0.57	0.39	0.143	ns	0.68	0.33	0.044	*	-1.97	0.84	0.019	*
S4	-0.68	0.39	0.083	ns	0.27	0.33	0.418	ns	-1.37	0.83	0.101	ns
S5	-0.05	0.39	0.889	ns	0.15	0.33	0.663	ns	-0.96	0.83	0.251	ns
N1	-0.35	0.39	0.370	ns	-0.73	0.33	0.030	*	-1.09	0.84	0.195	ns
N2	-0.96	0.39	0.015	*	-0.08	0.34	0.810	ns	0.56	0.84	0.501	ns
N3	-0.50	0.39	0.199	ns	-0.01	0.33	0.983	ns	0.01	0.83	0.986	ns
N4	-0.43	0.39	0.276	ns	0.26	0.33	0.433	ns	-0.76	0.83	0.359	ns
N5	-0.12	0.39	0.760	ns	0.09	0.33	0.787	ns	-0.06	0.83	0.941	ns
Side×Subject												
Dominant×S2	-7.84	2.47	0.002	**	9.80	2.14	0.000	***	0.69	5.27	0.895	ns
Dominant×S3	-3.28	2.47	0.185	ns	9.53	2.11	0.000	***	4.30	5.29	0.417	ns
Dominant×S4	0.84	2.47	0.734	ns	13.39	2.11	0.000	***	16.74	5.39	0.002	**
Dominant×S5	-5.82	2.47	0.019	*	13.20	2.12	0.000	***	-0.25	5.30	0.963	ns
Dominant×N1	-5.11	2.47	0.039	*	19.06	2.12	0.000	***	-19.50	5.38	0.000	***
Dominant×N2	-3.61	2.47	0.145	ns	7.06	2.12	0.001	***	-38.38	5.27	0.000	***
Dominant×N3	3.08	2.47	0.214	ns	-0.55	2.11	0.796	ns	11.28	5.27	0.033	*
Dominant×N4	-3.14	2.47	0.205	ns	7.42	2.11	0.000	***	10.45	5.28	0.048	*
Dominant×N5	-4.63	2.47	0.062	ns	-12.84	2.12	0.000	***	4.145	5.45	0.415	ns
Muscle×Subject												
Glute×S2	12.38	2.47	0.000	***	-11.86	2.18	0.000	***	-3.36	5.27	0.524	ns
Glute×S3	0.62	2.47	0.803	ns	-9.94	2.11	0.000	***	15.80	5.32	0.003	**
Glute×S4	8.50	2.47	0.001	***	-12.13	2.14	0.000	***	-0.02	5.27	0.997	ns
Glute×S5	8.60	2.47	0.001	***	-10.65	2.14	0.000	***	4.14	5.27	0.432	ns
Glute×N1	11.81	2.47	0.000	***	-19.59	2.12	0.000	***	-5.70	5.30	0.283	ns
Glute×N2	4.85	2.47	0.051	ns	-13.60	2.12	0.000	***	0.76	5.31	0.886	ns
Glute×N3	4.61	2.47	0.063	ns	-8.20	2.12	0.000	***	-14.16	5.27	0.008	**
Glute×N4	12.74	2.47	0.000	***	-19.98	2.18	0.000	***	-7.94	5.30	0.135	ns
Glute×N5	9.95	2.47	0.000	***	-19.17	2.15	0.000	***	-6.29	5.31	0.238	ns
R^2_{adj}	71.2%				87.7%				79.8%			

*The quantitative predictor CD0 was included in the regression on CD25 and the quantitative predictor CD25 was included in the regression on CD75.

Table 3-8. Cycling Protocol: Regressions on RD measurements (ms)

	RD0				RD75				RD25			
Term	Coef	SE	P-Value	Sig.	Coef	SE	P-Value	Sig.	Coef	SE	P-Value	Sig.
Constant	59.13	4.97	0.000	***	47.18	3.83	0.000	***	112.51	14.18	0.000	***
CycleTime	6.58	0.98	0.000	***	1.50	0.68	0.029	*	9.95	2.17	0.000	***
CycleTime^2	-0.573	0.07	0.000	***	-0.298	0.052	0.000	***	-0.536	0.17	0.002	**
RD0/RD75*					0.84	0.03	0.000	***	1.06	0.10	0.000	***
Side												
Dominant	7.70	4.30	0.074	ns	0.457	2.85	0.873	ns	-48.57	9.08	0.000	***
Muscle												
Glute	-0.27	4.30	0.951	ns	8.66	2.84	0.002	**	1.52	9.09	0.867	ns
Subject												
S2	-14.27	6.80	0.036	*	-1.90	4.52	0.675	ns	-25.10	14.34	0.081	ns
S3	8.61	6.80	0.206	ns	11.55	4.50	0.011	*	-12.61	14.43	0.383	ns
S4	-20.07	6.80	0.003	**	23.51	4.54	0.000	***	-10.91	14.32	0.447	ns
S5	-12.09	6.80	0.076	ns	3.26	4.51	0.470	ns	-19.36	14.33	0.177	ns
N1	4.61	6.80	0.498	ns	3.11	4.49	0.489	ns	-22.68	14.33	0.114	ns
N2	46.40	6.80	0.000	***	4.13	4.75	0.385	ns	12.02	14.93	0.421	ns
N3	18.20	6.80	0.008	**	1.68	4.53	0.711	ns	55.05	14.41	0.000	***
N4	35.95	6.80	0.000	***	9.92	4.65	0.033	*	-37.70	14.85	0.012	*
N5	-11.47	6.80	0.092	ns	1.55	4.51	0.730	ns	-22.25	14.33	0.121	ns
Side×Muscle												
Dominant×Glute	3.77	2.59	0.147	ns	-0.83	1.72	0.629	ns	4.71	5.47	0.390	ns
CycleTime×Subject												
S2	0.20	0.92	0.830	ns	0.69	0.61	0.256	ns	-5.49	1.93	0.005	**
S3	-0.38	0.92	0.678	ns	0.81	0.61	0.184	ns	-6.57	1.93	0.001	***
S4	0.65	0.92	0.477	ns	1.92	0.61	0.002	**	-3.32	1.94	0.088	ns
S5	-1.79	0.92	0.052	ns	0.77	0.61	0.206	ns	-9.62	1.93	0.000	***
N1	-1.51	0.92	0.099	ns	-0.07	0.61	0.912	ns	-4.85	1.93	0.012	*
N2	-1.87	0.92	0.041	*	0.28	0.61	0.642	ns	-1.75	1.93	0.366	ns
N3	0.72	0.92	0.433	ns	0.21	0.61	0.731	ns	-5.84	1.93	0.003	**
N4	-1.53	0.92	0.095	ns	0.47	0.61	0.439	ns	-5.99	1.93	0.002	**
N5	0.58	0.92	0.530	ns	1.33	0.61	0.040	*	-3.72	1.94	0.055	ns
Side×Subject												
Dominant×S2	5.20	5.80	0.370	ns	6.51	3.83	0.090	ns	34.59	12.25	0.005	**
Dominant×S3	-12.83	5.80	0.027	*	-6.72	3.85	0.082	ns	46.75	12.33	0.000	***
Dominant×S4	23.56	5.80	0.000	***	-4.50	3.91	0.250	ns	15.46	12.30	0.209	ns
Dominant×S5	11.12	5.80	0.056	ns	13.19	3.85	0.001	***	112.59	12.40	0.000	***
Dominant×N1	-17.71	5.80	0.002	**	10.59	3.88	0.007	**	43.01	12.21	0.000	***
Dominant×N2	-5.91	5.80	0.309	ns	8.77	3.84	0.023	*	0.33	12.21	0.979	ns
Dominant×N3	-40.81	5.80	0.000	***	-38.01	4.06	0.000	***	-0.94	14.14	0.947	ns
Dominant×N4	-3.01	5.80	0.603	ns	8.88	3.83	0.021	*	67.93	12.22	0.000	***
Dominant×N5	42.10	5.80	0.000	***	-7.76	4.08	0.058	ns	71.94	12.50	0.000	***
Muscle×Subject												
Glute×S2	-0.58	5.80	0.920	ns	-8.64	3.83	0.025	*	2.02	12.24	0.869	ns
Glute×S3	-10.19	5.80	0.080	ns	-1.95	3.85	0.612	ns	12.30	12.25	0.316	ns
Glute×S4	8.30	5.80	0.153	ns	-18.09	3.84	0.000	***	23.67	12.25	0.054	ns
Glute×S5	3.52	5.80	0.544	ns	-4.16	3.83	0.278	ns	4.85	12.20	0.692	ns
Glute×N1	-2.77	5.80	0.633	ns	-9.06	3.83	0.019	*	-0.59	12.25	0.962	ns
Glute×N2	-14.35	5.80	0.014	*	-9.53	3.86	0.014	*	-2.19	12.39	0.860	ns
Glute×N3	-2.75	5.80	0.636	ns	-8.15	3.83	0.034	*	-11.64	12.25	0.342	ns
Glute×N4	-1.83	5.80	0.752	ns	-9.06	3.83	0.019	*	-3.26	12.25	0.790	ns
Glute×N5	-9.20	5.80	0.113	ns	-7.55	3.84	0.050	*	3.50	12.30	0.776	ns
R^2_{adj}	69.6%				88.8%				66.2%			

*The quantitative predictor RD0 was included in the regression on RD75 and the quantitative predictor RD75 was included in the regression on RD25.

Table 3-9. Cycling Protocol: Descriptive statistics of the rates of change for each variable

Variable	Rate Type*	Units†	Mean	SD	Slowest	Fastest	Quadratic
T_{max}	N/A	$\mathrm{Nm/min}$	-0.066	0.029	-0.032	-0.104	0.0025 $\mathrm{Nm/min^2}$
T_{avg}	N/A	$\mathrm{Nm/min}$	-0.037	0.013	-0.022	-0.057	0.0019 $\mathrm{Nm/min^2}$
CD0	Overall	$\mathrm{ms/min}$	0.998	0.476	0.35	1.92	-0.017 $\mathrm{ms/min^2}$
CD25	Relative to CD0	$\mathrm{ms/min}$	0.183	0.349	0.05	0.81	-0.089 $\mathrm{ms/min^2}$
CD25	Overall	$\mathrm{ms/min}$	1.211	0.702	0.43	2.79	-0.107 $\mathrm{ms/min^2}$
CD75	Relative to CD25	$\mathrm{ms/min}$	1.473	0.785	0.07	2.6	-0.169 $\mathrm{ms/min^2}$
CD75	Overall	$\mathrm{ms/min}$	2.913	0.752	1.46	3.85	-0.296 $\mathrm{ms/min^2}$
RD0	Overall	$\mathrm{ms/min}$	6.087	1.073	4.71	7.30	-0.573 $\mathrm{ms/min^2}$
RD75	Relative to RD0	$\mathrm{ms/min}$	2.141	0.616	1.43	3.42	-0.298 $\mathrm{ms/min^2}$
RD75	Overall	$\mathrm{ms/min}$	7.254	1.298	5.69	9.49	-0.779 $\mathrm{ms/min^2}$
RD25	Relative to RD75	$\mathrm{ms/min}$	5.235	2.687	0.33	9.95	-0.536 $\mathrm{ms/min^2}$
RD25	Overall	$\mathrm{ms/min}$	12.924	3.162	7.00	17.40	-1.362 $\mathrm{ms/min^2}$

*For CD (RD) measurements the overall rate is relative to the instant stimulation began (ended).
†The unit min represents the number of minutes cycling.

3.2.2.2 Delay

From Tables 3-7 and 3-8, it can be seen that CycleTime, CycleTime$\times$Subject, and CycleTime^2 are significant predictors and hence fatigue (induced by cycling) has a significant effect on the FES-induced EMD confirming the other hypothesis of this chapter.

3.3 Discussion

An important observation of this study is that similar trends occurred across the different populations in this study, which is likely due to the fact that the energy conversion process resulting from the application of an electric field to the generation of torque is largely invariant to the causation of different NCs. Therefore, the data for all participants were combined when generating the plots and performing the regressions for the angle protocol.

3.3.1 Angle Protocol

Participants with and without NCs were recruited in this study. Interestingly, both populations displayed similar trends, and hence, the data for all participants were combined when generating the plots and performing the regressions. Similarly, in the Cycling Protocol it was observed that although variability may exist between participants with and without NCs, the overall trends were consistent across the different populations.

By inspection of Figures 3-3 and 3-4, the CD and RD appear to behave differently. The crank angle appears to have a smaller, although still significant, effect on the RD compared to the CD. Furthermore, from the regression results in Tables 3-2 to 3-5 it was determined that the crank angle and the muscle combination have a significant effect on the EMD during FES-cycling. Since the lower limb position is a function of the crank angle, it could be concluded that the EMD is a function of the lower limb position during FES-cycling. The finding that the EMD is a function of the lower limb position is true, in general, and is agnostic to the specific exercise being performed. However, different

exercises may result in a different combination of muscle groups being active at a given time, which would impact the model. Future studies would be required to establish specific models of the EMD for these other activities.

3.3.2 Cycling Protocol

Although the results of this study, such as those in Table 3-6, can be compared to the results of prior studies, all prior studies focused on single joint tasks where the effects of more complicated tasks that require multiple muscle groups at once were not considered. Previous studies also only focused on the initial CD and not the time to produce different levels of torque or force production (CD25 or CD75) and few considered the RD [33].

3.3.2.1 Torque

Prior studies have investigated the change in torque or force production as a result of fatigue [33, 109][4] . In Rampichini *et al.* [109], after two minutes of stimulation to the gastrocnemius medialis the peak force decreased from 687 N to 639 N and in Downey *et al.* [33]*,* FES over a 5 minute duration in the quadriceps femoris resulted in the peak torque decreasing from 25.05 Nm to 5.35 Nm. However, it is unknown how the torque production will vary as a result of FES-cycling. In Fig. 3-5, the peak and average torques decreased as the cycling time increased. As a muscle fatigues, the force that it generates decreases, thus Fig. 3-5 confirms the hypothesis that FES-cycling does induce fatigue. The median peak torque was found to be 1.59 Nm (0.70 Nm) before cycling and 1.03 Nm (0.51 Nm) after 10 minutes of cycling for the participants without (with) NCs. A one-tail, unpaired t-test was performed using the combined data across all cycling times to conclude that T_{max} and T_{avg} are significantly smaller (P-value < 0.001) for participants with NCs than those with none. Future attempts to minimize FES-cycling induced fatigue can be compared against the rates and findings of this chapter.

[4] In [33, 109] results were for clinically healthy participants.

3.3.2.2 Delay

Recently studies have investigated EMD changes due to FES induced fatigue [33, 109]. Rampichini *et al.* [109] reports that after two minutes of stimulation to the gastrocnemius medialis the EMD increased from 26.85 ms to 31.74 ms. Downey *et al.* [33] reports that FES over a 5 minute duration in the quadriceps femoris from a high-fatiguing protocol (10 s of stimulation every 15 s) resulted in CD0 increasing from 52.06 ms to 128.34 ms. From Fig. 7 in [33], it can be seen that the low-fatiguing protocol (5 s of stimulation every 15 s) caused CD0 to increase from 52 ms to 62 ms. In the present study, the quadriceps femoris and the gluteal muscle groups were stimulated over 10 minutes of FES-induced cycling resulting in an increased median of CD0 from 54.0 ms to 59.8 ms after 10 minutes of cycling. From [33], a protocol that only changes the duration of stimulation can result in a significant difference in the change in CD0 from before to after the protocol. Therefore, the variation between the change in CD0 across different studies is likely due to a variation in stimulation intensity or duration for each study.

As indicated in Fig. 3-6, CD0 tends to increase with cycling time, indicating CD0 increased with fatigue; thus as T_{max} decreased (Fig. 3-5), CD0 increased. This is consistent with the finding in [95], where it was found that at lower isometric forces the delay was larger. From Fig. 3-6, it can be seen that the other EMD measurements do not generally increase with cycling time. After normalizing each EMD measurement by its respective peak torque measurement, the normalized EMD tended to increase with time indicating that T_{max} has a strong influence on the EMD. Therefore, it is possible that EMD varies with fatigue because fatigue causes T_{max} to decrease.

By inspection of Fig. 3-6 and Tables 3-6 and 3-9 it can be seen that the EMD was different for the participants with NCs and those with none. A two-tail, unpaired t-test indicated that CD0, CD25, CD75, and RD0 were significantly different (P-value < 0.001) for able-bodied participants and those with NCs (Table 3-6). From Table 3-6,

participants with NCs had on average a 48.5% smaller median T_{max} than the able-bodied participants, which likely contributes to the difference between the groups. The results in Tables 3-6 and 3-9 provide results on the EMD for both groups of participants as well as a combination, which can be used to bound the torque and EMD and their rates of change. A diverse population was recruited because it was desired for the bounds to represent a varied population.

Another finding of this study is that the CD and RD are not the same. For example, using the CD0 and RD0 data for all participants, a two-tail, unpaired t-test was used to conclude that CD0 and RD0 are different (P-value < 0.001). The difference between the CD and RD measurements is also apparent in Fig. 3-6. In Table 3-9, it is noticeable that the RD increases with cycling time at a faster rate than the CD. Therefore, the cycling protocol confirms a conclusion from the angle protocol, that the CD and RD are different. Additionally, the regression results in Tables 3-7 and 3-8 confirm that the muscle group, the side, and the interaction Side$\times$Muscle were statistically significant (P-value < 0.05) predictors of the EMD, indicating that the EMD varies among different muscle groups.

3.3.3 Closed-Loop Control

The results in this chapter can be used to improve the future development of closed-loop controllers for FES-cycling, such as those in Chapters 4-8, by providing insight into how the torque and EMD should be modeled and by establishing a range of expected values for the torque and the EMD. For example, the results indicate that future control designs should include different delays in the dynamic model for the CD, RD, and each muscle combination. Furthermore, when developing an estimator of the EMD, it should allow for the EMD to be a function of the crank angle. To account for inter-subject variability, previous closed-loop controllers for FES systems typically utilize robust control design methods, which require the delay to be lower and upper bounded by known constants [11–13]. The EMD bounds are important because they are

used to determine when to apply/cease stimulation in an effort to properly time when FES should be applied so that muscle contractions occur at times that yield effective torque production, which can potentially reduce the rate of fatigue. The results in this chapter provide the control designer with a range of expected bounds for each EMD measurement. The bounds on the rate of change of each EMD measurement can likewise inform adaptive update laws that estimate the delay to yield a more accurate estimate of the EMD throughout an experiment, which will improve performance.

3.4 Concluding Remarks

This chapter used plots and statistical results to confirm the hypothesis that FES-induced cycling will result in the torque and EMD varying with cycling time. Another finding is that the crank angle has a a significant effect on the EMD during FES-cycling. The EMD was divided into six different measurements to better understand how the EMD varied with time. To aid future control development, bounds were established on the torque and EMD and on the rate of change of both. Additionally, the study indicated that the CD and RD are different and that the EMD varies between muscle combinations. The results in this study can be used to inform the development of closed-loop controllers that account for the existence of a time-varying EMD. The findings of this chapter also indicate that the EMD should be modeled as angle dependent. These future efforts may lead to improved assistive devices and rehabilitative treatments. Additional studies could further investigate the effects of fatigue on the EMD at various crank angles.

CHAPTER 4
ROBUST CADENCE TRACKING FOR SWITCHED FES-CYCLING WITH AN UNKNOWN TIME-VARYING INPUT DELAY

In this chapter, closed-loop FES and motor controllers are implemented on the FES-cycle dynamic model introduced in Chapter 2 to yield cadence tracking. Stimulation is applied to three of the major muscle groups of the leg (i.e., quadriceps, hamstrings, gluteals). Additionally, delay-dependent switching conditions, which are presented in Chapter 2, and a robust control method are developed to account for an unknown time-varying input delay of a switched system. The results in Chapter 3 are used to bound the EMD in this chapter and the subsequent chapters. A Lyapunov-like analysis is performed to yield semi-global exponential cadence tracking to an ultimate bound. Experiments were performed on six able-bodied participants and four participants with NCs to validate the developed controller. The proposed controller resulted in an average cadence error of 0.01 $\pm$ 2.00 RPM for the able-bodied participants and 0.01 $\pm$ 2.72 RPM for participants with NCs. The experimental results validate the controller and indicate that delay compensation can result in an improved FES-cycling experience when compared to a controller of the same form, but without delay compensation. This chapter demonstrates the first control development and associated stability analysis for a switched uncertain nonlinear dynamic FES system with unknown time-varying input delays.

4.1 Control Development

The control objective is for the bicycle crank to track a smooth desired trajectory $q_d, \dot{q}_d, \ddot{q}_d : \mathbb{R}_{\geq 0} \to \mathbb{R}$ despite the presence of uncertainties in the nonlinear dynamic model and an unknown time-varying input delay. The measurable cadence tracking error, denoted by $\dot{e} : \mathbb{R}_{\geq 0} \to \mathbb{R}$, is defined as

$$\dot{e} \triangleq \dot{q}_d - \dot{q}, \tag{4–1}$$

where, the measurable crank position tracking error, denoted by $e : \mathbb{R}_{\geq 0} \to \mathbb{R}$, is defined as

$$e \triangleq q_d - q. \tag{4–2}$$

To facilitate the subsequent analysis, a measurable auxiliary tracking error, denoted by $r : \mathbb{R}_{\geq 0} \to \mathbb{R}$, is defined as

$$r \triangleq \dot{e} + \alpha_1 e + \alpha_2 e_u, \tag{4–3}$$

where $\alpha_1, \alpha_2 \in \mathbb{R}_{\geq 0}$ are selectable constants. The auxiliary error signal, denoted by $e_u : \mathbb{R}_{\geq 0} \to \mathbb{R}$, is designed to inject a delay-free input term into the closed-loop error system and is defined as

$$e_u \triangleq -\int_{t-\hat{\tau}}^{t} u(\theta)\, d\theta. \tag{4–4}$$

The open-loop error system is obtained by taking the time derivative of (4–3), solving (2–18) for $\ddot{q}$, using (4–2) and (4–4), setting $\tau_{vol} = 0$, and adding and subtracting $M^{-1}B_M^{\tau}u_{\hat{\tau}} + e$ to obtain

$$\dot{r} = -e + \chi + M^{-1}B_M^{\tau}\left(u_{\hat{\tau}} - u_{\tau}\right) - M^{-1}B_E u_e + \left(\alpha_2 - M^{-1}B_M^{\tau}\right)u_{\hat{\tau}} - \alpha_2 u, \tag{4–5}$$

where the auxiliary term, denoted by $\chi : \mathcal{Q} \times \mathbb{R} \times \mathbb{R}_{\geq 0} \to \mathbb{R}$, is defined as

$$\chi \triangleq \ddot{q}_d + M^{-1}\left(V\dot{q} + G + P + b_c\dot{q} + d\right) + \alpha_1\dot{e} + e.$$

Note that volitional contributions are not considered in this chapter, thus τ_{vol} in (2–18) is set to 0. By using Properties 2.1-2.6, χ can be bounded as

$$|\chi| \leq \Phi + \rho\left(\|z\|\right)\|z\|, \tag{4–6}$$

where $\Phi \in \mathbb{R}_{>0}$ is a known constant, $\rho(\cdot)$ is a positive, strictly increasing, and radially unbounded function, and $z \in \mathbb{R}^3$ is a composite error vector defined as

$$z \triangleq \begin{bmatrix} e & r & e_u \end{bmatrix}^T. \tag{4–7}$$

Based on the open-loop error system in (4–5) and the subsequent stability analysis, the FES and motor controller are designed respectively as

$$u = k_s r, \tag{4–8}$$

$$u_e = k_1 \text{sgn}\left(r\right) + \left(k_2 + k_3\right) r, \tag{4–9}$$

where k_s, k_1, k_2, $k_3 \in \mathbb{R}_{>0}$ are selectable constants, and sgn $(\cdot)$ denotes the signum function. Substituting (4–8) and (4–9) into (4–5) yields the closed-loop error system

$$\begin{aligned} \dot{r} &= -e + \chi + k_s M^{-1} B_M^{\tau} \left(r_{\hat{\tau}} - r_{\tau}\right) - M^{-1} B_E \left(k_1 \text{sgn}\left(r\right) + \left(k_2 + k_3\right) r\right) \\ &\quad + \left(\alpha_2 - M^{-1} B_M^{\tau}\right) k_s r_{\hat{\tau}} - \alpha_2 k_s r. \end{aligned} \tag{4–10}$$

LK functionals, denoted by Q_1, $Q_2 : \mathbb{R}_{\geq 0} \to \mathbb{R}_{>0}$, are designed to facilitate the subsequent stability analysis as

$$Q_1 \triangleq \frac{1}{2} \left(\varepsilon_1 \omega_1 + \varepsilon_3 \omega_3\right) k_s \int_{t-\hat{\tau}}^{t} r\left(\theta\right)^2 d\theta, \tag{4–11}$$

$$Q_2 \triangleq \frac{\omega_2 k_s}{\hat{\tau}} \int_{t-\hat{\tau}}^{t} \int_{s}^{t} r\left(\theta\right)^2 d\theta ds, \tag{4–12}$$

where $\varepsilon_1, \varepsilon_3, \omega_1, \omega_2, \omega_3 \in \mathbb{R}_{>0}$ are selectable constants. Based on the subsequent stability analysis, auxiliary bounding constants denoted by $\beta_1, \beta_2, \delta_1, \delta_2 \in \mathbb{R}_{>0}$ are defined as

$$\beta_1 \triangleq \min\left(\alpha_1 - \frac{\varepsilon_2 \alpha_2^2}{2},\ k_s \left(\frac{1}{2}\alpha_2 - \varepsilon_1 \omega_1 - \varepsilon_3 \omega_3 - \omega_2\right),\ \frac{\omega_2}{3 k_s \hat{\tau}^2} - \frac{1}{2\varepsilon_2} - \frac{\omega_3 k_s}{\varepsilon_3}\right), \tag{4–13}$$

$$\beta_2 \triangleq \min\left(\alpha_1 - \frac{\varepsilon_2 \alpha_2^2}{2},\ \frac{c_e}{c_M} k_2 - k_s \left(\varepsilon_3 \omega_3 + \omega_2\right),\ \frac{\omega_2}{3 k_s \hat{\tau}^2} - \frac{1}{2\varepsilon_2} - \frac{\omega_3 k_s}{\varepsilon_3}\right), \tag{4–14}$$

$$\delta_1 \triangleq \min\left(\frac{\beta_1}{2},\ \frac{2\omega_2}{3\hat{\tau}\left(\varepsilon_1 \omega_1 + \varepsilon_3 \omega_3\right)},\ \frac{1}{3\hat{\tau}}\right), \tag{4–15}$$

$$\delta_2 \triangleq \min\left(\frac{\beta_2}{2},\ \frac{2\omega_2}{3\hat{\tau}\left(\varepsilon_1 \omega_1 + \varepsilon_3 \omega_3\right)},\ \frac{1}{3\hat{\tau}}\right), \tag{4–16}$$

where $\varepsilon_2 \in \mathbb{R}_{>0}$ is a selectable constant.

4.2 Stability Analysis

In the subsequent analysis, switching times are denoted by $\{t_n^i\}$, $i \in \{m, e\}$, $n \in \{0, 1, 2, ...\}$, which denote the instants in time when B_M^τ becomes nonzero $(i = m)$ and when B_M^τ becomes zero $(i = e)$. A positive definite, continuously differentiable, common Lyapunov function candidate that is defined on a domain $\mathcal{D} \subseteq \mathbb{R}^5$ and denoted by $V_L : \mathcal{D} \to \mathbb{R}_{>0}$ is defined as

$$V_L \triangleq \frac{1}{2}e^2 + \frac{1}{2}r^2 + \frac{1}{2}\omega_3 e_u^2 + Q_1 + Q_2, \tag{4–17}$$

which satisfies the following inequalities:

$$\lambda_1 \|y\|^2 \leq V_L \leq \lambda_2 \|y\|^2, \tag{4–18}$$

where $y \in \mathbb{R}^5$ is defined as

$$y \triangleq \begin{bmatrix} z & \sqrt{Q_1} & \sqrt{Q_2} \end{bmatrix}^T, \tag{4–19}$$

and $\lambda_1, \lambda_2 \in \mathbb{R}_{>0}$ are known constants defined as

$$\lambda_1 \triangleq \min\left(\frac{1}{2}, \frac{\omega_3}{2}\right), \quad \lambda_2 \triangleq \max\left(1, \frac{\omega_3}{2}\right).$$

For the subsequent stability analysis, let the set of initial conditions be defined as

$$S_{\mathcal{D}} \triangleq \left\{y \in \mathcal{D} \mid \|y\| < \sqrt{\tfrac{\lambda_1}{\lambda_2}}\gamma\right\}, \tag{4–20}$$

where $\gamma \in \mathbb{R}_{>0}$ is a known constant and is defined as[1] $\gamma \triangleq \inf\{\rho^{-1}((\sqrt{\kappa}, \infty))\}$, where $\kappa \triangleq \min\left(\frac{1}{2}\beta_1\alpha_2 k_s, \frac{2c_e}{c_M}k_3\beta_2\right)$.

Theorem 4.1. *The closed-loop error system in* (4–10) *is uniformly ultimately bounded in the sense that*

$$\|y(t)\|^2 \leq \frac{\lambda_2}{\lambda_1}\|y(t_0)\|^2 \exp\left(-\lambda_3(t - t_0)\right) + \frac{v}{\lambda_1\lambda_3}\left(1 - \exp\left(-\lambda_3(t - t_0)\right)\right), \tag{4–21}$$

[1] For a set A, the inverse image is defined as $\rho^{-1}(A) \triangleq \{a \mid \rho(a) \in A\}$.

where $v \triangleq \frac{1}{\alpha_2 k_s}\left(\Phi + k_s \bar{\tilde{\tau}} \Upsilon \frac{c_B}{c_m}\right)^2$, $\Upsilon \in \mathbb{R}_{>0}$ *is a known constant and* $\lambda_3 \triangleq \lambda_2^{-1} \min(\delta_1, \delta_2)$, $\forall t \in [t_0, \infty)$, *provided* $y(t_0) \in S_{\mathcal{D}}$, *and the following gain conditions are satisfied:*

$$\alpha_1 > \frac{\varepsilon_2 \alpha_2^2}{2},\ \alpha_2 > 2(\varepsilon_1 \omega_1 + \varepsilon_3 \omega_3 + \omega_2), \tag{4–22}$$

$$\omega_2 > 3 k_s \hat{\tau}^2 \left(\frac{1}{2\varepsilon_2} + \frac{\omega_3 k_s}{\varepsilon_3}\right),\ \sqrt{\lambda_1^{-1}\lambda_3^{-1} v} < \gamma, \tag{4–23}$$

$$k_1 \geq \frac{c_M}{c_e}\left(\Phi + k_s \Upsilon \hat{\tau} \left|\alpha_2 - \varepsilon_1 \omega_1\right|\right), \tag{4–24}$$

$$k_2 > \frac{k_s c_M}{c_e}(\varepsilon_3 \omega_3 + \omega_2),\ k_3 > 0, \tag{4–25}$$

$$\max\left(\left|\alpha_2 - \frac{c_b}{c_M}\right|, \left|\alpha_2 - \frac{c_B}{c_m}\right|\right) \leq \varepsilon_1 \omega_1. \tag{4–26}$$

Proof. The solution to the time derivative of (4–17) exists almost everywhere (a.e.) within $t \in [t_0, \infty)$, because the motor controller, B_M^{τ}, and B_E are discontinuous. A generalized time derivative of V_L, denoted by $\dot{\tilde{V}}_L$, exists such that $\dot{V}_L(y) \overset{\text{a.e.}}{\in} \dot{\tilde{V}}_L(y)$. Let $y(t)$ for $t \in [t_0, \infty)$ be a Filippov solution to the differential inclusion $\dot{y} \in K[h](y)$ and let $h : \mathbb{R}^5 \to \mathbb{R}^5$ be defined as $h \triangleq \begin{bmatrix} \dot{e} & \dot{r} & \dot{e}_u & \sqrt{\dot{Q}_1} & \sqrt{\dot{Q}_2} \end{bmatrix}^T$ (see [110]). Substituting the time derivative of (4–2)-(4–4) and (4–10) into $\dot{\tilde{V}}_L(y)$, applying the Leibniz Rule on (4–11)-(4–12), and using (4–8) yields

$$\begin{aligned} \dot{\tilde{V}}_L \subseteq\ & e(r - \alpha_1 e - \alpha_2 e_u) + \omega_3 e_u k_s (r_{\hat{\tau}} - r) + r\left[-e + \chi + k_s M^{-1} K\left[B_M^{\tau}\right](r_{\hat{\tau}} - r_{\tau})\right. \\ & \left. - M^{-1} K[B_E]\left(k_1 K[\text{sgn}(r)] + (k_2 + k_3) r\right) + \left(\alpha_2 - M^{-1} K\left[B_M^{\tau}\right]\right) k_s r_{\hat{\tau}} - \alpha_2 k_s r\right] \\ & + \tfrac{1}{2}(\varepsilon_1 \omega_1 + \varepsilon_3 \omega_3) k_s (r^2 - r_{\hat{\tau}}^2) + \tfrac{\omega_2 k_s}{\hat{\tau}}\left(\hat{\tau} r^2 - \int_{t-\hat{\tau}}^{t} r(\theta)^2 d\theta\right), \end{aligned} \tag{4–27}$$

where, $K[\text{sgn}(\cdot)] = SGN(\cdot)$ such that $SGN(\cdot) = \{1\}$ if $(\cdot) > 0$, $[-1, 1]$ if $(\cdot) = 0$, and $\{-1\}$ if $(\cdot) < 0$.

When $B_M^{\tau} > 0$, the rider's muscles are generating a force, that is to say, the FES effect is present in the system (i.e., $t \in \left[t_n^m, t_{n+1}^e\right)$). From the switching laws in (2–10) and (2–13), whenever $B_M^{\tau} > 0$, there are two cases: $B_E = 0$ or $B_E > 0$. When $B_E = 0$, the system is being controlled solely by the delayed FES input, which is the more restrictive

case. In fact, (4–27) with $B_E > 0$ can be upper bounded by (4–27) with $B_E = 0$. Therefore, the subsequent proof omits the case when $B_M^{\tau} > 0$ and $B_E > 0$.

Setting $B_E = 0$, canceling common terms, using Properties 2.1 and 2.8, designing ε_1 and ω_1 such that $\max\left(\left|\alpha_2 - \frac{c_b}{c_M}\right|, \left|\alpha_2 - \frac{c_B}{c_m}\right|\right) \leq \varepsilon_1\omega_1$, and using the fact that $\dot{V}_L(y) \overset{\text{a.e.}}{\in} \dot{\tilde{V}}_L(y)$, (4–27) can be upper bounded as

$$\begin{aligned}\dot{V}_L \overset{\text{a.e.}}{\leq} & -\alpha_1 e^2 + \alpha_2 |e e_u| + k_s \tfrac{c_B}{c_m} |r| \left|r_{\hat{\tau}} - r_{\tau}\right| - \alpha_2 k_s r^2 + \tfrac{1}{2}\left(\varepsilon_1\omega_1 + \varepsilon_3\omega_3\right) k_s \left(r^2 - r_{\hat{\tau}}^2\right) \\ & + k_s\varepsilon_1\omega_1 |r r_{\hat{\tau}}| + \omega_3 k_s |e_u r_{\hat{\tau}}| + \omega_3 k_s |e_u r| + |r| |\chi| + \tfrac{\omega_2 k_s}{\hat{\tau}}\left(\hat{\tau} r^2 - \int_{t-\hat{\tau}}^{t} r(\theta)^2 \, d\theta\right).\end{aligned} \tag{4–28}$$

Provided that $\|y(\cdot)\| < \gamma, \ \forall \cdot \in [t_0, t)$, where $\gamma \in \mathbb{R}_{>0}$ is a known constant, it can be shown by using (4–6), (4–10), Properties 2.1-2.9, and the fact that $\|z\| \leq \|y\|$,that

$$\dot{r}(\cdot) \leq c_1 + c_2\gamma + c_3\gamma^2 \leq \Upsilon, \tag{4–29}$$

$\forall \cdot \in [t_0, t)$, where Υ is a constant and $c_1, c_2, c_3 \in \mathbb{R}_{>0}$ are known constants. Since $\dot{r}(\cdot) \leq \Upsilon, \ \forall \cdot \in [t_0, t)$, from (4–29), the Mean Value Theorem (MVT) and Property 2.11 can be used to obtain the following upper bound upper

$$k_s \frac{c_B}{c_m} |r| \left|r_{\hat{\tau}} - r_{\tau}\right| \leq k_s \bar{\tilde{\tau}} \Upsilon \frac{c_B}{c_m} |r| . \tag{4–30}$$

Using Young's Inequality, the subsequent inequalities can be developed

$$|e e_u| \leq \frac{1}{2\varepsilon_2\alpha_2} e_u^2 + \frac{\varepsilon_2\alpha_2}{2} e^2, \tag{4–31}$$

$$|r r_{\hat{\tau}}| \leq \frac{1}{2} r^2 + \frac{1}{2} r_{\hat{\tau}}^2, \tag{4–32}$$

$$|e_u r_{\hat{\tau}}| \leq \frac{1}{2\varepsilon_3} e_u^2 + \frac{\varepsilon_3}{2} r_{\hat{\tau}}^2, \tag{4–33}$$

$$|e_u r| \leq \frac{1}{2\varepsilon_3} e_u^2 + \frac{\varepsilon_3}{2} r^2. \tag{4–34}$$

Substituting (4–6) and (4–31)-(4–34) into (4–28), using (4–30), and completing the squares yields

$$\begin{aligned}\dot{V}_L &\overset{\text{a.e.}}{\leq} -\left(\alpha_1 - \tfrac{\varepsilon_2\alpha_2^2}{2}\right)e^2 + \left(\tfrac{1}{2\varepsilon_2} + \tfrac{\omega_3 k_s}{\varepsilon_3}\right)e_u^2 - k_s\left(\tfrac{1}{2}\alpha_2 - \varepsilon_1\omega_1 - \varepsilon_3\omega_3 - \omega_2\right)r^2 \\ &\quad + \tfrac{1}{\alpha_2 k_s}\left(\Phi + k_s\bar{\tilde{\tau}}\Upsilon\tfrac{c_B}{c_m}\right)^2 + \tfrac{1}{\alpha_2 k_s}\rho^2\left(\|z\|\right)\|z\|^2 - \tfrac{\omega_2 k_s}{\hat{\tau}}\int_{t-\hat{\tau}}^{t} r\left(\theta\right)^2 d\theta.\end{aligned} \tag{4–35}$$

An upper bound for e_u^2 can be obtained by using the Cauchy-Schwarz inequality and (4–8) to yield

$$e_u^2 \leq \hat{\tau}k_s^2\int_{t-\hat{\tau}}^{t} r\left(\theta\right)^2 d\theta, \tag{4–36}$$

and Q_2 can be bounded above by

$$Q_2 \leq \omega_2 k_s\int_{t-\hat{\tau}}^{t} r\left(\theta\right)^2 d\theta. \tag{4–37}$$

Consequently, the following upper bound can be determined by utilizing (4–11), (4–36), and (4–37) to yield

$$-\tfrac{\omega_2 k_s}{\hat{\tau}}\int_{t-\hat{\tau}}^{t} r\left(\theta\right)^2 d\theta \leq -\tfrac{\omega_2}{3k_s\hat{\tau}^2}e_u^2 - \tfrac{2\omega_2}{3\hat{\tau}(\varepsilon_1\omega_1+\varepsilon_3\omega_3)}Q_1 - \tfrac{1}{3\hat{\tau}}Q_2. \tag{4–38}$$

Subsequently, the fact that $\|z\| \leq \|y\|$, substituting (4–38) into (4–35), and imposing the aforementioned gain conditions in (4–22)-(4–26), (4–35) can be bounded above as

$$\dot{V}_L \overset{\text{a.e.}}{\leq} -\left(\tfrac{1}{2}\beta_1 - \tfrac{1}{\alpha_2 k_s}\rho^2\left(\|y\|\right)\right)\|z\|^2 - \tfrac{1}{2}\beta_1\|z\|^2 - \tfrac{2\omega_2}{3\hat{\tau}(\varepsilon_1\omega_1+\varepsilon_3\omega_3)}Q_1 - \tfrac{1}{3\hat{\tau}}Q_2 + v, \tag{4–39}$$

where β_1 is defined in (4–13) and v is defined in (4–21). Provided $y\left(t_n^m\right) \in \mathcal{D}$, where

$$\mathcal{D} \triangleq \left\{y \in \mathbb{R}^5 \mid \|y\| < \gamma\right\}, \tag{4–40}$$

then (4–39) can be further bounded as

$$\dot{V}_L \overset{\text{a.e.}}{\leq} -\delta_1\|y\|^2 + v, \tag{4–41}$$

where δ_1 is defined in (4–15). From the inequality in (4–18), (4–41) can be bounded above as

$$\dot{V}_L \overset{\text{a.e.}}{\leq} -\frac{\delta_1}{\lambda_2} V_L + v, \tag{4–42}$$

$\forall t \in \left[t_n^m, t_{n+1}^e\right)$.

When $B_M^\tau = 0$, the muscles are not generating a force, that is, the FES effect is absent from the system (i.e., $t \in \left[t_n^e, t_{n+1}^m\right)$). The switching laws in (2–10) and (2–13) were designed such that whenever $B_M^\tau = 0$ that $B_E > 0$ (i.e., the system is controlled solely by the motor). Setting $B_M^\tau = 0$, canceling common terms, using Properties 2.1, 2.8, and 2.9, noticing that $\alpha_2 = \varepsilon_1\omega_1 + (\alpha_2 - \varepsilon_1\omega_1)$, and using the fact that $\dot{V}_L(y) \overset{\text{a.e.}}{\in} \dot{\tilde{V}}_L(y)$, (4–27) can be upper bounded as

$$\begin{aligned}\dot{V}_L \overset{\text{a.e.}}{\leq}\ & -\alpha_1 e^2 + \alpha_2 |e e_u| + |r|\,|\chi| - \tfrac{c_e}{c_M} k_1 |r| - \tfrac{c_e}{c_M}(k_2 + k_3) r^2 + \varepsilon_1\omega_1 k_s |r r_{\hat{\tau}}| \\ & -\varepsilon_1\omega_1 k_s r^2 + |\alpha_2 - \varepsilon_1\omega_1|\, k_s |r|\,|r_{\hat{\tau}} - r| + \omega_3 k_s |e_u r_{\hat{\tau}}| + \omega_3 k_s |e_u r| \\ & + \tfrac{1}{2}(\varepsilon_1\omega_1 + \varepsilon_3\omega_3) k_s (r^2 - r_{\hat{\tau}}^2) + \tfrac{\omega_2 k_s}{\hat{\tau}} \left(\hat{\tau} r^2 - \textstyle\int_{t-\hat{\tau}}^t r(\theta)^2\, d\theta\right).\end{aligned} \tag{4–43}$$

Substituting (4–6) and (4–31)-(4–34) into (4–43), selecting gains according to (4–24), completing the squares on $|r|\,|\chi|$, and using the MVT yields

$$\begin{aligned}\dot{V}_L \overset{\text{a.e.}}{\leq}\ & -\left(\alpha_1 - \tfrac{\varepsilon_2\alpha_2^2}{2}\right) e^2 + \left(\tfrac{1}{2\varepsilon_2} + \tfrac{\omega_3 k_s}{\varepsilon_3}\right) e_u^2 - \left(\tfrac{c_e}{c_M} k_2 - k_s(\varepsilon_3\omega_3 + \omega_2)\right) r^2 \\ & + \tfrac{c_M \rho^2(\|z\|)\|z\|^2}{4 c_e k_3} - \tfrac{\omega_2 k_s}{\hat{\tau}} \textstyle\int_{t-\hat{\tau}}^t r(\theta)^2\, d\theta.\end{aligned} \tag{4–44}$$

Following a similar development as the $B_M^\tau > 0$ case, (4–44) can be bounded above by

$$\dot{V}_L \overset{\text{a.e.}}{\leq} -\frac{\delta_2}{\lambda_2} V_L, \tag{4–45}$$

$\forall t \in \left[t_n^e, t_{n+1}^m\right)$, provided that $y(t_n^e) \in \mathcal{D}$. Hence, an overall upper bound for both (4–42) and (4–45) can be obtained as

$$\dot{V}_L \overset{\text{a.e.}}{\leq} -\lambda_3 V_L + v, \tag{4–46}$$

where $\lambda_3 \triangleq \lambda_2^{-1} \min(\delta_1, \delta_2)$ denotes the most conservative decay rate over all regions of the crank (i.e., $\forall t \in [t_0, \infty)$). It is also verified that (4–17) is a common Lyapunov

function across every crank region. The differential inequality in (4–46) can be solved to yield

$$V_L(t) \leq \left(V_L(t_0) - \lambda_3^{-1} v\right) \exp\left(-\lambda_3 (t - t_0)\right) + \lambda_3^{-1} v, \tag{4–47}$$

$\forall t \in [t_0, \infty)$, provided $y(t_n^m), y(t_n^e) \in \mathcal{D}, \forall n$ and $\|y(\cdot)\| < \gamma, \ \forall \cdot \in [t_0, t)$. Note that an equivalent condition to $y(t_n^m), y(t_n^e) \in \mathcal{D}$ is that $\|y(t_n^m)\| < \gamma$ and $\|y(t_n^e)\| < \gamma$. It could be shown that a sufficient condition for $y(t_n^m), y(t_n^e) \in \mathcal{D}$ and $\|y(\cdot)\| < \gamma, \ \forall \cdot \in [t_0, t)$ is that $y(t_0) \in S_{\mathcal{D}}$ and the gain condition in (4–23) is satisfied. Therefore, provided that $y(t_0) \in S_{\mathcal{D}}$ and the aforementioned gain conditions are met, (4–17) can be used with (4–47) to yield the exponential bound in (4–21). Using (4–17) and (4–46) it can be shown that $e, r, e_u \in \mathcal{L}_\infty$. By (4–8) and (4–9), $u, u_e \in \mathcal{L}_\infty$ and the remaining signals are bounded. □

4.3 Extension

An extension of the developed controllers in (4–8) and (4–9) to improve the gain conditions is to allow for the motor to always be activated. This change is reflected by modifying the motor switching condition from (2–13) to the following

$$\sigma_e \triangleq 1. \tag{4–48}$$

The stability analysis follows directly from the above analysis.

For comparative purposes, an additional controller/switching signal combination can be created to compensate for the system dynamics in (2–18) if the FES input delay was considered to be negligible. This “Delay-free” controller can be generated by removing the delay-compensating term e_u from the auxiliary tracking error system in (4–3), such that

$$r \triangleq \dot{e} + \alpha_1 e, \tag{4–49}$$

and using (4–8) and (4–9) with this modified error system. Additionally, since the delay is assumed to be negligible, the switching signals do not need to compensate for the

delay and can be defined as

$$\sigma_m(q) \triangleq \begin{cases} 1, & q \in \mathcal{Q}_m \\ 0, & \text{otherwise} \end{cases}, \tag{4–50}$$

$$\sigma_e(q) \triangleq \begin{cases} 1, & q \in \mathcal{Q}_{KDZ} \\ 0, & \text{otherwise} \end{cases}, \tag{4–51}$$

such as in [3]. The stability analysis for the delay-free controller can be developed using a method similar to [3].

4.4 Experiment

The performance of the developed controllers and switching signals in (2–10), (2–13), (4–8), and (4–9), henceforth collectively labeled as Controller A, were validated through experiments on both able-bodied participants and participants with NCs. To better examine the performance of Controller A compared to alternative cadence tracking controllers, the extension and delay-free controllers described in the Extension section were implemented, henceforth labeled as Controller B and Controller C, respectively. To allow for the best comparison, all three controllers were designed to have the same form and the same objective of cadence tracking. By comparing the three controllers, insights are provided on the effect of delay compensation and the effect of switching the motor on and off.

4.4.1 Experimental Testbed

The experimental testbed used in this chapter is the FES cycle that is introduced in Chapter 2.

4.4.2 Experimental Methods

An experimental protocol was performed on six able-bodied participants and four participants with NCs. The demographic information for each participant is shown in Table 4-1. Able-bodied participants are referred to by the letter “P” followed by their participant number, while participants with NCs are referred to by the letter “N” followed

Table 4-1. Participant Demographics

Participant	Age	Sex	Condition	Time Since Diagnosis
P1	24	M	None	- -
P2	26	M	None	- -
P3	21	F	None	- -
P4	24	M	None	- -
P5	22	F	None	- -
P6	24	M	None	- -
N1	26	M	Spina Bifida (L5-S1)	26yr
N2	58	M	Quadriplegia	5yr
N3	57	F	Multiple Sclerosis	10yr
N4	42	F	Cerebral Palsy	42yr

by their participant number. Each participant gave written informed consent approved by the University of Florida Institutional Review Board. During the experiment, each participant was instructed to relax and make no volitional effort to either assist or resist the FES or electric motor input (i.e., to be a passive rider, blind to the desired or actual trajectory). The experiment was repeated three times for each participant with the only change being the implemented controller. Controllers A, B, and C were implemented in a random order for the experiment. For simplicity, experiments are subsequently referred to by the participant number followed by the controller letter; for example N1A refers to the first neurological participant for Controller A.

Before the experiments began, the electrodes were placed on each muscle group (quadriceps, hamstrings, and gluteals) and the participant was seated on the cycle with their feet secured using the orthotic boots, as shown in Figure 2-1. The seat was adjusted to ensure the participant's comfort while cycling. Measurements as detailed in [3] were performed to determine the desired FES regions of the crank for each participant. The cycle was then run at 50 RPM and open-loop stimulation was applied to one muscle group at a time to determine a comfort limit for each muscle, called the comfort threshold. If during an experiment the participants comfort threshold was reached, the stimulation was saturated.

The experimental protocol lasted 180 s. The first 20 s consisted of the motor tracking a smooth cadence ramp from zero to $\dot{q}_d = 50$ RPM, at which point either Controller A, B, or C was implemented for the remainder of the experiment. The goal of the remaining 160 s of the experiment was to track a constant desired cadence of 50 RPM, similar to [1]. This protocol was repeated for each controller.

4.5 Results

Experiments were conducted using Controllers A, B, and C on both able-bodied participants and those with NCs. Each controller was implemented on each participant for a single trial. The demographics of the four neurological participants are shown in Table 4-1. Participant N2 has quadriplegia and felt little sensation in his limbs resulting in higher stimulation thresholds. Participants N1, N3, and N4 were more sensitive to the stimulation resulting in lower stimulation thresholds, with Participant N4 being the most sensitive. Experiments were performed on participants with a range of neuromuscular conditions to demonstrate each controller's stability over a range of rider capabilities.

The cadence error, motor input, and FES input for both able-bodied participants and participants with NCs are displayed in Table 4-2. To highlight the performance of Controllers A, B, and C, the cadence tracking results and control inputs over the entire experiment are displayed in Figures 4-1 and 4-3 for Participants P1 and N2, respectively, and the control inputs over approximately 3 cycles are displayed in Figure 4-2 for participant P1. Typical results for both able-bodied participants and participants with NCs are represented by the results of Participant P1. The results of Participant N2 are also depicted because his results deviated from that of Participant P1 and because he is quadriplegic and unable to provide volitional effort; thus, any muscle produced force is caused solely due to the controllers.

4.6 Discussion

The experimental results conducted on both able-bodied and neurologically impaired populations demonstrate the validity of Controller A in tracking cadence despite

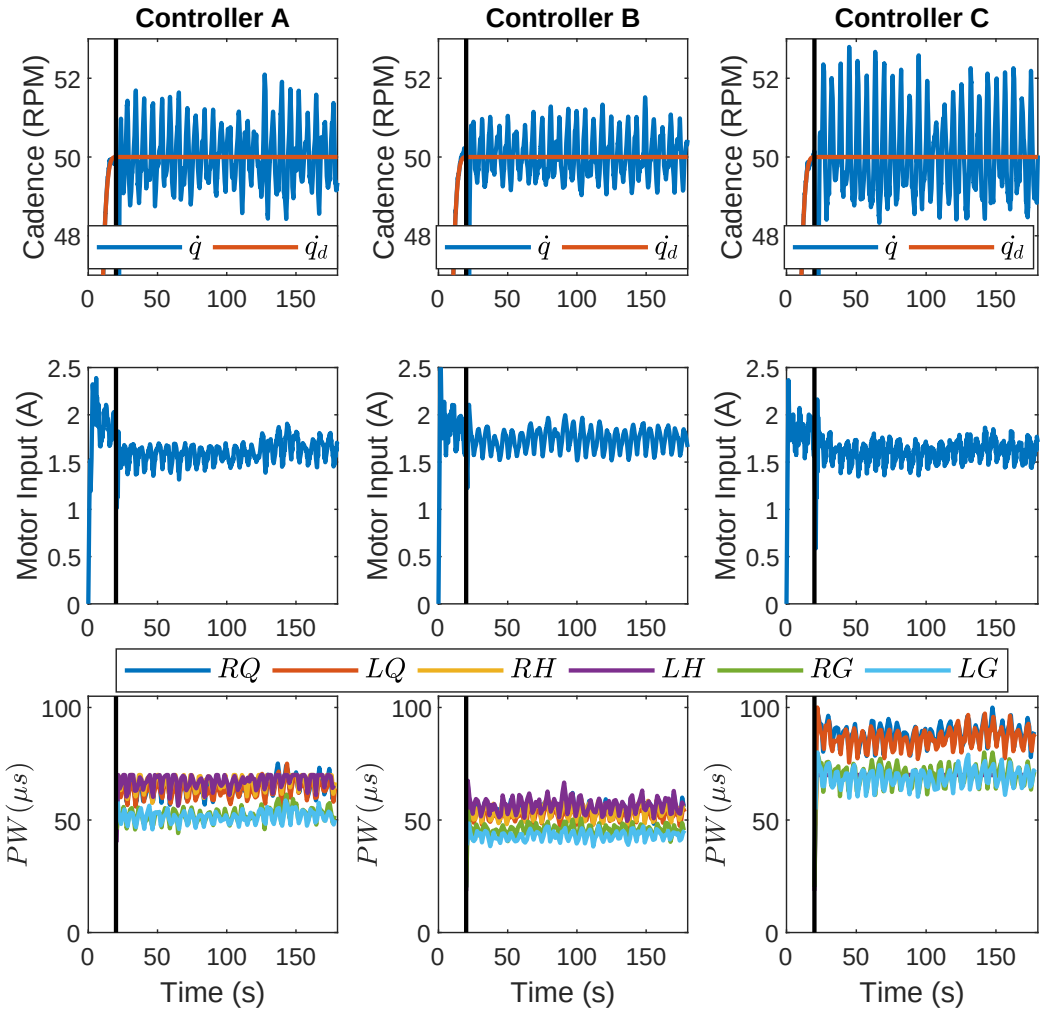

Figure 4-1. The desired versus the filtered cadence (top), filtered motor input (middle), and the peak FES input pulse width (PW) for each FES region applied to the right (R) and left (L) quadriceps (Q), hamstring (H), and gluteal (G) (bottom) are depicted for Controllers A, B, and C from left to right for participant P1. The vertical black line indicates the time when steady-state was reached. A 1.2 s moving average filter was used on the actual cadence and the motor input for visual clarity.

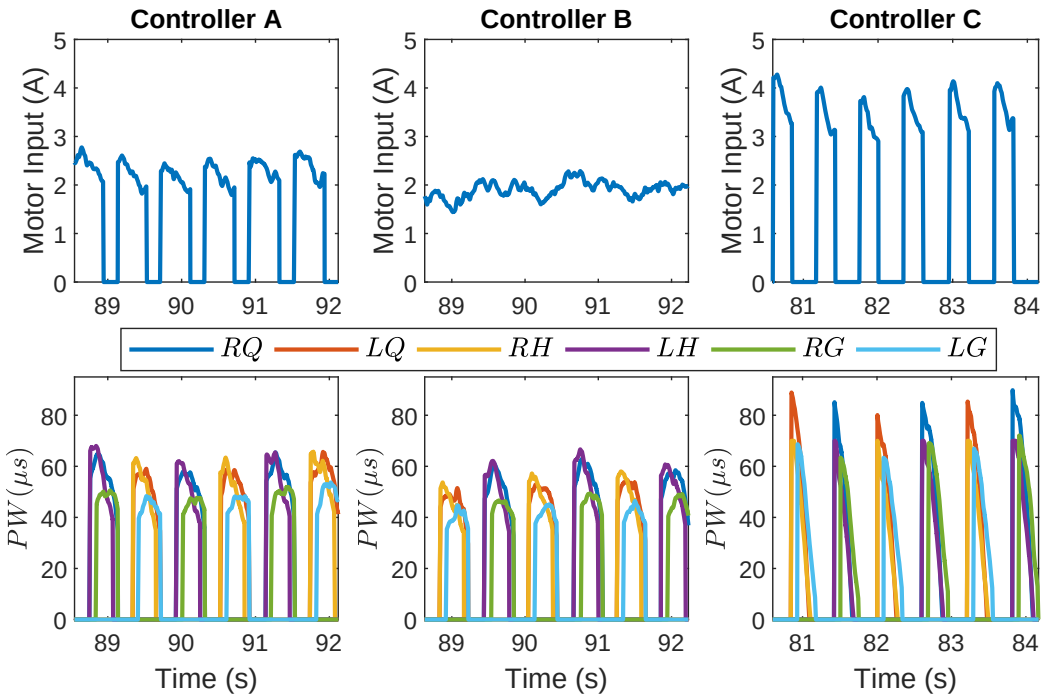

Figure 4-2. The motor input (top) and the FES inputs (bottom) over approximately three crank cycles are depicted for Controllers A, B, and C from left to right for participant P1.

uncertainties in the system and an unknown time-varying input delay as is indicated by Figures 4-1 and 4-3. In fact, for the able-bodied participants, the average standard deviation of the cadence tracking error was less than 3 RPM for each controller as illustrated in Table 4-2. For the participants with NCs, Controllers A and B outperformed Controller C in cadence tracking, as depicted in Table 4-2 and Figure 4-3. Controller B had the best cadence tracking as indicated by Table 4-2 because Controller B maintained motor control throughout the experiment. Controller B was designed to achieve the best possible tracking performance by the controllers in (4–8) and (4–9). Controller C had the largest standard deviations for cadence tracking errors (Table 4-2).

Typical motor and FES inputs over 3 cycles for each participant are represented by Participant P1's results, which are depicted in Figure 4-2 for each controller. Note, the FES inputs for Controller A and B appear to have a similar shape, while those of

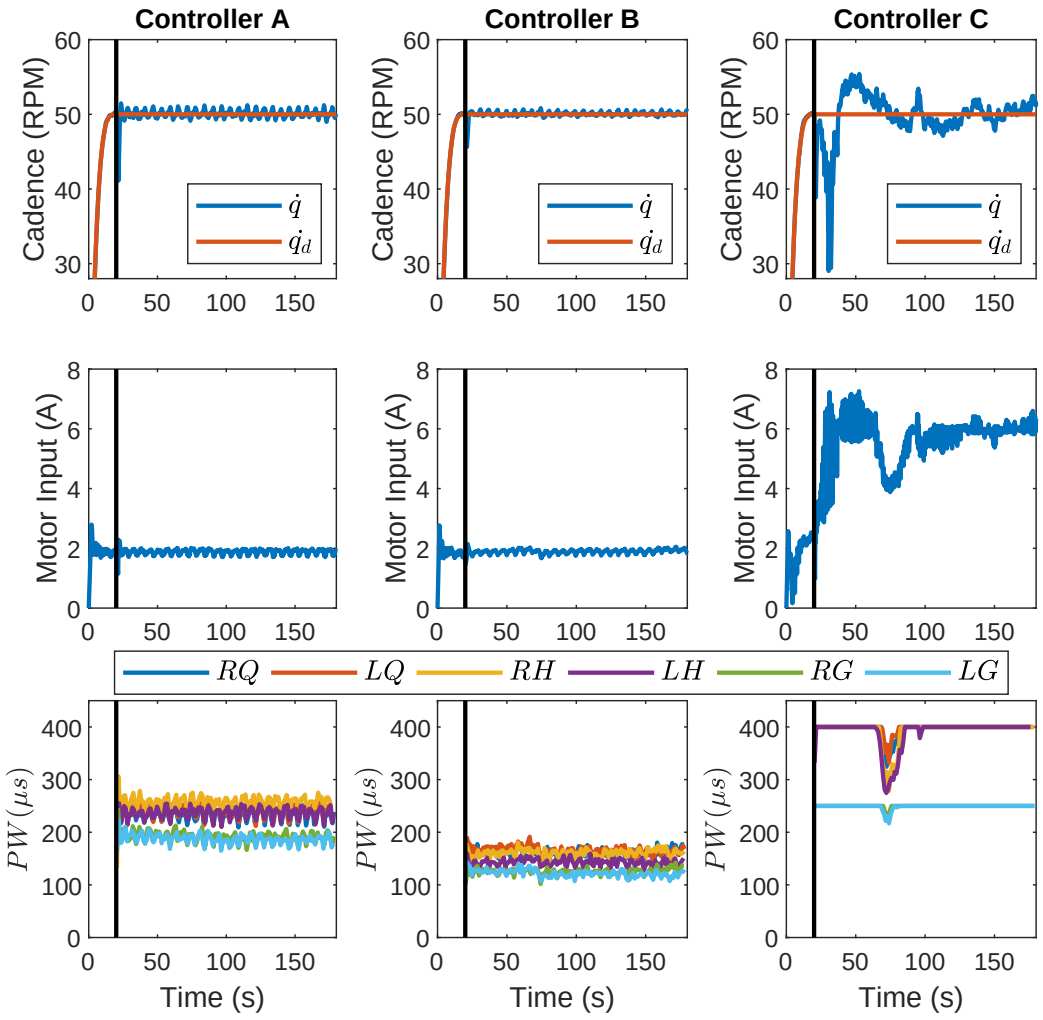

Figure 4-3. The desired versus the filtered cadence (top), filtered motor input (middle), and the peak FES input pulse width (PW) for each FES region applied to the right (R) and left (L) quadriceps (Q), hamstring (H), and gluteal (G) (bottom) are depicted for Controllers A, B, and C from left to right for participant N2. The vertical black line indicates the time when steady-state was reached. A 1.2 s moving average filter was used on the actual cadence and the motor input for visual clarity.

Controller C were initially very high and followed by a sharp decrease, causing it to appear triangular.

For Participants P1 and N2, the FES and motor inputs across the experiment for each controller are depicted in Figures 4-1 and 4-3. In Figure 4-3, it can be seen that Controller C produced a saturated FES input to each muscle for most of the experiment for Participant N2. From Table 4-2 and Figures 4-1 and 4-3, it is clear that Controller C required higher FES inputs than Controllers A and B. In fact, for able-bodied participants, Controllers B and C had average peak FES inputs that were 12.6% lower and 9.6% higher than Controller A, respectively. For participants with a NC, Controllers B and C had average peak FES inputs that were 30.0% lower and 41.3% higher than Controller A, respectively. Therefore, it can be noted that Controller B tends to decrease the required FES input. However, for each participant, Table 4-2 indicates that on average the FES is on 69.8%, 70.3%, and 46.3% of the time for Controllers A, B, and C, respectively. Thus Controller C increased the FES input but the FES is on for a shorter amount of time. Although the FES duration is shorter for Controller C, participants commonly indicated that Controller C felt less comfortable, because it resulted in higher FES inputs, when compared to Controllers A and B.

For each participant, the average motor input for each controller is depicted in Table 4-2. For the able-bodied participants, the motor input was 6.5% higher for Controller B when compared to Controller A and C. For participants with a NC, the motor input was about 53% higher for Controller C than for Controller A and Controller B. Overall, the differences between motor input for each participant and controller were fairly similar, with the exception of the much larger input for Participant N2 and Controller C. This result is noteworthy because, although the motor is on the least for Controller C, as indicated by Table 4-2 and depicted in Figure 4-2, the average motor input over one cycle was about the same for each controller. Since Participant N2 had poor cadence

tracking with Controller C, the motor required much larger inputs to maintain the stability of the system.

Controller C on average had larger cadence tracking errors and higher FES inputs when compared to Controllers A and B, resulting in the worst performance. Additionally, for Participant N2, Controller C resulted in the largest overall tracking errors and highest motor and FES inputs (Table 4-2). Controller C does not account for the delay, which results in the muscle contractions starting too late and thus occurring in less efficient regions of the crank cycle, contributing to the poor tracking performance relative to Controllers A and B. Controller B had the best tracking performance; however, in general it caused the FES inputs to be lower than the other controllers. The challenge with Controller B is that the motor is always active, as is often the case in current clinical practice, and both the motor and FES have the same cadence tracking control objective. Therefore, it is possible that for some participants the FES may be too low to even elicit muscle contractions since the tracking could solely be achieved by the motor. FES has been shown to be beneficial for rehabilitation and it is desired for the participant to contribute as much as possible [20, 24, 25]. Controller A, although it did not perform as well as Controller B, had much better tracking than Controller C and resulted, on average, in more FES being applied than Controller B, while still being at a comfortable level. In fact, for the participants with NCs in Table 4-2, the standard deviation of the cadence error, average motor input, and average peak FES input is 60.7%, 52.8%, and 41.3% larger, respectively, for Controller C than Controller A.

4.7 Concluding Remarks

In this chapter, delay-dependent switching conditions, which are presented in Chapter 2, and robust cadence tracking controllers are developed for a switched uncertain nonlinear dynamic system in the presence of bounded unknown additive disturbances and an unknown time-varying input delay. A Lyapunov-like stability analysis was performed on the proposed controllers, which guarantees semi-global exponential tracking

to an ultimate bound. An extension of the proposed controller is provided to maintain motor control throughout the crank cycle (as opposed to switching the motor on and off), and for comparison, a third controller was developed assuming the system had no input delay. Experiments were performed on six able-bodied participants and four participants with NCs to compare the performance of these three controllers. The results indicate that the proposed controller exhibited the desired performance of cadence tracking with FES contributions with an average cadence error of 0.01 ± 2.00 RPM for the able-bodied participants and 0.01 ± 2.72 RPM for participants with NCs.

Table 4-2. Comparative results for able-bodied and neurological population during steady state operation: reported as Average±Standard Deviation

Controller	Participant	Cadence Error (RPM)	Motor Input (A)*	FES Input (μs)†	FES on time (%)‡
A	P1	0.06±2.16	1.60±0.13	60.97±3.40	63.71
	P2	0.06±2.66	1.94±0.29	78.54±6.82	65.19
	P3	0.05±2.38	1.65±0.15	76.64±3.97	65.95
	P4	-0.04±1.40	1.15±0.13	36.61±2.52	66.32
	P5	-0.02±1.86	1.50±0.12	31.85±1.58	67.91
	P6	-0.03±1.53	1.39±0.09	21.74±0.46	72.44
	Average	**0.01±2.00**	**1.54±0.15**	**51.06±3.12**	**66.92**
	N1	0.00±2.10	1.32±0.09	40.28±1.92	74.96
	N2	0.00±2.70	1.87±0.13	224.25±12.51	73.54
	N3	0.03±2.96	2.01±0.16	52.43±2.39	72.61
	N4	0.00±3.14	1.84±0.13	36.39±2.39	74.90
	Average	**0.01±2.72**	**1.76±0.13**	**88.34±4.81**	**74.00**
B	P1	0.01±1.27	1.73±0.14	51.04±3.44	64.02
	P2	0.05±1.52	2.05±0.26	63.79±6.95	66.21
	P3	0.03±1.22	1.86±0.15	64.05±4.16	66.50
	P4	-0.03±0.80	1.14±0.13	37.61±2.28	65.15
	P5	-0.01±1.25	1.62±0.15	30.36±1.57	68.09
	P6	-0.02±0.66	1.41±0.08	20.83±0.30	72.85
	Average	**0.00±1.12**	**1.64±0.15**	**44.61±3.12**	**67.14**
	N1	-0.03±0.87	1.30±0.08	30.98±1.12	75.43
	N2	-0.04±1.08	1.89±0.11	146.28±7.67	74.12
	N3	-0.02±0.93	2.04±0.15	39.05±2.25	73.90
	N4	-0.05±1.34	1.88±0.12	30.91±0.87	76.38
	Average	**-0.04±1.06**	**1.78±0.12**	**61.80±2.98**	**74.96**
C	P1	0.09±3.29	1.61±0.14	75.31±5.26	43.15
	P2	0.10±3.86	1.87±0.27	83.78±5.91	39.11
	P3	0.09±3.68	1.78±0.21	82.66±3.63	38.70
	P4	-0.03±1.93	1.04±0.11	35.91±3.08	48.65
	P5	-0.02±2.32	1.53±0.12	34.03±1.14	45.58
	P6	0.00±2.00	1.40±0.09	24.12±0.23	62.39
	Average	**0.04±2.85**	**1.54±0.16**	**55.97±3.25**	**46.26**
	N1	-0.02±2.70	1.27±0.10	44.87±2.13	49.17
	N2	0.23±6.72	5.55±0.93	345.80±16.83	44.23
	N3	0.08±4.11	2.05±0.26	67.09±4.91	49.30
	N4	0.08±3.97	1.87±0.16	41.57±1.47	43.05
	Average	**0.09±4.37**	**2.69±0.36**	**124.83±6.33**	**46.44**

*For post-processing, a single crank-cycle (a moving window of approximately 1.2 s) averaging filter was applied on the motor input.
†The average and standard deviation of the applied stimulation was calculated using the maximum stimulation delivered to each muscle group for each FES region.
‡This variable represents the average percentage of a single crank cycle that FES was applied to at least one of the muscle groups.

CHAPTER 5
ROBUST CADENCE TRACKING FOR SWITCHED FES-CYCLING USING A TIME-VARYING ESTIMATE OF THE UNKNOWN ELECTROMECHANICAL DELAY

Building upon our preliminary work in Chapter 4, the contributions of this chapter include innovations in the control development and stability analysis to yield exponential cadence tracking closed-loop FES/motor controllers that compensate for time-varying, nonlinear, and uncertain dynamics, unknown disturbances, switching between actuators (e.g., between muscle groups and the motor), fatigue, and the unknown time-varying muscle delay between stimulation application and the production of muscle force, called the EMD. An additional innovation is that the EMD is estimated via a function that varies with time and accounts for fatigue, which is generated using the results from Chapter 3. Furthermore, an improved delay compensation term is included in the error system to better compensate for the EMD. Control authority is maintained and efficient muscle contractions are produced through the development of FES/motor switching conditions that are both EMD and state dependent, as presented in Chapter 2. Furthermore, experiments were conducted to validate the developed control system, which produced an average cadence error of -0.01$\pm$1.35 RPM across five able-bodied participants and -0.05$\pm$1.38 RPM across four participants with NCs. A statistical analysis was performed to conclude that compensating for the delay significantly improves the cadence tracking capability when compared to a controller of the same form, but without delay compensation. This chapter provides the first control development and stability analysis that implements a time-varying EMD estimate to compensate for an unknown, nonlinear, switched, dynamic FES system with unknown time-varying input delays.

5.1 Control Development

The objective of this chapter is to track a desired cadence. The measurable position and cadence tracking errors, represented by $e, \dot{e} : \mathbb{R}_{\geq 0} \to \mathbb{R}$, respectively, are defined as

$$e \triangleq q_d - q, \tag{5–1}$$

$$\dot{e} \triangleq \dot{q}_d - \dot{q}, \tag{5–2}$$

where the desired position and cadence of the bicycle crank are sufficiently smooth and represented by $q_d, \dot{q}_d : \mathbb{R}_{\geq 0} \to \mathbb{R}$, respectively. To aid the stability analysis and compensate for the EMD, measurable auxiliary errors, represented by $r, e_u : \mathbb{R}_{\geq 0} \to \mathbb{R}$, are defined as

$$r \triangleq \dot{e} + \alpha_1 e + \alpha_2 e_u, \tag{5–3}$$

$$e_u \triangleq -\int_{t-\hat{\tau}(t)}^{t} \sigma_s(\theta)\, u(\theta)\, d\theta, \tag{5–4}$$

where $\alpha_1, \alpha_2 \in \mathbb{R}_{\geq 0}$ denote selectable constants, $\hat{\tau} : \mathbb{R}_{>0} \to \mathbb{R}$ denotes an estimate of the EMD, and $\sigma_s : \mathbb{R}_{\geq 0} \to \{0, 1\}$ denotes a switching signal that indicates when stimulation is being applied to any muscle group as designed in (2–12). A predictor for the estimate of the EMD is designed as

$$\dot{\hat{\tau}} = \text{proj}\left(g\left(t, q, \dot{q}, \hat{\tau}\right)\right), \tag{5–5}$$

where proj $(\cdot)$ represents the smooth projection operator from [111], which is designed to bound the EMD estimate such that $\underline{\tau} \leq \hat{\tau} \leq \bar{\tau}$. In (5–5), $g : \mathbb{R}_{\geq 0} \times \mathcal{Q} \times \mathbb{R} \times \mathbb{R}_{>0} \to \mathbb{R}$ represents a continuous function that updates the EMD estimate. For example, in Chapter 3, the EMD is estimated during FES-cycling by using $\hat{\tau}(t) = A + Bt + Ct^2, \forall t \in [0, 10]$, where $t \in \mathbb{R}_{\geq 0}$ denotes the cycling run time in minutes, and $A, B, C \in \mathbb{R}$ are constants with statistical information provided in Tables 3-6 and 3-9. Thus, $g(t) = B + 2Ct, \forall t \in [0, 10]$ is used during the subsequent experiments to estimate the EMD.

The open-loop error system is derived by substituting (5–2) and (5–4) into (5–3), taking the time derivative, multiplying by M, adding/subtracting $B_M^{\tau} u_{\hat{\tau}} + e$, and substituting in (2–18) to yield

$$\begin{aligned} M\dot{r} &= -Vr - e + B_M^{\tau}\left(u_{\hat{\tau}} - u_{\tau}\right) - B_E u_e - \sigma_s M \alpha_2 u \\ &\quad + \left(\sigma_{s,\hat{\tau}} M \alpha_2 - B_M^{\tau}\right) u_{\hat{\tau}} - \sigma_{s,\hat{\tau}} M \alpha_2 \dot{\hat{\tau}} u_{\hat{\tau}} + \chi, \end{aligned} \tag{5–6}$$

where $\chi : \mathcal{Q} \times \mathbb{R} \times \mathbb{R} \times \mathbb{R}_{\geq 0} \to \mathbb{R}$ is an auxiliary term defined as

$$\chi \triangleq M\ddot{q}_d + V\left(\dot{q}_d + \alpha_1 e + \alpha_2 e_u\right) + G + P + b_c\dot{q} + d + M\alpha_1\dot{e} + e - \tau_{vol},$$

which, by using Properties 2.1-2.7, can be bounded as

$$|\chi| \leq \Phi + \rho\left(\|z\|\right)\|z\|, \tag{5–7}$$

where $\rho\left(\cdot\right)$ is a radially unbounded, positive, and strictly increasing function, $\Phi \in \mathbb{R}_{>0}$ is a known constant, and $z \in \mathbb{R}^3$ is defined as

$$z \triangleq \begin{bmatrix} e & r & e_u \end{bmatrix}^T. \tag{5–8}$$

Based on (5–6) and the subsequent analysis, the motor and FES controllers are defined as

$$u_e \triangleq k_1 \text{sgn}\left(r\right) + \sigma_e\left(k_2 + k_3\right) r, \tag{5–9}$$

$$u \triangleq k_s r, \tag{5–10}$$

respectively, where $k_1, k_2, k_3, k_s \in \mathbb{R}_{>0}$ represent selectable constants, sgn $(\cdot)$ denotes the signum function, and $\sigma_e : \mathcal{Q} \times \{0,\, 1\} \to \{0,\, 1\}$ represents a switching signal for the motor as defined in (2–13).

Remark 5.1. The first motor term remains on for all time to yield exponential position and cadence tracking and to improve the overall performance. Note that during implementation, a small value is sufficient for k_1; thus, the first motor term would result in a relatively small motor input for all time. However, if it is desired to include the switching signal, σ_e, on the first motor term, refer to the development in [13]. The cost of including σ_e on the first motor term is that a uniformly ultimately bounded result is obtained, which complicates the analysis and yields poorer control performance.

Substituting (5–9) and (5–10) into (5–6) yields the closed-loop error system

$$\begin{aligned} M\dot{r} &= -Vr - e + \chi - B_E\left(k_1 \text{sgn}\left(r\right) + \sigma_e\left(k_2 + k_3\right) r\right) + k_s B_M^{\tau}\left(r_{\hat{\tau}} - r_{\tau}\right) \\ &\quad + \left(\sigma_{s,\hat{\tau}} M\alpha_2 - B_M^{\tau}\right) k_s r_{\hat{\tau}} - \sigma_s M\alpha_2 k_s r - \sigma_{s,\hat{\tau}} M\alpha_2 k_s \dot{\hat{\tau}} r_{\hat{\tau}}. \end{aligned} \tag{5–11}$$

To facilitate the subsequent analysis, LK functionals, represented by $Q_1,\, Q_2 : \mathbb{R}_{\geq 0} \to \mathbb{R}_{>0}$, are defined as

$$Q_1 \triangleq \frac{1}{2} k_s \left(\omega_4\left(\varepsilon_1\omega_1 + c_M\alpha_2\varepsilon_4\right) + \varepsilon_3\omega_3\right) \int_{t-\hat{\tau}}^{t} r\left(\theta\right)^2 d\theta, \tag{5–12}$$

$$Q_2 \triangleq \frac{\omega_2 k_s}{\bar{\tau}} \int_{t-\bar{\tau}}^{t} \int_{s}^{t} r\left(\theta\right)^2 d\theta ds, \tag{5–13}$$

and auxiliary bounding constants, represented by $\beta_1, \beta_2, \delta_1, \delta_2 \in \mathbb{R}$, are defined as

$$\begin{aligned} \beta_1 \triangleq \min\Big(&\alpha_1 - \tfrac{\varepsilon_2\alpha_2^2}{2},\; k_s\left[\tfrac{1}{2}c_m\alpha_2 - \varepsilon_3\omega_3 - \omega_2 - \tfrac{1}{2}\left(\varepsilon_1\omega_1 + c_M\alpha_2\varepsilon_4\right)\left(1+\omega_4\right)\right], \\ &\tfrac{\omega_2}{3k_s\bar{\tau}^2} - \tfrac{1}{2\varepsilon_2} - \tfrac{k_s\omega_3}{2\varepsilon_3}\left(2+\varepsilon_4\right)\Big), \end{aligned} \tag{5–14}$$

$$\begin{aligned} \beta_2 \triangleq \min\Big(&\alpha_1 - \tfrac{\varepsilon_2\alpha_2^2}{2},\; \tfrac{1}{2}c_e k_2 - k_s\left[\varepsilon_3\omega_3 + \omega_2 + \tfrac{1}{2}\left(\varepsilon_1\omega_1 + c_M\alpha_2\varepsilon_4\right)\left(1+\omega_4\right)\right], \\ &\tfrac{\omega_2}{3k_s\bar{\tau}^2} - \tfrac{1}{2\varepsilon_2} - \tfrac{k_s\omega_3}{2\varepsilon_3}\left(2+\varepsilon_4\right)\Big), \end{aligned} \tag{5–15}$$

$$\delta_1 \triangleq \min\left(\tfrac{\beta_1}{2},\; \tfrac{2\omega_2}{3\bar{\tau}\left(\omega_4\left(\varepsilon_1\omega_1 + c_M\alpha_2\varepsilon_4\right) + \varepsilon_3\omega_3\right)},\; \tfrac{1}{3\bar{\tau}}\right), \tag{5–16}$$

$$\delta_2 \triangleq \min\left(\tfrac{\beta_2}{2},\; \tfrac{2\omega_2}{3\bar{\tau}\left(\omega_4\left(\varepsilon_1\omega_1 + c_M\alpha_2\varepsilon_4\right) + \varepsilon_3\omega_3\right)},\; \tfrac{1}{3\bar{\tau}}\right), \tag{5–17}$$

$$\omega_4 = \frac{1}{1-\varepsilon_4}, \tag{5–18}$$

where $\varepsilon_1, \varepsilon_2, \varepsilon_3, \varepsilon_4, \omega_1, \omega_2, \omega_3, \omega_4 \in \mathbb{R}_{>0}$ represent selectable constants, $\Upsilon \in \mathbb{R}_{>0}$ is a known constant, and $\beta_1, \beta_2, \delta_1, \delta_2 \in \mathbb{R}_{>0}$ provided that the following sufficient conditions are satisfied

$$\alpha_1 > \frac{\varepsilon_2\alpha_2^2}{2}, \quad \omega_2 > 3k_s\bar{\tau}^2\left(\frac{1}{2\varepsilon_2} + \frac{k_s\omega_3}{2\varepsilon_3}\left(2+\varepsilon_4\right)\right), \tag{5–19}$$

$$\omega_1 \geq \frac{1}{\varepsilon_1}\max\left(\left|c_M\alpha_2 - c_b\right|, \left|c_m\alpha_2 - c_B\right|\right), \tag{5–20}$$

$$c_m\alpha_2 > \left(\varepsilon_1\omega_1 + c_M\alpha_2\varepsilon_4\right)\left(1+\omega_4\right) + 2\varepsilon_3\omega_3 + 2\omega_2, \tag{5–21}$$

$$k_1 \geq \frac{1}{c_e}\left(\Phi + k_s c_B \Upsilon\left(\bar{\tau} - \underline{\tau}\right) + k_s \bar{\tau} \Upsilon \max\left(c_b, c_m \alpha_2\right)\right), \tag{5–22}$$

$$k_2 > \frac{2k_s}{c_e}\left(\varepsilon_3 \omega_3 + \frac{1}{2}\left(1 + \omega_4\right)\left(\varepsilon_1 \omega_1 + c_M \alpha_2 \varepsilon_4\right) + \omega_2\right), \tag{5–23}$$

$$k_3 \geq \frac{k_s}{c_e} \max\left(c_b, c_m \alpha_2\right), \quad \left|\dot{\hat{\tau}}\right| \leq \varepsilon_4 < 1. \tag{5–24}$$

5.2 Stability Analysis

To facilitate the subsequent analysis, let switching times be denoted by $\{t_n^i\}$, $i \in \{m,\, e\}$, $n \in \{0, 1, 2, ...\}$, which denote the time instances when σ_e becomes zero $(i = m)$ or nonzero $(i = e)$. A positive definite and continuously differentiable common Lyapunov functional candidate $V_L : \mathcal{D} \to \mathbb{R}_{\geq 0}$ is defined as

$$V_L \triangleq \frac{1}{2}e^2 + \frac{1}{2}Mr^2 + \frac{1}{2}\omega_3 e_u^2 + Q_1 + Q_2, \tag{5–25}$$

where $\mathcal{D}, S_{\mathcal{D}} \subseteq \mathbb{R}^5$ denote open connected sets that are defined as

$$\mathcal{D} \triangleq \left\{y \in \mathbb{R}^5 \,|\, \|y\| < \gamma\right\}, \tag{5–26}$$

$$S_{\mathcal{D}} \triangleq \left\{y \in \mathbb{R}^5 \mid \|y\| < \sqrt{\tfrac{\lambda_1}{\lambda_2}}\gamma\right\}, \tag{5–27}$$

where $\gamma \in \mathbb{R}_{>0}$ represents a known constant defined as[1] $\gamma \leq \inf\left\{\rho^{-1}\left(\left(\sqrt{\min\left(\beta_1 c_m \alpha_2 k_s, \beta_2 c_e k_2\right)}, \infty\right)\right)\right\}$. Based on Property 2.1, the candidate common Lyapunov functional in (5–25) can be bounded as

$$\lambda_1 \|y\|^2 \leq V_L \leq \lambda_2 \|y\|^2, \tag{5–28}$$

where $\lambda_1, \lambda_2 \in \mathbb{R}_{>0}$ and $y \in \mathbb{R}^5$ are known and defined as

$$\lambda_1 \triangleq \frac{1}{2}\min\left(1, c_m, \omega_3\right), \quad \lambda_2 \triangleq \max\left(1, \frac{c_M}{2}, \frac{\omega_3}{2}\right),$$

[1] For a set A, the inverse image is defined as $\rho^{-1}(A) \triangleq \{a \mid \rho(a) \in A\}$.

$$y \triangleq \left[\begin{array}{cccc} z^T & \sqrt{Q_1} & \sqrt{Q_2} \end{array} \right]^T. \tag{5–29}$$

Theorem 5.1. *For the switched cycle-rider system in* (2–18)*, the motor and FES controllers defined in* (5–9) *and* (5–10) *yield semi-global exponential cadence tracking in the sense that*

$$\|y(t)\| \leq \sqrt{\frac{\lambda_2}{\lambda_1}} \|y(t_0)\| \exp\left(-\frac{1}{2}\lambda_3(t-t_0)\right), \tag{5–30}$$

$\forall t \in [t_0, \infty)$*, where* $\lambda_3 \triangleq \lambda_2^{-1} \min(\delta_1, \delta_2)$*, provided that the sufficient conditions in* (5–19)-(5–24) *are satisfied and* $y(t_0) \in S_{\mathcal{D}}$*.*

Remark 5.2. The gain conditions are feasible. As an example, if the system had the following realistic parameters (for simplicity units are not included) $c_m = 20$, $c_M = 25$, $k_m = 100, \forall m \in \mathcal{M}$, $c_b = 8$, $c_B = 10$, $\underline{\tau} = 0.07$, $\overline{\tau} = 0.1$, Φ =7.9, $\Upsilon = 20$, $k_e = 1$, and $c_e = 5$, then the gains $k_s = 0.5$, $\alpha_1 = 0.41$, $\alpha_2 = 0.41$, $k_1 = 3.8$, $k_2 = 1.7$, and $k_3 = 0.82$, would satisfy the gain conditions in (5–19)-(5–24).

Proof. For $t \in [t_0, \infty)$, let $y(t)$ be a Filippov solution to $\dot{y} \in K[h](y)$, where $h \triangleq \left[\begin{array}{ccccc} \dot{e} & \dot{r} & \dot{e}_u & \sqrt{\dot{Q}_1} & \sqrt{\dot{Q}_2} \end{array} \right]^T$ (see [110]) and $K[\cdot]$ is defined in [112]. Since the controllers in (5–9) and (5–10) are discontinuous, the time derivative of (5–25) exists within $t \in [t_0, \infty)$ almost everywhere (a.e.) such that $\dot{V}_L(y) \overset{\text{a.e.}}{\in} \dot{\tilde{V}}_L(y)$, where $\dot{\tilde{V}}_L$ represents the generalized time derivative of (5–25) along $\dot{y} = h(y)$. Using (5–3), (5–10), (5–11), and the calculus of $K[\cdot]$ from [113], and applying the Leibniz integral rule to (5–4), (5–12), and (5–13) yields

$$\begin{aligned} \dot{\tilde{V}}_L \subseteq\ & e(r - \alpha_1 e - \alpha_2 e_u) + \tfrac{1}{2}\dot{M} r^2 + r(-Vr - e + \chi + k_s K[B_M^\tau](r_{\hat{\tau}} - r_\tau) \\ & - B_E(k_1 K[\text{sgn}(r)] + K[\sigma_e](k_2 + k_3) r) - K[\sigma_s] M \alpha_2 k_s r \\ & - K[\sigma_{s,\hat{\tau}}] M \alpha_2 k_s \dot{\hat{\tau}} r_{\hat{\tau}} + (K[\sigma_{s,\hat{\tau}}] M \alpha_2 - K[B_M^\tau]) k_s r_{\hat{\tau}}\Big) \\ & + \omega_3 e_u \left(-K[\sigma_s] k_s r + K[\sigma_{s,\hat{\tau}}] k_s r_{\hat{\tau}} \left(1 - \dot{\hat{\tau}}\right)\right) + \tfrac{\omega_2 k_s}{\bar{\tau}} \left(\bar{\tau} r^2 - \int_{t-\bar{\tau}}^t r(\theta)^2 d\theta\right) \\ & + \tfrac{1}{2} k_s (\omega_4 (\varepsilon_1 \omega_1 + c_M \alpha_2 \varepsilon_4) + \varepsilon_3 \omega_3) \left(r^2 - \left(1 - \dot{\hat{\tau}}\right) r_{\hat{\tau}}^2\right), \end{aligned} \tag{5–31}$$

Table 5-1. Summary of all possible switching cases

Case Number	σ_s	$\sigma_{s,\hat{\tau}}$	$\sigma_{s,\tau}{}^*$	σ_e
1	1	1	1	0
2	1	1	1	1
3	1	1	0	1
4	1	0	1	1
5	1	0	0	1
6	0	1	1	1
7	0	0	1	1
8	0	1	0	1
9	0	0	0	1

*From (2–12), (2–19), and Property 2.8, $B_M^{\tau} = 0$ if and only if $\sigma_{s,\tau} = 0$.

where, $K\left[\text{sgn}\left(\cdot\right)\right] = SGN\left(\cdot\right)$ and $SGN\left(\cdot\right) = \{1\}$ if $\left(\cdot\right) > 0$, $[-1, 1]$ if $\left(\cdot\right) = 0$, and $\{-1\}$ if $\left(\cdot\right) < 0$. By examination of (5–31) and the switching conditions defined in (2–11), (2–12), and (2–13) it can be seen that nine unique cases exist as summarized in Table 5-1. Case 1 in Table 5-1 represents the only case when $\sigma_e = 0$, which only occurs when FES-induced muscle forces are present (i.e., $t \in \left[t_n^m, t_{n+1}^e\right)$). Cases 2-9 will subsequently be considered simultaneously by using an overall upper bound, since $\sigma_e = 1$ across each case.

During a given case each switching signal is constant; thus, Case 1 can be investigated by setting $K\left[\sigma_s\right] = 1$, $K\left[\sigma_{s,\hat{\tau}}\right] = 1$, and $K\left[\sigma_e\right] = 0$. By invoking Properties 2.1, 2.8, and 2.9 (e.g., to bound M, $K\left[B_M^{\tau}\right]$, and B_E), choosing ε_1 and ω_1 such that $\max\left(\left|c_M\alpha_2 - c_b\right|, \left|c_m\alpha_2 - c_B\right|\right) \leq \varepsilon_1\omega_1$, requiring that $\left|\dot{\hat{\tau}}\right| \leq \varepsilon_4 < 1$, and recalling that $\dot{V}_L\left(y\right) \overset{\text{a.e.}}{\in} \dot{\tilde{V}}_L\left(y\right)$ then (5–31) can be upper bounded as

$$\begin{aligned}\dot{V}_L \overset{\text{a.e.}}{\leq}\ & -\alpha_1 e^2 + \alpha_2\left|ee_u\right| + \left|r\right|\left|\chi\right| + k_s c_B\left|r\left(r_{\hat{\tau}} - r_{\tau}\right)\right| - k_1 c_e\left|r\right| - c_m\alpha_2 k_s r^2 \\ & + k_s\left(\varepsilon_1\omega_1 + c_M\alpha_2\varepsilon_4\right)\left|r r_{\hat{\tau}}\right| + k_s\omega_3\left|e_u r\right| + k_s\omega_3\left(1 - \dot{\hat{\tau}}\right)\left|e_u r_{\hat{\tau}}\right| \\ & + \tfrac{1}{2}k_s\left(\omega_4\left(\varepsilon_1\omega_1 + c_M\alpha_2\varepsilon_4\right) + \varepsilon_3\omega_3\right) r^2 + \tfrac{\omega_2 k_s}{\bar{\tau}}\left(\bar{\tau} r^2 - \int_{t-\bar{\tau}}^{t} r\left(\theta\right)^2 d\theta\right) \\ & - \tfrac{1}{2}k_s\left(\omega_4\left(\varepsilon_1\omega_1 + c_M\alpha_2\varepsilon_4\right) + \varepsilon_3\omega_3\right)\left(1 - \dot{\hat{\tau}}\right) r_{\hat{\tau}}^2.\end{aligned} \tag{5–32}$$

Selecting ω_4 according to (5–18), applying Young's Inequality, and simplifying the resulting expression yields

$$\begin{aligned}\dot{V}_L \overset{\text{a.e.}}{\leq} & -\left(\alpha_1 - \tfrac{\varepsilon_2\alpha_2^2}{2}\right)e^2 + \left(\tfrac{1}{2\varepsilon_2} + \tfrac{k_s\omega_3}{2\varepsilon_3}(2+\varepsilon_4)\right)e_u^2 + |r|\,|\chi| + k_s c_B\,|r\,(r_{\hat{\tau}} - r_\tau)| \\ & -k_1 c_e\,|r| + k_s\left(\tfrac{1}{2}(\varepsilon_1\omega_1 + c_M\alpha_2\varepsilon_4)(1+\omega_4) + \varepsilon_3\omega_3\right)r^2 - c_m\alpha_2 k_s r^2 \\ & +k_s\omega_2 r^2 - \tfrac{\omega_2 k_s}{\bar{\tau}}\int_{t-\bar{\tau}}^{t} r\,(\theta)^2\,d\theta.\end{aligned} \tag{5–33}$$

Provided that $\|y\,(\cdot)\| < \gamma,\ \forall \cdot \in [t_0, t)$, then (5–7), (5–8), (5–11), (5–29), and Properties 2.1, 2.8, and 2.9 can be used to conclude that $\dot{r}\,(\cdot) < c_1 + c_2\gamma + c_3\gamma^2 \leq \Upsilon,\ \forall \cdot \in [t_0, t)$, where $c_1, c_2, c_3 \in \mathbb{R}_{>0}$ are known constants. Hence, by invoking the MVT on the $(r_{\hat{\tau}} - r_\tau)$ term in (5–33), substituting (5–7) into (5–33), completing the squares on $-\frac{1}{2}c_m\alpha_2 k_s r^2 + |r|\,\rho\,(\|z\|)\,\|z\|$, grouping terms, and imposing (5–22) yields

$$\begin{aligned}\dot{V}_L \overset{\text{a.e.}}{\leq} & -\left(\alpha_1 - \tfrac{\varepsilon_2\alpha_2^2}{2}\right)e^2 + \left(\tfrac{1}{2\varepsilon_2} + \tfrac{k_s\omega_3}{2\varepsilon_3}(2+\varepsilon_4)\right)e_u^2 + \tfrac{1}{2c_m\alpha_2 k_s}\rho^2\,(\|z\|)\,\|z\|^2 \\ & -k_s\left(\tfrac{1}{2}c_m\alpha_2 - \tfrac{1}{2}(\varepsilon_1\omega_1 + c_M\alpha_2\varepsilon_4)(1+\omega_4) - \varepsilon_3\omega_3 - \omega_2\right)r^2 \\ & -\tfrac{\omega_2 k_s}{\bar{\tau}}\int_{t-\bar{\tau}}^{t} r\,(\theta)^2\,d\theta.\end{aligned} \tag{5–34}$$

To further simplify (5–34), the following bounds for e_u^2 (via Cauchy-Schwarz inequality), Q_1, and Q_2 can be developed

$$e_u^2 \leq \bar{\tau}k_s^2\int_{t-\bar{\tau}}^{t} r^2\,(\theta)\,d\theta, \tag{5–35}$$

$$Q_1 \leq \frac{1}{2}k_s\left(\omega_4\left(\varepsilon_1\omega_1 + c_M\alpha_2\varepsilon_4\right) + \varepsilon_3\omega_3\right)\int_{t-\bar{\tau}}^{t} r\,(\theta)^2\,d\theta, \tag{5–36}$$

$$Q_2 \leq \omega_2 k_s\int_{t-\bar{\tau}}^{t} r\,(\theta)^2\,d\theta. \tag{5–37}$$

Based on (5–35)-(5–37),

$$-\tfrac{\omega_2 k_s}{\bar{\tau}}\int_{t-\bar{\tau}}^{t} r\,(\theta)^2\,d\theta \leq -\tfrac{\omega_2}{3k_s\bar{\tau}^2}e_u^2 - \tfrac{2\omega_2}{3\bar{\tau}(\omega_4(\varepsilon_1\omega_1 + c_M\alpha_2\varepsilon_4) + \varepsilon_3\omega_3)}Q_1 - \tfrac{1}{3\bar{\tau}}Q_2. \tag{5–38}$$

Using the fact that $\|y\| \geq \|z\|$ and using (5–14), (5–16), (5–28), and (5–38)

$$\dot{V}_L \overset{\text{a.e.}}{\leq} -\frac{\delta_1}{\lambda_2}V_L, \tag{5–39}$$

$\forall t \in \left[t_n^m, t_{n+1}^e\right)$, provided that $y(t) \in \mathcal{D}, \forall t \in \left[t_n^m, t_{n+1}^e\right)$ and $\|y(\cdot)\| < \gamma, \ \ \forall \cdot \in [t_0, t)$, where the latter expression is equivalent to $y(\cdot) \in \mathcal{D}, \forall \cdot \in [t_0, t)$.

Cases 2-9 from Table 5-1 represent the cases when $\sigma_e = 1$ (i.e., $t \in \left[t_n^e, t_{n+1}^m\right)$). To facilitate the subsequent analysis an overall upper bound is determined for Cases 2-9. Note that the following inequality holds by individually considering each case, selecting ε_1 and ω_1 such that $c_M\alpha_2 - c_b \leq |c_M\alpha_2 - c_b| \leq \varepsilon_1\omega_1$ and $c_B - c_m\alpha_2 \leq |c_m\alpha_2 - c_B| \leq \varepsilon_1\omega_1$, and using Properties 2.1 and 2.8:

$$k_s \left|\sigma_{s,\hat{\tau}} M\alpha_2 - B_M^\tau\right| |rr_{\hat{\tau}}| \ \ \leq \ \ k_s\varepsilon_1\omega_1 |rr_{\hat{\tau}}| + k_s \max(c_b, c_m\alpha_2) |rr_{\hat{\tau}}|. \tag{5–40}$$

Using the inequality in (5–40), invoking Properties 2.1, 2.8, and 2.9, recalling that $\dot{V}_L(y) \overset{\text{a.e.}}{\in} \dot{\tilde{V}}_L(y)$, canceling common terms, and requiring $\left|\dot{\hat{\tau}}\right| \leq \varepsilon_4 < 1$, the inequality in (5–31) can be upper bounded for Cases 2-9 as

$$\begin{aligned}
\dot{V}_L \ \overset{\text{a.e.}}{\leq} \ & -\alpha_1 e^2 + \alpha_2 |ee_u| + |r||\chi| - c_e k_1 |r| + k_s(\varepsilon_1\omega_1 + c_M\alpha_2\varepsilon_4)|rr_{\hat{\tau}}| \\
& -c_e(k_2 + k_3) r^2 + k_s \max(c_b, c_m\alpha_2)|rr_{\hat{\tau}}| + k_s c_B |r(r_{\hat{\tau}} - r_\tau)| \\
& + k_s\omega_3 |e_u r| + k_s\omega_3 \left(1 - \dot{\hat{\tau}}\right)|e_u r_{\hat{\tau}}| + \tfrac{1}{2}k_s(\omega_4(\varepsilon_1\omega_1 + c_M\alpha_2\varepsilon_4) + \varepsilon_3\omega_3) r^2 \\
& - \tfrac{1}{2}k_s(\omega_4(\varepsilon_1\omega_1 + c_M\alpha_2\varepsilon_4) + \varepsilon_3\omega_3)\left(1 - \dot{\hat{\tau}}\right) r_{\hat{\tau}}^2 + \tfrac{\omega_2 k_s}{\bar{\tau}}\left(\bar{\tau} r^2 - \int_{t-\bar{\tau}}^t r(\theta)^2 d\theta\right).
\end{aligned} \tag{5–41}$$

Applying the MVT, selecting the gain conditions in (5–22) and (5–24), and substituting (5–7) into (5–41) yields

$$\begin{aligned}
\dot{V}_L \ \overset{\text{a.e.}}{\leq} \ & -\alpha_1 e^2 + \alpha_2 |ee_u| - c_e k_2 r^2 + \|r\| \rho(\|z\|) \|z\| + k_s(\varepsilon_1\omega_1 + c_M\alpha_2\varepsilon_4)|rr_{\hat{\tau}}| \\
& + k_s\omega_3 |e_u r| + k_s\omega_3 \left(1 - \dot{\hat{\tau}}\right)|e_u r_{\hat{\tau}}| - \tfrac{\omega_2 k_s}{\bar{\tau}} \int_{t-\bar{\tau}}^t r(\theta)^2 d\theta \\
& + \tfrac{1}{2}k_s(\omega_4(\varepsilon_1\omega_1 + c_M\alpha_2\varepsilon_4) + \varepsilon_3\omega_3) r^2 + \omega_2 k_s r^2 \\
& - \tfrac{1}{2}k_s(\omega_4(\varepsilon_1\omega_1 + c_M\alpha_2\varepsilon_4) + \varepsilon_3\omega_3)\left(1 - \dot{\hat{\tau}}\right) r_{\hat{\tau}}^2.
\end{aligned} \tag{5–42}$$

A further upper bound for (5–42) is obtained by following a similar development as for Case 1 as

$$\dot{V}_L \overset{\text{a.e.}}{\leq} -\frac{\delta_2}{\lambda_2} V_L, \tag{5–43}$$

$\forall t \in \left[t_n^e, t_{n+1}^m\right)$, provided $y(t) \in \mathcal{D}$, $\forall t \in \left[t_n^e, t_{n+1}^m\right)$, and $y(\cdot) \in \mathcal{D}, \forall \cdot \in [t_0, t)$.

Upper bounding (5–39) and (5–43), and defining $\lambda_3 \triangleq \lambda_2^{-1} \min(\delta_1, \delta_2)$ yields an overall upper bound $\forall t \in [t_0, \infty)$ as

$$\dot{V}_L \overset{\text{a.e.}}{\leq} -\lambda_3 V_L, \tag{5–44}$$

which confirms that (5–25) is a common Lyapunov-like function for every case. Solving the differential inequality in (5–44) yields

$$V_L(t) \leq V_L(t_0) \exp\left(-\lambda_3 (t - t_0)\right), \ \forall t \in [t_0, \infty), \tag{5–45}$$

provided that $y(t) \in \mathcal{D}, \forall t \in [t_0, \infty)$. The result in (5–30) is obtained by using (5–28) and (5–45). A sufficient condition for $y(t) \in \mathcal{D}, \forall t \in [t_0, \infty)$ is that the gains k_m, k_e, k_s, α_1, α_2, k_1, k_2, and k_3 are selected so that $y(t_0) \in S_{\mathcal{D}}$. From (5–9), (5–10), (5–25) and (5–44), $e, r, e_u, u, u_e \in \mathcal{L}_\infty$ and the remaining signals are bounded. □

5.3 Experiment

Henceforth, we will label the motor and FES controllers defined in (5–9) and (5–10), the subsequently defined "delay-free" version of (5–9) and (5–10), and $u_e = 0$ and $u = 0$ (i.e., no motor or FES assistance) as Controllers A, B, and C, respectively. Controller B represents the motor and FES controllers that compensate for the switched system in (2–18) if the EMD was assumed to be negligible. Controller B is generated by redefining (5–3) as $r \triangleq \dot{e} + \alpha_1 e$, redefining (2–11) and (2–13) as in [3]

$$\sigma_m(q) \triangleq \begin{cases} 1, & q \in \mathcal{Q}_m \\ 0, & \text{otherwise} \end{cases}, \ \sigma_e(q) \triangleq \begin{cases} 1, & q \in \mathcal{Q}_{KDZ} \\ 0, & \text{otherwise} \end{cases}, \tag{5–46}$$

and using (5–9) and (5–10) with these modified signals. Therefore, insights on the importance/effect of EMD compensation can be obtained by comparing the performance of Controllers A and B.

Table 5-2. Participant Demographics

Participant	Age	Sex	Condition	Time Since Diagnosis
S1	22	F	None	- -
S2	22	M	None	- -
S3	22	F	None	- -
S4	22	F	None	- -
S5	21	F	None	- -
N1	42	F	Cerebral Palsy	42yr
N2	55	F	Multiple Sclerosis	25yr
N3	54	M	Multiple Sclerosis	10yr
N4	26	M	Spina Bifida (L5-S1)	26yr

5.3.1 Experimental Testbed

The experimental testbed used in this chapter is the FES cycle that is introduced in Chapter 2.

5.3.2 Experimental Methods

The demographics of the participants included in this study are summarized in Table 5-2, where able-bodied participants and participants with NCs are indicated by an identifying number preceded by the letter “S” or “N”, respectively. Written informed consent was provided by each participant as approved by the University of Florida Institutional Review Board (IRB201600881). To allow for equal comparison and to represent the clinical case when a participant is unable to contribute volitionally, passive therapy experiments were performed on the able-bodied participants, which consisted of the rider being instructed to remain passive (i.e., provide no volitional effort) and the rider being blind to the tracking performance. To investigate various clinical conditions, active therapy experiments were performed on the participants with NCs, which consisted of the rider being shown a real-time plot of the actual versus desired cadence, and each rider was asked to contribute to the tracking objective to the best of their ability.

In preparation for the experiments, the participant was secured on the cycle seat with their feet in orthotic boots (Össur Rebound Air Tall) connected at the pedals and electrodes (Axelgaard ValuTrode CF7515) were placed on the lower limb muscles (i.e.,

gluteals, hamstrings, quadriceps) and connected to the stimulator. Measurements (i.e., seat position, limb lengths, etc.) were then obtained as detailed in [3] to calculate the desired regions of the crank for a contraction of each muscle group (i.e., $\mathcal{Q}_m$). The cycle speed was then continuously increased to 50 RPM via the motor and stimulation was applied in an open-loop manner to determine a comfort limit on the stimulation for each muscle group. During the subsequent experiments, the FES inputs were saturated at a comfort limit indicated by the participant for each muscle group.

A preliminary trial was performed before each experiment that used Controller A to obtain an initial estimate of the EMD, $\hat{\tau}(t_0)$. Using the procedure detailed in Chapter 3, $\hat{\tau}(t_0)$ was obtained by fixing the crank at an efficient angle and then stimulating the quadriceps of the dominant leg for 0.25 s. The stimulation and torque data were then examined to calculate the CD25 measurement of the EMD, which was used as $\hat{\tau}(t_0)$. To update the EMD, recall that $g(t) = B + 2Ct$ was used, where the terms B and C are obtained by using Table 3-9 in Chapter 3.

Remark 5.3. Note that although the EMD may vary between each muscle group and each leg, the problem was simplified by using the measured EMD from the quadriceps of the dominant leg as $\hat{\tau}(t_0)$. From experience, the quadriceps muscle from the dominant leg tends to produce the highest torques. Furthermore, although the EMD is measured six different ways in Chapter 3, this chapter uses the CD25 measurement to represent the EMD, which represents the delay between the onset of stimulation to the instant that the output torque reached 25% of the maximum torque level.

After the cycle speed was increased to 50 RPM during the first 20 s, Controller A, B, or C was implemented for the remaining 120 s, called the steady-state period, to track a constant desired cadence of 50 RPM. The controllers were implemented at the start of the steady-state period so that the initial tracking errors and stimulation inputs would be minimal, which consequently increases the comfort of the participant and delays the onset of fatigue. Experiments using Controllers A and B for the able-bodied participants

were implemented in a random order. Controller C was implemented before Controller A for the participants with NCs since Controller C provides no FES inputs, which would yield minimal fatigue and provide an unassisted and unfatigued baseline performance for each participant. No practice was allowed for the able-bodied participants; however, a single practice trial was permitted for each controller for the participants with NCs since they provided volition. Between each experiment, rest periods of five minutes were provided.

5.4 Results

5.4.1 Results from Able-Bodied Participants

To compare Controllers A and B, descriptive statistics of the experimental results (i.e., the peak and root mean square (RMS) cadence errors, FES effort, and motor effort) are included in Table 5-3 for the able-bodied participants. To visually depict typical results for the able-bodied participants, the cadence tracking performance and control inputs are shown in Figure 5-1 for Participant S1 using Controllers A and B. On average across the able-bodied participants, Controllers A and B had a cadence tracking error of -0.01$\pm$1.35 RPM and -0.01$\pm$2.84 RPM, respectively, and FES was applied (to a minimum of one muscle group) 62.3% and 61.2% of the time, respectively.

5.4.1.1 Statistical analysis

Using the data provided in Table 5-3, paired difference statistical tests were performed on the RMS and peak cadence errors, the average and standard deviation of the motor effort, the percent of FES application time, and the average and standard deviation of the FES effort, to compare the performance of Controllers A and B. The Shapiro-Wilk's normality test was used to conclude that the paired difference data was approximately normal. One-sided paired t-tests were executed to conclude that the peak (P-Value = 0.001) and RMS (P-Value < 0.001) cadence errors, and the motor (P-Value < 0.001) and FES (P-Value = 0.027) standard deviations were significantly smaller for Controller A than for Controller B. However, Controllers A and B had no significant effect

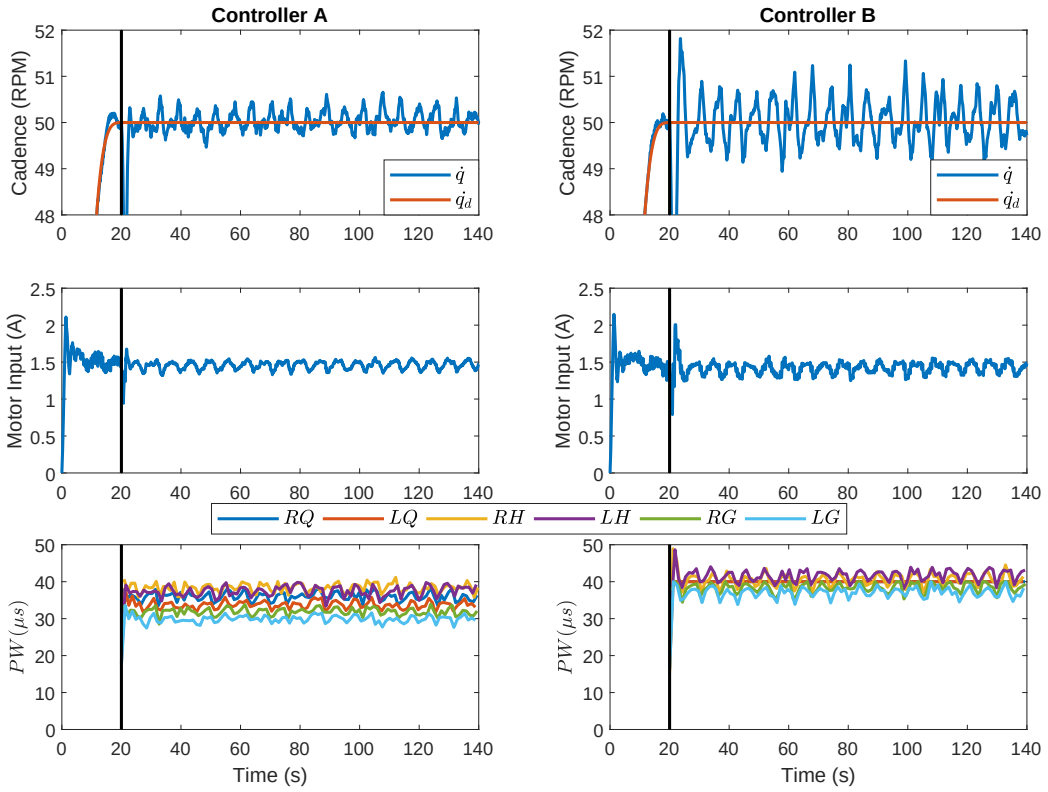

Figure 5-1. The actual ($\dot{q}$) versus desired ($\dot{q}_d$) cadence (top), motor input (middle), and peak stimulation input (i.e., pulsewidth or PW) for each FES region applied to the right (R) and left (L) gluteal (G), hamstring (H), and quadriceps (Q) (bottom) are depicted for Controller A (left) and Controller B (right) for participant S1. The black line indicates steady-state and a 1.2 s moving average filter was applied to $\dot{q}$ and the motor input.

Table 5-3. Experimental results for the able-bodied participants during steady state

Controller	Participant	RMS Cadence Error (RPM)	Peak Cadence Error (RPM)*	Motor Effort (A)†	FES Effort (μs)‡
A	S1	1.69	7.81	1.46±1.09	34.52±1.47
	S2	1.72	4.81	1.73±1.13	36.70±1.83
	S3	1.24	4.10	1.70±0.82	39.47±1.93
	S4	1.02	5.63	1.78±0.80	25.56±1.14
	S5	1.11	3.47	1.53±0.83	18.22±0.38
	Average	**1.35**	**5.17**	**1.64±0.93**	**30.89±1.35**
B	S1	2.95	14.18	1.42±1.98	39.49±2.14
	S2	3.67	12.14	1.75±2.33	38.06±2.06
	S3	2.71	6.87	1.63±1.61	38.06±3.02
	S4	2.45	10.19	1.89±1.78	27.22±1.27
	S5	2.46	9.38	1.53±1.58	19.10±0.65
	Average	**2.85**	**10.55**	**1.65±1.86**	**32.39±1.83**

*The maximum value of $|\dot{e}|$.
†The average $\pm$ standard deviation of $|u_E|$.
‡The average $\pm$ standard deviation of the maximum stimulation delivered to each muscle group within each FES region.

on the percent of FES application time (P-Value = 0.176), or the average motor (P-Value = 0.377) and FES (P-Value = 0.176) efforts.

5.4.1.2 Discussion

Consistent with the statistical results, Figure 5-1 indicates that Controller A reduced the cadence tracking error and the variance of the motor and FES inputs for Participant S1, when compared to Controller B. It can further be seen from Figure 5-1 that the FES inputs tended to be higher for Controller B than for Controller A for Participant S1, which was not true in general for each participant. Overall, it can be concluded that Controller A, relative to Controller B, improved the cadence tracking performance while simultaneously reducing the variance of the control inputs.

5.4.2 Results from Participants with NCs

Since Controller A improved the tracking performance relative to Controller B, comparative experiments were performed on the participants with NCs using Controller C instead of Controller B. Recall that Controller C provides no assistance to determine the participant's ability to track the desired cadence on their own volition. Descriptive

Table 5-4. Experimental results for the participants with NCs during steady state

Controller	Participant	RMS Cadence Error (RPM)	Peak Cadence Error (RPM)*	Motor Input (A)†	FES Input (μs)‡
A	N1	1.53	4.70	1.25$\pm$0.88	18.11$\pm$2.17
	N2	1.75	4.88	1.74$\pm$1.12	26.11$\pm$0.75
	N3	1.26	4.93	1.76$\pm$1.07	44.42$\pm$1.82
	N4	1.01	5.37	1.34$\pm$0.77	32.98$\pm$1.51
	Average	**1.39**	**4.97**	**1.52$\pm$0.96**	**30.40$\pm$1.56**
C	N1	3.62	14.08	0.00$\pm$0.00	0.00$\pm$0.00
	N2	3.39	24.36	0.00$\pm$0.00	0.00$\pm$0.00
	N3	2.62	14.18	0.00$\pm$0.00	0.00$\pm$0.00
	N4	4.53	27.94	0.00$\pm$0.00	0.00$\pm$0.00
	Average	**3.54**	**20.14**	**0.00$\pm$0.00**	**0.00$\pm$0.00**

*The maximum value of $|\dot{e}|$.
†The average $\pm$ standard deviation of $|u_E|$.
‡The average $\pm$ standard deviation of the maximum stimulation delivered to each muscle group within each FES region.

statistics of the experimental results, for Controllers A and C, are included in Table 5-4 for the participants with NCs. Typical cadence tracking results for the participants with NCs, for both controllers, are represented in Figure 5-2 for Participant N1. On average across the participants with NCs, FES was applied 64.8% of the time for Controller A, and the average cadence tracking error was -0.05$\pm$1.38 RPM and 0.53$\pm$3.37 RPM for Controllers A and C, respectively.

5.4.2.1 Statistical analysis

Using the cadence data in Table 5-4, paired statistical tests (i.e., one-sided paired t-test and Shapiro-Wilk's test) were performed to conclude normality of the data and that peak (P-Value = 0.011) and RMS (P-Value = 0.010) cadence errors were significantly smaller for Controller A than for Controller C. The cadence tracking performance for Participant N1 and both controllers can also be seen in Figure 5-2, which further emphasizes the improved tracking performance under Controller A relative to Controller C. It can thus be concluded that Controller A tracked the desired cadence better than Controller C, which was expected due to Controller C providing no motor or FES assistance.

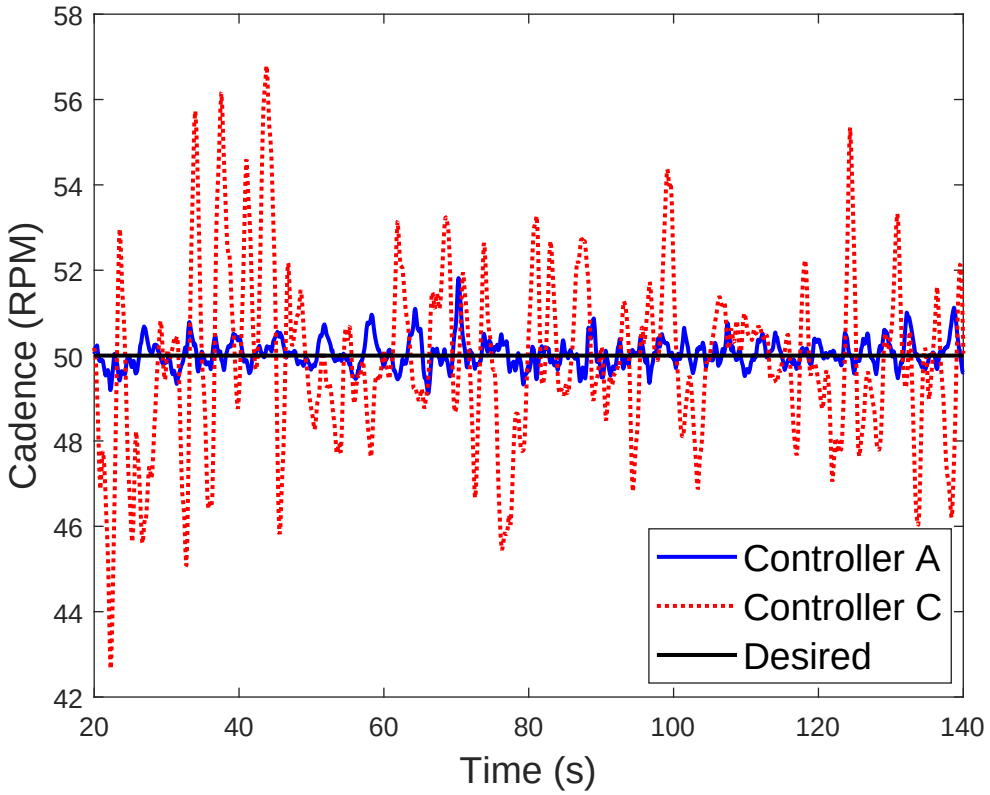

Figure 5-2. The filtered (1.2 s moving average filter) cadence tracking performance is depicted for participant N1 and Controllers A (blue) and C (red).

5.4.2.2 Discussion

Overall, the results for Controller A in Tables 5-3 and 5-4, and Figures 5-1 and 5-2 demonstrate the ability of Controller A to achieve cadence tracking despite uncertain volitional contributions from each participant with a NC, uncertainties and nonlinearities in the dynamics, a time-varying and unknown EMD, unknown disturbances, and a range of capabilities of each participant (e.g., due to some participants being able-bodied and others having a variety of NCs). Thus, Controller A has proven to be a safe and effective cadence tracking controller for individuals with varied capabilities during both active and passive therapy exercises.

5.5 Concluding Remarks

In this chapter, FES/motor controllers and a time-varying estimate of the EMD are developed to compensate for a switched, delayed, nonlinear, and uncertain FES cycle system with uncertain volitional effort and disturbances. A switched Lyapunov stability analysis was performed to conclude exponential cadence tracking. Control authority was maintained and efficient muscle contractions were produced through the development of EMD and state dependent switching signals, which are included in Chapter 2. To enable comparisons, an alternative control system was created under the assumption that the EMD was negligible, with the same form as the developed controllers. Passive therapy experiments were then conducted on five able-bodied participants to compare the developed control system against the "EMD-free" control system, which resulted in cadence errors of 0.01 ± 1.35 RPM and -0.01 ± 2.84 RPM, respectively, and it was concluded that compensating for the EMD significantly improved the cadence tracking performance. Using the developed controllers, active therapy experiments were subsequently conducted on four participants with NCs and produced an average cadence error of -0.05 ± 1.38 RPM.

CHAPTER 6
SATURATED CONTROL OF A SWITCHED FES-CYCLE WITH AN UNKNOWN TIME-VARYING INPUT DELAY

In this chapter, saturated FES and motor controllers are developed for an FES-cycle that ensure safety and comfort of the participant, while likewise being robust to uncertain parameters in the dynamics, unknown disturbances, and an unknown time-varying input delay. Since each participant has varying levels of sensitivity to FES it is desired to saturate/bound the stimulation input to ensure comfort and safety. A Lyapunov-based stability analysis is performed to ensure uniformly ultimately bounded cadence tracking, and a preliminary experiment was performed on a single participant to validate the designed control system and demonstrated a cadence of 48.24 $\pm$ 2.09 RPM for a desired cadence of 50 RPM. This chapter demonstrates the first use of saturated control to compensate for the EMD during a coordinated FES task (e.g., FES-cycling) that requires switching control between multiple electrodes and a motor.

6.1 Control Development

One objective is for the bicycle crank to track a desired cadence, denoted by $\dot{q}_d : \mathbb{R}_{\geq 0} \to \mathbb{R}$, despite the dynamic model being uncertain and having an unknown time-varying input delay. To quantify the control objective a measurable cadence tracking error, $\dot{e} : \mathbb{R}_{\geq 0} \to \mathbb{R}$, is defined as

$$\dot{e} \triangleq \dot{q}_d - \dot{q}. \tag{6–1}$$

A measurable auxiliary tracking error, $r : \mathbb{R}_{\geq 0} \to \mathbb{R}$, is defined as

$$r \triangleq \dot{e} + \alpha e_u, \tag{6–2}$$

where $\alpha \in \mathbb{R}_{\geq 0}$ is a selectable constant. The auxiliary error signal, $e_u : \mathbb{R}_{\geq 0} \to \mathbb{R}$, is defined as

$$e_u \triangleq -\int_{t-\hat{\tau}}^{t} \sigma_s(\theta)\, u(\theta)\, d\theta, \tag{6–3}$$

and is used to inject a delay-free input into the closed-loop error system. The constant estimate of the delay is denoted by $\hat{\tau} \in \mathbb{R}_{>0}$ and by Property 2.11, the delay estimation error, $\tilde{\tau} = \tau - \hat{\tau}$, can be upper bounded such that $|\tilde{\tau}| \leq \overline{\tilde{\tau}}$, where $\overline{\tilde{\tau}} \in \mathbb{R}_{>0}$ is a known constant. The switching signal, $\sigma_s : \mathbb{R}_{\geq 0} \to \{0, 1\}$, is defined in (2–12) and is used to indicate when stimulation is applied.

The open-loop error system is obtained by substituting (6–1) and (6–3) into (6–2) and taking the time derivative of (6–2), solving (2–18) for $\ddot{q}$ and substituting into the time derivative of (6–2), and adding and subtracting $\frac{B_M^\tau}{M} u_{\hat{\tau}}$ to yield

$$\dot{r} = \chi + \tfrac{B_M^\tau}{M} \left(u_{\hat{\tau}} - u_\tau \right) - \tfrac{B_E}{M} u_e + \left(\sigma_{s,\hat{\tau}} \alpha - \tfrac{B_M^\tau}{M} \right) u_{\hat{\tau}} - \sigma_s \alpha u, \tag{6–4}$$

where $\chi : \mathcal{Q} \times \mathbb{R} \times \mathbb{R}_{\geq 0} \to \mathbb{R}$ is defined as $\chi \triangleq \ddot{q}_d + \frac{1}{M} \left[V \dot{q} + G + P + b_c \dot{q} + d \right]$. By using Properties 2.1-2.6, (6–1), and (6–2), the auxiliary term χ can be bounded as

$$|\chi| \leq \Phi + \rho \left(\|z\| \right) \|z\|, \tag{6–5}$$

where $\Phi \in \mathbb{R}_{>0}$ is a known constant, $\rho(\cdot)$ is a positive, strictly increasing, radially unbounded, and globally invertible function, and $z \in \mathbb{R}^2$ is a composite error vector defined as

$$z \triangleq \begin{bmatrix} r & e_u \end{bmatrix}^T. \tag{6–6}$$

A secondary control objective is to design saturated FES and motor controllers that can meet the cadence tracking objective. Based on the open-loop error system in (6–4), the bound in (6–5), and the subsequent stability analysis, the FES and motor control inputs are designed as

$$u \triangleq k_s \tanh(r), \tag{6–7}$$

and

$$u_e \triangleq k_1 \text{sgn}(r) + k_2 \tanh(r), \tag{6–8}$$

respectively, where $k_s,\, k_1,\, k_2 \in \mathbb{R}_{>0}$ are selectable constants and sgn $(\cdot)$ denotes the signum function.

Remark 6.1. A sliding mode term is included in the motor controller to achieve asymptotic cadence tracking if the motor control input was always available. However, since the FES controller does not have a sliding mode term, the overall cadence tracking result yields an ultimate bound. Therefore, the sliding mode term could be removed from the motor controller if desired, and an overall maximum ultimate bound could be determined.

Notice that the FES and motor control inputs are bounded by selectable gain constants, since $|u| \leq k_s$ and $|u_e| \leq k_1 + k_2$. Note, the stimulation input (i.e. pulse width) to each of the rider's muscles is defined as $u_m \triangleq k_m \sigma_m u, \forall m \in \mathcal{M}$, and the stimulation input can be bounded by $|u_m| \leq k_m k_s, \forall m \in \mathcal{M}$. Likewise, the current input to the motor is defined as $u_E \triangleq k_e \sigma_e u_e$ and can be bounded by $|u_E| \leq k_e \left(k_1 + k_2\right)$. The bounds on the FES controller allow for the maximum stimulation input to be limited, resulting in a safer and more comfortable experience for the participant. Likewise, the current input into the motor is limited to ensure the input does not exceed the motor specifications. Substituting (6–7) and (6–8) into (6–4) yields the closed-error system

$$\begin{aligned} \dot{r} &= \chi + k_s \tfrac{B_M^\tau}{M} \left(\tanh\left(r_{\hat{\tau}}\right) - \tanh\left(r_\tau\right)\right) - \tfrac{B_E}{M} \left(k_1 \text{sgn}\left(r\right) + k_2 \tanh\left(r\right)\right) \\ &\quad + \left(\sigma_{s,\hat{\tau}} \alpha - \tfrac{B_M^\tau}{M}\right) k_s \tanh\left(r_{\hat{\tau}}\right) - \sigma_s \alpha k_s \tanh\left(r\right). \end{aligned} \tag{6–9}$$

To facilitate the subsequent stability analysis, and based on the closed-loop error system in (6–9), the following LK functionals $Q_1,\, Q_2 : \mathbb{R}_{\geq 0} \to \mathbb{R}_{>0}$ are defined as

$$Q_1 \triangleq \frac{1}{2} \left(\varepsilon_1 \omega_1 + \varepsilon_2 \omega_2\right) k_s \int_{t-\hat{\tau}}^{t} \tanh^2\left(r\left(\theta\right)\right) d\theta, \tag{6–10}$$

$$Q_2 \triangleq \frac{\omega_3 k_s}{\hat{\tau}} \int_{t-\hat{\tau}}^{t} \int_{s}^{t} \tanh^2\left(r\left(\theta\right)\right) d\theta ds, \tag{6–11}$$

where $\varepsilon_1, \varepsilon_2, \omega_1, \omega_2, \omega_3 \in \mathbb{R}_{>0}$ are selectable constants. Further, the auxiliary bounding constants $\beta, \beta_1, \beta_2, \delta \in \mathbb{R}_{>0}$ are defined as

$$\beta \triangleq \min\left(\beta_1, \beta_2\right), \tag{6–12}$$

$$\beta_1 \triangleq \min\left(k_s\left(\tfrac{1}{2}\alpha - \varepsilon_1\omega_1 - \varepsilon_2\omega_2 - \omega_3\right),\ \tfrac{\omega_3}{3k_s\hat{\tau}^2} - \tfrac{\omega_1 k_s}{\varepsilon_1},\ \tfrac{\omega_3}{3\hat{\tau}\left(\frac{1}{2}(\varepsilon_1\omega_1+\varepsilon_2\omega_2)\right)},\ \tfrac{1}{3\hat{\tau}}\right), \tag{6–13}$$

$$\beta_2 \triangleq \min\left(\tfrac{c_e}{2c_M}k_{21} - k_s\left(\varepsilon_1\omega_1 + \varepsilon_2\omega_2 + \omega_3\right),\ \tfrac{\omega_3}{3k_s\hat{\tau}^2} - \tfrac{\omega_1 k_s}{\varepsilon_1},\ \tfrac{\omega_3}{3\hat{\tau}\left(\frac{1}{2}(\varepsilon_1\omega_1+\varepsilon_2\omega_2)\right)},\ \tfrac{1}{3\hat{\tau}}\right), \tag{6–14}$$

$$\delta \triangleq \max\left(\tfrac{1}{\alpha k_s}, \tfrac{c_M}{2c_e k_{21}}\right), \tag{6–15}$$

and the gain conditions are defined as

$$\alpha > 2\left(\varepsilon_1\omega_1 + \varepsilon_2\omega_2 + \omega_3\right), \quad \omega_3 > \frac{3k_s^2\hat{\tau}^2\omega_1}{\varepsilon_1}, \tag{6–16}$$

$$\varepsilon_2\omega_2 \geq \max\left(\left|\alpha - \tfrac{c_b}{c_M}\right|, \left|\alpha - \tfrac{c_B}{c_m}\right|\right), \tag{6–17}$$

$$k_1 \geq \tfrac{c_M}{c_e}\left(\Phi + k_s\overline{\tilde{\tau}}\Upsilon\tfrac{c_B}{c_m} + k_s\hat{\tau}\Upsilon\max\left(\tfrac{c_b}{c_M}, \alpha\right)\right), \tag{6–18}$$

$$k_2 \geq k_{21} + k_{22}, \tag{6–19}$$

$$k_{21} > \tfrac{2c_M k_s}{c_e}\left(\varepsilon_1\omega_1 + \varepsilon_2\omega_2 + \omega_3\right), \tag{6–20}$$

$$k_{22} \geq \tfrac{k_s c_M}{c_e}\max\left(\tfrac{c_b}{c_M}, \alpha\right), \tag{6–21}$$

where $k_{21}, k_{22} \in \mathbb{R}_{>0}$ are selectable constants, and $\Upsilon \in \mathbb{R}_{>0}$ is a subsequently defined known bounding constant.

6.2 Stability Analysis

Let switching times be denoted by $\{t_n^i\}$, $i \in \{m, e\}$, $n \in \{0, 1, 2, ...\}$, which represent the time instances when B_E becomes zero $(i = m)$, or the time instances when B_E becomes nonzero $(i = e)$. Let $V_L : \mathcal{D} \to \mathbb{R}_{\geq 0}$ denote a positive definite, continuously differentiable, common Lyapunov function candidate on a domain $\mathcal{D} \subseteq \mathbb{R}^4$, that is defined as

$$V_L \triangleq \ln\left(\cosh\left(r\right)\right) + \frac{1}{2}\omega_1 e_u^2 + Q_1 + Q_2. \tag{6–22}$$

By using (2–23), (6–22) can be bounded as

$$\underbrace{\lambda_1 \ln\left(\cosh\left(\|y\|\right)\right)}_{\phi_1(\|y\|)} \leq V_L \leq \underbrace{\lambda_2 \|y\|^2}_{\phi_2(\|y\|)}, \tag{6–23}$$

where $y \in \mathbb{R}^4$ is defined as

$$y \triangleq \begin{bmatrix} z^T & \sqrt{Q_1} & \sqrt{Q_2} \end{bmatrix}^T, \tag{6–24}$$

and $\lambda_1, \lambda_2 \in \mathbb{R}_{>0}$ are known constants defined as

$$\lambda_1 \triangleq \min\left(1, \frac{\omega_1}{2}\right), \quad \lambda_2 \triangleq \max\left(1, \frac{\omega_1}{2}\right).$$

Theorem 6.1. *For the cycle-rider dynamics in* (2–18)*, along with Properties 2.1-2.11, the FES and motor control inputs defined in* (6–7) *and* (6–8) *ensure uniformly ultimately bounded tracking in the sense that*

$$\|y(t)\| < \overline{d}, \quad \forall t > T\left(\overline{d}, \|y(t_0)\|\right), \tag{6–25}$$

where $\overline{d}, T \in \mathbb{R}_{>0}$ *denote the ultimate bound, and the ultimate time to reach the ultimate bound, respectively, provided the gain conditions in* (6–16)-(6–21) *are satisfied, along with the following sufficient gain condition*

$$\tfrac{\beta}{2\delta} \geq \rho^2(\overline{\mu})(\overline{\mu}+1)^2, \tag{6–26}$$

where $\overline{\mu} \in \mathbb{R}_{>0}$ *is defined as* $\overline{\mu} \triangleq \max\left(\overline{d}, \|y(t_0)\|\right)$.

Remark 6.2. It can be proven that these gain conditions are feasible. As an example, if the system had the following realistic parameters (for simplicity units are not included) $c_m = 20$, $c_M = 25$, $k_m = 1000, \forall m \in \mathcal{M}$, $c_b = 80$, $c_B = 100$, $\hat{\tau} = 0.08$, $\overline{\tilde{\tau}} = 0.015$, Φ =0.11, $\rho(\|y\|) = 0.023 + 0.002\|y\|$, $\Upsilon = 6$, $k_e = 1$, and $c_e = 5$, and provided that $\|y(t_0)\| \leq 6$, then the gains $k_s = 0.2$, $\alpha = 4.1$, $k_1 = 2.9$, and $k_2 = 8.2$, would satisfy the gain conditions in (6–16)-(6–26). Note that these sufficient gain conditions represent a worst-case scenario and in practice the gains can be relaxed as discussed in [1].

Table 6-1. Summary of all possible switching cases

Case Number	σ_s	$\sigma_{s,\hat{\tau}}$	$\sigma_{s,\tau}$*	σ_e†
1	1	1	1	0
2	1	1	1	1
3	1	1	0	1
4	1	0	1	1
5	1	0	0	1
6	0	1	1	1
7	0	0	1	1
8	0	1	0	1
9	0	0	0	1

*From (2–19), (2–12), and Property 2.8, $B_M^{\tau} = 0$ if and only if $\sigma_{s,\tau} = 0$.
†From (2–20) and Property 2.9, $B_E = 0$ if and only if $\sigma_e = 0$.

Proof. Since the motor controller, B_E, and B_M^{τ} are discontinuous, a generalized solution to the time derivative of (6–22) exists almost everywhere (a.e.) within $t \in [t_0, \infty)$, and $\dot{V}_L(y) \overset{\text{a.e.}}{\in} \dot{\tilde{V}}_L(y)$, where $\dot{\tilde{V}}_L$ is the generalized time derivative of V_L. Let $y(t)$ for $t \in [t_0, \infty)$ be a Filippov solution to the differential inclusion $\dot{y} \in K[h](y)$, where $K[\cdot]$ is defined as in [112], and let $h : \mathbb{R}^4 \to \mathbb{R}^4$ be defined as $h \triangleq \left[\begin{array}{cccc} \dot{r} & \dot{e}_u & \sqrt{\dot{Q}_1} & \sqrt{\dot{Q}_2} \end{array} \right]^T$ (see [110]). Using the calculus of $K[\cdot]$ from [113], applying the Leibniz integral rule to (6–3), (6–10), (6–11), and using (6–9) yields the following generalized time derivative of (6–22)

$$\begin{aligned} \dot{\tilde{V}}_L \subseteq\ & \tanh(r) \left(\chi + k_s \tfrac{K[B_M^{\tau}]}{M} \left(\tanh(r_{\hat{\tau}}) - \tanh(r_{\tau}) \right) - K[\sigma_s] \alpha k_s \tanh(r) \right. \\ & - \tfrac{K[B_E]}{M} \left(k_1 K[\text{sgn}(r)] + k_2 \tanh(r) \right) + \left(K[\sigma_{s,\hat{\tau}}] \alpha - \tfrac{K[B_M^{\tau}]}{M} \right) k_s \tanh(r_{\hat{\tau}}) \Big) \\ & + \omega_1 k_s e_u \left(-K[\sigma_s] \tanh(r) + K[\sigma_{s,\hat{\tau}}] \tanh(r_{\hat{\tau}}) \right) \\ & + \tfrac{1}{2} \left(\varepsilon_1 \omega_1 + \varepsilon_2 \omega_2 \right) k_s \left(\tanh^2(r) - \tanh^2(r_{\hat{\tau}}) \right) \\ & + \tfrac{\omega_3 k_s}{\hat{\tau}} \left(\hat{\tau} \tanh^2(r) - \textstyle\int_{t-\hat{\tau}}^{t} \tanh^2(r(\theta)) \, d\theta \right), \end{aligned} \tag{6–27}$$

where, $K[\text{sgn}(\cdot)] = SGN(\cdot)$ such that $SGN(\cdot) = \{1\}$ if $(\cdot) > 0$, $[-1, 1]$ if $(\cdot) = 0$, and $\{-1\}$ if $(\cdot) < 0$. To obtain a result for all time, the expression in (6–27) must be evaluated for each possible switching condition combination. From the switching conditions defined in (2–11), (2–12), and (2–13) and the expression in (6–27) it can be seen that there exists 9 unique cases, which are summarized in Table 6-1. First, Case 1 will be

examined and then Cases 2-9 will be examined using an overall upper bound.

Case 1 in Table 6-1 represents the only case when the motor is not in use, which occurs only when FES-induced muscle contractions are present in the system (i.e., $t \in \left[t_n^m, t_{n+1}^e\right)$). Note, during Case 1 the switching signals are constant; therefore, $K\left[B_M^\tau\right]$ can be bounded using Property 2.8 as $c_b \leq K\left[B_M^\tau\right] \leq c_B$, $K\left[\sigma_s\right] = 1$, $K\left[\sigma_{s,\hat{\tau}}\right] = 1$, and $K\left[B_E\right] = 0$. Therefore, setting $K\left[\sigma_s\right] = 1$, $K\left[\sigma_{s,\hat{\tau}}\right] = 1$, and $K\left[B_E\right] = 0$, using Properties 2.1 and 2.8, choosing ε_2 and ω_2 such that $\max\left(\left|\alpha - \frac{c_b}{c_M}\right|, \left|\alpha - \frac{c_B}{c_m}\right|\right) \leq \varepsilon_2\omega_2$, and using the fact that $\dot{V}_L\left(y\right) \overset{\text{a.e.}}{\in} \dot{\tilde{V}}_L\left(y\right)$ allows (6–27) to be evaluated during Case 1 and upper bounded as follows

$$\begin{aligned}\dot{V}_L \overset{\text{a.e.}}{\leq}\ & \left|\tanh\left(r\right)\right|\left|\chi\right| - \alpha k_s \tanh^2\left(r\right) + k_s\tfrac{c_B}{c_m}\left|\tanh\left(r\right)\right|\left|\left(\tanh\left(r_{\hat{\tau}}\right) - \tanh\left(r_\tau\right)\right)\right| \\ & + k_s\varepsilon_2\omega_2\left|\tanh\left(r\right)\tanh\left(r_{\hat{\tau}}\right)\right| + \omega_3 k_s \tanh^2\left(r\right) + \omega_1 k_s\left|e_u \tanh\left(r\right)\right| \\ & + \omega_1 k_s\left|e_u \tanh\left(r_{\hat{\tau}}\right)\right| + \tfrac{1}{2}\left(\varepsilon_1\omega_1 + \varepsilon_2\omega_2\right)k_s\left(\tanh^2\left(r\right) - \tanh^2\left(r_{\hat{\tau}}\right)\right) \\ & - \tfrac{\omega_3 k_s}{\hat{\tau}}\int_{t-\hat{\tau}}^{t}\tanh^2\left(r\left(\theta\right)\right)d\theta.\end{aligned} \tag{6–28}$$

Provided that $\left\|y\left(\cdot\right)\right\| < \gamma,\ \ \forall \cdot \in \left[t_0, t\right)$, it could be shown using Properties 2.1, 2.8, and 2.9, (6–5), (6–9), and the fact that $\left\|y\right\| \geq \left\|z\right\|$ that

$$\dot{r}\left(\cdot\right) \leq c_1 + c_2\gamma + c_3\gamma^2 \leq \Upsilon, \tag{6–29}$$

$\forall \cdot \in \left[t_0, t\right)$, where $c_1, c_2, c_3 \in \mathbb{R}_{>0}$ are known constants. Now, using (6–29), the MVT can be used to further bound (6–28) as

$$\begin{aligned}\dot{V}_L \overset{\text{a.e.}}{\leq}\ & \left(\left|\chi\right| + k_s\bar{\bar{\tau}}\Upsilon\tfrac{c_B}{c_m}\right)\left|\tanh\left(r\right)\right| - \alpha k_s\tanh^2\left(r\right) + k_s\varepsilon_2\omega_2\left|\tanh\left(r\right)\tanh\left(r_{\hat{\tau}}\right)\right| \\ & + \omega_3 k_s\tanh^2\left(r\right) + \omega_1 k_s\left|e_u\tanh\left(r\right)\right| + \omega_1 k_s\left|e_u\tanh\left(r_{\hat{\tau}}\right)\right| \\ & + \tfrac{1}{2}\left(\varepsilon_1\omega_1 + \varepsilon_2\omega_2\right)k_s\left(\tanh^2\left(r\right) - \tanh^2\left(r_{\hat{\tau}}\right)\right) - \tfrac{\omega_3 k_s}{\hat{\tau}}\int_{t-\hat{\tau}}^{t}\tanh^2\left(r\left(\theta\right)\right)d\theta.\end{aligned} \tag{6–30}$$

Using Young's Inequality to upper bound select terms in (6–30) yields the following upper bound

$$\dot{V}_L \overset{\text{a.e.}}{\leq} \left(|\chi| + k_s\overline{\tilde{\tau}}\Upsilon\tfrac{c_B}{c_m}\right)|\tanh(r)| - \alpha k_s \tanh^2(r) + k_s\left(\varepsilon_1\omega_1 + \varepsilon_2\omega_2 + \omega_3\right)\tanh^2(r) + \left(\tfrac{\omega_1 k_s}{\varepsilon_1}\right)e_u^2 - \tfrac{\omega_3 k_s}{\hat{\tau}}\int_{t-\hat{\tau}}^{t}\tanh^2(r(\theta))\,d\theta. \tag{6–31}$$

Substituting (6–5) into (6–31) and completing the squares on the $|\tanh(r)|$ terms yield

$$\dot{V}_L \overset{\text{a.e.}}{\leq} -k_s\left(\tfrac{1}{2}\alpha - \varepsilon_1\omega_1 - \varepsilon_2\omega_2 - \omega_3\right)\tanh^2(r) - \tfrac{\omega_3 k_s}{\hat{\tau}}\int_{t-\hat{\tau}}^{t}\tanh^2(r(\theta))\,d\theta + \left(\tfrac{\omega_1 k_s}{\varepsilon_1}\right)e_u^2 + \tfrac{1}{\alpha k_s}\left(\rho^2(\|z\|)\|z\|^2 + \left(\Phi + k_s\overline{\tilde{\tau}}\Upsilon\tfrac{c_B}{c_m}\right)^2\right). \tag{6–32}$$

To facilitate the analysis, the Cauchy-Schwarz inequality can be used with (6–3) and (6–7) to yield

$$e_u^2 \leq \hat{\tau}k_s^2\int_{t-\hat{\tau}}^{t}\tanh^2(r(\theta))\,d\theta. \tag{6–33}$$

Furthermore, Q_2 can be upper bounded as

$$Q_2 \leq \omega_3 k_s\int_{t-\hat{\tau}}^{t}\tanh^2(r(\theta))\,d\theta. \tag{6–34}$$

The following inequality is obtained by using (6–10), (6–33), and (6–34):

$$-\tfrac{\omega_3 k_s}{\hat{\tau}}\int_{t-\hat{\tau}}^{t}\tanh^2(r(\theta))\,d\theta \leq -\tfrac{\omega_3}{3k_s\hat{\tau}^2}e_u^2 - \tfrac{\omega_3}{3\hat{\tau}\left(\frac{1}{2}(\varepsilon_1\omega_1+\varepsilon_2\omega_2)\right)}Q_1 - \tfrac{1}{3\hat{\tau}}Q_2. \tag{6–35}$$

Substituting (6–35) into (6–32) and using the definition of β_1 in (6–13) yields

$$\dot{V}_L \overset{\text{a.e.}}{\leq} -\beta_1\|x\|^2 + \tfrac{1}{\alpha k_s}\rho^2(\|z\|)\|z\|^2 + v, \tag{6–36}$$

$\forall t \in \left[t_n^m, t_{n+1}^e\right)$, provided that $\|y(\cdot)\| < \gamma,\ \forall\cdot \in [t_0, t)$, where $x \in \mathbb{R}^4$ is defined as

$$x \triangleq \begin{bmatrix} \tanh(r) & e_u & \sqrt{Q_1} & \sqrt{Q_2} \end{bmatrix}^T, \tag{6–37}$$

and the auxiliary constant, $v \in \mathbb{R}_{>0}$, is defined as

$$v \triangleq \tfrac{1}{\alpha k_s}\left(\Phi + k_s\overline{\tilde{\tau}}\Upsilon\tfrac{c_B}{c_m}\right)^2. \tag{6–38}$$

Now the Cases 2-9 from Table 6-1 will be considered, which represent the cases when the motor is active (i.e., $t \in \left[t_n^e, t_{n+1}^m\right)$). An overall upper bound for Cases 2-9 is determined to facilitate the analysis. Note, by individually considering each case, utilizing Properties 2.1 and 2.8, and selecting ε_2 and ω_2 such that $\alpha - \frac{c_b}{c_M} \leq \left|\alpha - \frac{c_b}{c_M}\right| \leq \varepsilon_2\omega_2$ and $\frac{c_B}{c_m} - \alpha \leq \left|\alpha - \frac{c_B}{c_m}\right| \leq \varepsilon_2\omega_2$, it could be proven that

$$\left|\left(K\left[\sigma_{s,\hat{\tau}}\right]\alpha - \frac{K\left[B_M^T\right]}{M}\right)\right| \leq \varepsilon_2\omega_2 + \max\left(\frac{c_b}{c_M}, \alpha\right). \tag{6–39}$$

The inequality in (6–27) can be upper bounded for Cases 2-9 by considering each case individually, using Properties 2.8 and 2.9, and utilizing the inequality in (6–39) to yield

$$\begin{aligned}\dot{V}_L \overset{\text{a.e.}}{\leq}\ & |\chi|\,|\tanh(r)| - \tfrac{c_e}{c_M}k_1\,|\tanh(r)| + k_s\tfrac{c_B}{c_m}\,|\tanh(r)|\,|(\tanh(r_{\hat{\tau}}) - \tanh(r_\tau))| \\ & -\tfrac{c_e}{c_M}k_2\tanh^2(r) + k_s\varepsilon_2\omega_2\,|\tanh(r)\tanh(r_{\hat{\tau}})| + \omega_1 k_s\,|e_u\tanh(r)| \\ & +\omega_1 k_s\,|e_u\tanh(r_{\hat{\tau}})| + k_s\max\left(\tfrac{c_b}{c_M}, \alpha\right)|\tanh(r)\tanh(r_{\hat{\tau}})| + \omega_3 k_s\tanh^2(r) \\ & +\tfrac{1}{2}\left(\varepsilon_1\omega_1 + \varepsilon_2\omega_2\right)k_s\left(\tanh^2(r) - \tanh^2(r_{\hat{\tau}})\right) - \tfrac{\omega_3 k_s}{\hat{\tau}}\int_{t-\hat{\tau}}^{t}\tanh^2(r(\theta))\,d\theta.\end{aligned} \tag{6–40}$$

Substituting (6–5) into (6–40), selecting the gains according to (6–18), (6–19), and (6–21), and applying the MVT yields

$$\begin{aligned}\dot{V}_L \overset{\text{a.e.}}{\leq}\ & \rho(\|z\|)\,\|z\|\,|\tanh(r)| - \tfrac{c_e}{c_M}k_{21}\tanh^2(r) + k_s\varepsilon_2\omega_2\,|\tanh(r)\tanh(r_{\hat{\tau}})| \\ & +\omega_1 k_s\,|e_u\tanh(r)| + \omega_1 k_s\,|e_u\tanh(r_{\hat{\tau}})| + \omega_3 k_s\tanh^2(r) \\ & +\tfrac{1}{2}\left(\varepsilon_1\omega_1 + \varepsilon_2\omega_2\right)k_s\left(\tanh^2(r) - \tanh^2(r_{\hat{\tau}})\right) - \tfrac{\omega_3 k_s}{\hat{\tau}}\int_{t-\hat{\tau}}^{t}\tanh^2(r(\theta))\,d\theta.\end{aligned} \tag{6–41}$$

Now, by following a similar development as for Case 1 the following upper bound for (6–41) can be obtained

$$\dot{V}_L \overset{\text{a.e.}}{\leq} -\beta_2\|x\|^2 + \frac{c_M}{2c_e k_{21}}\rho^2(\|z\|)\,\|z\|^2, \tag{6–42}$$

$\forall t \in \left[t_n^e, t_{n+1}^m\right)$, provided that $\|y(\cdot)\| < \gamma,\ \forall \cdot \in [t_0, t)$, where β_2 is defined in (6–14).

An upper bound for every case can be obtained by upper bounding both (6–36) and (6–42) by

$$\dot{V}_L \overset{\text{a.e.}}{\leq} -\beta \|x\|^2 + \delta \rho^2 (\|z\|) \|z\|^2 + v, \tag{6–43}$$

$\forall t \in [t_0, \infty)$, where

$$\delta \triangleq \max\left(\tfrac{1}{\alpha k_s}, \tfrac{c_M}{2c_e k_{21}}\right). \tag{6–44}$$

From (6–43), (6–22) can be considered a common Lyapunov-like function across the entire crank cycle (i.e., for every case [114]). Additionally, notice that $\beta > 0$ provided the gain conditions in (6–16)-(6–20) are satisfied. Using (2–24), (6–24), and (6–37) it can be proven that $\|x\|^2 \geq \tanh^2(\|y\|)$. Furthermore, (6–43) can be upper bounded by using the fact that $\|y\| \geq \|z\|$ and $\|x\|^2 \geq \tanh^2(\|y\|)$ to yield

$$\dot{V}_L \overset{\text{a.e.}}{\leq} -\underbrace{\frac{\beta}{2} \tanh^2(\|y\|)}_{\phi_3(\|y\|)} + v, \tag{6–45}$$

$\forall t \in [t_0, \infty)$, provided that $\|y(\cdot)\| < \gamma, \ \forall \cdot \in [t_0, t)$ and that the following inequality is satisfied for all time

$$-\frac{\beta}{2} \tanh^2(\|y\|) + \delta \rho^2(\|y\|) \|y\|^2 \leq 0. \tag{6–46}$$

The expression in (6–46) can be rewritten as follows

$$\rho^2(\|y\|) \left(\frac{\|y\|}{\tanh(\|y\|)}\right)^2 \leq \frac{\beta}{2\delta}. \tag{6–47}$$

A sufficient condition for (6–47) is obtained by using the properties in (2–25) as

$$\rho^2(\|y\|) (\|y\| + 1)^2 \leq \frac{\beta}{2\delta}. \tag{6–48}$$

Notice that the left-hand side of (6–48) is strictly increasing with respect to $\|y\|$. Therefore, the condition in (6–48) implies that $\|y\|$ must be bounded. Let γ denote the maximum value of $\|y\|$ such that (6–48) holds. Thus, (6–48) is satisfied for all time if $\|y(t)\| \leq \gamma, \forall t \in [t_0, \infty)$. Therefore, a sufficient condition for $\|y(\cdot)\| < \gamma, \ \forall \cdot \in [t_0, t)$ is that the condition in (6–48) is satisfied for all time. Given (6–23) and (6–45), $\|y(\cdot)\|$ is

uniformly ultimately bounded [115] in the sense that

$$\|y(t)\| \leq \overline{d}, \quad \forall t \geq T\left(\overline{d}, \|y(t_0)\|\right), \tag{6–49}$$

provided the gain conditions in (6–16)-(6–20) and the sufficient condition in (6–48) are satisfied for all time. In (6–49), $\bar{d}$ denotes the ultimate bound of $\|y(t)\|$ and is determined according to [115] as

$$\bar{d} > \left(\phi_1^{-1} \circ \phi_2\right)\left(\phi_3^{-1}(v)\right), \tag{6–50}$$

where ϕ_1 and ϕ_2 are defined in (6–23), ϕ_3 is defined in (6–45), v is defined in (6–38), and T denotes the ultimate time to reach the ultimate bound and is defined as [115]

$$T \triangleq \begin{cases} 0 & \|y(t_0)\| \leq \kappa \\ \frac{\phi_2(\|y(t_0)\|) - \phi_1\left(\left(\phi_2^{-1} \circ \phi_1\right)\left(\bar{d}\right)\right)}{\phi_3\left(\phi_2^{-1} \circ \phi_1\right)\left(\bar{d}\right) - v} & \|y(t_0)\| > \kappa. \end{cases} \tag{6–51}$$

where $\kappa \triangleq \left(\phi_2^{-1} \circ \phi_1\right)\left(\bar{d}\right)$. From (6–49), a sufficient condition for (6–48) to be satisfied for all time is provided in (6–26), which is expressed in terms of the initial condition and the ultimate bound of the composite error signal $\|y\|$. □

6.3 Experiment

6.3.1 Experimental Testbed

The experimental testbed used in this chapter is the FES cycle that is introduced in Chapter 2.

6.3.2 Experimental Methods

Experiments on a 28 year old male able-bodied participant were performed to validate the controllers in (6–7) and (6–8). The participant gave written informed consent approved by the University of Florida Institutional Review Board (IRB201600881). The participant was instructed to be a passive rider and make no volitional effort to either assist or resist the electric motor input or FES input during the experiment. The participant was blind to the desired and actual trajectory. For simplicity, in this

experiment only the quadriceps femoris muscle group was stimulated; however, the analysis is valid for the quadriceps femoris, hamstrings, and gluteal muscle groups. During the first 20 s of the experiment the motor tracked a smooth cadence ramp from zero to $\dot{q}_d = 50$ RPM. At that point the FES and motor controllers were implemented according to the developed control design. For the next 160 s, a constant desired cadence of 50 RPM was tracked. The lower thresholds of the torque transfer ratios were used to determine the range of crank angles corresponding to the stimulation of each muscle and activation of the motor. The gains were selected as $k_1 = 0.5$, $k_2 = 15$, $k_s = 1$, and $\alpha = 0.1$. The time-varying input delay was estimated as $\hat{\tau} = 0.1$ s. For use in (2–11), the delay upper bound was selected as $\bar{\tau} = 0.12$ s, respectively.

6.3.3 Results and Discussion

Figure 6-1 depicts the motor current input (top plot) and the FES pulse width delivered to the participant's RQ and LQ (bottom plot) throughout the experiment. Recall that a smooth cadence ramp up to 50 RPM occurred over the first 20 s of the experiment. Figure 6-2 depicts the subject's tracking performance during the experiment, quantified by the actual cadence versus desired cadence (top plot), and by the cadence error (bottom plot). An average cadence of 48.24 $\pm$ 2.09 RPM with a maximum peak error of 9.1 RPM was achieved during the experiment. The offset in the cadence error could likely be improved by modifying the error system to include a position error term. A position error term would be like the integral term of a Proportional-Integral-Derivative (PID) controller to reduce the steady-state error [116]. The control inputs over a single crank cycle are shown in Figure 6-3. These preliminary experimental results successfully demonstrate the ability of the controllers in (6–7) and (6–8) to achieve uniformly ultimately bounded tracking performance despite unknown disturbances, uncertainty in the lower limb dynamics, and an unknown time-varying FES input delay for a single healthy participant.

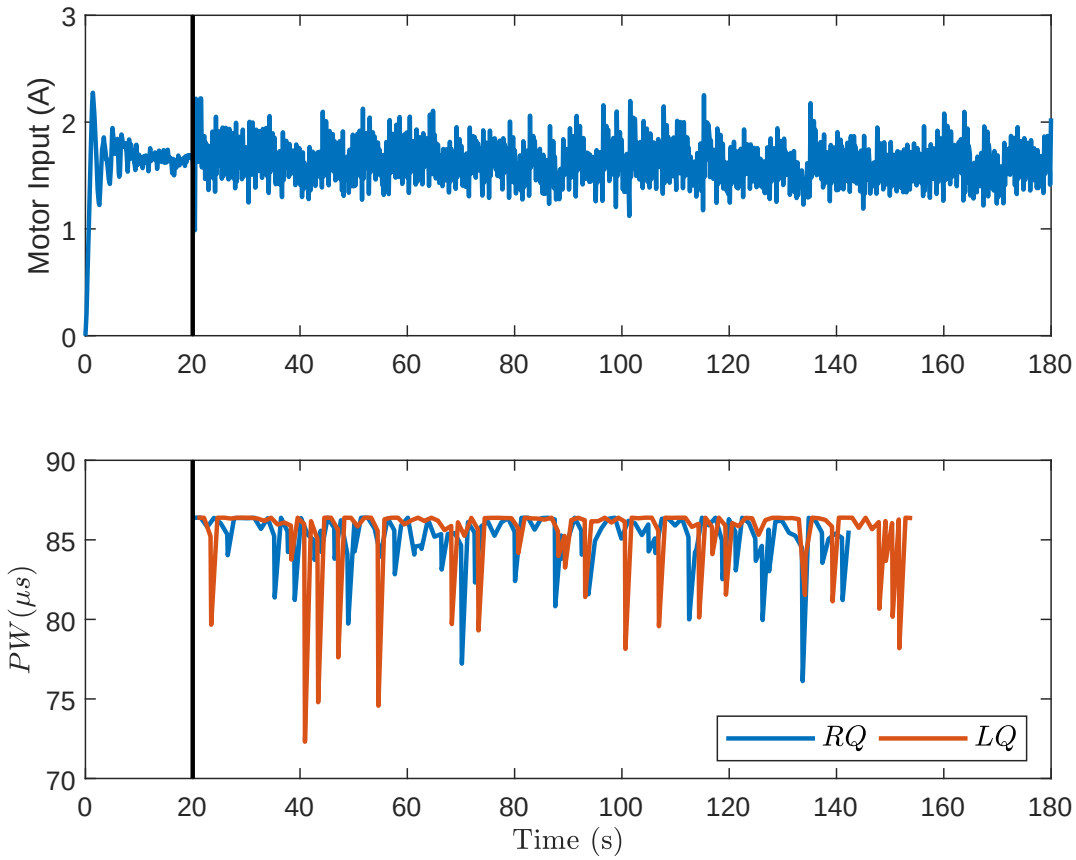

Figure 6-1. The filtered motor input (top) and the peak FES input pulse width (PW) applied to the right (RQ) and left (LQ) quadriceps femoris for each FES region (bottom). The vertical black line indicates the time when the developed controllers were activated. A 1.2 s moving average filter was used on the motor input for visual clarity. The effect of the saturated FES control input can be seen in the bottom plot.

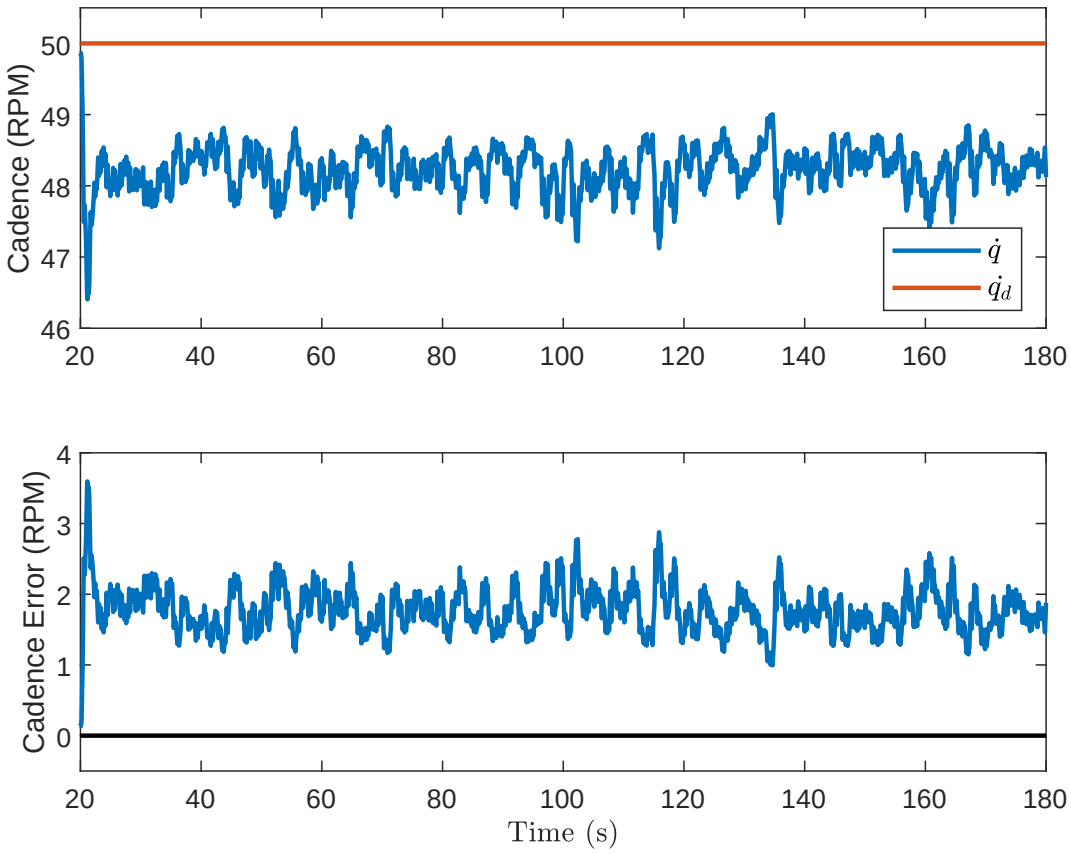

Figure 6-2. The desired versus the actual cadence (top) and the cadence error (bottom) after the designed control system was activated. For visual clarity, a solid black line marks zero error. A 1.2 s moving average filter was applied to $\dot{q}$ and $\dot{e}$ for visual clarity.

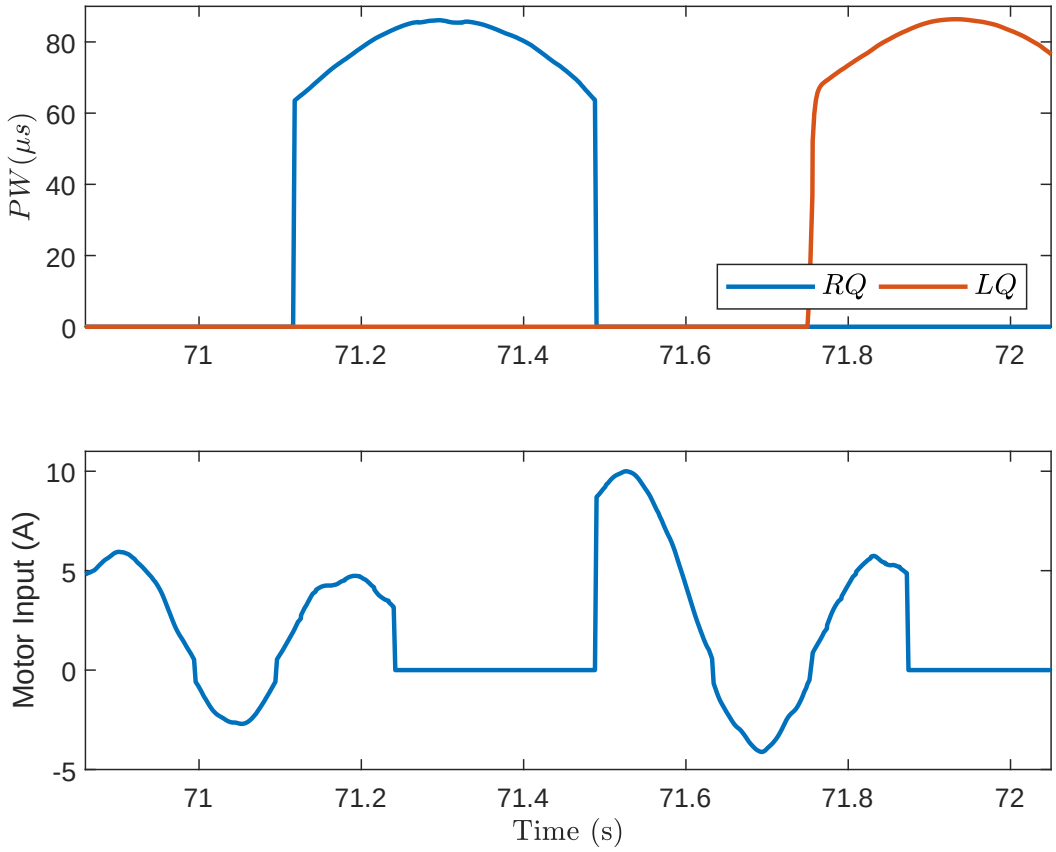

Figure 6-3. The FES input (top) and the motor input (bottom) over approximately one crank cycle.

6.4 Concluding Remarks

In this chapter, new FES and motor controllers are developed for the FES cycle to yield cadence tracking. Compared to Chapter 4, a saturated control system is developed such that the upper bound of both the motor and FES controller is known a priori and can be adjusted by modifying the feedback control gains. Consequently, the participant's safety and comfort are improved. A Lyapunov-like analysis was performed to ensure uniformly ultimately bounded cadence tracking for an uncertain nonlinear dynamic switched system, unknown bounded additive disturbances, and an unknown time-varying input delay. Additionally, switching conditions that are presented in Chapter 2 were developed to activate/deactivate stimulation to yield effective muscle contractions. A preliminary experiment on a single participant was performed to validate the motor and FES controllers, which indicated that an offset occurred in the cadence error. Chapter 7 seeks to improve the cadence tracking performance by ensuring both position and cadence tracking, while simultaneously providing saturated FES inputs. Furthermore, extensive experiments are performed in Chapter 7 to compare the controllers developed in this chapter and those developed in Chapter 7.

CHAPTER 7
POSITION AND CADENCE TRACKING OF A MOTORIZED FES-CYCLE WITH AN UNKNOWN TIME-VARYING INPUT DELAY USING SATURATED FES CONTROL

In this chapter, similar to Chapter 6, we develop a saturated closed-loop FES controller that compensates for the EMD. However, in this chapter the control development and stability analysis is modified to yield exponential position and cadence tracking compared to uniformly ultimately bounded cadence tracking that is ensured in Chapter 6. Furthermore, this chapter results in less conservative gain conditions compared to Chapter 6. The motivation of this chapter is to include position tracking as a control objective in an effort to improve the cadence tracking performance as discussed in Chapter 6. Contributions of this chapter result from the design and analysis innovations to compensate for switching between the different muscles and motor control inputs, compensating for the inherent uncertain nonlinear dynamics, compensating for the time-varying unknown input delay resulting from the complex electrochemical FES muscle torque production process, and compensating for saturation in the evoked torque due to fatigue, available muscle mass, or stimulation sensitivity. An important feature of the bound on the developed saturated FES controller is that it is known a priori, similar to the saturated controllers in Chapter 6, and can be adjusted by tuning the control gains to limit the stimulation levels, providing a more comfortable experience for the participant. The performance of the controllers developed in this chapter were then compared to the control system developed in Chapter 6 through a series of experiments on nine participants (five able-bodied and four with NCs). For the controllers developed in this chapter and those developed in Chapter 6, the experiments for the non-informed passive able-bodied participants resulted in average cadence tracking errors of -0.03$\pm$1.69 RPM and 3.90$\pm$3.36 RPM, respectively, and the experiments for the participants with NCs resulted in average cadence tracking errors of -0.04$\pm$1.98 RPM and 0.53$\pm$3.37 RPM, respectively, for a desired cadence of 50 RPM.

7.1 Control Development

The first control objective of the FES-cycle system is for the crank to track a sufficiently smooth desired position $q_d : \mathbb{R}_{\geq 0} \to \mathbb{R}$ and desired cadence $\dot{q}_d : \mathbb{R}_{\geq 0} \to \mathbb{R}$, which is complicated by the existence of uncertainties in the dynamic model and the unknown time-varying EMD. The tracking control objective is quantified by a measurable position tracking error, denoted by $e : \mathbb{R}_{\geq 0} \to \mathbb{R}$, and defined as

$$e \triangleq q_d - q, \tag{7–1}$$

and a measurable cadence tracking error, denoted by $\dot{e} : \mathbb{R}_{\geq 0} \to \mathbb{R}$, and defined as

$$\dot{e} \triangleq \dot{q}_d - \dot{q}. \tag{7–2}$$

Motivated by the desire to inject a delay-free FES input into the open- and closed-loop error systems, an auxiliary signal $e_u : \mathbb{R}_{\geq 0} \to \mathbb{R}$ is designed as

$$e_u \triangleq -\int_{t-\hat{\tau}}^{t} \sigma_s(\theta)\, u(\theta)\, d\theta, \tag{7–3}$$

where $\hat{\tau} \in \mathbb{R}_{>0}$ denotes a constant estimate of the EMD, and σ_s is defined in (2–12). The EMD estimation error is defined as $\tilde{\tau} \triangleq \tau - \hat{\tau}$, which can be upper bounded by applying Property 2.11 as $|\tilde{\tau}| \leq \overline{\tilde{\tau}}$, where $\overline{\tilde{\tau}} \in \mathbb{R}_{>0}$ is a known constant. Motivated to aid the subsequent stability analysis and to include e in the closed-loop error system, the time derivative of the auxiliary signal $e_f : \mathbb{R}_{\geq 0} \to \mathbb{R}$ is designed as

$$\dot{e}_f \triangleq \cosh^2(e_f)\left(-k_1 r + e - \alpha_3 \tanh(e_f)\right), \tag{7–4}$$

where hyperbolic functions are used to facilitate the saturated control design, $e_f(0) = 0$, and $k_1, \alpha_3 \in \mathbb{R}_{>0}$ are selectable constants. A measurable auxiliary tracking error, $r : \mathbb{R}_{\geq 0} \to \mathbb{R}$, is defined as

$$r \triangleq \dot{e} + \alpha_1 e + \tanh(e_f) + \alpha_2 e_u, \tag{7–5}$$

where $\alpha_1, \alpha_2 \in \mathbb{R}_{>0}$ are selectable constants. To obtain the open-loop error system, we substitute (7–2) into (7–5) and take the time derivative of (7–5), apply Leibniz integral rule to (7–3) to obtain $\dot{e}_u$, solve (2–18) for $\ddot{q}$, substitute in (7–4), and add and subtract $B_M^{\tau} M^{-1} u_{\hat{\tau}} + e$ to yield

$$\dot{r} = \chi + \frac{B_M^{\tau}}{M}\left(u_{\hat{\tau}} - u_{\tau}\right) - \frac{B_E}{M} u_e - k_1 r - \sigma_s \alpha_2 u + \left(\sigma_{s,\hat{\tau}} \alpha_2 - \frac{B_M^{\tau}}{M}\right) u_{\hat{\tau}} - e, \tag{7–6}$$

where $\chi : \mathcal{Q} \times \mathbb{R} \times \mathbb{R} \times \mathbb{R}_{\geq 0} \to \mathbb{R}$ is defined as

$$\chi \triangleq \ddot{q}_d + M^{-1}\left[V\dot{q} + G + P + b_c \dot{q} + d - \tau_{vol}\right] + 2e + \alpha_1 \dot{e} - \alpha_3 \tanh\left(e_f\right). \tag{7–7}$$

By using (7–2), (7–5), and Properties 2.1-2.7,

$$|\chi| \leq \Phi + \rho\left(\|z\|\right)\|z\|, \tag{7–8}$$

where $\Phi \in \mathbb{R}_{>0}$ is a known constant, $\rho\left(\cdot\right)$ is a globally invertible, positive, radially unbounded, and strictly increasing function, and $z \in \mathbb{R}^4$ is a composite error vector defined as

$$z \triangleq \begin{bmatrix} e & r & e_u & \tanh(e_f) \end{bmatrix}^T. \tag{7–9}$$

The second control objective of the FES-cycle system is to design a saturated FES control input to ensure the comfort of the participant. The FES and motor control inputs are designed, based on (7–6) and the subsequent stability analysis, as

$$u \triangleq -\frac{k_1}{\alpha_2} \tanh\left(e_f\right), \tag{7–10}$$

$$u_e \triangleq \frac{c_M}{c_e}\left(\sigma_e k_2 r + k_3 \operatorname{sgn}\left(r\right)\right), \tag{7–11}$$

where $\operatorname{sgn}\left(\cdot\right)$ denotes the signum function, and $k_1,\ k_2,\ k_3 \in \mathbb{R}_{>0}$ are selectable constants. The motor switching signal, denoted by σ_e, is defined in (2–13). A feature of the FES control input is that $|u| \leq \frac{k_1}{\alpha_2}$, and thus it can be bounded by selectable gain constants. The stimulation input (i.e. pulse width) to each muscle group is defined as $u_m \triangleq k_m \sigma_m u, \forall m \in \mathcal{M}$, resulting in a bounded stimulation input since

$|u_m| \leq \frac{k_m k_1}{\alpha_2}, \forall m \in \mathcal{M}$. Therefore, the stimulation input into each muscle can be bounded a priori by selectable constants to ensure a more comfortable and safer experience for the rider. The motor control input is defined as $u_E \triangleq k_e u_e$. The closed-loop error system is obtained by substituting (7–10) and (7–11) into (7–6) to yield

$$\begin{aligned} \dot{r} &= \chi + \tfrac{B_M^\tau}{M}\left(u_{\hat{\tau}} - u_\tau\right) - k_1 r - e - \tfrac{B_E}{M}\tfrac{c_M}{c_e}\left(\sigma_e k_2 r + k_3 \mathsf{sgn}\left(r\right)\right) \\ &\quad + \sigma_s k_1 \mathsf{tanh}\left(e_f\right) + \left(\sigma_{s,\hat{\tau}}\alpha_2 - \tfrac{B_M^\tau}{M}\right) u_{\hat{\tau}}. \end{aligned} \tag{7–12}$$

To facilitate the subsequent stability analysis, LK functionals $Q_1,\, Q_2 : \mathbb{R}_{\geq 0} \to \mathbb{R}_{>0}$ are defined as

$$Q_1 \triangleq \frac{1}{2}\left(\varepsilon_1\omega_1 + \omega_2\right)\int_{t-\hat{\tau}}^{t} u^2\left(\theta\right) d\theta, \tag{7–13}$$

$$Q_2 \triangleq \frac{\omega_3}{\hat{\tau}}\int_{t-\hat{\tau}}^{t}\int_{s}^{t} u^2\left(\theta\right) d\theta ds, \tag{7–14}$$

and auxiliary bounding constants $\beta_1, \beta_2, \delta_1, \delta_2 \in \mathbb{R}$ are defined as

$$\beta_1 \triangleq \min\left(\alpha_1 - \tfrac{\alpha_2\varepsilon_2}{2},\, \tfrac{1}{2}\left(k_1 - \omega_2\right),\, \tfrac{\omega_3}{3\hat{\tau}^2} - \tfrac{\alpha_2}{2\varepsilon_2} - \tfrac{\omega_1}{\varepsilon_1},\, \alpha_3 - \tfrac{k_2^2}{\alpha_2^2}\left(\varepsilon_1\omega_1 + \tfrac{1}{2}\omega_2 + \omega_3\right)\right), \tag{7–15}$$

$$\beta_2 \triangleq \min\left(\alpha_1 - \tfrac{\alpha_2\varepsilon_2}{2},\, k_2 - \tfrac{1}{2}\omega_2,\, \tfrac{\omega_3}{3\hat{\tau}^2} - \tfrac{\alpha_2}{2\varepsilon_2} - \tfrac{\omega_1}{\varepsilon_1},\, \alpha_3 - \tfrac{k_1}{2} - \tfrac{k_1^2}{\alpha_2^2}\left(\varepsilon_1\omega_1 + \tfrac{1}{2}\omega_2 + \omega_3\right)\right), \tag{7–16}$$

$$\delta_1 \triangleq \min\left(\tfrac{1}{2}\beta_1,\, \tfrac{\omega_3}{3\hat{\tau}\left(\frac{1}{2}\left(\varepsilon_1\omega_1 + \omega_2\right)\right)},\, \tfrac{1}{3\hat{\tau}}\right), \tag{7–17}$$

$$\delta_2 \triangleq \min\left(\tfrac{1}{2}\beta_2,\, \tfrac{\omega_3}{3\hat{\tau}\left(\frac{1}{2}\left(\varepsilon_1\omega_1 + \omega_2\right)\right)},\, \tfrac{1}{3\hat{\tau}}\right), \tag{7–18}$$

where $\varepsilon_1, \varepsilon_2, \omega_1, \omega_2, \omega_3 \in \mathbb{R}_{>0}$ are selectable constants. To ensure that (7–15)-(7–18) are positive, the following gain conditions must be satisfied

$$\alpha_1 > \frac{1}{2}\alpha_2\varepsilon_2, \quad k_1 > \omega_2, \quad k_2 > \frac{1}{2}\omega_2, \tag{7–19}$$

$$k_3 \geq \Phi + \bar{\tilde{\tau}}\Upsilon\tfrac{c_B}{c_m} + \tfrac{k_1}{\alpha_2}\max\left(\tfrac{c_b}{c_M}, \alpha_2\right), \tag{7–20}$$

$$\omega_2 \geq \max\left(\left|\alpha_2 - \tfrac{c_b}{c_M}\right|, \left|\alpha_2 - \tfrac{c_B}{c_m}\right|\right), \tag{7–21}$$

$$\omega_3 > 3\hat{\tau}^2\left(\tfrac{\alpha_2}{2\varepsilon_2} + \tfrac{\omega_1}{\varepsilon_1}\right), \tag{7–22}$$

$$\alpha_3 > \frac{1}{2}k_1 + \frac{k_1^2}{\alpha_2^2}\left(\varepsilon_1\omega_1 + \frac{1}{2}\omega_2 + \omega_3\right), \tag{7–23}$$

where $\Upsilon \in \mathbb{R}_{>0}$ is a known constant.

7.2 Stability Analysis

Switching times are denoted by $\{t_n^i\}$, $i \in \{m, e\}$, $n \in \{0, 1, 2, ...\}$, which represent the instants in time when σ_e becomes zero $(i = m)$ or nonzero $(i = e)$. A common Lyapunov function candidate, $V_L : \mathcal{D} \to \mathbb{R}_{\geq 0}$, that is continuously differentiable and positive definite is defined on a domain $\mathcal{D} \subseteq \mathbb{R}^6$ as

$$V_L \triangleq \frac{1}{2}e^2 + \frac{1}{2}r^2 + \frac{1}{2}\omega_1 e_u^2 + \frac{1}{2}\tanh^2(e_f) + Q_1 + Q_2. \tag{7–24}$$

The common Lyapunov function candidate in (7–24) can be bounded as

$$\lambda_1 \|y\|^2 \leq V_L \leq \lambda_2 \|y\|^2, \tag{7–25}$$

where $\lambda_1, \lambda_2 \in \mathbb{R}_{>0}$ are known constants defined as

$$\lambda_1 \triangleq \min\left(\frac{1}{2}, \frac{\omega_1}{2}\right), \quad \lambda_2 \triangleq \max\left(1, \frac{\omega_1}{2}\right),$$

and $y \in \mathbb{R}^6$ is defined as

$$y \triangleq \begin{bmatrix} z^T & \sqrt{Q_1} & \sqrt{Q_2} \end{bmatrix}^T. \tag{7–26}$$

Let $S_{\mathcal{D}}$ be defined as

$$S_{\mathcal{D}} \triangleq \left\{y \in \mathcal{D} \mid \|y\| < \sqrt{\tfrac{\lambda_1}{\lambda_2}}\gamma\right\}, \tag{7–27}$$

where $\gamma \in \mathbb{R}_{>0}$ is a known constant defined as[1] $\gamma \leq \inf\{\rho^{-1}((\kappa, \infty))\}$, where $\kappa \triangleq \sqrt{\frac{1}{2}k_1 \min(\beta_1, \beta_2)}$.

Theorem 7.1. *For the motorized FES cycle-rider dynamics in* (2–18) *and Properties 2.1-2.11, the controllers defined in* (7–10) *and* (7–11) *yield exponential cadence tracking*

[1] For a set A, the inverse image is defined as $\rho^{-1}(A) \triangleq \{a \mid \rho(a) \in A\}$.

in the sense that

$$\|y(t)\| \leq \sqrt{\frac{\lambda_2}{\lambda_1}} \|y(t_0)\| \exp\left(-\frac{\lambda_3}{2}(t-t_0)\right), \tag{7–28}$$

$\forall t \in [t_0, \infty)$ *, where* $\lambda_3 \triangleq \lambda_2^{-1} \min(\delta_1, \delta_2)$*, provided* $y(t_0) \in S_{\mathcal{D}}$*, and the gain conditions in* (7–19)-(7–23) *are satisfied.*

Proof. Since the FES and motor controllers are discontinuous, a generalized solution exists almost everywhere (a.e.) within $t \in [t_0, \infty)$ for the time derivative of (7–24), denoted by $\dot{\tilde{V}}_L$, such that $\dot{V}_L(y) \overset{\text{a.e.}}{\in} \dot{\tilde{V}}_L(y)$. Let $y(t)$ be a Filippov solution to the differential inclusion $\dot{y} \in K[h](y)$ for $t \in [t_0, \infty)$, where $K[\cdot]$ is defined as in [112], and let $h : \mathbb{R}^6 \to \mathbb{R}^6$ be defined as $h \triangleq \left[\begin{array}{cccccc} \dot{e} & \dot{r} & \dot{e}_u & \dot{\tanh}(e_f) & \sqrt{\dot{Q}_1} & \sqrt{\dot{Q}_2} \end{array}\right]^T$ (see [110]). Using the calculus of $K[\cdot]$ from [113], using (7–4), (7–5), and (7–12), applying the Leibniz integral rule to (7–3), (7–13), (7–14), and canceling common terms yield the following generalized time derivative of (7–24),

$$\begin{aligned} \dot{\tilde{V}}_L \subseteq\ & e\left(-\alpha_1 e - \alpha_2 e_u\right) + r\left[\frac{K\left[B_M^\tau\right]}{M}\left(u_{\hat{\tau}} - u_\tau\right) - \frac{B_E}{M}\frac{c_M}{c_e}\left(K[\sigma_e] k_2 r + k_3 K[\text{sgn}(r)]\right)\right. \\ & \left. + \chi - k_1 r + K[\sigma_s] k_1 \text{tanh}(e_f) + \left(K[\sigma_{s,\hat{\tau}}]\alpha_2 - \frac{K\left[B_M^\tau\right]}{M}\right) u_{\hat{\tau}}\right] \\ & + \omega_1 e_u\left(-K[\sigma_s] u + K[\sigma_{s,\hat{\tau}}] u_{\hat{\tau}}\right) + \tanh(e_f)\left(-k_1 r - \alpha_3 \text{tanh}(e_f)\right) \\ & + \tfrac{1}{2}\left(\varepsilon_1\omega_1 + \omega_2\right)\left(u^2 - u_{\hat{\tau}}^2\right) + \tfrac{\omega_3}{\hat{\tau}}\left(\hat{\tau}u^2 - \int_{t-\hat{\tau}}^{t} u^2(\theta)\, d\theta\right), \end{aligned} \tag{7–29}$$

where, $K[\text{sgn}(\cdot)] = SGN(\cdot)$ such that $SGN(\cdot) = \{1\}$ if $(\cdot) > 0$, $[-1, 1]$ if $(\cdot) = 0$, and $\{-1\}$ if $(\cdot) < 0$. Evaluating the expression in (7–29) for each potential combination of the switching signals will yield a result for all time. By inspection of (7–29) and the switching conditions in (2–11), (2–12), and (2–13), there exists nine unique combinations as summarized in Table 5-1. Subsequently, Case 1 will be considered, followed by an examination of Cases 2-9 using an overall upper bound.

From Table 5-1, Case 1 represents the only case when $\sigma_e = 0$ (i.e., $t \in \left[t_n^m, t_{n+1}^e\right)$), which occurs when FES forces are occurring. Notice that the switching signals are

constant during a given case; thus, during Case 1, $K[\sigma_s] = 1$, $K[\sigma_{s,\hat{\tau}}] = 1$, $K[\sigma_e] = 0$, and by Property 2.8, $c_b \leq K[B_M^{\tau}] \leq c_B$. Setting $K[\sigma_s] = 1$, $K[\sigma_{s,\hat{\tau}}] = 1$, and $K[\sigma_e] = 0$, choosing ω_2 such that $\max\left(\left|\alpha_2 - \frac{c_b}{c_M}\right|, \left|\alpha_2 - \frac{c_B}{c_m}\right|\right) \leq \omega_2$, using the fact that $\dot{V}_L(y) \overset{\text{a.e.}}{\in} \dot{\tilde{V}}_L(y)$, and using Properties 2.1, 2.8, and 2.9 yields the following upper bound for (7–29) during Case 1,

$$\begin{aligned}\dot{V}_L \overset{\text{a.e.}}{\leq}\ & -\alpha_1 e^2 + \alpha_2 |e e_u| + \tfrac{c_B}{c_m}|r||u_{\hat{\tau}} - u_{\tau}| + |r||\chi| - k_3|r| - k_1 r^2 + \omega_2 |u_{\hat{\tau}} r| \\ & + \omega_1 |e_u u| + \omega_1 |e_u u_{\hat{\tau}}| - \alpha_3 \tanh^2(e_f) + \tfrac{1}{2}(\varepsilon_1\omega_1 + \omega_2)(u^2 - u_{\hat{\tau}}^2) \\ & + \tfrac{\omega_3}{\hat{\tau}}\left(\hat{\tau}u^2 - \int_{t-\hat{\tau}}^{t} u^2(\theta)\, d\theta\right).\end{aligned} \tag{7–30}$$

Using (7–4), (7–10), and (7–26) it could be shown that $\dot{u}(\cdot) \leq \Upsilon,\ \forall \cdot \in [t_0, t)$ provided that $\|y(\cdot)\| < \gamma,\ \forall \cdot \in [t_0, t)$. Since $\dot{u}(\cdot) \leq \Upsilon,\ \forall \cdot \in [t_0, t)$, the MVT can be applied to upper bound (7–30) as

$$\begin{aligned}\dot{V}_L \overset{\text{a.e.}}{\leq}\ & -\alpha_1 e^2 + \alpha_2 |e e_u| + \bar{\tilde{\tau}}\Upsilon\tfrac{c_B}{c_m}|r| + |r||\chi| - k_3|r| - k_1 r^2 + \omega_2 |u_{\hat{\tau}} r| + \omega_1 |e_u u| \\ & + \omega_1 |e_u u_{\hat{\tau}}| - \alpha_3 \tanh^2(e_f) + \tfrac{1}{2}(\varepsilon_1\omega_1 + \omega_2)(u^2 - u_{\hat{\tau}}^2) + \tfrac{\omega_3}{\hat{\tau}}\left(\hat{\tau}u^2 - \int_{t-\hat{\tau}}^{t} u^2(\theta)\, d\theta\right).\end{aligned} \tag{7–31}$$

Substituting (7–8) into (7–31), applying the gain condition in (7–20), and completing the squares on the $|r|\rho(\|z\|)\|z\|$ term yields

$$\begin{aligned}\dot{V}_L \overset{\text{a.e.}}{\leq}\ & -\alpha_1 e^2 + \alpha_2 |e e_u| - \tfrac{1}{2}k_1 r^2 + \omega_2 |u_{\hat{\tau}} r| + \omega_1 |e_u u| + \omega_1 |e_u u_{\hat{\tau}}| - \alpha_3 \tanh^2(e_f) \\ & + \tfrac{1}{2}(\varepsilon_1\omega_1 + \omega_2)(u^2 - u_{\hat{\tau}}^2) + \omega_3 u^2 - \tfrac{\omega_3}{\hat{\tau}}\int_{t-\hat{\tau}}^{t} u^2(\theta)\, d\theta + \tfrac{1}{2k_1}\rho^2(\|z\|)\|z\|^2.\end{aligned} \tag{7–32}$$

Applying Young's Inequality and using (7–10) yields

$$\begin{aligned}\dot{V}_L \overset{\text{a.e.}}{\leq}\ & -\left(\alpha_1 - \tfrac{\alpha_2\varepsilon_2}{2}\right)e^2 + \left(\tfrac{\alpha_2}{2\varepsilon_2} + \tfrac{\omega_1}{\varepsilon_1}\right)e_u^2 - \tfrac{1}{2}(k_1 - \omega_2)r^2 - \alpha_3 \tanh^2(e_f) \\ & + \tfrac{k_1^2}{\alpha_2^2}\left(\varepsilon_1\omega_1 + \tfrac{1}{2}\omega_2 + \omega_3\right)\tanh^2(e_f) - \tfrac{\omega_3}{\hat{\tau}}\int_{t-\hat{\tau}}^{t} u^2(\theta)\, d\theta + \tfrac{1}{2k_1}\rho^2(\|z\|)\|z\|^2.\end{aligned} \tag{7–33}$$

We can bound Q_2 as

$$Q_2 \leq \omega_3 \int_{t-\hat{\tau}}^{t} u^2(\theta)\, d\theta, \tag{7–34}$$

and then apply the Cauchy-Schwarz inequality to (7–3) to obtain

$$e_u^2 \leq \hat{\tau} \int_{t-\hat{\tau}}^{t} u^2(\theta)\, d\theta. \tag{7–35}$$

From (7–13), (7–34) , and (7–35),

$$-\tfrac{\omega_3}{\hat{\tau}} \int_{t-\hat{\tau}}^{t} u^2(\theta)\, d\theta \leq -\tfrac{\omega_3}{3\hat{\tau}\left(\frac{1}{2}(\varepsilon_1\omega_1+\omega_2)\right)} Q_1 - \tfrac{\omega_3}{3\hat{\tau}^2} e_u^2 - \tfrac{1}{3\hat{\tau}} Q_2. \tag{7–36}$$

Substituting (7–36) into (7–33), using the fact that $\|y\| \geq \|z\|$, and using (7–9), (7–15), (7–17), and (7–25) yields

$$\dot{V}_L \overset{\text{a.e.}}{\leq} -\frac{\delta_1}{\lambda_2} V_L, \tag{7–37}$$

$\forall t \in \left[t_n^m, t_{n+1}^e\right)$, provided that $\|y(\cdot)\| < \gamma, \ \forall \cdot \in [t_0, t)$ and provided $y(t_n^m) \in \mathcal{D}$, where

$$\mathcal{D} \triangleq \{y \in \mathbb{R}^6 \mid \|y\| < \gamma\}. \tag{7–38}$$

The condition $y(t_n^m) \in \mathcal{D}$ is equivalent to requiring $\|y(t_n^m)\| < \gamma$.

Cases 2-9 from Table 5-1 all include $\sigma_e = 1$ (i.e., $t \in \left[t_n^e, t_{n+1}^m\right)$). To facilitate the development of an overall upper bound for Cases 2-9, notice that by considering each case individually, selecting ω_2 according to (7–21), and using Properties 2.1 and 2.8, it could be shown that

$$\left| \left(K\left[\sigma_{s,\hat{\tau}}\right] \alpha_2 - \tfrac{K\left[B_M^{\tau}\right]}{M} \right) \right| \leq \omega_2 + \max\left(\tfrac{c_b}{c_M}, \alpha_2\right). \tag{7–39}$$

An overall upper bound of (7–29) for Cases 2-9 is obtained by considering each case individually, using Properties 2.1, 2.8, and 2.9, and using (7–39) to yield

$$\begin{aligned} \dot{V}_L \overset{\text{a.e.}}{\leq}\ & -\alpha_1 e^2 + \alpha_2 |e e_u| + |r|\,|\chi| - k_3 |r| - k_1 r^2 + \tfrac{c_B}{c_m} |r|\,|u_{\hat{\tau}} - u_{\tau}| - k_2 r^2 + \omega_2 |u_{\hat{\tau}} r| \\ & + \max\left(\tfrac{c_b}{c_M}, \alpha_2\right) |u_{\hat{\tau}} r| - \alpha_3 \mathsf{tanh}^2(e_f) + \omega_1 |e_u u| + \omega_1 |e_u u_{\hat{\tau}}| + k_1 |r \tanh(e_f)| \\ & + \tfrac{1}{2}(\varepsilon_1\omega_1 + \omega_2)(u^2 - u_{\hat{\tau}}^2) + \tfrac{\omega_3}{\hat{\tau}} \left(\hat{\tau} u^2 - \int_{t-\hat{\tau}}^{t} u^2(\theta)\, d\theta \right). \end{aligned} \tag{7–40}$$

Substituting (7–8) into (7–40), completing the squares on $|r|\,\rho\left(\|z\|\right)\|z\|$, using Young's Inequality on $|r\tanh\left(e_f\right)|$, and using the fact that $|u_{\hat{\tau}}r| \leq \frac{k_1}{\alpha_2}|r|$ yields

$$\begin{aligned}\dot{V}_L \overset{\text{a.e.}}{\leq} & -\alpha_1 e^2 + \alpha_2 |e e_u| + |r|\,\Phi - k_3|r| - k_2 r^2 + \tfrac{1}{2k_1}\rho^2\left(\|z\|\right)\|z\|^2 + \tfrac{c_B}{c_m}|r|\,|u_{\hat{\tau}} - u_\tau| \\ & + \omega_2 |u_{\hat{\tau}} r| + \tfrac{k_1}{\alpha_2}\max\left(\tfrac{c_b}{c_M}, \alpha_2\right)|r| + \omega_1 |e_u u| - \left(\alpha_3 - \tfrac{1}{2}k_1\right)\tanh^2\left(e_f\right) \\ & + \tfrac{1}{2}\left(\varepsilon_1\omega_1 + \omega_2\right)\left(u^2 - u_{\hat{\tau}}^2\right) + \omega_1 |e_u u_{\hat{\tau}}| + \tfrac{\omega_3}{\hat{\tau}}\left(\hat{\tau}u^2 - \int_{t-\hat{\tau}}^{t} u^2(\theta)\,d\theta\right).\end{aligned} \tag{7–41}$$

An upper bound for (7–41) is obtained by following a development similar to Case 1 to yield

$$\dot{V}_L \overset{\text{a.e.}}{\leq} -\frac{\delta_2}{\lambda_2} V_L, \tag{7–42}$$

$\forall t \in \left[t_n^e, t_{n+1}^m\right)$, provided that $y\left(t_n^e\right) \in \mathcal{D}$ and $\|y(\cdot)\| < \gamma,\ \forall \cdot \in [t_0, t)$.

An upper bound across all cases (i.e., $\forall t \in [t_0, \infty)$) is obtained by using (7–37) and (7–42) to yield

$$\dot{V}_L \overset{\text{a.e.}}{\leq} -\lambda_3 V_L, \tag{7–43}$$

where $\lambda_3 \triangleq \lambda_2^{-1}\min\left(\delta_1, \delta_2\right)$, which can be solved to yield

$$V_L(t) \leq V_L(t_0)\exp\left(-\lambda_3(t - t_0)\right), \tag{7–44}$$

provided that $y\left(t_n^m\right), y\left(t_n^e\right) \in \mathcal{D}, \forall n$, and provided that $\|y(\cdot)\| < \gamma,\ \forall \cdot \in [t_0, t)$. Using (7–25) with (7–44) yields the result in (7–28). A sufficient condition for $y\left(t_n^m\right), y\left(t_n^e\right) \in \mathcal{D}, \forall n$, and $\|y(\cdot)\| < \gamma,\ \forall \cdot \in [t_0, t)$ is that $y(t_0) \in S_{\mathcal{D}}$. From (7–24) and (7–44), $e, r, e_u \in \mathcal{L}_\infty$, and from (7–10) and (7–11), $u, u_e \in \mathcal{L}_\infty$ and the remaining signals are bounded. □

7.3 Experiment

Let the FES and motor controllers developed in (7–10) and (7–11), the control system developed in Chapter 6, and $u = 0$ and $u_e = 0$ (i.e., no control assistance) be henceforth labeled as Controllers A, B, and C, respectively. Controllers A and B

Table 7-1. Participant Demographics

Participant	Age	Sex	Condition	Time Since Diagnosis
S1	22	F	None	- -
S2	22	M	None	- -
S3	22	F	None	- -
S4	22	F	None	- -
S5	21	F	None	- -
N1	26	M	Spina Bifida (L5-S1)	26yr
N2	55	F	Multiple Sclerosis	25yr
N3	54	M	Multiple Sclerosis	10yr
N4	42	F	Cerebral Palsy	42yr

both have a cadence tracking objective; however, Controller A also includes a position tracking objective in an effort to improve the cadence tracking performance.

7.3.1 Experimental Testbed

The experimental testbed used in this chapter is the FES cycle that is introduced in Chapter 2.

7.3.2 Experimental Methods

Experiments were performed on nine participants, including four with NCs, whose demographics are shown in Table 7-1. Each participant provided written informed consent approved by the University of Florida Institutional Review Board (IRB201600881). Able-bodied participants, who were blind to the desired and actual trajectory, were instructed to be a passive rider and make no volitional effort to either assist or resist the electric motor input or FES input during the experiment. The able-bodied participants were asked to provide no volitional contribution for equal comparison and to simulate the potential lack of volitional contribution by some (e.g., spinal cord injured) patients in a clinical setting. To further examine the performance of the control methods in an alternative clinical condition (i.e., active therapy), participants with NCs were asked to pedal volitionally, and FES was added as required. Furthermore, the participants with NCs were asked to contribute to the cadence tracking objective to the best of their ability,

and they were shown, exclusively, a plot of the actual and desired cadence in real-time during the experiment.

Prior to the experiments, electrodes were placed over the quadriceps, hamstrings, and gluteal muscle groups. The participant was seated on the cycle, and their feet were secured to the pedals using orthotic boots. The seat of the cycle was adjusted for each participant's comfort and to ensure a minimum bend of at least 15 degrees in the knee across all angles of the crank cycle. The participant specific desired FES regions for each muscle ($\mathcal{Q}_m$) were determined by recording various measurements (i.e., seat position, limb lengths, etc.) as defined in [3]. The motor was then used to ramp the cycle up to 50 RPM, and open-loop stimulation was applied to one muscle group at a time. The stimulation was incrementally increased until the participant's comfort limit was determined, and this limit was recorded for each muscle group. Recall that Controllers A and B utilize saturated FES controllers, thus the comfort limits were used to inform the selection of control gains to saturate the FES input at or below each muscle's comfort limit.

During the first 20 s of an experiment the motor tracked a smooth cadence ramp from zero to $\dot{q}_d = 50$ RPM. For the remaining 160 s (the steady-state portion of the experiment), either Controller A, B, or C was implemented and a constant desired cadence of 50 RPM was tracked. For the able-bodied participants, Controllers A and B were implemented in a random order. For the participants with NCs, a run was first performed using Controller C and then a run was performed using Controller A. Since participants with NCs provided volition, they were allowed a single practice run for each controller.

7.4 Results

7.4.1 Results from Able-Bodied Participants

The experimental results (i.e., root mean square (RMS) and peak cadence errors, motor effort, and FES effort) of the able-bodied population are summarized in Table

Table 7-2. Comparative results for the able-bodied participants during steady state operation

Controller	Participant	RMS Cadence Error (RPM)	Peak Cadence Error (RPM)*	Motor Effort (A)†	FES Effort (μs)‡
A	S1	1.62	6.59	1.53$\pm$1.20	19.76$\pm$0.80
	S2	1.99	12.76	1.71$\pm$1.26	36.12$\pm$2.58
	S3	1.80	10.38	1.59$\pm$0.95	35.42$\pm$0.44
	S4	1.68	8.16	1.68$\pm$1.03	12.25$\pm$2.30
	S5	1.35	9.12	1.54$\pm$0.90	15.49$\pm$1.43
	Average	**1.69**	**9.40**	**1.61$\pm$1.07**	**23.81$\pm$1.51**
B	S1	4.86	13.99	1.59$\pm$1.81	36.21$\pm$2.60
	S2	4.90	12.65	1.71$\pm$1.80	38.57$\pm$1.29
	S3	3.99	11.98	2.41$\pm$2.18	67.48$\pm$1.54
	S4	6.08	15.64	2.48$\pm$2.61	29.17$\pm$0.76
	S5	5.93	14.84	2.00$\pm$2.21	23.02$\pm$0.89
	Average	**5.15**	**13.82**	**2.04$\pm$2.12**	**38.89$\pm$1.41**

*The maximum value of $|\dot{e}|$.
†The average $\pm$ standard deviation of $|u_E|$.
‡The average $\pm$ standard deviation of the maximum stimulation delivered to each muscle group within each FES region.

7-2 for Controllers A and B. Figure 7-1 depicts a plot of the desired cadence versus the actual cadence and plots of the control inputs for Participant S1 when using either Controller A or B, which represent a typical result for the able-bodied participants. Furthermore, it was determined that on average, across each able-bodied participant, Controllers A and B applied FES to at least one muscle group during 59.7% and 62.5% of the experiment, respectively, and resulted in an average cadence tracking error of -0.03$\pm$1.69 RPM and 3.90$\pm$3.36 RPM, respectively.

7.4.1.1 Statistical analysis

A series of statistical tests were performed to determine the impact of each controller on the cadence tracking performance and the control inputs. The statistical tests were performed on the following measurements: RMS cadence error, peak cadence error, average motor and FES inputs, motor and FES input standard deviations, and the percent of time that FES was applied. Since only two controllers (Controllers A and B) were used on each able-bodied participant, a paired difference test was used on each

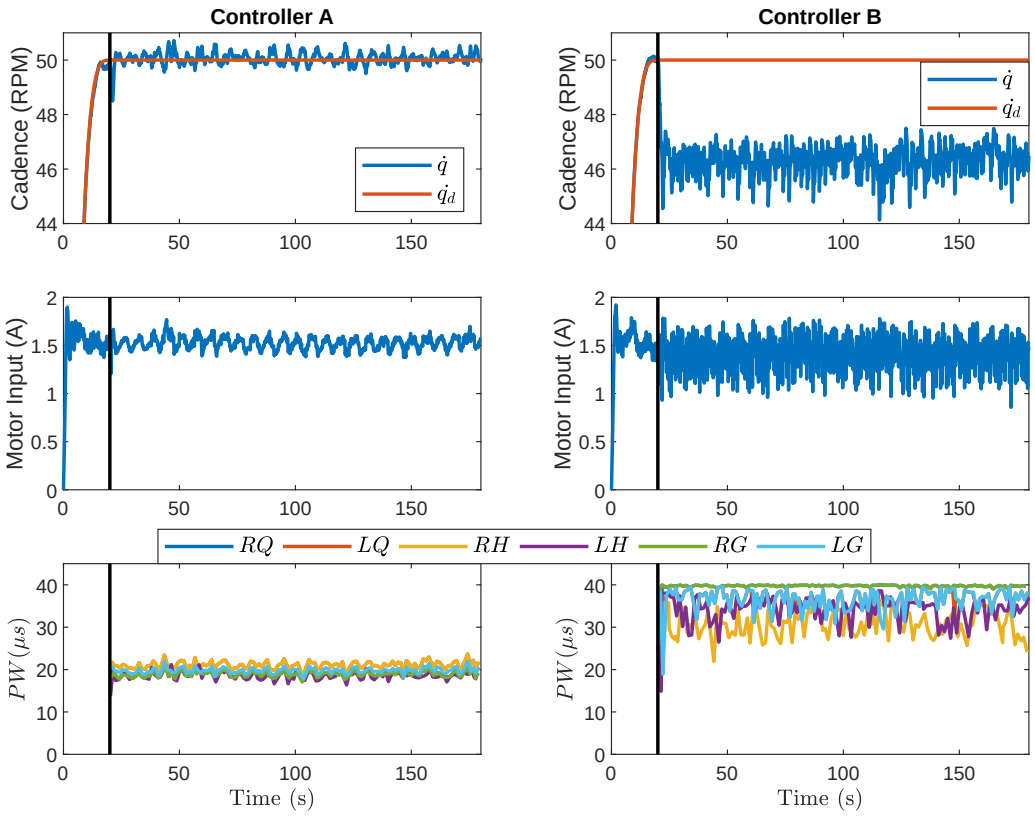

Figure 7-1. The actual versus desired cadence after steady-state was reached (top), motor input (middle), and peak FES pulsewidth (PW) input for each FES region applied to the left (L) and right (R) quadriceps (Q), hamstring (H), and gluteal (G) (bottom) are shown for Controller A (left) and Controller B (right) for participant S1. For visual clarity, a 1.2 s moving average filter was applied to the actual cadence ($\dot{q}$) and the motor input. Steady-state is indicated by the vertical black line. Note that stimulation of the RG was saturated at 40 μs, which resulted in the flat portions of the FES input for Controller B.

measurement; however, due to the small sample size (n = 5), the Shapiro-Wilk's test for normality, whose null hypothesis is that the population is normally distributed, was used to conclude that the difference data (i.e., the difference between each controller pair for each participant) was approximately normal for each measurement (P-Value > 0.05). Therefore, a series of one-sided paired t-tests were performed to conclude that the RMS cadence error (P-Value < 0.001), peak cadence error (P-Value = 0.023), average motor effort (P-Value = 0.034), motor effort standard deviation (P-Value = 0.003), average FES effort (P-Value = 0.020), and percent of time that FES was applied (P-Value = 0.014) were significantly larger for Controller B than for Controller A. Further, it was determined that the controller had no statistically significant effect on the FES effort standard deviation (P-Value = 0.445).

7.4.1.2 Discussion

From the statistical analysis and inspection of Figure 7-1, it can be concluded that Controller A outperformed Controller B by reducing the cadence tracking error while simultaneously requiring less motor and FES effort, including requiring FES to be applied over a smaller duration of time. Furthermore, it is clear from Figure 7-1 that Controller B resulted in a offset of the cadence error, whereas Controller A resulted in a negligible steady-state cadence error. Controller A was developed to reduce the steady-state cadence error produced by Controller B by including a position and cadence error term in the error system. It was theorized that the position error term would act like the integral term of a Proportional-Integral-Derivative (PID) controller to reduce the steady-state error [116], which was confirmed by the performance of Controller A relative to Controller B.

7.4.2 Results from Participants with NCs

Since Controller A outperformed Controller B, Controller B was not used on the participants with NCs and Controller C was instead used for comparison. The experimental results for the population with NCs are summarized in Table 7-3 for Controllers

Table 7-3. Comparative results for the participants with NCs during steady state operation

Controller	Participant	RMS Cadence Error (RPM)	Peak Cadence Error (RPM)*	Motor Input (A)†	FES Input (μs)‡
A	N1	1.98	8.86	1.29±0.84	32.22±1.65
	N2	1.57	7.69	1.46±0.81	14.70±0.53
	N3	2.19	6.72	0.93±0.44	37.72±6.57
	N4	2.16	7.74	1.68±1.08	22.49±3.31
	Average	**1.98**	**7.75**	**1.34±0.79**	**26.78±3.01**
C	N1	4.53	27.94	0.00±0.00	0.00±0.00
	N2	3.39	24.36	0.00±0.00	0.00±0.00
	N3	2.62	14.18	0.00±0.00	0.00±0.00
	N4	3.62	14.08	0.00±0.00	0.00±0.00
	Average	**3.54**	**20.14**	**0.00±0.00**	**0.00±0.00**

*The maximum value of $|\dot{e}|$.
†The average ± standard deviation of $|u_E|$.
‡The average ± standard deviation of the maximum stimulation delivered to each muscle group within each FES region.

A and C. The cadence tracking results for Controllers A and C are depicted in Figure 7-2 for Participant N1, which represents a typical result for the participants with NCs.

Across each participant with NCs, it was also determined that Controllers A and C resulted in an average cadence tracking error of -0.04±1.98 RPM and 0.53±3.37 RPM, respectively, and that, for Controller A, FES was applied to at least one muscle group during 57.4% of the experiment.

7.4.2.1 Statistical analysis

To compare the cadence tracking performance of Controllers A and C, statistical tests were performed on the RMS and peak cadence errors. As was done for the results of the able-bodied participants, normality was confirmed using the Shapiro-Wilk's test and then one-sided paired t-tests were performed to conclude that the RMS (P-Value = 0.019) and peak (P-Value = 0.015) cadence errors were significantly larger for Controller C than Controller A.

7.4.2.2 Discussion

The statistical analysis confirms that Controller A improves the cadence tracking performance relative to Controller C, which is expected since Controller C provides no

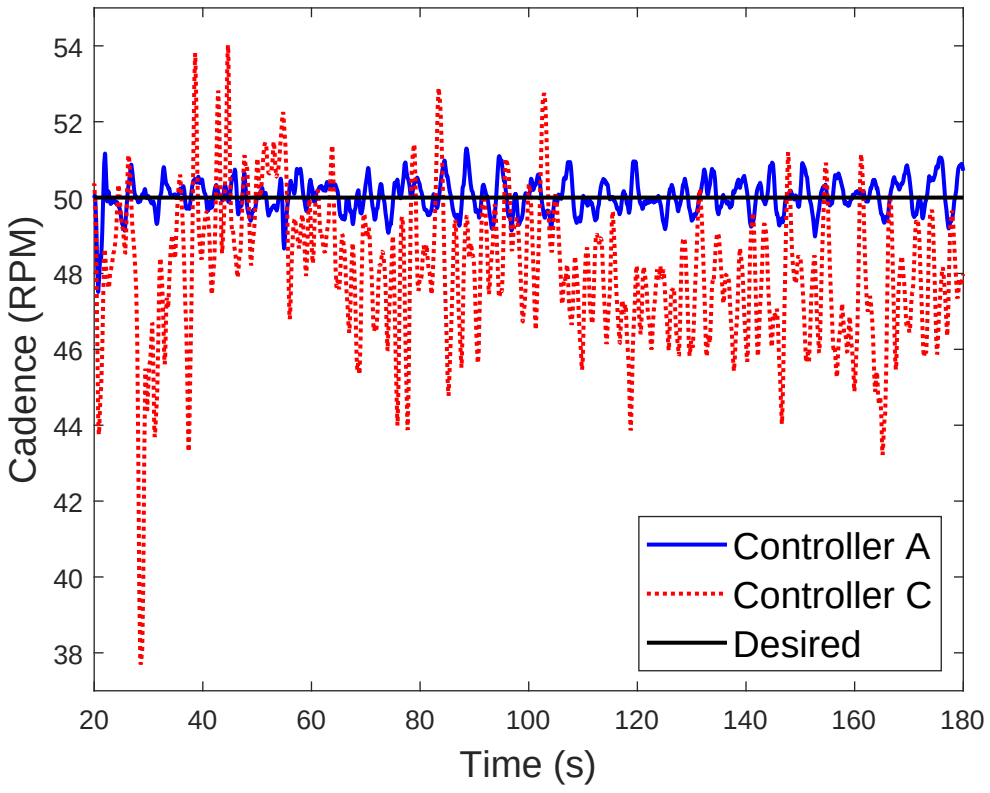

Figure 7-2. The filtered cadence tracking results for participant N1 are shown for Controllers A (blue) and C (red), where a 1.2 s moving average filter was applied for visual clarity.

control assistance to meet the control objectives. Furthermore, the experimental results in Table 7-3 and Figure 7-2 demonstrate the cadence tracking capability of Controller A despite the existence of an unknown time-varying EMD, presence of volitional effort from participants with a wide range of NCs, unknown disturbances, and uncertainty in the lower limb dynamics. Therefore, Controller A has demonstrated potential as a cadence tracking controller that saturates the FES input and is robust to a range of uncertainties, which can safely be used during both passive and active therapy exercises.

7.5 Concluding Remarks

In this chapter, the safety/comfort and tracking performance of a participant during FES-cycling is improved by the development of a switched and saturated FES control system that is robust to uncertainties in the dynamic model, unknown disturbances, and an unknown time-varying EMD. Exponential position and cadence tracking are guaranteed by a Lyaponov-based stability analysis. An important feature of the control system is that the bound on the FES controller can be set a priori to be within the tolerable range of the participant to ensure comfort. Furthermore, state and delay dependent switching conditions were developed to properly activate/deactivate the motor and the FES of each muscle group to ensure efficient muscle contractions.

A series of experiments were performed on five able-bodied participants and four participants with NCs to validate the performance of the developed controller. For able-bodied participants, the developed controller and the controllers in Chapter 6 resulted in an average cadence tracking error of -0.03$\pm$1.69 RPM and 3.90$\pm$3.36 RPM, respectively. For the participants with NCs, the developed controller and the controllers in Chapter 6 produced an average cadence tracking error of -0.04$\pm$1.98 RPM and 0.53$\pm$3.37, respectively.

CHAPTER 8
ROBUST CADENCE AND POWER TRACKING ON A SWITCHED FES CYCLE WITH AN UNKNOWN ELECTROMECHANICAL DELAY

In prior chapters, the control objective was to ensure position and/or cadence tracking; however, in this chapter a dual objective control structure for simultaneous position/cadence and power tracking is developed. The FES and motor controllers are designed to track a desired power and cadence, respectively, and a Lyapunov-based switched systems analysis is performed to guarantee uniformly ultimately bounded power tracking and global exponential cadence tracking for a switched, delayed, nonlinear, and uncertain FES-cycling system. Due to intermittent FES application there exists uncontrolled periods for the power tracking objective, which requires a dwell-time analysis, which was further complicated by the existence of the EMD. A unique challenge in this problem is that there is an unknown time-varying input delay to produce force, and a different unknown time-varying residual input delay where force is still produced after stimulation is removed. These delays impact the dwell-time conditions that dictate stimulation timing, and if not properly accounted for can lead to undesired effects such as antagonistic muscles exerting force at the same time or potential instabilities. The proposed controllers were validated by experimental analysis of four participants with NCs and five able-bodied participants, and yielded average power and cadence tracking errors of 0.01 ± 0.09 watts (W) and -0.05 ± 0.65 RPM, respectively, for the able-bodied participants and 0.01 ± 1.11 W and -0.07 ± 1.17 RPM, respectively, for the participants with NCs. This chapter provides the first dual objective control structure, along with the corresponding stability analysis, for an unknown, nonlinear, switched, dynamic FES system with an unknown time-varying EMD.

8.1 Control Development

Assumption 8.1. Similar to [41], an active estimate of τ_M, denoted by $\hat{\tau}_M : \mathbb{R}_{\geq 0} \to \mathbb{R}$, can be developed (refer to Section 8.3.2) such that

$$\tilde{\tau}_M \triangleq \hat{\tau}_M - \tau_M, \tag{8–1}$$

where τ_M is defined in (2–7) and $\tilde{\tau}_M : \mathbb{R}_{\geq 0} \to \mathbb{R}$ denotes the bounded estimation error (i.e., $|\tilde{\tau}_M| \leq c_{est}$, where $c_{est} \in \mathbb{R}_{\geq 0}$ is known).

8.1.1 Position/Cadence Error System

The position tracking error, $e_1 : \mathbb{R}_{\geq 0} \to \mathbb{R}$, is defined as

$$e_1 \triangleq q_d - q, \tag{8–2}$$

where $q_d : \mathbb{R}_{\geq 0} \to \mathbb{R}$ denotes the smooth and bounded desired position (i.e., $q_d, \dot{q}_d, \ddot{q}_d \in \mathcal{L}_\infty$). To aid the subsequent stability analysis, an auxiliary error $e_2 : \mathbb{R}_{\geq 0} \to \mathbb{R}$ is defined as

$$e_2 \triangleq \dot{e}_1 + \alpha_1 e_1, \tag{8–3}$$

where $\dot{e}_1 \triangleq \dot{q}_d - \dot{q}$ quantifies the cadence tracking objective, and $\alpha_1 \in \mathbb{R}_{\geq 0}$ denotes a selectable constant. The open-loop position/cadence error system is obtained by taking the time derivative of (8–3), multiplying by M, adding and subtracting e_1, and using (2–18), (8–2), and (8–3) to yield

$$M\dot{e}_2 = \chi_1 - e_1 - Ve_2 - \tau_M - B_E u_e, \tag{8–4}$$

where $\chi_1 \triangleq M\left(\ddot{q}_d + \alpha_1 \dot{e}_1\right) + V\left(\dot{q}_d + \alpha_1 e_1\right) + G + P + b_c\dot{q} + d + e_1$. Based on (8–4) and the stability analysis, the motor controller is designed as

$$u_e = \frac{1}{B_E}\left(k_1 e_2 + \left(k_2 + k_3 \|y\| + k_4 \|y\|^2\right) \text{sgn}\left(e_2\right) - \hat{\tau}_M\right), \tag{8–5}$$

where $y \triangleq \begin{bmatrix} e_1 & e_2 \end{bmatrix}^T$, sgn $(\cdot)$ represents the signum function, and $k_1,\, k_2,\, k_3,\, k_4 \in \mathbb{R}_{>0}$ are selectable constants, and B_E is defined in (2–21). In this chapter, recall that the motor is active for all $t \geq t_0$ (i.e., the motor switching signal is defined as $\sigma_e \triangleq 1$). Substituting (8–5) into (8–4) and using (8–1) yields the closed-loop position/cadence error system

$$M\dot{e}_2 = \chi - e_1 - Ve_2 - k_1 e_2 - \left(k_2 + k_3 \|y\| + k_4 \|y\|^2\right) \text{sgn}\left(e_2\right), \tag{8–6}$$

where $\chi \triangleq \chi_1 + \tilde{\tau}_M$, which can be bounded by Assumption 8.1 and Properties 2.1-2.6 as

$$|\chi| \leq c_1 + c_2 \|y\| + c_3 \|y\|^2, \tag{8–7}$$

where $c_1,\, c_2,\, c_3 \in \mathbb{R}_{>0}$ are known constants.

8.1.2 Torque Error System

The integral torque error, $e_3 : \mathbb{R}_{\geq 0} \to \mathbb{R}$, is defined as [117]

$$e_3 \triangleq \int_{t_0}^{t} \left(\tau_{M,d}(\theta) - \hat{\tau}_M(\theta)\right) d\theta, \tag{8–8}$$

where $\tau_{M,d} : \mathbb{R}_{\geq 0} \to \mathbb{R}$ is the bounded desired torque (i.e., $\tau_{M,d} \in \mathcal{L}_\infty$). Applying Leibniz's Rule to take the time derivative of (8–8) yields the torque tracking error

$$\dot{e}_3 = \tau_{M,d}(t) - \hat{\tau}_M(t). \tag{8–9}$$

The form of (8–8) is used to enable the FES controller to influence (8–9), and thus, the subsequently designed torque error system [117]. An auxiliary signal, $e_4 : \mathbb{R}_{\geq 0} \to \mathbb{R}$, is designed as

$$e_4 \triangleq -\int_{t-\hat{\tau}}^{t} u\left(\theta\right) d\theta, \tag{8–10}$$

to provide delay compensation by injecting a delay free FES input into the closed-loop error system. To facilitate the subsequent stability analysis, an auxiliary torque error,

$r : \mathbb{R} \times \mathbb{R} \to \mathbb{R}$, is defined as

$$r \triangleq \alpha_2 e_3 + \alpha_3 e_4, \tag{8–11}$$

where $\alpha_2, \alpha_3 \in \mathbb{R}_{>0}$ are selectable constants.

The open-loop torque error system is obtained by taking a time derivative of (8–11), adding and subtracting $\alpha_2 B_M^{\tau} u_{\hat{\tau}}$, substituting in (8–1), and using $\tau_M = B_M^{\tau} u_{\tau} + \tau_{vol}$ to yield

$$\dot{r} = \alpha_2 \chi_2 + \alpha_2 B_M^{\tau} \left(u_{\hat{\tau}} - u_{\tau} \right) - \alpha_3 u + \left(\alpha_3 - \alpha_2 B_M^{\tau} \right) u_{\hat{\tau}}, \tag{8–12}$$

where B_M^{τ} is defined in (2–19) and $\chi_2 \triangleq \tau_{M,d} - \tau_{vol} - \tilde{\tau}_M$, which can be bounded using Property 2.7 and Assumption 8.1 as $|\chi_2| \leq c_4$, where $c_4 \in \mathbb{R}_{>0}$ is known. Based on (8–12) and the stability analysis, the FES controller is defined as

$$u = k_s r, \tag{8–13}$$

where $k_s \in \mathbb{R}_{>0}$ is a selectable constant and the FES switching signals are defined in (2–10). Due to the form of (8–8), the FES controller cannot be applied before t_0. The closed-loop torque error system is obtained by substituting (8–13) into (8–12) to yield

$$\dot{r} = \alpha_2 \chi_2 + \alpha_2 k_s B_M^{\tau} \left(r_{\hat{\tau}} - r_{\tau} \right) - \alpha_3 k_s r + \left(\alpha_3 - \alpha_2 B_M^{\tau} \right) k_s r_{\hat{\tau}}. \tag{8–14}$$

Furthermore, the subsequent analysis is facilitated by defining LK functionals, $Q_1, Q_2 : \mathbb{R}_{\geq 0} \to \mathbb{R}_{\geq 0}$, as

$$Q_1 \triangleq \frac{1}{2} \left(\alpha_3 - c_b \alpha_2 + \varepsilon_1 \omega_1 \right) k_s \int_{t-\hat{\tau}}^{t} r\left(\theta\right)^2 d\theta, \tag{8–15}$$

$$Q_2 \triangleq \frac{\omega_2 k_s}{\hat{\tau}} \int_{t-\hat{\tau}}^{t} \int_{s}^{t} r\left(\theta\right)^2 d\theta ds, \tag{8–16}$$

where $\varepsilon_1, \omega_1, \omega_2 \in \mathbb{R}_{>0}$ are selectable constants.

8.2 Stability Analysis

Due to intermittent FES application, the cases when the muscles are active ($B_M^{\tau} > 0$) and inactive ($B_M^{\tau} = 0$) must be analyzed along with a consideration of the switching

between cases. A common Lyapunov function candidate is used in Theorems 8.1-8.3 to establish the decay rate (when $B_M^\tau > 0$), growth rate (when $B_M^\tau = 0$), and overall boundedness of $\|z\|$. Theorems 8.1 and 8.2 require the assumption that $\|z(\cdot)\| \leq \gamma, \forall \cdot \in [t_0, t)$, where $\gamma \in \mathbb{R}_{>0}$ is a known constant, where the assumption is proven in Theorem 8.3. To aid the analysis in Theorems 8.1-8.3, let the switching instances be denoted as $\{t_n^i\}, i \in \{m, e\}, n \in \{1, 2, ...\}$, where t_n^m and t_n^e denote the time instances when B_M^τ becomes nonzero and zero for the n-th time, respectively. Furthermore, define $t_0^e \triangleq t_0$ since it is known that FES forces are not present at t_0 (i.e., $B_M^\tau = 0$ initially) due to the FES controller not being applied before t_0. In Theorem 8.4, the position and cadence errors are proven to be globally exponentially stable, and the motor controller is shown to be bounded.

Define the continuously differentiable, positive definite Lyapunov function candidates, $V_1 : \mathbb{R} \times \mathbb{R} \times \mathbb{R}_{\geq 0} \times \mathbb{R}_{\geq 0} \to \mathbb{R}_{\geq 0}$ and $V_2 : \mathbb{R} \times \mathbb{R} \to \mathbb{R}_{\geq 0}$, as

$$V_1 \triangleq \frac{1}{2} r^2 + \frac{1}{2} \omega_1 e_4^2 + Q_1 + Q_2, \tag{8–17}$$

$$V_2 \triangleq \frac{1}{2} e_1^2 + \frac{1}{2} M e_2^2, \tag{8–18}$$

which can be bounded as

$$\lambda_1 \|z\|^2 \leq V_1 \leq \lambda_2 \|z\|^2, \tag{8–19}$$

$$\beta_1 \|y\|^2 \leq V_2 \leq \beta_2 \|y\|^2, \tag{8–20}$$

where $\lambda_1 \triangleq \min\left(\frac{1}{2}, \frac{\omega_1}{2}\right)$, $\lambda_2 \triangleq \max\left(1, \frac{\omega_1}{2}\right)$, $\beta_1 \triangleq \min\left(\frac{1}{2}, \frac{c_m}{2}\right)$, $\beta_2 \triangleq \max\left(\frac{1}{2}, \frac{c_M}{2}\right)$, $z \in \mathbb{R}^4$ is defined as

$$z \triangleq \begin{bmatrix} r & e_4 & \sqrt{Q_1} & \sqrt{Q_2} \end{bmatrix}^T, \tag{8–21}$$

and y is defined following (8–5). Auxiliary constants $\delta_1, \delta_2, \lambda, \lambda_3, \lambda_4, v, v_1, v_2 \in \mathbb{R}_{>0}$ are defined to aid the subsequent stability analysis as

$$\delta_1 \triangleq \min\left(\frac{1}{4}\alpha_3 k_s, \frac{\omega_2}{3k_s\hat{\tau}^2} - \frac{\omega_1 k_s}{\varepsilon_1}, \frac{2\omega_2}{3\hat{\tau}(\alpha_3 - c_b\alpha_2 + \varepsilon_1\omega_1)}, \frac{1}{3\hat{\tau}}\right), \tag{8–22}$$

$$\delta_2 \triangleq \varepsilon_2 + k_s \left(\varepsilon_1 \omega_1 + \omega_2\right), \tag{8–23}$$

$$\lambda \triangleq \lambda_3 \Delta t_{min}^m - \lambda_4 \Delta t_{max}^e, \tag{8–24}$$

$$\lambda_3 \triangleq \lambda_2^{-1} \delta_1, \quad \lambda_4 \triangleq \lambda_1^{-1} \delta_2, \tag{8–25}$$

$$v \triangleq \tfrac{v_1}{\lambda_3} \exp\left(\lambda_4 \Delta t_{max}^e\right)\left(1 - \exp\left(-\lambda_3 \Delta t_{min}^m\right)\right) - \tfrac{v_2}{\lambda_4}\left(1 - \exp\left(\lambda_4 \Delta t_{max}^e\right)\right), \tag{8–26}$$

$$v_1 \triangleq \frac{\overline{\tilde{\tau}} \Upsilon^2}{k_s} + \frac{\alpha_2^2 c_4^2}{\alpha_3 k_s}, \tag{8–27}$$

$$v_2 \triangleq \frac{\left(\alpha_2 c_4 + k_s c_b \alpha_2 \hat{\tau} \Upsilon\right)^2}{4\varepsilon_2}, \tag{8–28}$$

where $\varepsilon_2, \Upsilon, \Delta t_{min}^m, \Delta t_{max}^e \in \mathbb{R}_{>0}$ denote a selectable constant, a known constant, the minimum allowable dwell-time for FES-induced muscle contractions, and the maximum allowable dwell-time for no FES-induced contractions, respectively. To aid the dwell-time analysis, define $\left\{t_j^i\right\}, i \in \{FES,\, KDZ\}, j \in \{1, 2, ...\}$, where t_j^{FES} and t_j^{KDZ} denote the known time instants when the crank enters $\mathcal{Q}_{FES}$ and $\mathcal{Q}_{KDZ}$ for the j-th time, respectively, and recall that the FES switching signals in (2–10) were designed to ensure that muscle contractions occur over the entire region $\mathcal{Q}_{FES}$. Achievable dwell-times can now be defined as

$$\Delta t_{min}^m \triangleq \min\left(t_j^{KDZ} - t_j^{FES}\right), \forall j, \tag{8–29}$$

$$\Delta t_{max}^e \triangleq \max\left(t_{j+1}^{FES} - t_j^{KDZ}\right), \forall j, \tag{8–30}$$

where Δt_{min}^m and Δt_{max}^e are dictated by a minimum and maximum allowable cadence after $\mathcal{Q}_{FES}$ has been defined.

Theorem 8.1. *For $B_M^\tau > 0$, $\|z(t)\|$ is uniformly ultimately bounded in the sense that*

$$\|z(t)\|^2 \leq \tfrac{\lambda_2}{\lambda_1}\|z(t_n^m)\|^2 \exp\left(-\lambda_3\left(t - t_n^m\right)\right) + \tfrac{v_1}{\lambda_1 \lambda_3}\left(1 - \exp\left(-\lambda_3\left(t - t_n^m\right)\right)\right), \tag{8–31}$$

$\forall t \in [t_n^m, t_n^e)$, $\forall n \in \{1, 2, ...\}$, *provided that Assumption 8.1 is satisfied,* $\|z(\cdot)\| < \gamma$, $\forall \cdot \in [t_0, t)$, *and the subsequent gain conditions are satisfied:*[1]

$$\alpha_3 \geq c_B \alpha_2, \quad \omega_2 \geq \frac{3\hat{\tau}^2 \omega_1 k_s^2}{\varepsilon_1}, \quad \alpha_3 k_s \hat{\tau} < 1, \tag{8–32}$$

$$\overline{\tilde{\tau}} \leq \frac{1}{k_s^2 \alpha_2^2 c_B^2} \left(4c_b \alpha_2 - 2\alpha_3 - 4\varepsilon_1 \omega_1 - 4\omega_2\right). \tag{8–33}$$

Proof. The solution to the time derivative of (8–17) exists almost everywhere (a.e.) within $t \in [t_0, \infty)$, because B_M^τ is discontinuous. A generalized time derivative of V_1, denoted by $\dot{\tilde{V}}_1$, exists such that $\dot{V}_1(z) \overset{\text{a.e.}}{\in} \dot{\tilde{V}}_1(z)$. Let $z(t)$ for $t \in [t_0, \infty)$ be a Filippov solution to the differential inclusion $\dot{z} \in K[h_1](z)$, where $h_1 \triangleq \begin{bmatrix} \dot{r} & \dot{e}_4 & \sqrt{\dot{Q}_1} & \sqrt{\dot{Q}_2} \end{bmatrix}^T$ (see [110]). Substituting (8–14) into $\dot{\tilde{V}}_1(z)$, applying Leibniz's Rule to (8–10), (8–15), and (8–16), using the fact that $\dot{V}_1(z) \overset{\text{a.e.}}{\in} \dot{\tilde{V}}_1(z)$, and upper bounding yields

$$\begin{aligned} \dot{V}_1 \overset{\text{a.e.}}{\leq} & \alpha_2 |r| |\chi_2| + \alpha_2 k_s B_M^\tau |r(r_{\hat{\tau}} - r_\tau)| - \alpha_3 k_s r^2 + k_s |\alpha_3 - \alpha_2 B_M^\tau| |r r_{\hat{\tau}}| \\ & + \omega_1 k_s (|e_4 r| + |e_4 r_{\hat{\tau}}|) + \tfrac{1}{2}(\alpha_3 - c_b \alpha_2 + \varepsilon_1 \omega_1) k_s (r^2 - r_{\hat{\tau}}^2) \\ & + \tfrac{\omega_2 k_s}{\hat{\tau}} \left(\hat{\tau} r^2 - \textstyle\int_{t-\hat{\tau}}^t r(\theta)^2 \, d\theta\right). \end{aligned} \tag{8–34}$$

Young's Inequality can be used to develop the subsequent inequalities

$$\begin{aligned} |r r_{\hat{\tau}}| &\leq \tfrac{1}{2} r^2 + \tfrac{1}{2} r_{\hat{\tau}}^2, \\ |e_4 r| &\leq \tfrac{1}{2\varepsilon_1} e_4^2 + \tfrac{\varepsilon_1}{2} r^2, \\ |e_4 r_{\hat{\tau}}| &\leq \tfrac{1}{2\varepsilon_1} e_4^2 + \tfrac{\varepsilon_1}{2} r_{\hat{\tau}}^2. \end{aligned} \tag{8–35}$$

Using Property 2.8 to bound B_M^τ, noticing that $|\alpha_3 - \alpha_2 B_M^\tau| \leq \alpha_3 - c_b \alpha_2$ provided that $\alpha_3 \geq c_B \alpha_2$, and inserting (8–35) into (8–34) yields

$$\begin{aligned} \dot{V}_1 \overset{\text{a.e.}}{\leq} & \alpha_2 |r| |\chi_2| + \alpha_2 k_s c_B |r(r_{\hat{\tau}} - r_\tau)| - \alpha_3 k_s r^2 + k_s (\alpha_3 - c_b \alpha_2 + \varepsilon_1 \omega_1 + \omega_2) r^2 \\ & + \left(\tfrac{\omega_1 k_s}{\varepsilon_1}\right) e_4^2 - \tfrac{\omega_2 k_s}{\hat{\tau}} \textstyle\int_{t-\hat{\tau}}^t r(\theta)^2 \, d\theta. \end{aligned} \tag{8–36}$$

[1] See Remark 8.1 regarding the feasibility of the gain conditions.

Using the fact that $|\chi_2| \leq c_4$ and completing the squares on $\alpha_2 |r| |\chi_2|$ yields

$$\begin{aligned} \dot{V}_1 \overset{\text{a.e.}}{\leq} & \alpha_2 k_s c_B |r (r_{\hat{\tau}} - r_\tau)| + \tfrac{\alpha_2^2 c_4^2}{\alpha_3 k_s} - k_s \left(c_b \alpha_2 - \tfrac{1}{2}\alpha_3 - \varepsilon_1 \omega_1 - \omega_2 \right) r^2 \\ & - \tfrac{1}{4}\alpha_3 k_s r^2 + \left(\tfrac{\omega_1 k_s}{\varepsilon_1} \right) e_4^2 - \tfrac{\omega_2 k_s}{\hat{\tau}} \textstyle\int_{t-\hat{\tau}}^{t} r (\theta)^2 \, d\theta. \end{aligned} \tag{8–37}$$

The Cauchy-Schwarz Inequality can be used with (8–13) on (8–10) to yield the following upper bound

$$e_4^2 \leq \hat{\tau} k_s^2 \int_{t-\hat{\tau}}^{t} r (\theta)^2 \, d\theta, \tag{8–38}$$

and the following upper bound for Q_2 can be obtained

$$Q_2 \leq \omega_2 k_s \int_{t-\hat{\tau}}^{t} r (\theta)^2 \, d\theta. \tag{8–39}$$

Using (8–15), (8–38), and (8–39) it can be shown that

$$- \frac{\omega_2 k_s}{3\hat{\tau}} \int_{t-\hat{\tau}}^{t} r (\theta)^2 \, d\theta \leq - \frac{2\omega_2}{3\hat{\tau} (\alpha_3 - c_b \alpha_2 + \varepsilon_1 \omega_1)} Q_1, \tag{8–40}$$

$$- \frac{\omega_2 k_s}{3\hat{\tau}} \int_{t-\hat{\tau}}^{t} r (\theta)^2 \, d\theta \leq - \frac{\omega_2}{3 k_s \hat{\tau}^2} e_4^2, \tag{8–41}$$

$$- \frac{\omega_2 k_s}{3\hat{\tau}} \int_{t-\hat{\tau}}^{t} r (\theta)^2 \, d\theta \leq - \frac{1}{3\hat{\tau}} Q_2. \tag{8–42}$$

A further upper bound for (8–37) can be obtained by using (8–40)-(8–42) to yield

$$\dot{V}_1 \overset{\text{a.e.}}{\leq} -\delta_1 \|z\|^2 - k_s \left(c_b \alpha_2 - \tfrac{1}{2}\alpha_3 - \varepsilon_1 \omega_1 - \omega_2 \right) r^2 + \alpha_2 k_s c_B |r (r_{\hat{\tau}} - r_\tau)| + \tfrac{\alpha_2^2 c_4^2}{\alpha_3 k_s}. \tag{8–43}$$

Provided that $\|z(\cdot)\| < \gamma, \ \forall \cdot \in [t_0, t)$, it can be shown that $\dot{r}(\cdot) \leq \Upsilon, \ \forall \cdot \in [t_0, t)$ by using (8–14), (8–21), the fact $|\chi_2| \leq c_4$, and Property 2.8. In fact, by using (8–14), the MVT, and the gain condition $\alpha_3 k_s \hat{\tau} < 1$ it can be shown that

$$\dot{r} \leq \tfrac{\alpha_2 (c_4 + c_B k_s \gamma)}{(1 - \alpha_3 k_s \hat{\tau})} \leq \Upsilon, \tag{8–44}$$

provided that $\|z(\cdot)\| < \gamma,\ \forall \cdot \in [t_0, t)$. Using the MVT and Property 2.11, (8–43) can be upper bounded as

$$\dot{V}_1 \overset{\text{a.e.}}{\leq} -\delta_1 \|z\|^2 - k_s \left(c_b\alpha_2 - \tfrac{1}{2}\alpha_3 - \varepsilon_1\omega_1 - \omega_2\right) r^2 + \alpha_2 k_s c_B \bar{\bar{\tau}} \Upsilon |r| + \tfrac{\alpha_2^2 c_4^2}{\alpha_3 k_s}. \tag{8–45}$$

By completing the squares and imposing the gain condition from (8–33), (8–45) can be bounded as

$$\dot{V}_1 \overset{\text{a.e.}}{\leq} -\delta_1 \|z\|^2 + v_1, \tag{8–46}$$

where δ_1 and v_1 are defined in (8–22) and (8–27), respectively. Using (8–19) and (8–25) allows (8–46) to be further bounded as

$$\dot{V}_1 \overset{\text{a.e.}}{\leq} -\lambda_3 V_1 + v_1. \tag{8–47}$$

Solving the differential inequality in (8–47) yields

$$V_1(t) \leq V_1(t_n^m) \exp\left(-\lambda_3 (t - t_n^m)\right) + \tfrac{v_1}{\lambda_3}\left(1 - \exp\left(-\lambda_3 (t - t_n^m)\right)\right), \tag{8–48}$$

$\forall t \in [t_n^m, t_n^e), \forall n \in \{1, 2, ...\}$, provided that $\|z(\cdot)\| < \gamma,\ \forall \cdot \in [t_0, t)$ and the gain conditions in (8–32) and (8–33) are met. By (8–19), the result in (8–31) is obtained. □

Theorem 8.2. *For $B_M^\tau = 0$, $\|z(t)\|$ can be upper bounded in the sense that*

$$\|z(t)\|^2 \leq \tfrac{\lambda_2}{\lambda_1}\|z(t_n^e)\|^2 \exp\left(\lambda_4 (t - t_n^e)\right) - \tfrac{v_2}{\lambda_1\lambda_4}\left(1 - \exp\left(\lambda_4 (t - t_n^e)\right)\right), \tag{8–49}$$

$\forall t \in \left[t_n^e, t_{n+1}^m\right), \forall n \in \{0, 1, 2, ...\}$*, provided that the gain conditions in* (8–32) *and* (8–33) *are satisfied, Assumption 8.1 is met, and* $\|z(\cdot)\| < \gamma,\ \forall \cdot \in [t_0, t)$*.*

Proof. Setting $B_M^\tau = 0$ in (8–34), adding and subtracting $k_s c_b \alpha_2 r r_{\hat{\tau}} + k_s c_b \alpha_2 r^2$, and using the MVT yields

$$\begin{aligned}\dot{V}_1 \overset{\text{a.e.}}{\leq}\ & |r|\left(\alpha_2 |\chi_2| + k_s c_b \alpha_2 \hat{\tau} \Upsilon\right) + k_s\left(\alpha_3 - c_b\alpha_2\right) r r_{\hat{\tau}} - k_s\left(\alpha_3 - c_b\alpha_2\right) r^2 \\ & + \omega_1 k_s\left(|e_4 r| + |e_4 r_{\hat{\tau}}|\right) + \tfrac{1}{2}\left(\alpha_3 - c_b\alpha_2 + \varepsilon_1\omega_1\right) k_s\left(r^2 - r_{\hat{\tau}}^2\right) \\ & + \tfrac{\omega_2 k_s}{\hat{\tau}}\left(\hat{\tau} r^2 - \textstyle\int_{t-\hat{\tau}}^t r(\theta)^2\, d\theta\right).\end{aligned} \tag{8–50}$$

Using a similar strategy as the case when $B_M^\tau > 0$, (8–50) can be bounded as

$$\dot{V}_1 \overset{\text{a.e.}}{\leq} \lambda_4 V_1 + v_2, \tag{8–51}$$

where δ_2, λ_4, and v_2 are defined in (8–23), (8–25), and (8–28), respectively. Solving the differential inequality in (8–51) yields

$$V_1(t) \leq V_1(t_n^e)\exp(\lambda_4(t-t_n^e)) + \tfrac{v_2}{\lambda_4}(\exp(\lambda_4(t-t_n^e))-1), \tag{8–52}$$

$\forall t \in \left[t_n^e, t_{n+1}^m\right)$ and $\forall n \in \{0,1,2,...\}$, provided that $\|z(\cdot)\| < \gamma,\ \forall \cdot \in [t_0, t)$ and the gain conditions in (8–32) and (8–33) are met. By (8–19), the result in (8–49) is obtained. □

Theorem 8.3. $\|z(t)\|$ *is bounded for all time in the sense that*

$$\|z(t)\| < \gamma, \forall t \in [t_0, \infty), \tag{8–53}$$

provided Assumption 8.1 is satisfied and the gain conditions in (8–32) *and* (8–33) *are satisfied in addition to the subsequent gain conditions*

$$\lambda_3 \Delta t_{min}^m > \lambda_4 \Delta t_{max}^e, \tag{8–54}$$

$$\frac{v}{1-\exp(-\lambda)} < \lambda_1 \gamma^2, \tag{8–55}$$

$$\tfrac{v_2}{\lambda_4}(\exp(\lambda_4 \Delta t_{max}^e) - 1) < \lambda_1 \gamma^2, \tag{8–56}$$

Proof. The ultimate bound can be determined by evaluating V_1 at the switching instances (i.e., $V_1(t_n^m)$). Using (8–48), (8–52), and the minimum and maximum allowable dwell-times (i.e., the worst case scenario) defined in (8–29) and (8–30), $V_1\left(t_{n+1}^m\right)$ can be bounded as

$$V_1\left(t_{n+1}^m\right) \leq V_1(t_n^m)\exp(-\lambda) + v,\ \forall n, \tag{8–57}$$

provided that the gain condition in (8–54) is satisfied, and provided that $\|z(\cdot)\| < \gamma,\ \forall \cdot \in \left[t_0, t_{n+1}^m\right), \forall n$, where λ and v are defined in (8–24) and (8–26), respectively. From

(8–19), it can be shown that a sufficient condition for $\|z(\cdot)\| < \gamma,\ \forall \cdot \in \left[t_0, t_{n+1}^m\right), \forall n$ is that $V_1(\cdot) < \lambda_1\gamma^2,\ \forall \cdot \in \left[t_0, t_{n+1}^m\right), \forall n$. Furthermore, note that V_1 is known from (8–17).

The remainder of the proof will establish the ultimate bound and sufficient conditions for $V_1(\cdot) < \lambda_1\gamma^2,\ \forall \cdot \in \left[t_0, t_{n+1}^m\right), \forall n$. First, recall that FES forces are not present over $t \in [t_0, t_1^m)$, thus we can apply (8–52) over $t \in [t_0, t_1^m)$ to yield

$$V_1(t) \ \leq \ V_1(t_0)\exp\left(\lambda_4\left(t - t_n^e\right)\right) + \tfrac{v_2}{\lambda_4}\left(\exp\left(\lambda_4\left(t - t_n^e\right)\right) - 1\right). \tag{8–58}$$

From (2–1) and the fact that each term in V_1 is a time-based integral (see (8–8), (8–10), (8–11), (8–15), (8–16), and (8–17)), it can be seen that $V_1(t_0) = 0$. Using (8–58), setting $V_1(t_0) = 0$, and assuming the worst case scenario (no muscle forces for the maximum allowable dwell-time), it could be shown that a sufficient condition for $V_1(t) < \lambda_1\gamma^2, \forall t \in [t_0, t_1^m)$ is that the condition in (8–56) is satisfied.

To determine the ultimate bound, we must consider when V_1 will converge, i.e., when $V_1\left(t_{n+1}^m\right) < V_1(t_n^m)$. From (8–57), V_1 will converge, for any n, whenever the following inequality holds (otherwise V_1 may diverge)

$$V_1(t_n^m) \ > \ \tfrac{v}{1-\exp(-\lambda)} \triangleq V_1^{UB}, \tag{8–59}$$

provided that $V_1(\cdot) < \lambda_1\gamma^2,\ \forall \cdot \in \left[t_0, t_{n+1}^m\right)$. It will subsequently be shown that $V_1^{UB} \in \mathbb{R}$ is the ultimate bound for V_1 . Further, provided that (8–55) is satisfied, notice that $V_1^{UB} < \lambda_1\gamma^2$.

There are two cases to consider, the case when (8–59) is not satisfied (i.e., $V_1(t_n^m) \leq V_1^{UB}$) and the case when (8–59) is satisfied (i.e., $V_1(t_n^m) > V_1^{UB}$), called Case 1 and Case 2, respectively.

For Case 1, it could be shown by using (8–57) that if $V_1(t_n^m) \leq V_1^{UB}$ then $V_1\left(t_{n+1}^m\right) \leq V_1^{UB}$ for any n, provided that $V_1(\cdot) < \lambda_1\gamma^2,\ \forall \cdot \in \left[t_0, t_{n+1}^m\right)$. Since $V_1(t_n^m) \leq V_1^{UB}$ implies $V_1\left(t_{n+1}^m\right) \leq V_1^{UB}$, it can be shown from the bounds in (8–48) and (8–52) that $V_1(\cdot) \leq V_1^{UB}, \forall \cdot \in \left[t_n^m, t_{n+1}^m\right]$, provided $V_1(\cdot) < \lambda_1\gamma^2,\ \forall \cdot \in [t_0, t_n^m)$. Thus, if $V_1(t_1^m) \leq V_1^{UB}$,

it can be shown that $V_1(t) \leq V_1^{UB}, \forall t \in [t_0, \infty)$ and hence from (8–19) and the fact that $V_1^{UB} < \lambda_1 \gamma^2$, $\|z(t)\| < \gamma, \forall t \in [t_0, \infty)$.

For Case 2, recall that $V_1\left(t_{n+1}^m\right) < V_1\left(t_n^m\right)$ and that the bound on $V_1(t)$ will decay $\forall t \in [t_n^m, t_n^e)$ according to (8–48) and will grow $\forall t \in \left[t_n^e, t_{n+1}^m\right)$ according to (8–52). However, since $V_1\left(t_{n+1}^m\right) < V_1\left(t_n^m\right)$, the bound on $V_1(t)$ will decay more during $[t_n^m, t_n^e)$ than it will grow during $\left[t_n^e, t_{n+1}^m\right)$. Therefore, $V_1(\cdot) \leq V_1\left(t_n^m\right), \forall \cdot \in \left[t_n^m, t_{n+1}^m\right]$, provided $V_1(\cdot) < \lambda_1 \gamma^2, \ \forall \cdot \in [t_0, t_n^m)$. Thus, for any n, if $V_1\left(t_n^m\right) > V_1^{UB}$ (i.e., the condition for Case 2), then $V_1\left(t_{n+1}^m\right) < V_1\left(t_n^m\right)$, which results in V_1 decaying towards V_1^{UB}, and if $V_1\left(t_n^m\right) \leq V_1^{UB}$, for any subsequent n, thereafter $V_1(\cdot) \leq V_1^{UB}, \forall t \in [t_n^m, \infty)$. Therefore, $\limsup_{t \to \infty} V_1(t) = V_1^{UB}$. Using the prior results and provided the conditions in (8–54)-(8–56) are satisfied, it can be seen that $V_1(\cdot) < \lambda_1 \gamma^2, \ \forall \cdot \in \left[t_0, t_{n+1}^m\right), \forall n$, and hence from (8–19) and the fact that $V_1^{UB} < \lambda_1 \gamma^2$, $\|z(\cdot)\| < \gamma, \ \forall \cdot \in [t_0, \infty)$.

Therefore, a sufficient condition for $\|z(\cdot)\| < \gamma, \ \forall \cdot \in [t_0, t)$ is that Assumption 8.1 and the gain conditions in (8–32), (8–33), and (8–54)-(8–56) are satisfied. From (8–11), (8–21), and (8–53) it can be shown that $e_3, r \in \mathcal{L}_\infty$ and thus from (8–13), $u \in \mathcal{L}_\infty, \forall t$. □

Remark 8.1. Provided that the EMD, the EMD estimation error, and the uncertainty of the FES control effectiveness (i.e., $|c_B - c_b|$) are sufficiently small, then the gain conditions are feasible. Iteration may be required when selecting the gains since the gain conditions are interconnected. A general strategy when selecting the gains is to select $\alpha_3 = c_B \alpha_2$, a larger value for k_m (increasing k_m increases c_b and c_B), and a smaller value for k_s and α_2. Furthermore, it is desired to increase Δt_{min}^m and to decrease Δt_{max}^e. To demonstrate the feasibility of the gain conditions, an example evolution of V_1 is generated by using (8–48) and (8–52) and is plotted in Figure 8-1.

Theorem 8.4 is now provided to establish the decay rate for the position and cadence error system for all time.

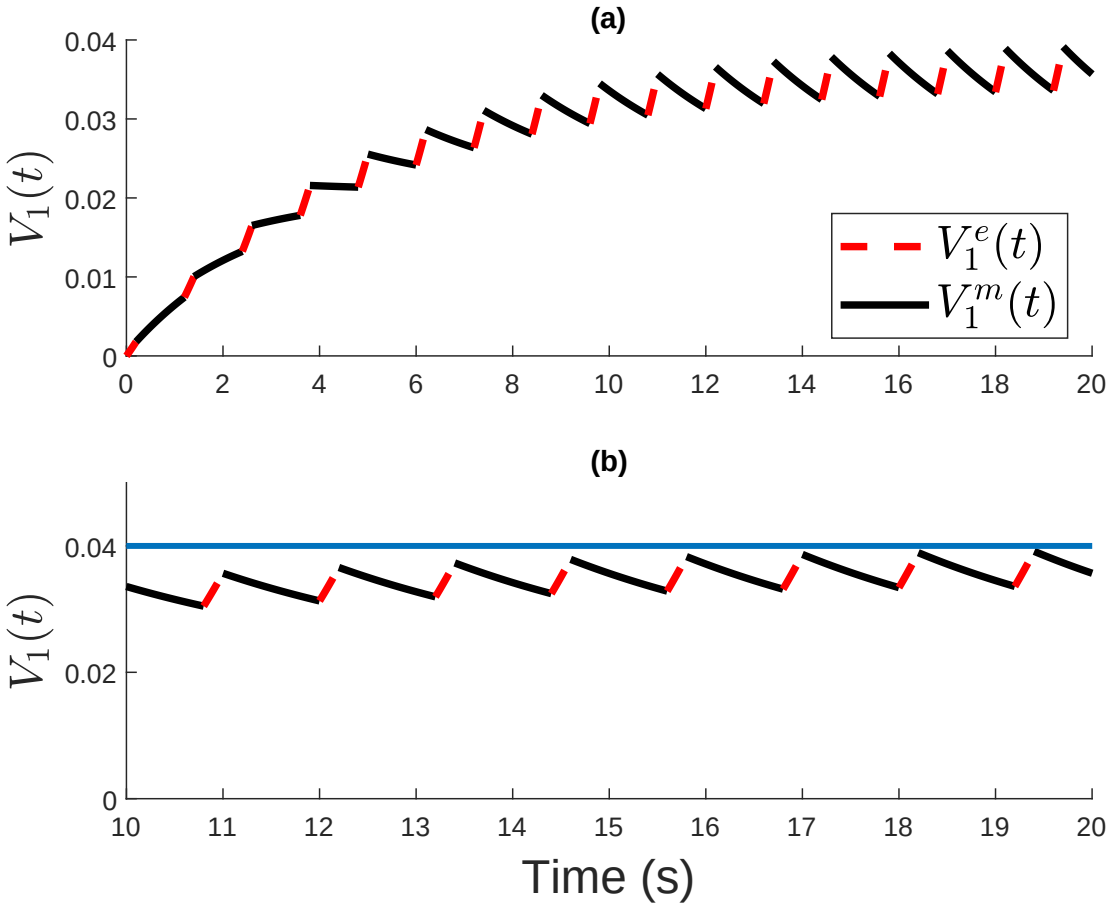

Figure 8-1. (a) An example evolution of V_1 over 20 s if the system had the parameters (for simplicity units are not included) $c_b = 35$, $c_B = 50$, $\Delta t^e = 0.2$, $\Delta t^m = 1.0$, $\hat{\tau} = 0.09$, $\bar{\bar{\tau}} = 0.01$, $\gamma = 0.29$, $\Upsilon = 0.5$, $c_4 = 0.55$, and the gains $k_s = 0.4$, $\alpha_2 = 0.07$, $\alpha_3 = 3.5$, and $k_m = 500$, $\forall m$, which satisfy the gain conditions in (8–32), (8–33), and (8–54)-(8–56). The exponential growth when in the uncontrolled region is denoted by V_1^e and the exponential decay in the controlled regions is denoted by V_1^m. Due to the form of V_1 in (8–17), $V_1(t_0) = 0$. The choice of Δt^m and Δt^e is for a constant cadence of 50 RPM with the muscle contractions (intermittently spread across 6 muscles) occurring over 83% of the cycle. (b) The same plot but focusing on the times between 10 s and 20 s and emphasizing the ultimate bound (indicated by the blue line).

Theorem 8.4. *The composite position and cadence error vector, y, is globally exponentially stable in the sense that*

$$\|y(t)\| \leq \sqrt{\frac{\beta_2}{\beta_1}} \|y(t_0)\| \exp\left(-\frac{\min(\alpha_1, k_1)}{2\beta_2}(t - t_0)\right), \tag{8–60}$$

$\forall t \in [t_0, \infty)$*, provided the following gain conditions are satisfied*

$$k_2 \geq c_1,\ k_3 \geq c_2,\ k_4 \geq c_3, \tag{8–61}$$

where c_1, c_2, and c_3 are introduced in (8–7)*.*

Proof. Since the motor controller is discontinuous the time derivative of (8–18) exists a.e. within $t \in [t_0, \infty)$ and $\dot{V}_2(y) \overset{\text{a.e.}}{\in} \dot{\tilde{V}}_2(y)$, where $\dot{\tilde{V}}_2$ is the generalized time derivative of (8–18). Let $y(t)$ for $t \in [t_0, \infty)$ be a Filippov solution to the differential inclusion $\dot{y} \in K[h_2](y)$, where $h_2 \colon \mathbb{R}^2 \to \mathbb{R}^2$ is defined as $h_2 \triangleq \begin{bmatrix} \dot{e}_1 & \dot{e}_2 \end{bmatrix}^T$ [110]. Substituting (8–3) and (8–6) into $\dot{\tilde{V}}_2(y)$, canceling common terms, using Property 2.10, and rearranging terms yields

$$\dot{\tilde{V}}_2 \subseteq -\alpha_1 e_1^2 + e_2 \chi - k_1 e_2^2 - \left(k_2 + k_3 \|y\| + k_4 \|y\|^2\right) K[\text{sgn}(e_2)] e_2. \tag{8–62}$$

Using (8–20) and (8–7), the fact that $\dot{V}_2(y) \overset{\text{a.e.}}{\in} \dot{\tilde{V}}_2(y)$, and provided the gain conditions in (8–61) are met, (8–62) can be bounded above as

$$\dot{V}_2 \overset{\text{a.e.}}{\leq} -\frac{\min(\alpha_1, k_1)}{\beta_2} V_2. \tag{8–63}$$

The differential inequality in (8–63) is solved to yield

$$V_2(t) \leq V_2(t_0) \exp\left(-\frac{\min(\alpha_1, k_1)}{\beta_2}(t - t_0)\right), \tag{8–64}$$

$\forall t \in [t_0, \infty)$. Provided the gain conditions in (8–61) are met, (8–20) can be used with (8–64) to yield the bound in (8–60). From (8–18) and (8–64) it can be seen that $e_1, e_2 \in \mathcal{L}_\infty$. From (8–21) and (8–53), $r \in \mathcal{L}_\infty$. From Properties 2.7 and 2.8, (8–1), and

Table 8-1. Participant Demographics

Participant	Age	Sex	Condition	Time Since Diagnosis
S1	28	M	None	- -
S2	22	F	None	- -
S3	28	M	None	- -
S4	24	M	None	- -
S5	23	F	None	- -
N1	26	M	Spina Bifida (L5-S1)	26yr
N2	55	F	Multiple Sclerosis	25yr
N3	54	M	Multiple Sclerosis	10yr
N4	42	F	Cerebral Palsy	42yr

the fact that $\tau_M \triangleq B_M^\tau k_s r_\tau + \tau_{vol}$ and $|\tilde{\tau}_M| \leq c_{est}$, it can be shown that $\tau_M, \hat{\tau}_M \in \mathcal{L}_\infty$, and by (8–5), $u_e \in \mathcal{L}_\infty$. □

8.3 Experiment

Henceforth, the combined efforts of the developed controllers in (8–5) and (8–13) and FES switching signals in (2–10) will be labeled as Controller A, the control structure developed in [41] (which assumed that the EMD was negligible) will be labeled as Controller B, and the developed motor controller in (8–5) alone will be labeled as Controller C. Controllers A and B have the same form (i.e., the motor tracks the position/cadence and the FES tracks the power); however, Controller A provides compensation for the EMD.

8.3.1 Experimental Testbed

The experimental testbed used in this chapter is the FES cycle that is introduced in Chapter 2.

8.3.2 Experimental Methods

Comparative experiments were performed on nine participants with the demographics summarized in Table 8-1, where participants with and without NCs are represented by the letter “N” and “S”, respectively, followed by an identifying number. Prior to participation, written informed consent approved by the UF Institutional Review Board

(IRB201600881) was provided. Experiments were either performed with or without volitional contributions by the participant, which are subsequently called active and passive therapy experiments, respectively. During the passive therapy experiments, the participants were blind to the actual/desired trajectories and were instructed to remain passive to simulate a situation where a participant is unable to provide voluntary contribution (e.g., due to muscle weakness or paralysis). During the active therapy experiments, the participants were shown a real-time plot of $e_3(t)$, exclusively, and were instructed to contribute to the best of their ability to the control objective, and FES was applied as required.

Prior to performing an experiment, Axelgaard ValuTrode CF7515 electrodes were placed over each muscle group (i.e., quadriceps, gluteal, and hamstrings) of a participant seated with their feet secured to the cycle using Össur Rebound Air Tall orthotic boots. The position of the cycle's seat was adjusted for comfort and so that the knees could not fully extend (i.e., the knees maintained a bend of at least 15 degrees). Measurements (i.e., limb lengths, seat position, etc.) were then made according to [3] to determine the participant's desired muscle contraction regions (i.e., $\mathcal{Q}_m$) for each muscle group. A FES comfort limit was obtained for each muscle group by running the cycle at 50 RPM and then applying and modulating open-loop stimulation, to one muscle group at a time, until the participant's comfort limit was determined for each muscle. Subsequently, the stimulation input to a given muscle was saturated if it exceeded the participant's comfort limit for that muscle.

A preliminary experiment was performed to estimate the passive torques of the cycle and rider about the crank, denoted by $\hat{\tau}_{pas}$. During this trial, FES was not applied and the rider was instructed to not provide volitional effort. The trial consisted of using the motor controller in (8–5) to run the cycle at 50 RPM (the desired cadence) while simultaneously recording the angular position and torque/power. An eighth-order Fourier fit was then applied to the recorded torque and position data to obtain $\hat{\tau}_{pas}$. An active

estimate of $\hat{\tau}_M$ could then be obtained by subtracting $\hat{\tau}_{pas}$ from the active torque sensor measurements, which satisfies Assumption 8.1.

The experimental protocol consisted of the motor controller associated with either Controller A, B, or C tracking a desired cadence that increased from 0 to 50 RPM over the first 30 s and then tracking 50 RPM for the remaining 90 s of the experiment (the steady-state portion of the experiment). After the cadence increase (i.e., t = 30 s), the corresponding FES controller was activated to track the desired power trajectory, denoted by $P_d : \mathbb{R}_{\geq 0} \to \mathbb{R}$ and defined as $P_d \triangleq \tau_{M,d}\dot{q}_d$, which smoothly increased from 0 to the desired power (1 W and 5 W for passive and active therapy experiments, respectively) and thereafter was held constant. Furthermore, the measured torque can be converted to the measured power, $P : \mathbb{R}_{\geq 0} \to \mathbb{R}$, by using $P \triangleq \hat{\tau}_M \dot{q}$. Passive therapy experiments (i.e., no volition) were performed on the able-bodied participants by implementing Controllers A and B in a random order. Active therapy experiments (i.e. with volition) were performed on the participants with NCs by implementing Controllers A and C in a random order. No practice was permitted for the able-bodied participants; however, the participants with NCs were permitted one practice run per controller since they provided volition. Subsequently, experiments are referred to as the participant number followed by the letter of the controller; for example, S1A denotes the experiment for participant S1 using Controller A.

8.4 Results

8.4.1 Results from Able-Bodied Participants

To validate Controller A, passive therapy experiments were performed on the able-bodied participants using Controllers A and B. The root mean square (RMS) and peak tracking (i.e., cadence and power) errors in addition to the required motor and FES effort are summarized in Table 8-2 for the able-bodied participants. The tracking (i.e., cadence and power) performance and control inputs (i.e., motor and FES) for participant S1, which depict a typical result, are provided in Figures 8-2 and 8-3 for Controller A and in

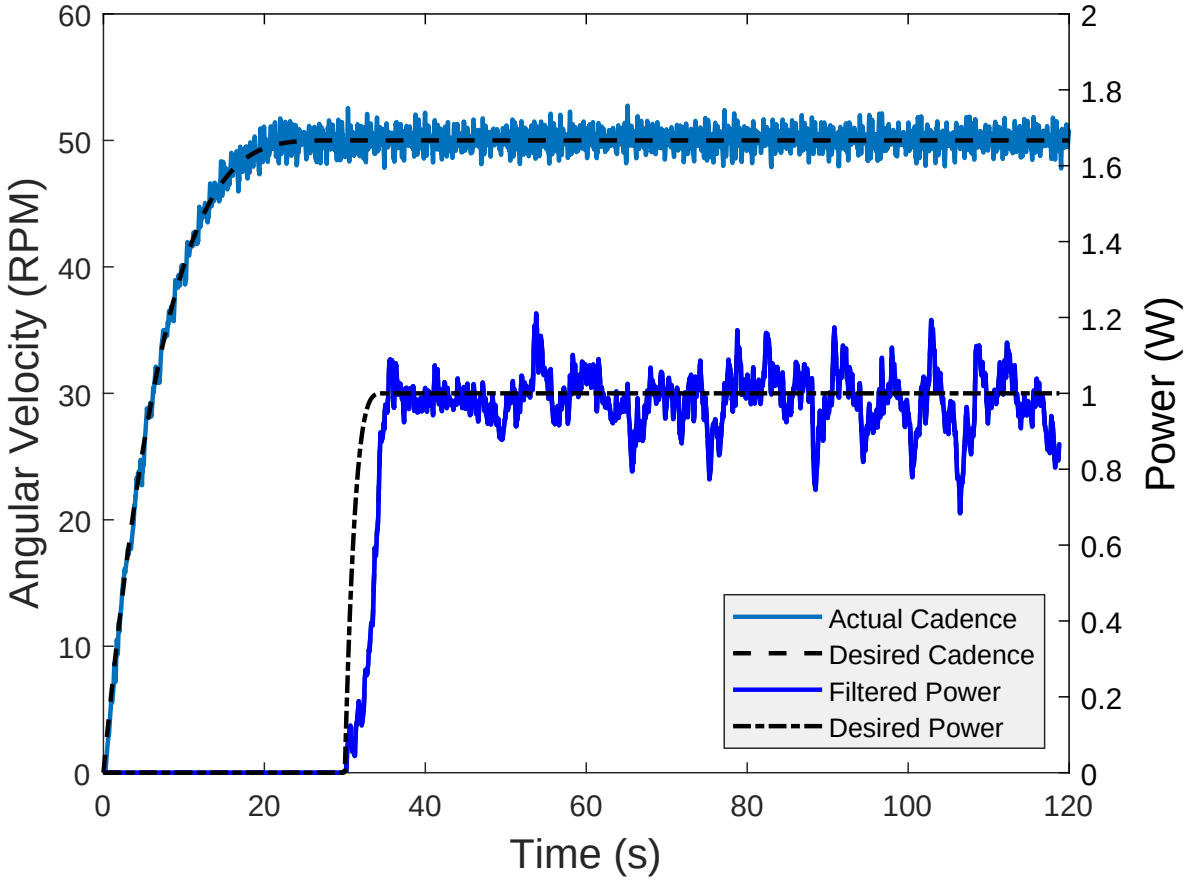

Figure 8-2. S1A: The desired versus the actual cadence and filtered power. For visual clarity, a two crank cycle (i.e., a moving window of 2.4 s) averaging filter was applied to the power.

Figures 8-4 and 8-5 for Controller B. Furthermore, across the able-bodied participants, Controllers A and B produced an average cadence error of -0.05$\pm$0.65 RPM and -0.05$\pm$0.73 RPM, respectively, an average integral torque error of 0.34$\pm$0.08 Nms and 1.13$\pm$0.76 Nms, respectively, and an average power error ($\dot{e}_3$) of 0.01$\pm$0.09 W and 0.38$\pm$0.18 W, respectively.

8.4.1.1 Statistical analysis

To compare the performance of Controllers A and B, paired difference statistical tests were implemented, using the data in Table 8-2, on the peak and RMS cadence ($\dot{e}_1$) , integral torque (e_3), and power tracking errors ($\dot{e}_3$), in addition to the average FES

Table 8-2. Comparative results for the able-bodied participants during steady state*,†

Controller	Participant	RMS Error $\dot{e}_1$ (RPM)	Peak Error $\dot{e}_1$ (RPM)	RMS Error e_3 (Nms)	Peak Error e_3 (Nms)	RMS Error $\dot{e}_3$ (W)‡	Peak Error $\dot{e}_3$ (W)‡	Motor Effort (A)‖	FES Effort (μs)#
A	S1	0.75	2.40	0.57	0.80	0.13	0.44	1.51±0.84	103.96±16.83
	S2	0.58	2.09	0.48	0.74	0.07	0.41	1.49±0.67	54.03±5.74
	S3	0.67	2.51	0.32	0.49	0.09	0.31	1.22±0.69	54.48±5.35
	S4	0.63	2.39	0.22	0.31	0.05	0.18	1.38±0.72	67.00±5.21
	S5	0.65	2.54	0.20	0.41	0.09	0.29	1.27±0.70	45.86±8.96
	Average	**0.66**	**2.38**	**0.36**	**0.55**	**0.09**	**0.32**	**1.37±0.73**	**65.07±8.42**
B	S1	0.74	2.57	2.56	4.92	0.43	0.86	1.61±0.81	123.17±17.33
	S2	0.72	2.31	1.73	3.48	0.77	0.96	1.65±0.82	61.49±8.63
	S3	0.89	2.99	0.13	0.32	0.27	0.83	1.44±0.77	67.82±10.78
	S4	0.64	1.95	1.99	3.86	0.79	1.02	1.55±0.74	72.40±16.24
	S5	0.68	2.42	0.45	0.73	0.16	0.58	1.30±0.73	44.89±7.02
	Average	**0.73**	**2.45**	**1.37**	**2.66**	**0.48**	**0.85**	**1.51±0.78**	**73.95±12.00**

*No volition was provided and the desired cadence and power were set to 50 RPM and 1 W, respectively.
†RMS error denotes the root mean square error and peak error denotes the maximum absolute value of the error over the entire experimental run.
‡For post-processing, a two crank cycle (i.e., a moving window of 2.4 s) averaging filter was applied.
‖The average $\pm$ standard deviation of $|u_E|$, where u_E denotes the current input to the motor.
#The average $\pm$ standard deviation of the maximum stimulation delivered to each muscle group during each FES region.

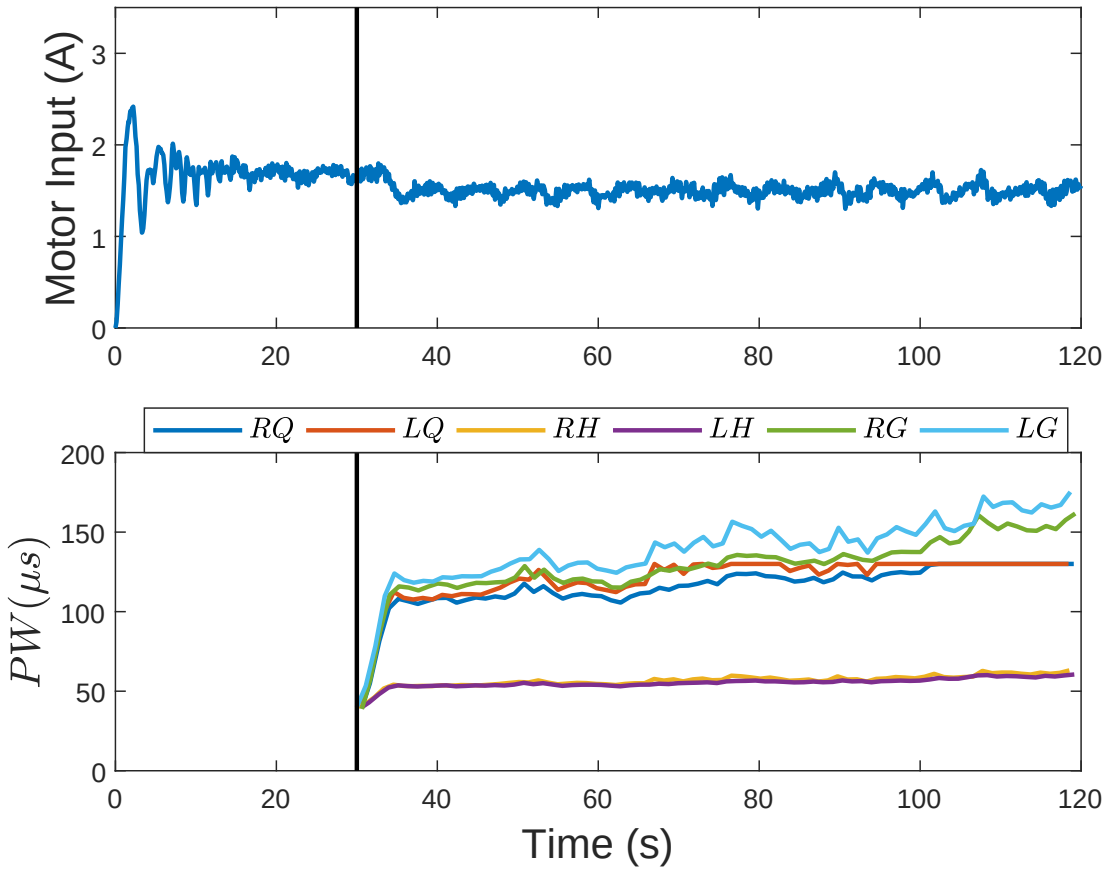

Figure 8-3. S1A: The filtered motor input using a 1.2 s moving average filter (top); and the maximum stimulation applied to the right (R) and left (L) quadriceps (Q), hamstring (H), and gluteal (G) for each FES region (bottom). Steady-state is indicated by the vertical black line. The flat portion of the FES input into the LQ is a result of saturating the input for rider comfort.

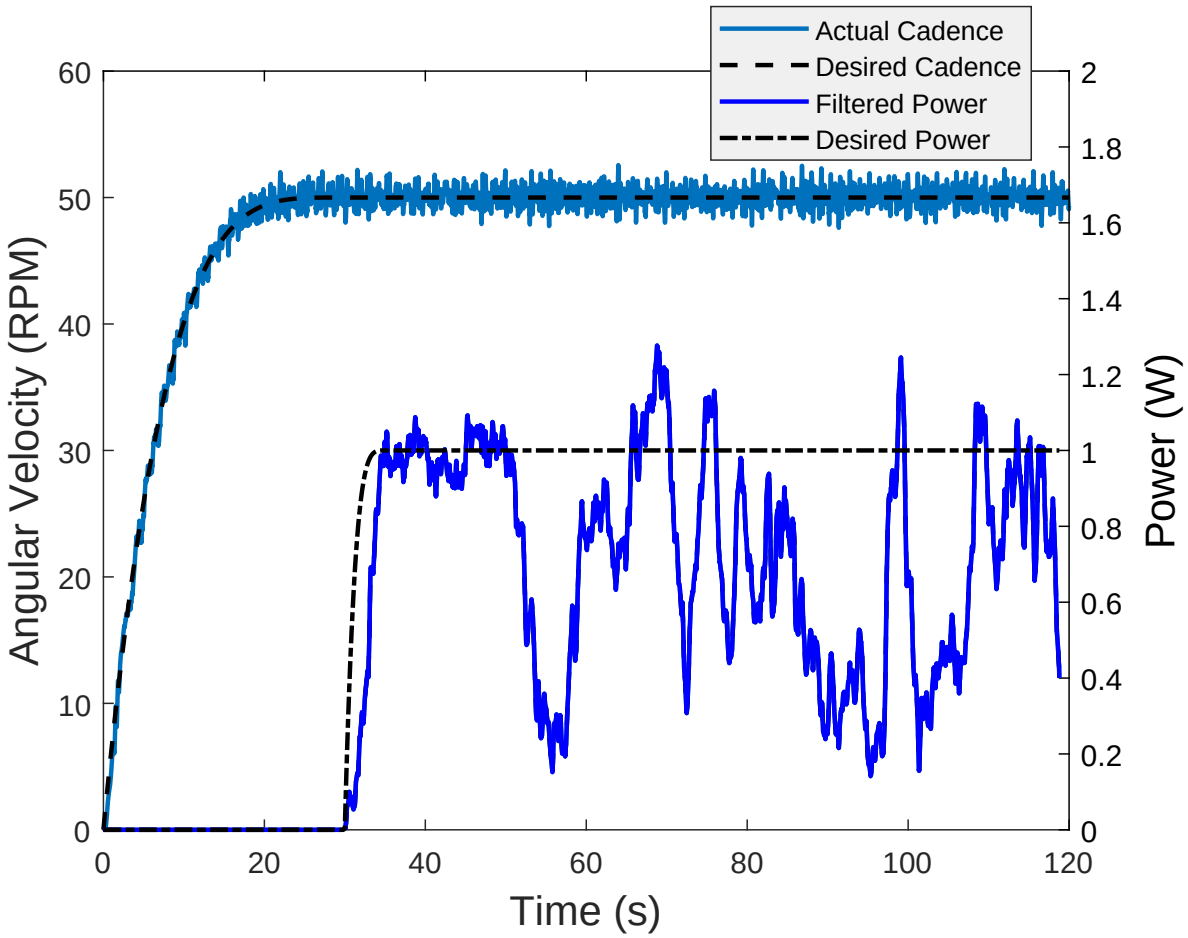

Figure 8-4. S1B: The desired versus the actual cadence and filtered power. For visual clarity, a two crank cycle (i.e., a moving window of 2.4 s) averaging filter was applied to the power.

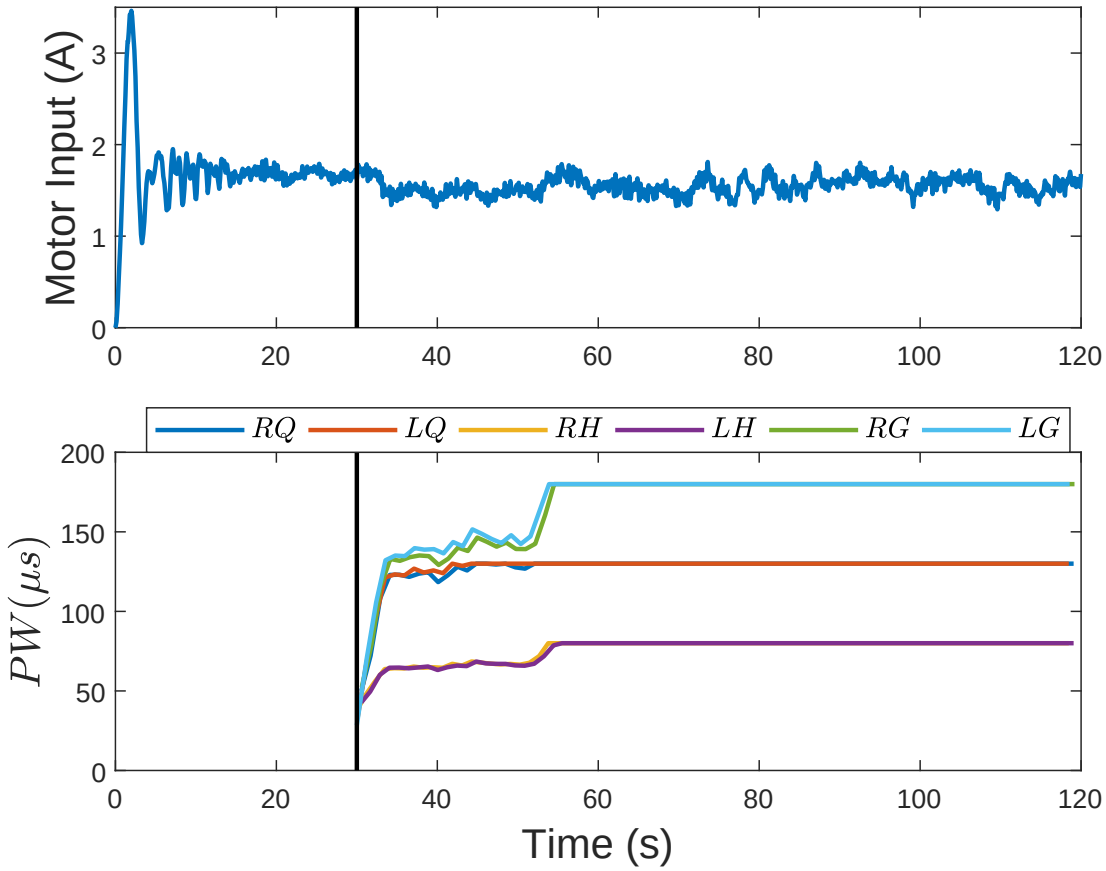

Figure 8-5. S1B: The filtered motor input using a 1.2 s moving average filter (top); and the maximum stimulation applied to the right (R) and left (L) quadriceps (Q), hamstring (H), and gluteal (G) for each FES region (bottom). Steady-state is indicated by the vertical black line. Note that the flat portions of the FES inputs are a result of saturating the stimulation input to each muscle to ensure participant comfort.

and motor effort, and the standard deviation of the FES and motor effort. Normality of the paired difference data for each measurement was confirmed using Shapiro-Wilk's normality test. One-sided paired t-tests were implemented to determine that the RMS (P-Value = 0.038) and peak (P-Value = 0.035) integral torque errors, RMS (P-Value = 0.022) and peak (P-Value = 0.002) power errors, and the average motor (P-Value = 0.008) and FES (P-Value = 0.031) effort were significantly larger for Controller B when compared to Controller A. However, no significant effect was determined between Controllers A and B for the RMS (P-Value = 0.072) and peak (P-Value = 0.357) cadence errors or the motor (P-Value = 0.074) and FES (P-Value = 0.092) standard deviations.

8.4.1.2 Discussion

From inspection of Figures 8-2 and 8-4, Controller A improves the torque/power tracking performance for participant S1, whereas the cadence tracking performance is essentially unaffected, which is consistent with the conclusions of the statistical analysis. Furthermore, from Figures 8-3 and 8-5 it is clear that the FES inputs for participant S1 tended to be higher for Controller B than Controller A, which is likewise consistent with the statistical analysis; however it is less visually clear that the average motor input for participant S1 was higher for Controller B than Controller A. Overall, it can be concluded that relative to Controller B, Controller A improved the torque/power tracking performance while requiring both a smaller average FES and motor effort.

Another interesting observation from Figures 8-3 and 8-5 is that, prior to saturation, the FES inputs tended to increase with time, which is indicative of the participant beginning to fatigue. In fact, in Figure 8-2 the power tracking appears to steadily worsen with time, likely as a result of fatigue. The development of methods (e.g., adaptive or optimal control) to further reduce fatigue while simultaneously providing compensation for the EMD is a focus of future efforts.

8.4.2 Results from Participants with NCs

Since Controller A improved the power/torque tracking and decreased the required control inputs, Controller B was not implemented on the participants with NCs. Recall that active therapy (i.e., with volitional effort) experiments were performed on the participants with NCs, therefore Controller C was implemented to determine how well the participant could track the desired power on their own volition. The results of the experiments using Controllers A and C on the participants with NCs are included in Table 8-3. A plot of the cadence and power tracking results for participant N1, which represent a typical result, are included in Figure 8-6 for Controller A and Figure 8-7 for Controller C. Furthermore, across the participants with NCs, Controllers A and C produced an average integral torque error of 0.23$\pm$0.44 Nms and 0.64$\pm$1.57 Nms, respectively, an average power error ($\dot{e}_3$) of 0.01$\pm$1.11 W and 0.01$\pm$1.95 W, respectively, and an average cadence error of -0.07$\pm$1.17 RPM for both controllers.

8.4.2.1 Statistical analysis

Statistical tests (i.e., Shapiro-Wilk and one-sided paired t-tests) were conducted to conclude normality and that RMS (P-Value = 0.045) and peak (P-Value = 0.028) integral torque error, and the peak power error (P-Value =0.03) were significantly larger for Controller C when compared to Controller A. Likewise, no significant effect was determined between Controllers A and C for the RMS (P-Value = 0.487) or peak (P-Value = 0.278) cadence error, the RMS power error (P-Value = 0.080), the average motor input (P-Value = 0.230), or the motor effort standard deviation (P-Value = 0.279).

8.4.2.2 Discussion

From the statistical analysis and by inspection of Figures 8-6 and 8-7, the torque/power tracking performance was improved when the FES controller from Controller A was implemented compared to Controller C, which provided no torque tracking assistance. The results in Table 8-3 and the statistical results demonstrate both the power and cadence tracking ability of Controller A, despite the uncertainties and

Table 8-3. Comparative results for the participants with NCs during steady state*,†

Controller	Participant	RMS Error $\dot{e}_1$ (RPM)	Peak Error $\dot{e}_1$ (RPM)	RMS Error e_3 (Nms)	Peak Error e_3 (Nms)	RMS Error $\dot{e}_3$ (W)‡	Peak Error $\dot{e}_3$ (W)‡	Motor Effort (A)‖	FES Effort (μs)#
A	N1	1.34	4.88	0.22	0.83	0.60	2.71	1.39±1.07	46.53±3.90
	N2	1.15	4.53	1.12	4.70	1.79	5.89	1.55±0.99	31.22±1.61
	N3	1.13	4.48	0.44	1.64	1.33	4.06	1.53±1.01	51.84±10.48
	N4	1.06	4.43	0.28	1.12	0.72	3.15	1.35±1.03	27.03±4.41
	Average	**1.17**	**4.58**	**0.52**	**2.07**	**1.11**	**3.95**	**1.45±1.02**	**39.15±5.10**
C	N1	1.18	4.76	0.41	1.58	0.90	4.97	1.22±0.85	0.00±0.00
	N2	0.93	3.79	3.20	7.95	3.03	7.28	1.22±0.78	0.00±0.00
	N3	1.17	4.58	1.00	4.64	1.26	7.80	1.48±0.98	0.00±0.00
	N4	1.42	7.33	2.23	7.04	2.64	10.13	1.54±1.23	0.00±0.00
	Average	**1.18**	**5.11**	**1.71**	**5.30**	**1.96**	**7.54**	**1.36±0.96**	**0.00±0.00**

*Volition was provided and the desired cadence and power were set to 50 RPM and 5 W, respectively.
†RMS error denotes the root mean square error and peak error denotes the maximum absolute value of the error over the entire experimental run.
‡For post-processing, a two crank cycle (i.e., a moving window of 2.4s) averaging filter was applied.
‖The average $\pm$ standard deviation of $|u_E|$, where u_E denotes the current input to the motor.
#The average $\pm$ standard deviation of the maximum stimulation delivered to each muscle group during each FES region.

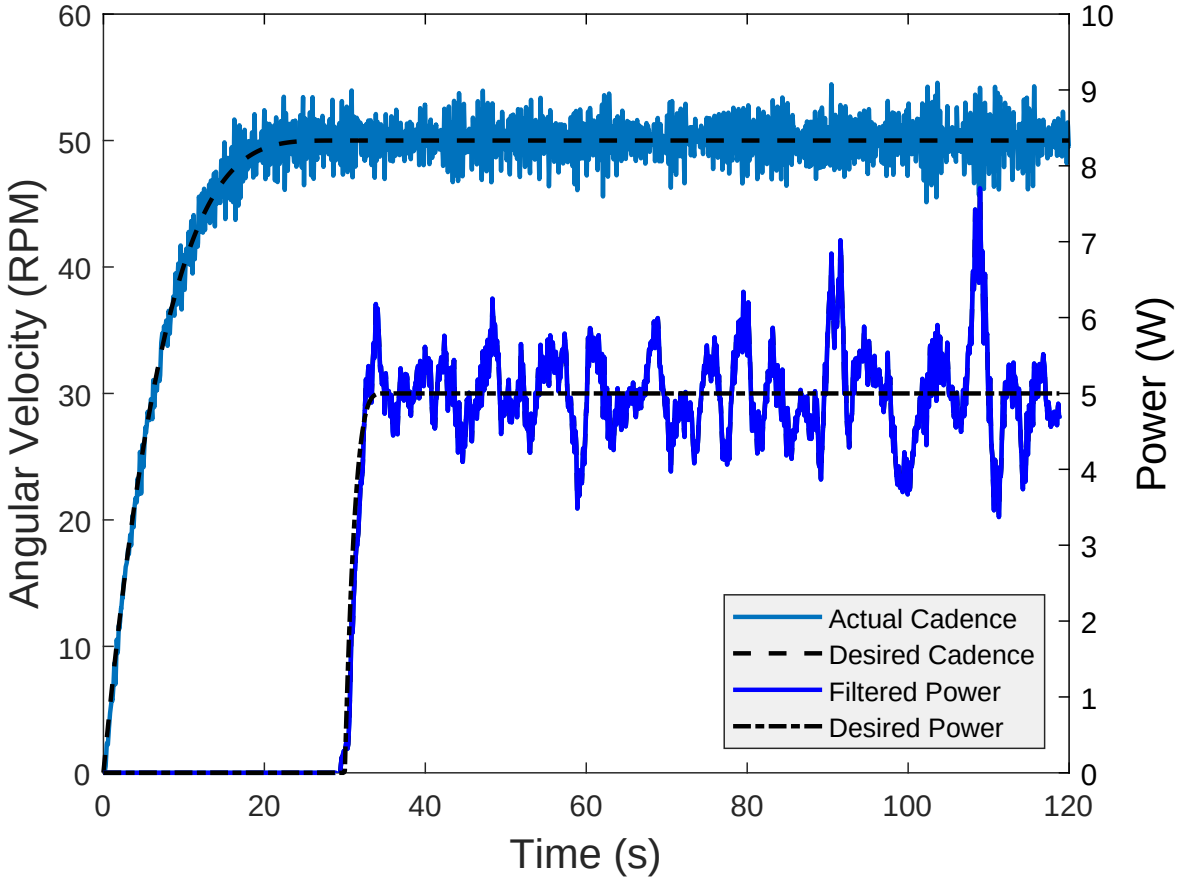

Figure 8-6. N1A: The desired versus the actual cadence and filtered power. For visual clarity, a two crank cycle (i.e., a moving window of 2.4 s) averaging filter was applied to the power.

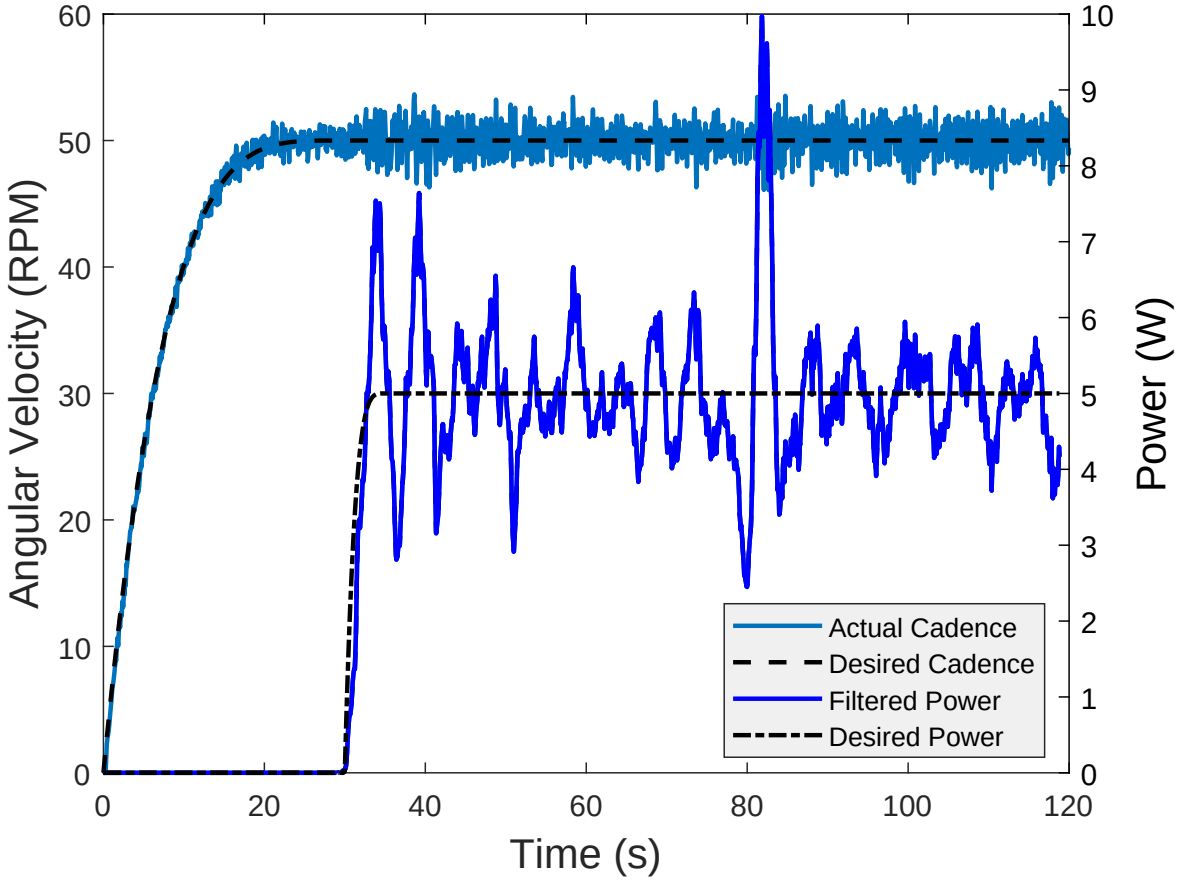

Figure 8-7. N1C: The desired versus the actual cadence and filtered power. For visual clarity, a two crank cycle (i.e., a moving window of 2.4 s) averaging filter was applied to the power.

time-varying nature associated with the rider-cycle system, including the wide-range of conditions of each participant, in addition to the effects of fatigue, the EMD, and volitional efforts. Overall, Controller A has proven its capability of achieving both cadence and power tracking for both passive and active therapy experiments on participants with and without NCs.

8.5 Concluding Remarks

In an effort to improve rehabilitation, a dual objective control system is developed in this chapter to track both PO and cadence using FES and motor controllers, respectively. The torque/power is tracked in real time by implementing a running integral of the torque tracking error. EMD compensation was provided by developing trigger conditions to properly time stimulation, LK functionals, and an auxiliary tracking error that injected a delay-free stimulation input into the closed-loop error system. A Lyapunov-like switched system analysis was performed to ensure exponential power tracking to an ultimate bound and global exponential cadence tracking for the uncertain, nonlinear, switched, and delayed cycle-rider system that was subject to uncertain disturbances such as an unknown volitional effort.

A series of comparative experiments were performed on nine participants, including four with a variety of NCs, to validate the developed FES and motor controllers. The proposed controllers produced average cadence and power tracking errors of -0.05$\pm$0.65 RPM and 0.01$\pm$0.09 W for the able-bodied participants, and -0.07$\pm$1.17 RPM and 0.01$\pm$1.11 W for the participants with NCs. A comparison was performed against non-delay compensating controllers of the same form as the proposed system, which demonstrated that compensating for the EMD improved the power tracking performance.

CHAPTER 9
CONCLUSION

NCs such as traumatic brain injury, stroke, spinal cord injury, and Parkinson's Disease, among others, often result in a deterioration of quality of life for affected individuals. In an effort to combat the severity of disability, reduce the cost of treatment of NCs, and limit the complications, researchers and clinicians have turned to technological solutions such as hybrid exoskeletons, which combine rehabilitation robots with FES to facilitate rehabilitative therapies. Control strategies for hybrid exoskeletons must be designed to ensure participant safety, while simultaneously promoting effective rehabilitation for participants with NCs. However, complications arise from uncertainties, nonlinearities, and time-varying properties of the dynamic system. Additionally, hybrid exoskeletons result in a physical human-robot interaction problem, where both the human (i.e., FES) and the robot (i.e., motor) are controlled and require control objectives. Moreover, hybrid exoskeletons are often a switched system (i.e., control switches between FES and a motor), which necessitates a switched systems stability analysis to guarantee system performance and to prevent injury. Furthermore, hybrid exoskeletons are complicated by the existence of an input delay, called the EMD, between the application/removal of FES and the onset/end of muscle force. To promote rehabilitation and safety, objectives such as position/cadence control, torque/power control, and saturated control have all been proposed and investigated to compensate for the EMD.

Throughout this dissertation, the EMD was characterized and stabilizing motor/FES controllers have been developed to safely implement human-robot interaction with an emphasis on compensating for the EMD of a switched hybrid exoskeleton system. Motivation for the use of hybrid exoskeletons, FES, and robots in rehabilitation settings is provided in Chapter 1. To establish the framework that this dissertation is built upon, a thorough literature review is provided in Chapter 1 on prior control strategies to compensate for systems with input delays, including hybrid exoskeleton systems with an

EMD. Throughout this dissertation, the hybrid exoskeleton of interest is a FES cycle, and the uncertain, nonlinear, switched, and time-varying cycle-rider dynamics are included in Chapter 2. Furthermore, Chapter 2 introduces the designed state and delay dependent switching signals that determine when to activate/deactivate both the motor and FES of each muscle group to ensure control authority is maintained, to produce efficient forward pedaling of the cycle crank, and to compensate for the EMD. The controllers in the subsequent chapters are designed to compensate for the EMD and to yield position, cadence, and/or power tracking.

In Chapter 3, two protocols are performed, measurements are made, and statistical analyses are performed to better understand the EMD. Plots and statistical results were used to confirm the hypothesis that FES-induced cycling will result in the torque and EMD varying with cycling time. Another finding is that the crank angle has a significant effect on the EMD during FES-cycling. The EMD was divided into six different measurements to better understand how the EMD varied with time. To aid future control development, bounds were established on the torque and EMD and on the rate of change of both. Additionally, the study indicated that the CD and RD are different and that the EMD varies between muscle combinations. The results in this study can be used to inform the development of closed-loop controllers that account for the existence of a time-varying EMD. The findings of this chapter also indicate that the EMD should be modeled as angle dependent. These future efforts may lead to improved assistive devices and rehabilitative treatments. The contributions of this chapter include the development of models for the EMD during FES cycling and the confirmation that the EMD is dependent on the cycling time and on the position of the lower limb.

In Chapter 4, delay-dependent switching conditions, which are presented in Chapter 2, and robust cadence tracking controllers are developed for a switched uncertain nonlinear dynamic system in the presence of bounded unknown additive disturbances and an unknown time-varying input delay. A Lyapunov-like stability analysis was performed

on the proposed controllers, which guarantees semi-global exponential tracking to an ultimate bound. An extension of the proposed controller is provided to maintain motor control throughout the crank cycle (as opposed to switching the motor on and off), and for comparison, a third controller was developed assuming the system had no input delay. Experiments were performed on six able-bodied participants and four participants with NCs to compare the performance of these three controllers. The results indicate that the proposed controllers exhibited the desired performance of cadence tracking with FES contributions and produced an average cadence error of 0.01 $\pm$ 2.00 RPM for the able-bodied participants and 0.01 $\pm$ 2.72 RPM for participants with NCs. The contributions of this chapter include developing the first EMD compensating controllers for a coordinated exercise, such as FES-cycling. Furthermore, experimental results demonstrated that compensating for the EMD improved the cadence tracking performance.

In Chapter 5, FES/motor controllers and a time-varying estimate of the EMD are developed to compensate for a switched, delayed, nonlinear, and uncertain FES cycle system with uncertain volitional effort and disturbances. A switched Lyapunov stability analysis was performed to conclude exponential cadence tracking. Control authority was maintained and efficient muscle contractions were produced through the development of EMD and state dependent switching signals, which are included in Chapter 2. To enable comparisons, an alternative control system was created under the assumption that the EMD was negligible, with the same form as the developed controllers. Passive therapy experiments were then conducted on five able-bodied participants to compare the developed control system against the “EMD-free” control system, which resulted in cadence errors of 0.01$\pm$1.35 RPM and -0.01$\pm$2.84 RPM, respectively, and it was concluded that compensating for the EMD significantly improved the cadence tracking performance. Using the developed controllers, active therapy experiments were subsequently conducted on four participants with NCs and produced

an average cadence error of -0.05$\pm$1.38 RPM. The contribution of this chapter include the modifications/improvements made in the control development and stability analysis, the implementation of a time-varying estimate of the EMD, and the series of experiments to validate the developed control system.

In Chapter 6, new FES and motor controllers are developed for the FES cycle to yield cadence tracking. Compared to Chapter 4, a saturated control system is developed such that the upper bound of both the motor and FES controller is known a priori and can be adjusted by modifying the feedback control gains. Consequently, the participant's safety and comfort are improved. A Lyapunov-like analysis was performed to ensure uniformly ultimately bounded cadence tracking for an uncertain nonlinear dynamic switched system, unknown bounded additive disturbances, and an unknown time-varying input delay. Additionally, switching conditions that are presented in Chapter 2 were developed to activate/deactivate stimulation to yield effective muscle contractions. A preliminary experiment on a single participant was performed to validate the motor and FES controllers. The contribution of this chapter is the first development of saturated controllers to compensate for the EMD of a switched system.

In Chapter 7, the safety/comfort and tracking performance of a participant during FES-cycling is improved by the development of a switched and saturated FES control system that is robust to uncertainties in the dynamic model, unknown disturbances, and an unknown time-varying EMD. Exponential position and cadence tracking are guaranteed by a Lyaponov-based stability analysis. An important feature of the control system is that the bound on the FES controller can be set a priori to be within the tolerable range of the participant to ensure comfort. Furthermore, state and delay dependent switching conditions were developed to properly activate/deactivate the motor and the FES of each muscle group to ensure efficient muscle contractions.
A series of experiments were performed on five able-bodied participants and four participants with NCs to validate the performance of the developed controller. For

able-bodied participants, the developed controller and the controllers in Chapter 6 resulted in an average cadence tracking error of -0.03$\pm$1.69 RPM and 3.90$\pm$3.36 RPM, respectively. For the participants with NCs, the developed controller and the controllers in Chapter 6 produced an average cadence tracking error of -0.04$\pm$1.98 RPM and 0.53$\pm$3.37, respectively. Future efforts include the development of an adaptive and saturated FES controller to better adapt to each individual participant, while ensuring participant comfort. The contributions of this chapter result from the design and analysis innovations to yield position and cadence tracking controllers, including a saturated FES controller, that compensate for the EMD of a switched FES system. Additionally, extensive experiments were provided to validate the performance of the controllers developed in Chapters 6 and 7.

In Chapter 8, a dual objective control system is developed to track both PO and cadence using FES and motor controllers, respectively. The torque/power is tracked in real time by implementing a running integral of the torque tracking error. EMD compensation was provided by developing trigger conditions to properly time stimulation, LK functionals, and an auxiliary tracking error that injected a delay-free stimulation input into the closed-loop error system. A Lyapunov-like switched system analysis was performed to ensure exponential power tracking to an ultimate bound and global exponential cadence tracking for the uncertain, nonlinear, switched, and delayed cycle-rider system that was subject to uncertain disturbances such as an unknown volitional effort. A series of comparative experiments were performed on nine participants, including four with a variety of NCs, to validate the developed FES and motor controllers. The proposed controllers produced average cadence and power tracking errors of -0.05$\pm$0.65 RPM and 0.01$\pm$0.09 W for the able-bodied participants, and -0.07$\pm$1.17 RPM and 0.01$\pm$1.11 W for the participants with NCs. A comparison was performed against non-delay compensating controllers of the same form as the proposed system, which demonstrated

that compensating for the EMD improved the power tracking performance. The contribution of this chapter includes the development of the first dual objective control structure that ensures simultaneous cadence and power tracking, along with the corresponding stability analysis, for an unknown, nonlinear, switched, dynamic FES system with an unknown time-varying EMD.

In this dissertation, experimental studies were conducted on participants with and without NCs and statistical analyses were performed to better understand the EMD. Using this improved understanding of the EMD, motor and FES controllers were developed to compensate for uncertainties, nonlinearities, time-varying properties in the dynamics, disturbances, fatigue, and the EMD. Extensive experiments were conducted to validate the performance of the developed EMD-compensating controllers for physical human-robot interaction on a FES cycle. Prior chapters include motor and FES control development, switched system stability analyses, experiments, and statistical analyses. Experiments were conducted on participants with a broad range of NCs, such as SCI, spina bifida, CP, and MS.

Future Work

Future work may include investigating the effects of fatigue on the EMD at various crank angles, developing methods to reduce the rate of FES-induced fatigue, developing improved estimates of the EMD (adaptive estimates in real time), developing improved methods to compensate for the EMD, implementing optimal or deep learning control algorithms to improve rehabilitation, or modifying desired trajectories online to avoid saturating muscles with stimulation. Furthermore, clinical trials should be performed to demonstrate the the clinical impacts of compensating for the EMD, the robustness of the developed control structures in this dissertation, and the rehabilitative effectiveness of closed-loop control methods over open-loop control methods that are common in current clinical practice.

REFERENCES

[1] C. A. Cousin, C. A. Rouse, V. H. Duenas, and W. E. Dixon, "Controlling the cadence and admittance of a functional electrical stimulation cycle," *IEEE Trans. Neural Syst. Rehabil. Eng.*, vol. 27, no. 6, pp. 1181–1192, June 2019.

[2] M. J. Bellman, T.-H. Cheng, R. J. Downey, and W. E. Dixon, "Stationary cycling induced by switched functional electrical stimulation control," in *Proc. Am. Control Conf.*, 2014, pp. 4802–4809.

[3] M. J. Bellman, R. J. Downey, A. Parikh, and W. E. Dixon, "Automatic control of cycling induced by functional electrical stimulation with electric motor assistance," *IEEE Trans. Autom. Science Eng.*, vol. 14, no. 2, pp. 1225–1234, April 2017.

[4] J. H. Rimmer and J. L. Rowland, "Health promotion for people with disabilities: implications for empowering the person and promoting disability-friendly environments," *Am. J. Lifestyle Med.*, vol. 2, no. 5, pp. 409–420, 2008.

[5] D. Newham and N. d. N. Donaldson, "FES cycling," *Op. Neuromod.*, pp. 395–402, 2007.

[6] E. J. Benjamin, M. J. Blaha, S. E. Chiuve, M. Cushman, S. R. Das, R. Deo, S. D. de Ferranti, J. Floyd, M. Fornage *et al.*, "Heart disease and stroke statistics - 2017 update," *Circulation*, vol. 135, no. 10, pp. 146–603, 2017.

[7] F. Anaya, P. Thangavel, and H. Yu, "Hybrid FES–robotic gait rehabilitation technologies: a review on mechanical design, actuation, and control strategies," *Int. J. Intell. Robot. Appl.*, pp. 1–28, 2018.

[8] R. Kobetic, C. S. To, J. R. Schnellenberger, M. L. Audu, T. C. Bulea, R. Gaudio, G. Pinault, S. Tashman, and R. J. Triolo, "Development of hybrid orthosis for standing, walking, and stair climbing after spinal cord injury," *J. Rehabil. Res. Dev.*, vol. 46, no. 3, pp. 447–462, 2009.

[9] V. K. Mushahwar, P. L. Jacobs, R. A. Normann, R. J. Triolo, and N. Kleitman, "New funtional electrical stimulation approaches to standing and walking," *J. Neural Eng.*, vol. 4, no. 3, pp. S181–S197, 2007.

[10] J. S. Petrofsky, "New algorithm to control a cycle ergometer using electrical stimulation," *Med. Biol. Eng. Comput.*, vol. 41, no. 1, pp. 18–27, Jan. 2003.

[11] B. C. Allen, C. Cousin, C. Rouse, and W. E. Dixon, "Cadence tracking for switched FES cycling with unknown input delay," in *Proc. IEEE Conf. Decis. Control*, Nice, Fr, Dec. 2019, pp. 60–65.

[12] B. Allen, C. Cousin, C. Rouse, and W. E. Dixon, "Cadence tracking for switched FES-cycling with unknown time-varying input delay," in *Proc. ASME Dyn. Syst. Control Conf.*, October 2019.

[13] B. C. Allen, K. Stubbs, and W. E. Dixon, “Robust cadence tracking for switched FES-cycling with an unknown time-varying input delay using a time-varying estimate,” in *IFAC World Congr.*, 2020.

[14] ——, “Robust power and cadence tracking on a motorized FES cycle with an unknown time-varying input delay,” in *Proc. IEEE Conf. Decis. Control*, 2020, pp. 3407–3412.

[15] B. C. Allen, K. J. Stubbs, and W. E. Dixon, “Saturated control of a switched FES-cycle with an unknown time-varying input delay,” in *IFAC Conf. Cyber-Phys. Hum.-Syst.*, 2020.

[16] D. J. Pons, C. L. Vaughan, and G. G. Jaros, “Cycling device powered by the electrically stimulated muscles of paraplegics,” *Med. Biol. Eng. Comput.*, vol. 27, no. 1, pp. 1–7, 1989.

[17] L. M. Schutte, M. M. Rodgers, F. E. Zajac, and R. M. Glaser, “Improving the efficacy of electrical stimulation-induced leg cycle ergometry: An analysis based on a dynamic musculoskeletal model,” *IEEE Trans. Rehabil. Eng.*, vol. 1, no. 2, pp. 109–125, Jun. 1993.

[18] B. C. Allen, K. Stubbs, and W. E. Dixon, “Adaptive trajectory tracking during motorized and FES-induced biceps curls via integral concurrent learning,” in *Proc. ASME Dyn. Syst. Control Conf.*, 2020.

[19] C. A. Rouse, B. C. Allen, and W. E. Dixon, “Switched control of motor assistance and functional electrical stimulation for biceps curls,” *Appl. Sci.*, vol. 22, no. 10, pp. 1–14, 2020.

[20] S. Ferrante, A. Pedrocchi, G. Ferrigno, and F. Molteni, “Cycling induced by functional electrical stimulation improves the muscular strength and the motor control of individuals with post-acute stroke,” *Eur. J. Phys. Rehabil. Med.*, vol. 44, no. 2, pp. 159–167, 2008.

[21] C.-W. Peng, S.-C. Chen, C.-H. Lai, C.-J. Chen, C.-C. Chen, J. Mizrahi, and Y. Handa, “Review: Clinical benefits of functional electrical stimulation cycling exercise for subjects with central neurological impairments,” *J. Med. Biol. Eng.*, vol. 31, pp. 1–11, 2011.

[22] A. T. Harrington, C. G. A. McRae, and S. C. K. Lee, “Evaluation of functional electrical stimulation to assist cycling in four adolescents with spastic cerebral palsy,” *J. Pediatr.*, vol. 2012, pp. 1–11, 2012.

[23] L. Griffin, M. Decker, J. Hwang, B. Wang, K. Kitchen, Z. Ding, and J. Ivy, “Functional electrical stimulation cycling improves body composition, metabolic and neural factors in persons with spinal cord injury,” *J. Electromyogr. Kinesiol.*, vol. 19, no. 4, pp. 614–622, 2009.

[24] T. Mohr, J. Pødenphant, F. Biering-Sørensen, H. Galbo, G. Thamsborg, and M. Kjær, "Increased bone mineral density after prolonged electrically induced cycle training of paralyzed limbs in spinal cord injured man," *Calcif. Tissue Int.*, vol. 61, no. 1, pp. 22–25, 1997.

[25] S. P. Hooker, S. F. Figoni, M. M. Rodgers, R. M. Glaser, T. Mathews, A. G. Suryaprasad, and S. C. Gupta, "Physiologic effects of electrical stimulation leg cycle exercise training in spinal cord injured persons," *Arch. Phys. Med. Rehabil.*, vol. 73, no. 5, pp. 470–476, 1992.

[26] V. R. Edgerton, R. D. de Leon, S. J. Harkema, J. A. Hodgson, N. London, D. J. Reinkensmeyer, R. R. Roy, R. J. Talmadge, N. J. Tillakaratne, W. Timoszyk, and A. Tobin, "Retraining the injured spinal cord," *J. Physiol.*, vol. 533, no. 1, pp. 15–22, 2001.

[27] V. Edgerton and R. R. Roy, "Paralysis recovery in humans and model systems," *Curr. Opin. Neurobiol.*, vol. 12, no. 6, pp. 658–667, 2002.

[28] K. Ragnarsson, "Functional electrical stimulation after spinal cord injury: current use, therapeutic effects and future directions," vol. 46, 2008, pp. 255–274.

[29] W. E. Dixon, E. Zergeroglu, D. M. Dawson, and B. T. Costic, "Repetitive learning control: A lyapunov-based approach," *IEEE Trans. Syst. Man Cybern. Part B Cybern.*, vol. 32, pp. 538–545, 2002.

[30] M. J. Bellman, T. H. Cheng, R. J. Downey, C. J. Hass, and W. E. Dixon, "Switched control of cadence during stationary cycling induced by functional electrical stimulation," *IEEE Trans. Neural Syst. Rehabil. Eng.*, vol. 24, no. 12, pp. 1373–1383, 2016.

[31] W. Ter Woerds, P. C. De Groot, D. H. Van Kuppevelt, and M. T. Hopman, "Passive leg movements and passive cycling do not alter arterial leg blood flow in subjects with spinal cord injury," *Phys. Ther.*, vol. 86, no. 5, pp. 636–645, 2006.

[32] L. Marchal-Crespo and D. J. Reinkensmeyer, "Review of control strategies for robotic movement training after neurologic injury," *J. Neuroeng. Rehabil.*, vol. 6, no. 1, 2009.

[33] R. Downey, M. Merad, E. Gonzalez, and W. E. Dixon, "The time-varying nature of electromechanical delay and muscle control effectiveness in response to stimulation-induced fatigue," *IEEE Trans. Neural Syst. Rehabil. Eng.*, vol. 25, no. 9, pp. 1397–1408, September 2017.

[34] E. S. Idsø, T. Johansen, and K. J. Hunt, "Finding the metabolically optimal stimulation pattern for FES-cycling," in *Proc. Conf. of the Int. Funct. Electrical Stimulation Soc.*, Bournemouth, UK, Sep. 2004.

[35] Z. Li, M. Hayashibe, C. Fattal, and D. Guiraud, “Muscle fatigue tracking with evoked emg via recurrent neural network: Toward personalized neuroprosthetics,” *Comput. Intell.*, vol. 9, no. 2, pp. 38–46, 2014.

[36] J. Ding, A. Wexler, and S. Binder-Macleod, “A predictive fatigue model. I. predicting the effect of stimulation frequency and pattern on fatigue,” *IEEE Trans. Rehabil. Eng.*, vol. 10, no. 1, pp. 48–58, 2002.

[37] K. J. Hunt, D. Hosmann, M. Grob, and J. Saengsuwan, “Metabolic efficiency of volitional and electrically stimulated cycling in able-bodied subjects,” *Med. Eng. Phys.*, vol. 35, no. 7, pp. 919–925, Jul. 2013.

[38] R. Berkelmans, “FES cycling,” *J. Autom. Control*, vol. 18, no. 2, pp. 73–76, 2008.

[39] K. J. Hunt, J. Fang, J. Saengsuwan, M. Grob, and M. Laubacher, “On the efficiency of FES cycling: A framework and systematic review,” *Technol. Health Care*, vol. 20, no. 5, pp. 395–422, 2012.

[40] H. Kawai, M. Bellman, R. Downey, and W. E. Dixon, “Closed-loop position and cadence tracking control for FES-cycling exploiting pedal force direction with antagonistic bi-articular muscles,” *IEEE Trans. Control Syst. Tech.*, vol. 27, no. 2, pp. 730–742, Feb. 2019.

[41] C. Cousin, V. Duenas, C. Rouse, M. Bellman, P. Freeborn, E. Fox, and W. E. Dixon, “Closed-loop cadence and instantaneous power control on a motorized functional electrical stimulation cycle,” *IEEE Trans. Control Sys. Tech.*, vol. 28, no. 6, pp. 2276–2291, November 2020.

[42] E. Cè, S. Rampichini, L. Agnello, A. Veicsteinas, and F. Esposito, “Effects of temperature and fatigue on the electromechanical delay components,” *Muscle Nerve*, vol. 47, pp. 566–576, 2013.

[43] K. H. Ha, S. A. Murray, and M. Goldfarb, “An approach for the cooperative control of FES with a powered exoskeleton during level walking for persons with paraplegia,” *IEEE Trans. Neural Syst. Rehabil. Eng.*, vol. 24, no. 4, pp. 455–466, 2016.

[44] A. Nordez, T. Gallot, S. Catheline, A. Guèvel, C. Cornu, and F. Hug, “Electromechanical delay revisited using very high frame rate ultrasound,” *J. Appl. Physiol.*, vol. 106, pp. 1970–1975, Jun. 2009.

[45] S. Obuz, R. J. Downey, J. R. Klotz, and W. E. Dixon, “Unknown time-varying input delay compensation for neuromuscular electrical stimulation,” in *IEEE Multi-Conf. Syst. and Control*, Sydney, Australia, Sep. 2015, pp. 365–370.

[46] S. Obuz, R. J. Downey, A. Parikh, and W. E. Dixon, “Compensating for uncertain time-varying delayed muscle response in isometric neuromuscular electrical stimulation control,” in *Proc. Am. Control Conf.*, 2016, pp. 4368–4372.

[47] N. Alibeji, N. Kirsch, S. Farrokhi, and N. Sharma, "Further results on predictor-based control of neuromuscular electrical stimulation," *IEEE Trans. Neural Syst. Rehabil. Eng.*, vol. 23, no. 6, pp. 1095–1105, 2015.

[48] N. Sharma, C. Gregory, and W. E. Dixon, "Predictor-based compensation for electromechanical delay during neuromuscular electrical stimulation," *IEEE Trans. Neural Syst. Rehabil. Eng.*, vol. 19, no. 6, pp. 601–611, 2011.

[49] I. Karafyllis, M. Malisoff, M. de Queiroz, M. Krstic, and R. Yang, "Predictor-based tracking for neuromuscular electrical stimulation," *Int. J. Robust Nonlin.*, vol. 25, no. 14, pp. 2391–2419, 2015.

[50] S. Zhou, D. Lawson, W. Morrison, and I. Fairweather, "Electromechanical delay in isometric muscle contractions evoked by voluntary, reflex and electrical stimulation," *Eur. J. Appl. Physiol. Occup. Physiol.*, vol. 70, no. 2, pp. 138–145, 1995.

[51] S. Zhou, "Acute effect of repeated maximal isometric contraction on electromechanical delay of knee extensor muscle," *J. Electromyogr. Kinesiol.*, vol. 6, pp. 117–127, 1996.

[52] M. Krstic, *Delay Compensation for Nonlinear, Adaptive, and PDE Systems*. Springer, 2009.

[53] L. Karafyllis and M. Krstic, *Predictor Feedback for Delay Systems: Implementations and Approximations*. Springer, 2017.

[54] M. Bagheri, P. Naseradinmousavi, and M. Krstic, "Feedback linearization based predictor for time delay control of a high-dof robot manipulator," *Automatica*, vol. 108, 2019.

[55] F. Mazenc and M. Malisoff, "Continuous discrete sequential observers for time-varying systems under sampling and input delays," *IEEE Trans. Autom. Control*, vol. 65, no. 4, pp. 1704–1709, 2020.

[56] F. Mazenc, M. Malisoff, and H. Ozbay, "Stability and robustness analysis for switched systems with time-varying delays," *SIAM J. CONTROL OPTIM.*, vol. 56, pp. 158–182, 2018.

[57] J.-P. Richard, "Time-delay systems: an overview of some recent advances and open problems," *Automatica*, vol. 39, no. 10, pp. 1667–1694, 2003.

[58] N. Bekiaris-Liberis and M. Krstic, "Compensation of time-varying input and state delays for nonlinear systems," *J. Dyn. Syst. Meas. Control*, vol. 134, no. 1, p. 011009, 2012.

[59] F. Mazenc, S. Niculescu, and M. Bekaik, "Stabilization of time-varying nonlinear systems with distributed input delay by feedback of plant's state," *IEEE Trans. Autom. Control*, vol. PP, no. 99, p. 1, 2012.

[60] M. Henson and D. Seborg, “Time delay compensation for nonlinear processes,” *Ind. Eng. Chem. Res.*, vol. 33, no. 6, pp. 1493–1500, 1994.

[61] J. Huang and F. Lewis, “Neural-network predictive control for nonlinear dynamic systems with time-delay,” *IEEE Trans. Neural Netw.*, vol. 14, no. 2, pp. 377–389, 2003.

[62] I. Chakraborty, S. Obuz, R. Licitra, and W. E. Dixon, “Control of an uncertain euler-lagrange system with known time-varying input delay: A pde-based approach,” in *Proc. Am. Control Conf.*, 2016, pp. 4344–4349.

[63] S. Obuz, J. R. Klotz, R. Kamalapurkar, and W. E. Dixon, “Unknown time-varying input delay compensation for uncertain nonlinear systems,” *Automatica*, vol. 76, pp. 222–229, February 2017.

[64] D. Bresch-Pietri and M. Krstic, “Delay-adaptive control for nonlinear systems,” *IEEE Trans. Autom. Control*, vol. 59, no. 5, pp. 1203–1218, 2014.

[65] W. Gao and Z. Jiang, “Adaptive optimal output regulation of discrete-time linear systems subject to input time-delay,” in *Proc. Am. Control Conf.*, 2018.

[66] A. Polyakov, D. Efimov, W. Perruquetti, and J.-P. Richard, “Output stabilization of time-varying input delay systems using interval observation technique,” *Automatica*, vol. 49, no. 11, pp. 3402–3410, 2013.

[67] D. Bresch-Pietri and M. Krstic, “Adaptive trajectory tracking despite unknown input delay and plant parameters,” *Automatica*, vol. 45, no. 9, pp. 2074–2081, 2009.

[68] D. Bresch-Pietri, J. Chauvin, and N. Petit, “Adaptive control scheme for uncertain time-delay systems,” *Automatica*, vol. 48, no. 8, pp. 1536–1552, 2012.

[69] D. Enciu, I. Ursu, and G. Tecuceanu, “Dealing with input delay and switching in electrohydraulic servomechanism mathematical model,” in *Proc. Dec. Inf. Tech. 5th Int. Conf. Control*, 2018.

[70] Y. Wang, X. Sun, and B. Wu, “Lyapunov Krasovskii functionals for input-to-state stability of switched non-linear systems with time-varying input delay,” *IET Control Theory Appl.*, 2015.

[71] F. Mazenc, M. Malisoff, and H. Ozbay, “Stability analysis of switched systems with time-varying discontinous delays,” in *Am. Control Conf.*, 2017.

[72] Y. Wang, X. Sun, and F. Mazenc, “Stability of switched nonlinear systems with delay and disturbance,” *Automatica*, vol. 69, 2016.

[73] Y. Wang, B. Niu, B. Wu, and X. Xie, “Asynchronous switching for switched nonlinear input delay systems with unstable subsystems,” *J. Franklin Inst.*, vol. 355, pp. 2912–2931, 2018.

[74] D. Yang, X. Li, and J. Qiu, “Output tracking control of delayed switched systems via state-dependent switching and dynamic output feedback,” *Nonlinear Anal. Hybrid Syst.*, vol. 32, pp. 294–305, 2019.

[75] M. Merad, R. J. Downey, S. Obuz, and W. E. Dixon, “Isometric torque control for neuromuscular electrical stimulation with time-varying input delay,” *IEEE Trans. Control Syst. Tech.*, vol. 24, no. 3, pp. 971–978, 2016.

[76] B. Zhou, Z. Lin, and G. Duan, “Stabilization of linear systems with input delay and saturation - a parametric Lyapunov equation approach,” *Int. J. Robust Nonlinear Control*, vol. 20, no. 13, pp. 1502–1519, 2010.

[77] B. Zhou and Z. Lin, “Parametric lyapunov equation approach to stabilization of discrete-time systems with input delay and saturation,” *IEEE Trans. Circuits Syst. I, Reg. Papers*, vol. 58, no. 11, pp. 2741 – 2754, 2011.

[78] Y.-Y. Cao, Z. Wang, and J. Tang, “Analysis and anti-windup design for time-delay systems subject to input saturation,” in *Proc. Int. Conf. Mechatron. Autom.*, 2007, pp. 1968–1973.

[79] F. Mazenc, S. Mondie, R. Francisco, P. Conge, I. Lorraine, and F. Metz, “Global asymptotic stabilization of feedforward systems with delay in the input,” *IEEE Trans. Autom. Control*, vol. 49, (5), pp. 844–850, 2004.

[80] M. Krstic, “Input delay compensation for forward complete and strict-feedforward nonlinear systems,” *IEEE Trans. Autom. Control*, vol. 55, pp. 287–303, Feb. 2010.

[81] N. Fischer, A. Dani, N. Sharma, and W. E. Dixon, “Saturated control of an uncertain nonlinear system with input delay,” *Automatica*, vol. 49, no. 6, pp. 1741–1747, 2013.

[82] Q. Zhou, C. Wu, and P. Shi, “Observer-based adaptive fuzzy tracking control of nonlinear systems with time delay and input saturation,” *Fuzzy Set. Syst.*, vol. 316, pp. 49–68, 2017.

[83] C. Fornusek and G. M. Davis, “Maximizing muscle force via low-cadence functional electrical stimulation cycling,” *J. Rehabil. Med.*, vol. 36, pp. 232–237, 2004.

[84] A. J. van Soest, M. Gföhler, and L. Casius, “Consequences of ankle joint fixation on FES cycling power output: a simulation study.” *Med. Sci. Sports Exerc.*, vol. 37, no. 5, pp. 797–806, 2005.

[85] M. Gföhler, T. Angeli, T. Eberharter, P. Lugner, W. Mayr, and C. Hofer, “Test bed with force-measuring crank for static and dynamic investigation on cycling by means of functional electrical stimulation,” *IEEE Trans. Neural Syst. Rehabil. Eng.*, vol. 9, no. 2, pp. 169–180, Jun. 2001.

[86] J. Szecsi, P. Krause, S. Krafczyk, T. Brandt, and A. Straube, “Functional output improvement in FES cycling by means of forced smooth pedaling,” *Med. Sci. Sports Exerc.*, vol. 39, no. 5, pp. 764–780, May 2007.

[87] V. Duenas, C. A. Cousin, V. Ghanbari, E. J. Fox, and W. E. Dixon, “Torque and cadence tracking in functional electrical stimulation induced cycling using passivity-based spatial repetitive learning control,” *Automatica*, vol. 115, pp. 1–9, 2020.

[88] M. Bellman, “Control of cycling induced by functional electrical stimulation: A switched systems theory approach,” Ph.D. dissertation, University of Florida, 2015.

[89] E. Ambrosini, S. Ferrante, T. Schauer, G. Ferrigno, F. Molteni, and A. Pedrocchi, “Design of a symmetry controller for cycling induced by electrical stimulation: preliminary results on post-acute stroke patients,” *Artif. Organs*, vol. 34, no. 8, pp. 663–667, Aug. 2010.

[90] K. J. Hunt, B. Stone, N.-O. Negård, T. Schauer, M. H. Fraser, A. J. Cathcart, C. Ferrario, S. A. Ward, and S. Grant, “Control strategies for integration of electric motor assist and functional electrical stimulation in paraplegic cycling: Utility for exercise testing and mobile cycling,” *IEEE Trans. Neural Syst. Rehabil. Eng.*, vol. 12, no. 1, pp. 89–101, Mar. 2004.

[91] A. Farhoud and A. Erfanian, “Fully automatic control of paraplegic FES pedaling using higher-order sliding mode and fuzzy logic control,” *IEEE Trans. Neural Syst. Rehabil. Eng.*, vol. 22, no. 3, pp. 533–542, 2014.

[92] C. Cousin, V. H. Duenas, C. Rouse, and W. E. Dixon, “Motorized functional electrical stimulation for torque and cadence tracking: A switched Lyapunov approach,” in *Proc. IEEE Conf. Decis. Control*, 2017, pp. 5900–5905.

[93] F. Baldissera, P. Cavallari, and G. Cerri, “Motoneuronal precompensation for the low-pass filter characteristics of muscle. a quantitative appraisal in cat muscle units,” *J. Physiol.*, pp. 611–627, 1998.

[94] L. D. Partridge, “Modifications of neural output signals by muscles: a frequency response study,” *J. Appl. Physiol.*, vol. 20, pp. 150–156, 1965.

[95] A. D. Vecchio, A. Ubeda, M. Sartori, J. M. Azorin, F. Felici, and D. Farina, “Central nervous system modulates the neuromechanical delay in a broad range for the control of muscle force,” *J. Appl. Physiol.*, pp. 1404–1410, 2018.

[96] C. A. Cousin, “Hybrid exoskeletons for rehabilitation: A nonlinear control approach,” Ph.D. dissertation, University of Florida, 2019.

[97] C. Rouse, “A switched systems approach to human-machine interaction,” Ph.D. dissertation, University of Florida, 2019.

[98] V. Duenas, “Functional electrical stimulation induced cycling using repetitive learning and passivity-based control,” Ph.D. dissertation, University of Florida, 2018.

[99] B. C. Allen, K. J. Stubbs, and W. E. Dixon, “Characterization of the time-varying nature of electromechanical delay during FES-cycling,” *IEEE Trans. Neural Syst. Rehabil. Eng.*, vol. 28, no. 10, pp. 2236–2245, 2020.

[100] ——, “Electromechanical delay during functional electrical stimulation induced cycling is a function of lower limb position,” *Disability and Rehabilitation: Assistive Technology*, vol. 0, no. 0, pp. 1–6, 2021.

[101] M. J. Bellman, T.-H. Cheng, R. Downey, and W. E. Dixon, “Cadence control of stationary cycling induced by switched functional electrical stimulation control,” in *Proc. IEEE Conf. Decis. Control*, 2014.

[102] V. H. Duenas, C. A. Cousin, A. Parikh, P. Freeborn, E. J. Fox, and W. E. Dixon, “Motorized and functional electrical stimulation induced cycling via switched repetitive learning control,” *IEEE Trans. Control Syst. Tech.*, vol. 27, no. 4, pp. 1468–1479, 2019.

[103] F. Zhang, D. M. Dawson, M. S. de Queiroz, and W. E. Dixon, “Global adaptive output feedback tracking control of robot manipulators,” *IEEE Trans. Autom. Control*, vol. 45, pp. 1203–1208, 2000.

[104] C. S. Bickel, C. M. Gregory, and J. C. Dean, “Motor unit recruitment during neuromuscular electrical stimulation: a critical appraisal,” *Eur. J. Appl. Physiol.*, vol. 111, no. 10, pp. 2399–2407, 2011.

[105] C. M. Gregory and C. S. Bickel, “Recruitment patterns in human skeletal muscle during electrical stimulation,” *Phys. Ther.*, vol. 85, no. 4, pp. 358–364, 2005.

[106] N. van Melick, B. M. Meddeler, T. J. Hoogeboom, M. Nijhuis-van der Sanden, and R. van Cingel, “How to determine leg dominance: The agreement between self-reported and observed performance in healthy adults,” *PLoS One*, vol. 12, 2017.

[107] N. Sharma, N. A. Kirsch, N. A. Alibeji, and W. E. Dixon, “A nonlinear control method to compensate for muscle fatigue during neuromuscular electrical stimulation,” *Front. Robot. AI*, vol. 4, p. 68, Dcember 2017.

[108] T. Muraoka, T. Muramatsu, T. Fukunaga, and H. Kanehisa, “Influence of tendon slack on electromechanical delay in the human medial gastrocnemius in vivo,” *J. Appl. Physiol.*, vol. 96, pp. 540–544, 2004.

[109] S. Rampichini, E. Cè, E. Limonta, and F. Esposito, “Effects of fatigue on the electromechanical delay components in gastrocnemius medialis muscle,” *Eur. J. Appl. Physiol.*, vol. 114, no. 3, pp. 639–651, 2014.

[110] N. Fischer, R. Kamalapurkar, and W. E. Dixon, "LaSalle-Yoshizawa corollaries for nonsmooth systems," *IEEE Trans. Autom. Control*, vol. 58, no. 9, pp. 2333–2338, Sep. 2013.

[111] Z. Cai, M. S. de Queiroz, and D. M. Dawson, "A sufficiently smooth projection operator," *IEEE Trans. Autom. Control*, vol. 51, no. 1, pp. 135–139, Jan. 2006.

[112] A. F. Filippov, "Differential equations with discontinuous right-hand side," in *Fifteen papers on differential equations*, ser. American Mathematical Society Translations - Series 2. American Mathematical Society, 1964, vol. 42, pp. 199–231.

[113] B. E. Paden and S. S. Sastry, "A calculus for computing Filippov's differential inclusion with application to the variable structure control of robot manipulators," *IEEE Trans. Circuits Syst.*, vol. 34, no. 1, pp. 73–82, Jan. 1987.

[114] S. Roy, S. B. Roy, and I. N. Kar, "Adaptive robust control of euler lagrange systems with linearly parametrizable uncertainty bound," *IEEE Trans. Control Syst. Technol.*, vol. 26, no. 5, pp. 1842–1850, 2018.

[115] M. Corless and G. Leitmann, "Continuous state feedback guaranteeing uniform ultimate boundedness for uncertain dynamic systems," *IEEE Trans. Autom. Control*, vol. 26, no. 5, pp. 1139–1144, 1981.

[116] R. J. Downey, T.-H. Cheng, M. J. Bellman, and W. E. Dixon, "Switched tracking control of the lower limb during asynchronous neuromuscular electrical stimulation: Theory and experiments," *IEEE Trans. Cybern.*, vol. 47, no. 5, pp. 1251–1262, May 2017.

[117] W. E. Dixon, A. Behal, D. M. Dawson, and S. Nagarkatti, *Nonlinear Control of Engineering Systems: A Lyapunov-Based Approach*. Birkhauser: Boston, 2003.

BIOGRAPHICAL SKETCH

Brendon C. Allen was born in 1991 in Jacksonville, Florida. He received his B.S. in mechanical engineering in December 2015 from the University of Florida and his M.S. in mechanical engineering in 2018 from Brigham Young University, Provo. As Brendon earned his M.S. degree, he worked in the BYU Neuromechanics research group under the supervision of Dr. Steven K. Charles. Brendon then joined the Nonlinear Controls and Robotics (NCR) research group to pursue his Ph.D. in August 2018 under the advisement of Dr. Warren E. Dixon in the Department of Mechanical and Aerospace Engineering. Brendon was a National Defense Science and Engineering Graduate (NDSEG) Fellow from 2019-2021. In August 2021, Brendon received his Ph.D. in mechanical engineering from the University of Florida. Brendon's research interests include rehabilitation robotics, Lyapunov-based nonlinear control techniques, and functional electrical stimulation.